

Geophysical and Lithological Characterization of the Ellerbek Valley Aquifer System

Von der Naturwissenschaftlichen Fakultät
der Gottfried Wilhelm Leibniz Universität Hannover
zur Erlangung des Grades

Doktor der Naturwissenschaften

- Dr. rer. nat. -

genehmigte Dissertation

von

M. Sc. Mohammed El Mahdi Siddig Abdelrahman

geboren am 23.05.1971 in El Gezira Aba, Sudan

2010

Referentin: Prof. Dr. Jutta Winsemann

Korreferent: Prof. Dr. Hans-Joachim Kümpel

Tag der Promotion: 14.12.2010

Erklärung zur Dissertation

Hierdurch erkläre ich, dass die Dissertation selbständig verfasst und alle benutzten Hilfsmittel sowie evtl. zur Hilfeleistungen herangezogenen Institutionen vollständig angegeben habe. Die Dissertation wurde nicht schon als Diplomarbeit oder ähnliche Prüfungsarbeit verwendet.

ABSTRACT

The Ellerbek Valley represents an important groundwater aquifer for water supply in Southern Schleswig-Holstein, Northern Germany. Geophysical methods including high resolution shallow seismic reflection surveys (P- and SH-wave profiling), Vertical Seismic Profiles (VSP), and airborne electromagnetics were applied on and across the valley, aimed at mapping and characterizing the groundwater aquifers in this valley and investigating the potential of these geophysical methods for analyzing such structures. Seismic data acquisition parameters of source and receiver set-ups resulted in high fold of coverage. Different imaging techniques were carried out in the seismic processing in order to optimize the imaging of the shallow subsurface structures. Common offset F-K DMO processing and integrated velocity analysis have improved the quality of the seismic sections. Steep dip FD time migration has imaged the seismic data better than the Kirchhoff time migration process. FK filtering has been used successfully to filter out Love waves that contaminate the SH-wave data. Vertical seismic profiling (VSP) provided ties to the surface seismic reflection profiling. Well logs are used to calibrate the seismic sections and to estimate petrophysical parameters of Pleistocene and Tertiary sediments.

The methods used successfully imaged (1) Tertiary sediments near the bottom of the fill of the buried valley; (2) Pleistocene sediment fill in the valley; and (3) Holocene sediments that cover the valley. Based on in-line borehole data for geologic control, the seismic profiles show distinctive seismic unconformities that correspond with identifiable lithological boundaries of Tertiary sediments. On the other hand, Pleistocene sediments fill the valley are characterized by complex reflection patterns or rather chaotic to transparent seismic facies. Secondary channels or cut-and-fill structures on meter to hundreds of meter scale were observed within the buried valley indicating a re-use of the existing buried valley during subsequent ice advances and retreats. Since erosion surfaces within the Pleistocene sediments are generally boundaries with some density and velocity contrasts, they are clearly seen with these acoustic methods even when they are not clearly indicated in borehole logs.

Setting up successful hydrogeological models requires detailed high quality 1-D, 2-D and/or 3-D observations. In the past, major progress has been achieved in this effort using borehole data integrated with geophysical measurements. To simply detect the presence of an approximately

2500-m wide buried valley, boreholes would need to be spaced a few meters apart and a much closer spacing would be necessary to obtain a good image of the valley shape. By contrast, the shallow high resolution seismic reflection method with 2.5-m horizontal trace spacing provides a powerful tool for mapping individual structures within Quaternary sediments. Although 2-D high-resolution seismic profiling techniques have limitations in imaging 3-D structures and environments, they offer, in the present study, opportunities for mapping the architecture of the glacial sediments and determining the distribution of porous sandy material down to some 500m depth, and imaging complex faults.

The subsurface geometry and structure of the Ellerbek Valley are well imaged on the seismic depth sections. Major subsurface stratigraphic units could be interpreted by correlating the seismic sections with the geophysical and lithological logs from wells. Moreover, the P- and S-wave velocities derived from surface and borehole seismic data are used to calculate the physical, petrophysical, and hydrogeological parameters of the Quaternary and Tertiary sediments.

The correlation of the key surface and borehole data demonstrates the effectiveness of these techniques for buried valley aquifer characterization.

Keywords: Buried Valley, Geophysical Methods, Groundwater.

ZUSAMMENFASSUNG

Die Ellerbeker Rinne stellt einen wichtigen Aquifer für die Trinkwasserversorgung im südlichen Schleswig-Holstein, Norddeutschland. Geophysikalische Methoden einschliesslich der hochauflösenden flachen Reflexionsseismik (P- und SH-Wellen-Profile), vertikale seismische Profile (VSP) und Hubschrauber-Elektromagnetik Methoden wurden über die Rinne angewandt, um die Grundwasserreservoirs in dieser Rinne zu charakterisieren und zu kartografieren und um das Potenzial dieser geophysikalischen Methoden zur Analyse solcher Strukturen zu untersuchen. Verschiedene bildgebende Verfahren wurden bei der Verarbeitung der seismischen Daten durchgeführt, um die Darstellung der flachen Strukturen zu optimieren. Gemeinsame Offset-FK-DMO-Verarbeitung und integrierte Geschwindigkeitsanalyse verbessern die Qualität der seismischen Abschnitte. Die steil abfallende FD-Zeit-Migration bildet die seismischen Daten besser ab als die Zeit-Kirchhoff-Migration. FK-Filter wurden erfolgreich verwendet, um Love-Wellen zu filtern, die die Daten der SH-Wellen verfälschen. Die vertikale seismische Profilierung (VSP) schafft Verknüpfungen mit der Oberflächen-Reflexionsseismik. Brunnenprotokolle werden verwendet, um die Interpretation der seismischen Abschnitte zu unterstützen und um petrophysikalische Parameter der Quartär- und Tertiär-Sedimente einzuschätzen.

Die verwendeten Methoden zeigten: 1) Tertiäre Sedimente unterhalb der verfüllten Rinne, 2) Pleistozäne Sedimente füllen die Rinne, und 3) Holozäne Sedimente oberhalb der Rinne. Basierend auf den Daten von in-line-Bohrungen zur geologischen Kontrolle zeigen die seismischen Profile sehr unterschiedliche seismische Einheiten und Geometrien, die tertiären Sedimenten entsprechen. Auf der anderen Seite, Pleistozäne Sedimente innerhalb der angenommenen quartären Rinne sind durch komplexe Reflexionsmuster oder eher chaotisch als transparente seismische Fazies charakterisiert. Erosionsstrukturen in der Rinne wurden beobachtet. Da Erosionsoberflächen in den quartären Sedimenten im allgemeinen Begrenzungen mit deutlichen Dichte und Geschwindigkeitskontrasten aufweisen, sind diese mit akustischen Methoden klar nachweisbar, auch wenn sie nicht eindeutig in den Bohrlochprotokollen angegeben werden. In den beiden untersuchten Bereichen führt die schicht tertiäre Ablagerungen zu starken und kontinuierlichen Reflexionen, wohingegen die quartären Sedimente kann lange kohärente Reflexionen aufweisen.

Das Erstellen hydrogeologischer Modelle erfordert detaillierte hochwertige 1-D, 2-D und 3-D Abbildungen. In der Vergangenheit wurden grosse Fortschritte erzielt, indem Bohrlochdaten und geophysikalische Messungen integriert wurden. Um eine etwa 2500 m breite verschüttete Rinnenfüllung zu lokalisieren, bräuchte man Bohrlöcher, die nur wenige Meter voneinander entfernt sind, und um ein besseres Bild der Rinnenform zu bekommen, müssten die Abstände zwischen den Bohrlöchern noch kleiner sein. Dagegen bietet die flache und hochauflösende seismische Reflexionsmethode mit 2,5 m horizontalem Abstand ein leistungsfähiges Werkzeug zur Abbildung einzelner Strukturen innerhalb der quartären Sedimente. Obwohl zweidimensionale hochauflösende seismische Profilierungstechniken bei der Abbildung von dreidimensionalen Strukturen nur begrenzt einsetzbar sind, bieten sie in der vorliegenden Studie die Möglichkeit zur Darstellung der Architektur glazialer Sediment, zur Bestimmung der Verteilung des sandigen Materials in 500 m Tiefe und zur Abbildung von Störungen im oberflächennahen Untergrund.

Die Lage und die Geometrie des Untergrundes der Ellerbeker Rinne sind gut auf den seismisch tiefen Abschnitten dargestellt. Bedeutende stratigrafische Einheiten könnten durch Korrelation der seismischen Abschnitte und der Bohrdaten interpretiert werden. Darüber hinaus werden die P- und S-Wellen-Geschwindigkeiten, die von seismischen Oberflächen und Bohrlochdaten abgeleitet wurden, erfolgreich bei der Berechnung der physikalischen, petrophysikalischen und hydrogeologischen Parameter der Grundwasserreservoirs der Rinnen und tertiären Sedimente eingesetzt werden.

Die Korrelation der verschiedenen Oberflächen und Bohrlochdaten zeigt die Wirksamkeit dieser Methoden zur Charakterisierung der Grundwasserreservoirs in der Rinne.

Schlagnworte: Rinne, Geophysikalischer Methoden, Grundwasser.

Acknowledgements

I would like to express my sincere thanks and gratitude to my promoter Prof. Dr. Hans-Joachim Kuempel, President of the Federal Institute for Geosciences and Natural Resources (BGR), Germany for his scientific guidance and much encouragement. His wide knowledge and experience have been of great value for me. His much support and fruitful discussion made my thesis work possible.

I am grateful to my co-promoter Prof. Dr. Jutta Winsermann of the Institute of Geology, Leibniz University of Hannover, for critical comments and fruitful suggestions which greatly contributed to improvement of this thesis.

Sincere wishes and all gratitude to Dr. Helga Wiederhold who has also supervised this work patiently with wide scientific guidance and interest.

I am greatly indebted to the Leibniz Institute for Applied Geophysics (LIAG) at Geozentrum, Hannover for offering a working place and all facilities for the data analyses as well as supplying the necessary data for this study. My thanks are extended to the staff of Section One (Seismic & Potential Methods) at the LIAG especially Dr. Hanna-Maria Rumpel, Dr. Gerald Gabriel, Dr. Thies Beilecke, Dr. Anton Hermann Bunes and Dr. Ulrich Polom for their help and fruitful discussions. I like to acknowledge the technical team of LIAG Mr. Vogel, D., Mr. Grossmann, E., Mr. Gruneberg, S., Mr. Rode, W. and Mr. Weitmueller W. for their technical assistance and help.

My loving thanks to my wife Ietidal who gave me much support during her stay with me in Hannover. Without her encouragement and support it would have been impossible for me to finish this work. My special gratitude is due to my family in Sudan for their continuous encouragement and support.

This research was financially supported by the University of Khartoum and the Ministry of the Higher Education of Sudan. I would like to express my deepest gratitude and thanks to these two organizations.

Table of Contents

ABSTRACT	IV
ZUSAMMENFASSUNG	VI
ACKNOWLEDGEMENTS	VIII
TABLE OF CONTENTS	IX
LIST OF TABLES	XII
LIST OF FIGURES	XIII
CHAPTER 1: INTRODUCTION	1
1.1 Background	1
1.2 Objectives of the Study	6
1.3 Location of the Study Area and Previous Work	9
1.4 Database	11
1.5 Thesis Structure	14
CHAPTER 2: GEOLOGY AND HYDROGEOLOGY	15
2.1 Overview	15
2.2 Upper Rotliegend	15
2.3 Zechstein Sequence	18
2.4 Triassic Sequence	18
2.5 Jurassic Sequence	19
2.6 Cretaceous Sequence	19
2.7 Tertiary Stratigraphy	20
2.8 Quaternary Stratigraphy	20
2.9 Groundwater Aquifer Systems in the Study Area	22
2.9.1 Tertiary Aquifers	23
2.9.2 Quaternary Aquifers	23
2.10 Groundwater Flow	24
CHAPTER 3: PHYSICAL PARAMETERS EVALUATION AND HYDROGEOLOGICAL RELEVANCE	27
3.1 General	27
3.2 Petrophysical Parameters	28
3.2.1 Porosity	28
3.2.2 Clay Content	30
3.2.3 Density	32
3.3 Hydraulic Conductivity	33
3.4 Elastic Parameters	34
3.4.1 Elastic Moduli	35
3.4.2 V_p - V_s Relations	38

CHAPTER 4: APPLICATION OF HIGH RESOLUTION SEISMIC METHODS-----	40
4.1 General-----	40
4.2 Fundamentals-----	40
4.2.1 Seismic Waves-----	41
4.2.2 Seismic Velocity-----	44
4.2.3 Seismic Reflection and Transmission-----	47
4.2.4 Resolution of Shallow Seismic Data-----	48
4.2.5 Limitations of Seismic Data-----	49
4.3 2-D Seismic Reflection Profiling with P- and SH-Waves-----	50
4.3.1 Data Acquisition-----	50
4.3.2 Data Analysis and Processing-----	54
4.4 Vertical Seismic Profiling-----	89
4.4.1 Zero-offset VSP-----	89
4.4.2 Instrumentation and Recording of the VSP Data-----	91
4.4.3 VSP Data Analysis and Processing-----	93
4.5 Time-Depth Conversion of Surface Seismic Data-----	103
4.6 Development of Workflow for Velocity Estimation Optimized for Geophysical Characterization-----	105
4.6.1 Comparison of CMP Seismic Velocity with VSP Data-----	106
 CHAPTER 5: INTERPRETATION-----	 109
5.1 Seismic Interpretation of P-Wave Profiles-----	109
5.1.1 Profile 4-----	109
5.1.2 Profile 5-----	112
5.2 Combined Interpretation of P- and SH-Wave Profiles-----	113
5.3 Integrated Interpretation-----	116
5.3.1 Surface Seismic and VSP Data-----	116
5.3.2 Surface Seismic and SkyTEM Data-----	119
5.3.3 Seismic Data, Lithology and Well Log Data-----	121
 CHAPTER 6: ESTIMATION OF PHYSICAL PARAMETERS-----	 123
6.1 General-----	123
6.2 Petrophysical Parameters-----	123
6.2.1 Porosity-----	123
6.2.2 Clay Content-----	124
6.2.3 Density-----	124
6.3 Hydraulic Conductivity-----	125
6.4 Elastic Parameters-----	127
6.4.1 Elastic Moduli-----	127
6.4.2 V_p - V_s Relations-----	130
 CHAPTER 7: DISCUSSION-----	 137
7.1 Overview-----	137
7.2 Surface Seismic Profiling-----	137
7.3 VSP and Seismic velocities derived physical parameters-----	144
7.4 Other Geophysical Data-----	148
 CHAPTER 8: CONCLUSIONS AND RECOMMENDATIONS-----	 151
8.1 Conclusions-----	151
8.2 Recommendations-----	152

REFERENCES	154
APPENDICES	167
APPENDIX A	167
APPENDIX B	169
APPENDIX C	171
CURRICULUM VITAE	174

List of Tables

1.1:	General information about the P- and SH-waves seismic profiles.....	12
1.2:	Borehole data: General information. Depths are calculated below the ground surface..	13
2.1:	Description of the Tertiary and Quaternary geological units in southern Schleswig-Holstein (from Wiederhold et al. 2002).....	25
4.1:	P-wave seismic data acquisition: equipments and parameters.....	52
4.2:	SH-wave seismic data acquisition: equipments and parameters.....	53
4.3:	P-wave seismic data processing sequence.....	58
4.4:	SH-wave seismic data processing sequence.....	79
4.5:	Different velocities and times at which the velocities are picked for most prominent reflections in the common velocity stacks (CVS) panels from the velocity analysis of our SH-wave profile.....	85
4.6:	Some objectives of Vertical Seismic Profiling (VSP) surveys (modified after Gilpatrick and Fouquet 1989).....	89
4.7:	VSP data acquisition: equipments and parameters.....	91
4.8:	VSP data processing sequence.....	92
6.1:	Average porosity, density and hydraulic conductivity values of the different geological units in the study area from empirical calculations.	126
6.2:	Ranges of Elastic parameters of different lithological units observed in the Ellerbek valley and its surrounding Tertiary horizons.....	129
6.3:	Average values of V_p and V_s (in m/s) and of V_p/V_s ratio for the Quaternary and Tertiary units. V_p and V_s values have been derived from VSP data.....	131
6.4:	Representative line fit equations for V_p/V_s versus depth in BH3914 and BH3786.....	134

List of Figures

- 1.1: Map showing the base of Quaternary deposits and the distribution of buried valleys for a large part of Northern Europe (Stackebrandt et al. 2001). BurVal pilot project areas are outlined by the rectangles: (1) Bording Valley, (2) Tyrsting Valley, (3) Rødekro Valley, (4) Ellerbeker Rinne, (5) Cuxhavener Rinne, (6) Groningen Valley (from BurVal Working Group 2006).8
- 1.2 Map showing the Ellerbek Valley and the location of seismic section perpendicular to the valley (modified after Scheer et al. 2006): Line 1 and 2 study by Gabriel et al (2003), locations of 2-D gravity data (after Gabriel et al. 2003) along line 1 and 2. 3-D gravity data (after Götze et al. 2009) cover the rectangle in the southern part of the valley. Seismic P4 and P5 are carried out within BurVal project and used in the present study..... 10
- 1.3 Detailed location of the P-wave profiles: profile 4 in the north and profile 5 in the south (in black), the SH-wave profile (in blue), contours of depth to the base Quaternary and the locations of boreholes with VSP data.....13
- 2.1 A: Structural overview of the Central European Basin system depth-to-pre-Permian surface within major NW-SE oriented fault systems: Central Graben (CG); Horn Graben (HG); Glueckstadt Graben (GG); Sorgenfrei-Tornquist Zone (STZ); Teisseyre-Tornquist Zone (TTZ); Horn Graben (HG) and Rheinsberg Trough (RT), (after Littke et al. 2008). B: Regional geological map showing sub-crop formations beneath Tertiary and Quaternary sediments (after Baldschuhn et al. 2001). The location of the Ellerbek valley is bounded by the dark blue lines. P4 and P5 represent the seismic profile4 and profile5, respectively. C: Cross section AA-BB shows the structure and geological units.....16-17
- 2.2: Simplified geological logs from BH3786 (A) and BH3914 (B). T. = Tertiary sediments; P. = Pleistocene sediments; H. = Holocene sediments; LC = Lauenburg Clay; UMC = Upper Mica Clay; ULS = Upper Lignite Sand; HC = Hamburg Clay; LLS = Lower

	Lignite Sand; LMC = Lower Mica Clay; C=clay; Si=silt; FS=fine sand; MS=medium sand; CS=coarse sand; Gr=gravel.....	22
2.3	Characteristic geological structure (salt domes and buried subglacial valleys) and groundwater situation in northern Germany; aquifers: white; clayey layers: light gray (after Gabriel et al. 2003).....	24
3.1:	Physical properties of sediments (Gabriel et al. 2003): influence of porosity and clay content on density, seismic velocity and electrical resistivity: (a) well-sorted, clay-free sediments, (b) reduction of the seismic impedance, density and p-wave velocity of sediments as function of porosity (Morgan 1969) normalized with respect to 30% porosity; (c) electrical resistivity as a function of grain size for fresh water saturated material (after TNO 1976); (d) clayey sediment, pore space partly filled with minerals, (e) porosity as a function of the clay content (artificial sand-clay mixture, Marion et al. 1992), (f) electrical resistivity related to clay content after Sen et al (1988).....	28
3.2:	P-velocity versus clay content in saturated sand-clay samples: a peak in velocity versus clay content occurs at 40 percent clay content. Velocity at the peak is 20 to 30 percent higher than for either pure clay or pure sand. The low values of velocity for the 85 percent clay content sample are attributed to length measurement errors (after Marion et al. 1992).....	30
4.1:	Types of seismic waves and ground particle motions: (a) P-wave, (b) S-wave, (c) Rayleigh wave and (d) Love wave (after Bolt 1982).....	41
4.2:	Waves generated at interface by incident P-wave. P_{inc} , P_{ref} , P_{trans} , S_{refl} and S_{trans} are the incident P-wave, reflected P-wave, transmitted P-wave, reflected S-wave and transmitted P-wave. θ_1 , θ'_1 and θ_2 are the angles of incident, reflection and transmission of P-wave. δ_1 and δ_2 angles of reflection of S-wave. ρ_1 , V_{P1} and V_{S1} are the density the velocity of P-wave and the velocity of S-wave of the upper medium. ρ_1 V_{P2} and V_{S2} are the density P-wave velocity and S-wave velocity of medium.....	43
4.3:	Instantaneous and interval velocities.....	45
4.4:	Three shot gathers with variable data quality from profile 4 with AGC (400 ms) applied. Data are displayed to 1000 ms. Shot gathers 30 (A) and 600 (C) are away from the	

buried valley location, whereas shot gather 125 (B) is in the location of the buried valley. The shot gathers 30 and 600 show stronger and clearer reflections than that shown by the shot gather 125. This is due to the fact that the reflections on the shot gathers 30 and 300 are from Tertiary horizons, whereas the reflections on shot gather 125 are from Quaternary sediments inside the valley. Letters highlight events: airwaves (a); noise traces (b); dipping reflectors (d); ground role (g); first arrivals (r).....55

- 4.5: Three shot gathers with variable data quality from profile 5 with AGC (400 ms) applied. Data are displayed to 1000 ms. Shot gathers 50 (A) and 351 (C) are out of the valley, whereas shot gather 240 (B) is inside the valley. The shot gather 25 and 351 show stronger reflections than that shown by the shot gather 240. This is due to relative homogeneity and continuity of the Tertiary horizons comparing to the heterogeneity of sediments in the valley. Letters highlight events: airwaves (a); noise traces (b); dipping reflectors (d); ground role (g); first arrivals (r).....56
- 4.6: Shot gathers 11 (A) and 91 (B) from the SH-wave profile. No processing has been performed. SR: SH-wave reflection; PR: P-wave reflection; LW: Love wave and BT: bad trace.....57
- 4.7: Raw and correlated vibrator traces (after Gadallah and Fisher, 2009).....59
- 4.8: Principle of static corrections: Shot and receivers are moved to a flat plane, the datum or reference surface. Near surface velocity changes are replaced by a correction velocity V_c (from Wiederhold 2006).....61
- 4.9: A Shot gather from profile4 without (left) and with (right) refraction statics applied. Reflection events show improvements in alignments given by the static corrections....61
- 4.10: Results of applying a prestack processing sequence to typical shot gathers from profile 4 (top) and profile 5 (bottom). Top and bottom mute are applied to eliminate first break and surface waves, respectively. AGC 400 (ms), Bandpass filter (50-70-150-200 Hz) are applied.65
- 4.11: Interactive velocity analysis display with the velocity spectrum (left panel); the NMO corrected gather (middle panel) and the function velocity stack (right panel). The

semblance panel shows the estimated RMS and interval velocity functions. The RMS velocity function is shown in the same time by the function velocity stacks panel.....68

4.12: Optimum stacking velocity fields determined by interactive analysis of semblance gathers after dip moveout. A: Stacking velocity field of profile 4. B: Stacking velocity field of profile 5. The stacking velocity ranges from 1400 to 2900 m/s in profile 4 and from 1600 to 2800 m/s in profile 5.....69

4.13: Interval velocity fields obtained from stacking velocity functions shown in Figure 4.13 A and B, respectively, using Dix's equation. A: the interval velocity field of profile 4; B: the interval velocity field of profile 5. The interval velocity ranges from 1300 to 3000 m/s in both profiles.....70

4.14: CMP traces of seismic energy (M) generated at sources points (S) reflected by a horizontal reflector and recorded at receiver points (R), before stacking (A) and after stacking (B).....71

4.15: Stacked sections of profile 4 without (A) and with (B) DMO applied. Bowtie features due to crossing reflections are obvious at CMP 200 (300 ms).....72

4.16: Stacked sections of profile 5 without (A) and with (B) DMO correction applied. Bowtie features due to crossing reflections are evident at CMP 600 (300 ms). The red line on top of the section (CMP 291-595) indicates the location of SH-wave profile.....73

4.17: Migrated time sections of profile 4 using Kirchhoff Time Migration (A) and Steep Dip FFD Time Migration (B).....76

4.18: Migrated time sections of profile 5 using Kirchhoff Time Migration (A) and Steep Dip Time Migration (B).....77

4.19: Uncorrelated (A) and correlated (B) SH-wave data (shot points 1, 2, 3 and 4). Each shot point has 121 channels. Channel number 121 is the vibroseis sweep channel.....80

4.20: Raw shot gathers 1 (left), 2 (middle) and 3 (right) before (A) and after pre-processing applied (B).....81

4.21: SH-wave raw shot gather before applying the FK filter (A), where coherent first arrivals are evident, and after applying the FK filter with some linear arrivals are eliminated (B).....82

4.22: Several CVS panels (A, B, C, D, E and F) from the SH-wave profile. Each panel is assigned the velocity value in m/s with which a certain reflection becomes most coherent.....84

4.23: Stacking velocity field of the SH-wave profile. Arrows on top show the CMPs at which a semblance velocity analysis was conducted. The lower velocity value is about 250 m/s shown at the top of the velocity field (Quaternary sediments). Higher velocity values are shown by Tertiary sediments in the bottom left part of the velocity field (about 750 m/s). Velocity ranges from 250 m/s for Quaternary sediments to 850 m/s for Tertiary sediments.....85

4.24: SH-wave stacked CMP section shows clear reflections of top and bottom of Lauenburg Clay at 200 and 500 ms (the two arrows on the right side). Other discontinuous reflections are also shown.....86

4.25: SH-wave time migrated section (A) and depth migrated section (B). Smearing effects due to the velocity field is evident in the bottom of the sections. The Lauenburg Clay (highlighted by two arrows on the right side) is shown between 200, 450 ms, and 30 and 70 m in top and bottom sections, respectively.....87

4.26: Schematic cross section of a typical VSP field layout indicating a survey borehole, seismic source, receiver, wireline and recording seismograph.....91

4.27: The waveform is rotated and separated to its 3 components: X (left), Y (middle) and Z (right) components. A: the components of the VSP at BH3914 and B: the components of the VSP at BH3786.....93

4.28: The VSP Z-component shows strong first arrivals, upgoing energy, tube waves and reflected tube waves. A: the Z-component of the VSP at BH3914 and B: the Z-component of the VSP at BH3786.....94

4.29:	Processed VSP data of BH3914 (A) and BH3786 (B). First break picking for velocity calculation is shown by red lines.....	95
4.30:	Cross section showing the source at the earth's surface and a receiver at depth h. The source is offset a horizontal distance (x) from the receiver. This configuration can be used to derive an average-velocity-with-depth function.....	96
4.31:	P- and S-wave interval velocities (V_p and V_s , respectively; in m/s) derived from VSP data from BH3914 (A) and BH3876 (B), correlated with the lithological logs of each borehole. Velocities are in m/s; horizontal lines follow the major geological units as shown by lithological columns. LC = Lauenburg Clay; UMC = Upper Mica Clay; ULS = Upper Lignite Sand; HC = Hamburg Clay; LLS = Lower Lignite Sand; LMC = Lower Mica Clay.....	97
4.32:	Separated upgoing energy of VSP at BH3914 (A) and BH3786 (B).....	100
4.33:	VSP results at BH3914: (a) upgoing waves, (b) upgoing waves corrected to tow-way-travel time, with top and bottom mute; (c) corridor stack repeated 5 times; and BH3786: (d) upgoing waves, (e) upgoing waves corrected to tow-way-travel time, with top and bottom mute and (f) corridor stack repeated 5 times.....	101
4.34:	Poststack depth migrated sections of profile 4 (A) and profile 5 (B) using interval velocity functions calculated from VSP at BH3914 and BH3786, respectively.....	103
4.35:	A velocity spectrum before DMO correction (A) and after DMO correction (B). Blue colour represents low semblance and red colour represents high semblance areas. V_{rms} is the RMS velocity and V_{int} is the interval velocity.....	105
4.36:	Measured interval velocity from CMP 800 of seismic profile 4 (dotted lines) compared with the VSP P-wave interval velocity function from BH3914 (solid line).....	106
4.37:	Measured interval velocity from CMP 700 of seismic profile 5 (dotted lines) compared with the VSP P-wave interval velocity function (solid line).....	106

4.38: Measured interval velocity from CMP 3500 of seismic SH-wave profile (dotted lines) compared with the VSP S-wave (V_s) interval velocity function from BH3786 (solid line)..... 107

5.1: A: Migrated depth section of profile 4 and B: geological interpretation of the migrated section showing identification of reflections with BH3914 superimposed. Dashed vertical to semi vertical lines represent interpreted fault planes. a is the Ellerbek valley floor; b, c, and d are secondary valleys; Unit5, Unit4, Unit3, Unit2 and Unit1 are interpreted seismic facies of the valley fill. Tertiary units: LC = Lauenburg Clay; UMC = Upper Mica Clay; ULS = Upper Lignite Sand; HC = Hamburg Clay; LLS = Lower Lignite Sand; LMC = Lower Mica Clay.....110

5.2: A: Migrated depth section of profile 5 and B: geological interpretation of the migrated section showing identification of reflections with BH3914 superimposed. Dashed vertical to semi vertical lines represent interpreted fault planes. a is the Ellerbek valley floor; b and c, and secondary valleys; Unit5, Unit4, Unit3, Unit2 and Unit1 are interpreted seismic facies of the valley fill. Tertiary units: LC = Lauenburg Clay; UMC = Upper Mica Clay; ULS = Upper Lignite Sand; HC = Hamburg Clay; LLS = Lower Lignite Sand; LMC = Lower Mica Clay. The double arrow line above the section highlights the corresponding location of the SH-wave section section.....113

5.3: A: Part of profile 5 that is analogous to SH-profile (CMP 291 to CMP 595; left panel) and the SH-wave profile (right panel). Both are imaged and vertically positioned so as depths correlate (common mid-points numbers on P- and SH-wave sections are different). B: the seismic sections are overlain by geological interpretation. Principal interpreted stratigraphic boundaries and faults are marked. Boundaries on the SH-profile show an interpreted shallow reflection in the Holocene sediments (purple horizontal line super imposed on two sections). Black vertical lines represent faults interpreted from both sections while purple vertical lines represent faults interpreted only from SH-waves. The oval shape on the bottom right of the two sections compares the reflection configurations which are chaotic in the P-wave section and well horizontal in the SH-wave section.....114

5.4: Geological model along seismic profile 5 (between CMP291 and CMP595) based on the integration of P- and S-wave depth sections. Purple coloured lines, both faults and geological boundaries, are interpreted only from the SH-wave profile. Unit1 to Unit5

are layers interpreted in Quaternary sediments bounded by unconformities (dotted thin lines). LC = Lauenburg Clay; UMC = Upper Mica Clay; ULS = Upper Lignite Sand; HC = Hamburg Clay; LLS = Lower Lignite Sand.....115

5.5: VSP corridor stack section at BH3914 inserted into the profile 4 seismic section (CMP 820) showing a close match of Hamburg Clay (HC) reflections. Other reflections around and below 200 ms, within the Lower Lignite Sand layer, are evident in the VSP and to lesser degree in the seismic section of profile 4.....116

5.6: VSP corridor stack section at BH3786 spliced into the profile 5 seismic section (CMP 780) showing a good match of the base Quaternary (Base Q) signature. An excellent match is also found at 300 ms. The arrow on the right side marks a coherent reflection of both dataset.....117

5.7: SkyTEM resistivity cross-section across the valley along a flight line close to the seismic profile 4 superimposed by seismic interpretation of profile 4 to 300 m depth, and the lithological log of BH3914.....119

5.8: SkyTEM resistivity cross-section across the valley along a flight line close to the seismic profile 5 superimposed by seismic interpretation of profile 5 to 200 m depth, and the lithological log of BH3786.....119

5.9: Seismic results of profile 4 (1), profile 5 (2) and lithological and geophysical logs of BH3914 and BH3786: (A) part of seismic reflection depth section; (B) VSP corridor stack section; (C) lithological log (D) Gamma ray patterns; (E) Gamma ray log and (F) Resistivity log.....121

6.1: Results of physical and petrophysical parameters calculation from P-wave interval velocity function (1): at BH3914 and (2): at BH3786. (A) Porosity log calculated using the velocity – porosity relation after Morgan (1969); (B) Density log calculated from V_p interval velocity function derived from VSP data using the velocity-density empirical relation after Hamilton (1971); (C) Hydraulic conductivity calculated from velocity values using the equation of Fechner (1998), (D) Clay content calculated from gamma log using equation 3.9 (after Western Atlas 1985); and the lithological logs of BH3914. LC = Lauenburg Clay; PS = Pleistocene Sands; UMC = Upper Mica Clay; ULS =

	Upper Lignite Sand; HC = Hamburg Clay; LLS = Lower Lignite Sand; LMC = Lower Mica Clay.....	125
6.2:	Elastic moduli derived from P- and SH-wave velocities (V_p and V_s) and densities measured (1): at BH3786 and (2): at BH3786. A is the rigidity modulus, B is the bulk modulus, C is Young's modulus and D is Poisson's ratio. LC = Lauenburg Clay; PS = Pleistocene Sands; LMC = Lower Mica Clay.....	128
6.3:	The plot of V_p versus V_s of BH3194 (A) and BH3786 (B). The regression linear functions are: $V_s=0.23V_p+24$ m/s and $V_s=0.65V_p-696$ m/s, respectively. These equations represent the lines in the Figure.....	130
6.4:	V_p/V_s versus depth and lithological logs of BH3914 (A) and BH3786 (B) showing a general decrease in V_p/V_s ratio with depth.....	131
6.5:	2-D interval velocity fields of P-wave profile 5 (A), SH-wave (B) and the V_p/V_s ratio (C). The 2-D P-wave interval velocity is resampled (between CMP300 to CMP600) to match the 2-D SH-wave velocity field. All fields are superimposed by the integrated interpretation of P- and SH-wave seismic data shown in Figure 5.4.....	133
6.6:	V_p/V_s versus depth for BH3914 (A) and BH 3786 (B). The regression lines, fit over the whole well, are shown ($V_p/V_s=-0.01z+5.1$ and $V_p/V_s=-0.7z+5.2$, respectively, where z is the depth in meters).....	134
6.7:	P- and SH-wave velocities are determined using full waveform VSP from BH3914 (A) and BH3786 (B). Plots of V_p/V_s versus V_p show tendency of the data to form clusters which correlate to certain types of sediments.....	135
6.8:	Correlation between P- and S-wave velocity ratio (V_p/V_s) versus S-wave velocity (V_s) from BH3914 (A) and BH3786 (B).....	135
7.1:	Part of the migrated seismic sections A: from profile 4 between CMP 120 and CMP 350; B: profile 5 between CMP 450 and CMP 650 show chaotic curve-like reflections in the areas marked by the rectangles.	141

- 7.2: A simplified geological section interpreted from profile 5 to illustrate a possible large secondary (?) valley (B) within the major Ellerbek valley (A).....142
- 7.3: Geological section across the Ellerbek Valley showing the Quaternary sediments fill the Ellerbek valley as well as Tertiary sediments. LC = Lauenburg Clay; UMC = Upper Mica Clay; ULS = Upper Lignite Sand; HC = Hamburg Clay; LLS = Lower Lignite Sand. The arrow points to Marine Mica Sand which appears on the west side of the valley.....142
- 7.4: Hypothetical schematic illustrations for the interpreted structural evolution of the Ellerbek Valley: (1) the Pre Quaternary situation; (2) after the Tertiary horizons were eroded by glacial activities and (3) the present day situation. Red boundaries are secondary valleys. LC = Lauenburg Clay; UMC = Upper Mica Clay; ULS = Upper Lignite Sand; HC = Hamburg Clay; LLS = Lower Lignite Sand; LMC = Lower Mica Clay. Numbers 1-5 represent sediment units of the valley infill as interpreted from seismic data.....149

Chapter 1: Introduction

1.1 Background

Buried valleys are geological structures that are extensively used as groundwater aquifers in Northern Germany (Gabriel et al. 2003, Gabriel 2006, Stackebrandt 2009). This is due to the fact that their infill is dominated by sandy material consisting mainly of glaciofluvial sands intercalated with silts and glaciolimnic silts and clays as well as boulder clays (Schwab and Ludwig 1996, Stackebrandt 2001). These valleys were formed in the last three major glaciations which covered most of the North Sea and adjacent continents (Gabriel 2006).

Buried valleys are wide spread in formally glaciated Northwest European lowlands (Huuse and Lykke-Anderson 2000). They have also been recognized in North America (e.g. Wright 1973, Boyd et al. 1988, Mooers 1989, Cutler et al. 2002, Russell et al. 2003, Hooke & Jennings 2006, Kehew et al. 2007) and Australia (e.g. de Broekert 2002, Holzschuh 2002). The existence of buried valleys and their importance for the occurrence and extent of groundwater resources have been known for several years (BurVal Working Group 2006). They are also scientifically important in providing evidence of preglacial drainage patterns (Greenhouse and Karrow 1994).

O'cofaigh (1996) defined buried valleys as elongated depressions with overdeepened areas along their floors cut into bedrock or unconsolidated sediments beneath marginal zones of large ice sheets (Jørgensen & Sanderson 2006). Stackebrandt (2009), in his review of subglacial channels of Northern Germany, mentioned that their contours and shapes show a significant relationship to the regional pre-Quaternary geology. In northern Europe they are described as up to hundreds of kilometers long, several kilometers wide and several hundreds of meters deep (Ehlers et al. 1984, Praeg 1996).

Origin of Buried Valleys

The origin of the buried valleys (or tunnel valleys) is not fully understood. O' Cofaigh (1996) pointed out that there is no completely satisfactory explanation of buried valley genesis. Huuse and Lykke-Anderson (2000) pointed out that the origin of buried valleys has been a matter of

intense debate for the last century. The origin of the buried valleys has been discussed by several authors (Boulton and Hindmarsh 1987, Mooers 1989 Winfield 1990, Ehlers and Wingfield 1991, Piotrowski 1994, O' Cofaigh 1996, Huuse and Lykke-Andersen 2000, Cutler et al. 2002; Kozłowski et al. 2005, Hooke & Jennings, 2006, Jørgensen & Sanderson 2006, Kirsch et al. 2006). O' Cofaigh (1996) grouped the assumptions for formation of buried valleys into three main theories:

- (1) Tunnel valley formation by subglacial sediment deformation,
- (2) Time-transgressive tunnel valley formation near ice margins, and
- (3) Tunnel valley formation by catastrophic subglacial sheet floods.

The sediment deformation theory has been developed by Boulton and Hindmarsh (1987), who proposed that shallow channels carrying subglacial meltwater are initiated by piping from the ice margin and would gradually be enlarged by the creep of deformable sediment toward the channel and the subsequent removal of the sediment by meltwater flow. Conflict to this hypothesis is based upon arguments questioning the existence of a fluid-pressure gradient toward the channels and the occurrence of buried valleys in bedrock lithologies, in which sediment deformation would not be possible (O'Cofaigh 1996). The theory of time transgressive formation close to the ice margin is supported by many authors. Mooers (1989) suggested the formation of buried valleys to be a more gradual, steady process, in which subglacial meltwater was augmented by diversion of supraglacial meltwater to the base of the glacier. On the other hand, most hypotheses invoke a sudden or catastrophic release of channelized subglacial meltwater (Winfield 1990, Ehlers and Wingfield 1991, Huuse and Lykke-Andersen 2000, Kirsch et al. 2006) because of the large clast size deposited in ice-marginal fans located at the termination of the channels (Piotrowski 1994) and the size and dimensions of the channels (Kozłowski et al. 2005). The sudden release of subglacial reservoirs is often attributed to failure of a permafrost seal at the margin (Piotrowski 1994, Cutler et al. 2002, Hooke & Jennings, 2006, Jørgensen & Sanderson 2006). Piotrowski (1997) and Hooke & Jennings (2006) suggested a cyclical process in which a seal is punctured and leads to a catastrophic release of an impoundment, followed by the reestablishment of the seal and the refilling of the impoundment. Hooke & Jennings (2006) proposed that piping and headword erosion back to meltwater impoundment initiate the outburst.

The Buried valleys differ from ordinary valleys in four ways: (1) they form interconnected anastomosing valley patterns, (2) their orientation is parallel to the assumed general Elsterian

ice flow direction, (3) overall network pattern suggests valleys to be part of one uniform hydrological system and (4) longitudinal profiles have an irregular base with many threshold (Van Dijke and Veldkamp 1996).

Buried valleys are aged during Pleistocene (Ehlers 1996). Stackebrandt (2009) pointed out that buried valleys were formed during all Pleistocene glaciations, but those of Elsterian age are most important and they are up to 500 m deep and 150 km long. Infill sediments of the valleys include sediments from Weichselian, Saalian and Elsterian glaciations and deposits from the Eemian and the Holsteinian interglacials (Jørgensen & Sanderson 2006) indicating that buried valleys have active geologic features at least since Elsterian glaciation.

Geophysical Studies of Buried Valleys

Buried valleys may be completely infilled by thick sedimentary successions, including glacial, glacialfluvial, glaciallacustrine, glaciomarine and non-glacial deposits, and may not have any clear topographic expression on the surface (O Cofaigh 1996). In such cases, detailed studies of borehole logs, geophysical data and sedimentary exposures are necessary to determine their morphology and extent (Benn and Evans 1998). Gabriel et al (2003) pointed out that buried valleys are not always visible at the surface and geophysical methods have often been applied to investigate these near-surface structures to provide a better understanding of their internal behaviour and geometrical structure. During the last few years extensive geophysical studies of buried valleys were carried out in NW Europe. A number of geophysical investigations of buried valleys have been documented in a special issue of the Journal of Applied Geophysics (Huuse et al. 2003). BurVal Working Group (2006) compiled an extensive geoscientific work in the BurVal Working Group book on mapping groundwater resources in buried glacial valleys in Denmark, Germany and the Netherlands. Most recent compiled studies on buried valley, on- and offshore, are presented in a special issue of Zeitschrift der Deutschen Gesellschaft fuer Geowissenschaften (Band 160.2009.Heft 3).

Offshore seismic data are extensively used in studying the morphology, distribution and infill stratigraphy of buried valleys. Huuse et al (2000) mapped buried valleys in the eastern Denmark North Sea based on over 6400 km of high-resolution 2-D seismic profiles coupled with sparse borehole information. Kluiving et al. (2003) interpreted a series of on- and offshore 2-D seismic profiles from the northern Netherlands integrated with gamma-ray, Vertical Seismic Profiles

and cuttings analysis from borehole onshore in order to establish a sedimentological model for the buried valleys fill. Praeg (2003) used 2-D and 3-D seismic data, originally acquired for petroleum exploration, in combination with borehole data to investigate buried mid-Pleistocene valleys southern UK and Dutch North Sea. The topography of a series of valleys extracted from 3-D data by Kristensen et al. (2007) shows undulating bottoms and adverse end slopes that are generally characteristic of subglacial valleys. Lutz et al (2009) mapped Pleistocene tunnel valleys in the German North Sea using 25000 km² 2-D and 3000 km³ 3-D marine seismic data. Their map covers new areas and reveals new tunnel valleys that were not deduced before. They differentiated 3 different generations of tunnel valleys in 3-D data and cut-and-fill structures within the tunnel valleys in 2-D data. Onshore 2-D High-resolution seismic surveys have been used for mapping ground water structures and imaging glacial deposits (Bradford et al. 1998, Wiederhold et al. 1998, Holzschuh 2002 Jørgensen et al. 2003). BurVal Working Group (2009) summarized results of 2-D seismic data applied in BurVal project pilot areas in North Sea region shown in Figure 1.1. They pointed out that seismic profiles can reveal the shape and internal structure of the buried valleys and surrounding layers.

Electromagnetic techniques have been extensively employed in characterization of Buried valleys. Jørgensen et al. (2003) presented an integrated application of time-domain electromagnetics (TEM) for the investigation of buried valleys in Denmark. Danielsen et al. (2003) presented a 2-D model study which showed the limitation of TEM 1-D inversion in the determination of the slopes of buried valleys. Gabriel et al. (2003) and Wiederhold et al (2005) summarized the results of different geophysical methods on buried valleys in Northern Germany including helicopter-borne electromagnetic (HEM) method. Bosch et al. (2009) used airborne EM with other geophysical and borehole data to develop a 3-D model for the incision of the Groningen valley in the Netherlands. Tezkan et al. (2009) used a special configuration for a transient electromagnetic survey in the area of Cuxhaven with the aim to look deeper and find the bottom of the valley with this method. They pointed out that larger EM transmitter can resolve deeper into buried valleys. Ground-based electromagnetic surveys have also been applied in the investigation of buried valleys (e.g. Baines et al. 2002, Jorgensen et al. 2003, Thomsen et al. 2004, Kilner et al. 2005, Jørgensen and Sandersen 2006, Bersezio et al. 2007).

Gravity measurements have recently been successfully integrated in the exploration of buried valleys in 2-D (Gabriel 2006) and 3-D (Götze et al. 2009). BurVal Working Group (2009) pointed out that gravity methods can be used to detect buried valleys of 1-km width, more than 200-m deep and filled with sediments different from the surrounding. Gravity measurements

have been carried out mainly to search for density contrast and map the lateral extent of buried valleys (e.g. Gabriel 2006, Møller et al. 2007 and Götze et al. 2009). Most successful results were obtained from bedrock areas in which buried valleys show up as gravity lows due to the increased porosity of the fill materials relative to bedrock (e.g. Wolfe and Richard 1996).

Groundwater Aquifers in Buried Valleys

The significance of Buried Valleys in groundwater exploration has become more apparent as traditional groundwater exploration from shallow aquifers is increasingly being compromised by pollution from industry and farming throughout the NW European lowlands (Huuse et al. 2003). Most frequently, the buried valleys host considerable groundwater aquifers, but they may also act as path ways for contaminants from the surface to percolate to deeper aquifers (Jørgensen & Sanderson 2009). However, the Buried Valleys can provide several tens of meters thick sands and gravels protected from surface pollution by some tens of meters of low permeability strata (Ehlers and Linke 1989; Piatewowski 1997).

Due to the mechanism of depositional conditions associated with advancing and retreating glaciers, these sediments are highly heterogeneous, such that their lithologies and hydraulic conductivities may change significantly over short distances (Siegenthaler and Huggenberges, 1993). This situation complicates the understanding of groundwater flow modeling and contaminant transport prediction, which require reliable information on 2-D and 3-D geometrics and distribution of shallow surface sedimentary structure.

One way to understand the structure and characteristics of the heterogeneous aquifers in a buried valley is by conventional hydrogeological investigations based on usually sparse boreholes and available outcrops. Information gathered by these methods is strongly localized. Therefore, geophysical methods may be useful in obtaining critical information concerning sedimentary structures and physical properties between such boreholes and outcrops.

The significance of each single geophysical method mainly depends on the physical properties and depths of the targeted geological structures. The state-of-art of combined use of several geophysical methods reduces the ambiguity of interpretation, but there is not the one “optimum combination of methods” for all applications. This study deals with the application of geophysical methods to characterize and map the geology and structure of groundwater aquifers

in the Ellerbek Buried Pleistocene Subglacial Valley and surrounding Tertiary horizons in Schleswig-Holstein, Northern Germany.

1.2 Objectives of the Study

In the years 2004-2006 a multidisciplinary geoscientific project, known as Buried Pleistocene Subglacial Valleys (BurVal) was carried out by Geoscientific institutions from Germany, the Netherlands, and Denmark focusing on the buried valleys in the North Sea region. The objective of the project was to develop geoscientific methods to be used for the investigations of groundwater aquifers found in Buried Pleistocene Subglacial Valleys (BurVal Working Group 2006).

Figure 1.1 shows the distribution of the BurVal pilot project areas in: Denmark (1. Bording Valley, 2. Tyrsting Valley and 3. Rødekro Valley), Germany (4. Ellerbek Valley, 5. Cuxhaven Valley) and the Netherlands (6. Groningen Valley). The Figure also shows the distribution of the buried valleys in North Europe as compiled by Stackebrandt et al (2001). The Ellerbek valley in Schleswig-Holstein, Northern Germany, is one of the pilot project areas of the BurVal project. In the present study we try to contribute to the BurVal project by exploring the structure and characteristics of the Ellerbek Valley aquifer system with sufficient detail to be useful for further groundwater studies concentrating on the southern part of the valley located between Tangstedt and Winzeldorf where good quality data exist.

The objectives of this study arise with respect to the importance of buried valley structures as a potential future resource of fresh water as well as an important key to paleoclimatic records. These objectives can be summarized in the following requirements: (1) the delineation of valley location and structure, (2) the nature and thicknesses of sediment fills, and (3) the estimation of the physical and petrophysical properties of the sediments present in the valley structure. The main goal of the present study is to use an integrated study of high resolution seismics and other geophysical methods and rock physics analysis to estimate the physical and petrophysical properties directly from in-situ geophysical measurements. The determination of the physical and petrophysical parameters of sediments provides ideas about the flow of the subsurface water and helps in understanding of propagation of seismic waves in the sediments.

To gather the information that is needed for an economical and ecological successful water supply, a reasonable combination of geoscientific and geophysical investigation methods should be used. It is an aim of this study to apply and evaluate those methods and give recommendations for the practical use.

In the course of this study we intend to address the following key questions related to the buried valley properties:

- How can we get optimal interval velocity models (for P- and SH-waves) for the near surface range?
- Is it possible to constrain the data by use of borehole data, electrical measurements and other geophysical data?
- Is it possible to derive realistic elastic parameters by combination of P- and SH-waves?
- Often the seismic section shows strong reflections but there is not hint on changes in the borehole lithologic column. So, what is the nature of the seismic reflections?

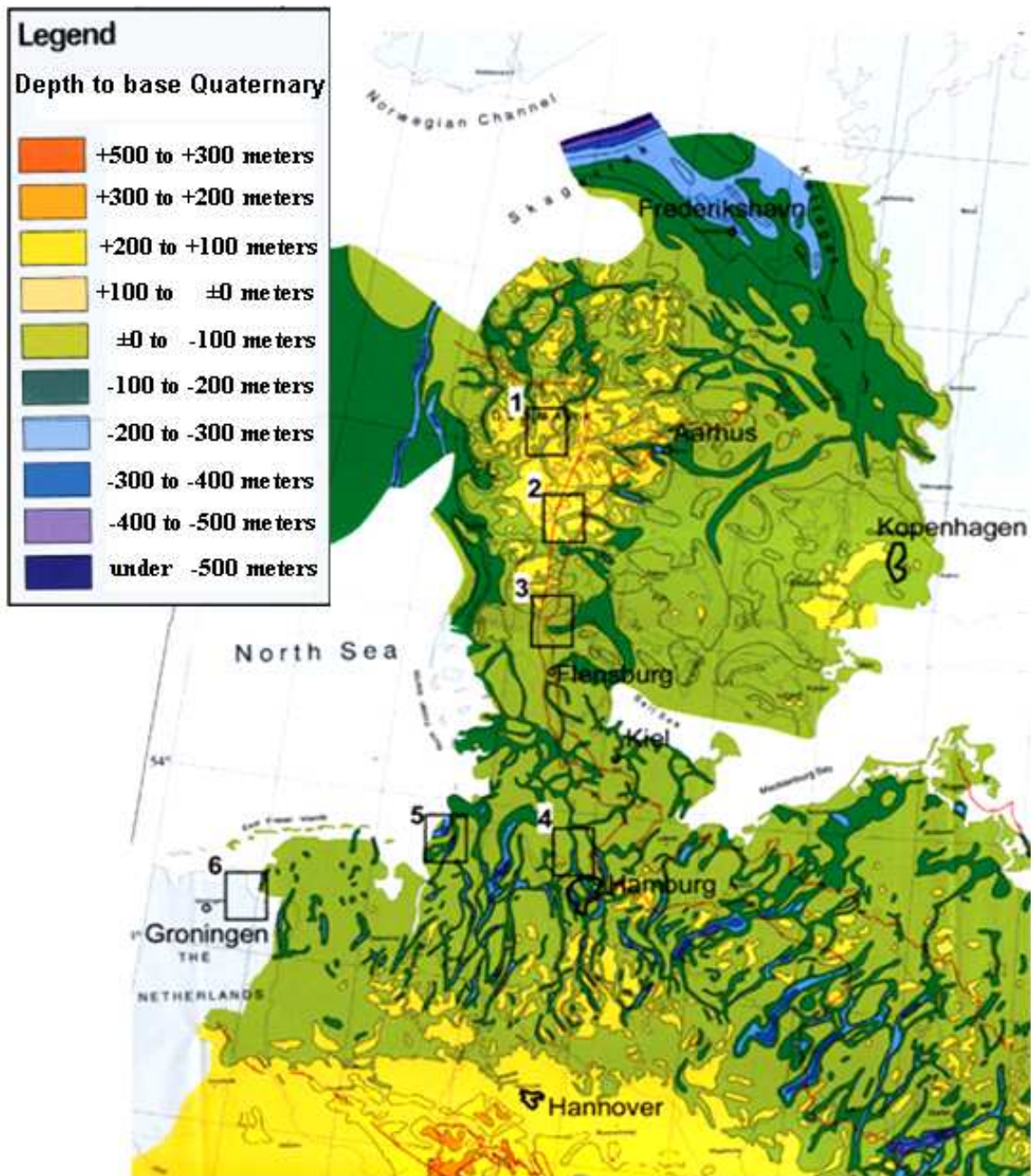


Figure 1.1: Map showing the base of Quaternary deposits and the distribution of buried valleys for a large part of Northern Europe (Stackebrandt et al. 2001). BurVal pilot project areas are outlined by the rectangles: (1) Bording Valley, (2) Tyrsting Valley, (3) Rødekro Valley, (4) Ellerbeker Rinne, (5) Cuxhavener Rinne, (6) Groningen Valley (from BurVal Working Group 2006).

1.3 Location of the Study Area and Previous Work

The Ellerbek valley is located in southern Schleswig-Holstein in North Germany. It extends in N-S direction for about several tens of kilometers. The investigated part is in the southern part of the valley which lies near the town of Tangstedt, about 15 km north of Hamburg. The general location of the study area (BurVal pilot project area No. 4) as well as the compiled distribution of buried valleys in North Sea region (after Stackebrandt 2001) is shown by Figure 1.1.

Several geological and geophysical investigations have been carried out in the study area to map the subsurface structure and understand the groundwater situation within the Ellerbek Valley in 1-D, 2-D and 3-D data. The geological situation and rough geometry of the Ellerbek Valley was explored initially by numerous deep drilling conducted by the water administrations of Schleswig-Holstein and Hamburg (e.g. Scheer 2001). Moreover, information about the base of the Quaternary and the buried valley is mainly based on water well data and data from exploration for hydrocarbons (Wiederhold 2006). Most of the boreholes were meant to be drilled in the middle of the respective buried valley (Gabriel et al. 2003). Figure 1.2 shows the buried valley which stretches for more than 30 km in a north-south direction from north of Barmstedt to the urban area of Hamburg. In its deepest parts, the basis of the Quaternary deposits lies more than 400 m below the sea level (Figure 1.3). The average width is about 2 km (Scheer et al. 2006).

Gabriel et al. (2003) utilized different geophysical methods including: 2-D seismic reflection profiling, gravimetric and airborne electromagnetic surveys across the Ellerbek valley near Bevern, about 11 km to the north of the present study area. They used two 2-D CMP seismic profiles (profiles 1 & 2 in Figure 1.2), two 2-D gravity profiles and a 2-D electromagnetic profile. They calibrated the geophysical results to borehole by means of Vertical Seismic Profiling (VSP) in order to map the lateral extent of the buried valley and characterize the infill sediments. The seismic results showed detailed structure of the buried valley with maximum depth 360 m. They observed chaotic reflections in the lower part of the valley fill and undisturbed reflections in the upper part. The gravity data showed a typical negative residual gravity anomaly of the valley, about 1.5 km wide and -0.5 mGal ($1 \text{ mGal} = 10^{-3} \text{ cm/s}^2$) in amplitude. The interpretation of the gravity anomaly was constrained by the seismic profile results. Gabriel et al (2003) interpreted EM profiles from helicopter-borne electromagnetic data (HEM) flown by the BGR (Siemon et al. 2001). They showed that the low resistivity layer at

the top of the valley sediments was due to clay layer which differ from the resistivity of the surrounding sands.

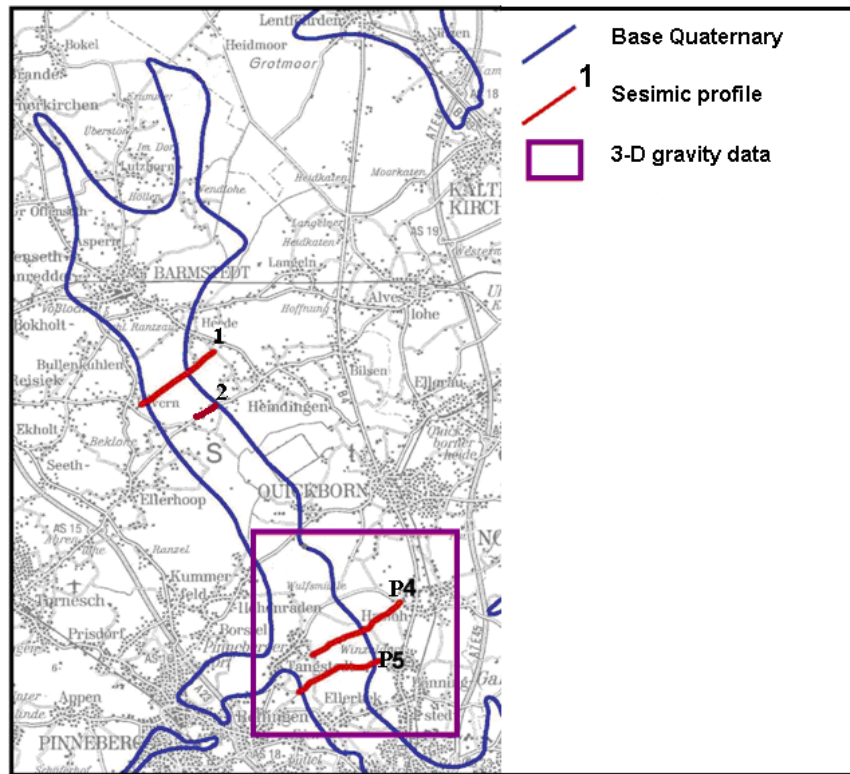


Figure 1.2: Map showing the Ellerbek Valley and the location of seismic section perpendicular to the valley (modified after Scheer et al. 2006): Line 1 and 2 study by Gabriel et al (2003), locations of 2-D gravity data (after Gabriel et al. 2003) along line 1 and 2. 3-D gravity data (after Götze et al. 2009) cover the rectangle in the southern part of the valley. Seismic P4 and P5 were carried out within BurVal project and used in the present study.

Tamiru (2009) conducted shallow seismic tomography to study the seismic velocity model of near surface lithology along profile 4 (Figure 1.2). She obtained P-wave velocity model to depth of 50 m with velocity contrast at 10, 30 and 50 m by a tomographic inversion of first arrival from conventional seismic data. She combined the P-wave velocity model (V_p) from P-wave profile with S-wave velocity (V_s) from SH-wave profile constrained by VSP data to make analysis of the velocity ratio (V_p/V_s) to extract lithological component for near-surface zone. She also combined the results of the seismic data with GPR, EM, and SIP to show near surface lithologic model.

Götze et al. (2009) conducted an integrated 3-D gravity study in the southern part of the Ellerbek Valley including the area of the preset study (Figure 1.2). They have generated Bouguer anomaly map from about 450 gravity points at 50 – 100 m point spacing. They observed that the measured gravity field was affected by a strong field due to salt structure. They calculated the later gravity field using regional gravity data, and subtracted from the measured gravity field resulting in residual gravity field of the area with values ranging from -1.0 to -1.5 mGal in the area of the valley. They analyzed the residual gravity field using curvature algorithms, Euler deconvolution and 3-D modelling resulting in 400 m depth of the Ellerbek Valley. Their analysis also showed a heterogeneous distribution of the density within the valley fill. Constraining the 3-D modelling by EM data, they delineated boulder clay layer and calculated density (3.0 g/cm^3) within the valley bottomed at 200m depth.

In summary, the initial and rough information about the valley shape, morphology and infill sediments, came from extrapolation of water well data, need to be refined. The previous seismic data showed variable details of the internal structure of the valley. Preliminary processing of seismic data was only applied to the data; therefore, more processing techniques need to be applied for better image of the buried valley and to facilitate detailed interpretation of the valley fill. The negative gravity anomaly was unique to Ellerbek valley compared to e.g. Bremerhaven-Cuxhaven buried valley studied by Gabriel et al. (2003). This negative gravity anomaly on the Ellerbek valley may indicate the sediments fill exhibit low density compared to the density of the surrounding sediments. From borehole data the infill sediments is dominated by coarse to fine sand (low density and high porosity) and the surrounding (Tertiary sediments) are dominated by fine sands and clays (High density and low porosity). The valley is covered by a high conductive layer which has been interpreted as clay layer. The Ellerbek Valley is incised in Tertiary sediments. It is more than 1.5 km wide, about 500 m deep, filled with sandy material of low density and high porosity and covered with clay layer of high electrical conductivity.

1.4 Database

1.4.1 Shallow Seismic data

The seismic data used in this study consist of two high-resolution seismic reflection profiles with P-waves (4.4 km and 3 km length, 2.5 CMP spacing, called profile 4 and profile 5, respectively), one high-resolution seismic profile with SH-wave (ca. 0.75 km, 0.5 m CMP

spacing, called SH-wave) and Vertical Seismic Profiles (VSP) in two boreholes close to the seismic lines (see Figure 1.3. General information about the seismic profiles is provided in Table 1.1.

The seismic surveys (excluding the SH-wave profile which was carried out during the course of the present work) have been performed within the BurVal project (Rumpel et al. 2005b).

Table 1.1: General information about the P- and SH-waves seismic profiles.

Profile	Acquisition date	Station number (in m), (field notes)	Profile geophone (PG) number	Vibration point number	CMP-points (number)	CMP-profile length (m)
Profile 4	30/05-07/06/2005	10-3425	1-684	1-683	3-1369	3415
Profile 5	03-06/07/2006	100-3105	1-402	1-401	2-1203	3000
SH-wave profile	26-28/06/2007	1001-1864	1-726	1-840	2000-3500	750

1.4.2 Well log data

A suite of geophysical well logs as well as lithological logs from two boreholes (BH3914 & BH3786) close to the seismic lines were used in this study. The well log dataset includes gamma-ray logs, and resistivity logs at each borehole and a density log at BH3914.

Wells used in this study were drilled and logged by the State Office for Agriculture, Environment and Rural Areas known as Landesamt fuer Natur und Umwelt des Landes Schleswig-Holstein (LANU). Table 1.2 provides some basic information about the boreholes used in the present study.

In addition to the above data, two airborne electromagnetic profiles from SkyTEM system data are also used to be integrated in the geological interpretation.

Table 1.2: Borehole data: General information. Depths are calculated below the ground surface and coordinate system is in UTM.

Well	X	Y	Total depth (m)	Diameter (m)	Aquifer formation	Depth to base Quaternary (m)	Water table (m)
BH3914	3558760	5950890	252	65	Tertiary sands	70	2.0
BH3786	3558160	5949620	432	65	Quaternary sands	412	7.5

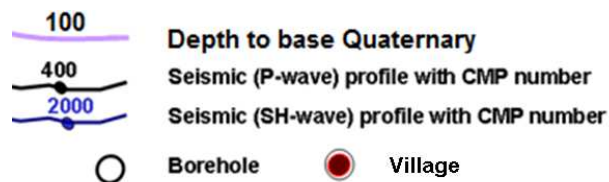


Figure 1.3: Detailed location of the P-wave profiles: profile 4 in the north and profile 5 in the south (in black), the SH-wave profile (in blue), contours of depth to the base Quaternary and the locations of boreholes with VSP data.

1.5 Thesis Structure

The thesis is divided into eight chapters. The present chapter contains the background and objectives for the research and describes the location of the study area, previous work in the study area, the data used and the structure of the thesis. Chapter two outlines the geology and hydrogeology of the study area. Chapter three outlines the physical, petrophysical and elastic characteristics of rocks and their hydrogeological relevance. Some fundamentals of the seismic methods are introduced in chapter four which is basically devoted to the processing of the high resolution seismic data (surface profiling and VSP). Chapter five focuses on interpretation of the geophysical data. Based on depth migrated seismic sections, a subsurface model and structures are delineated. Integrated interpretations of different geophysical data are also carried out. Chapter six gives preliminary estimations of some physical, elastic parameters as well as hydraulic parameters of the Quaternary and Tertiary sediments present in the study area. A number of specialized models that describe the seismic velocity-physical parameters behaviour of clastic rocks are applied to the available data. Relations between seismic observables (P- and S-wave velocities) and rock properties are investigated, and direct relations are obtained. The results are discussed in chapter seven. Chapter eight provides the conclusion of the work and some recommendations are given.

Chapter 2: Geology and Hydrogeology

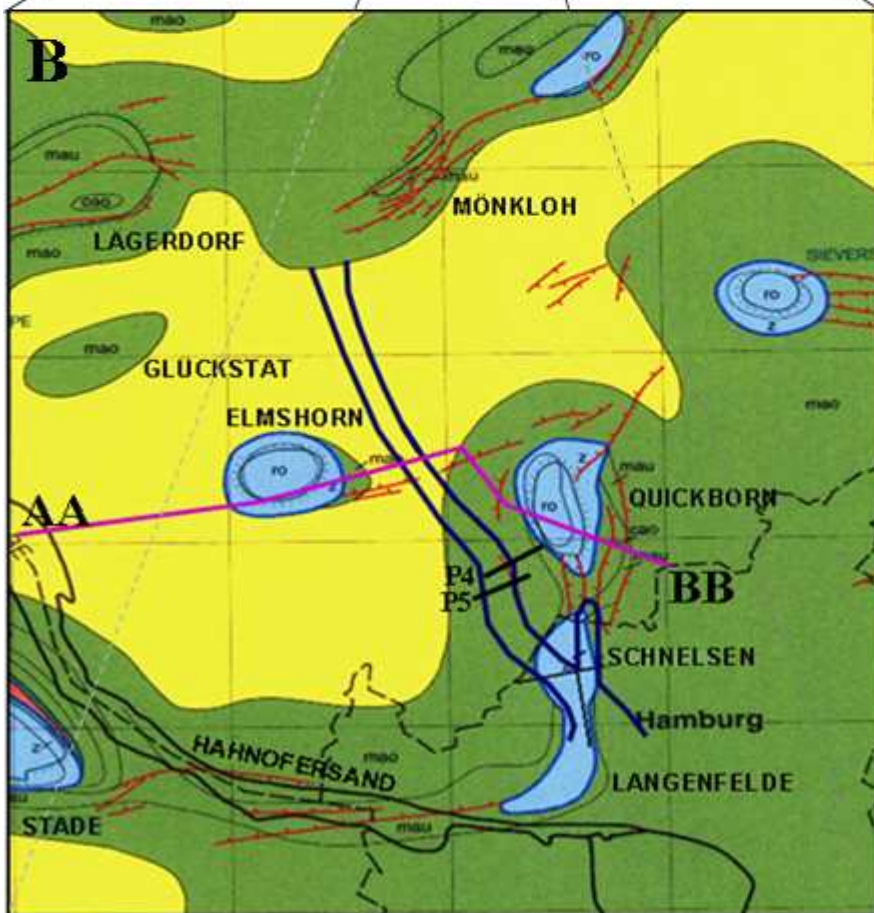
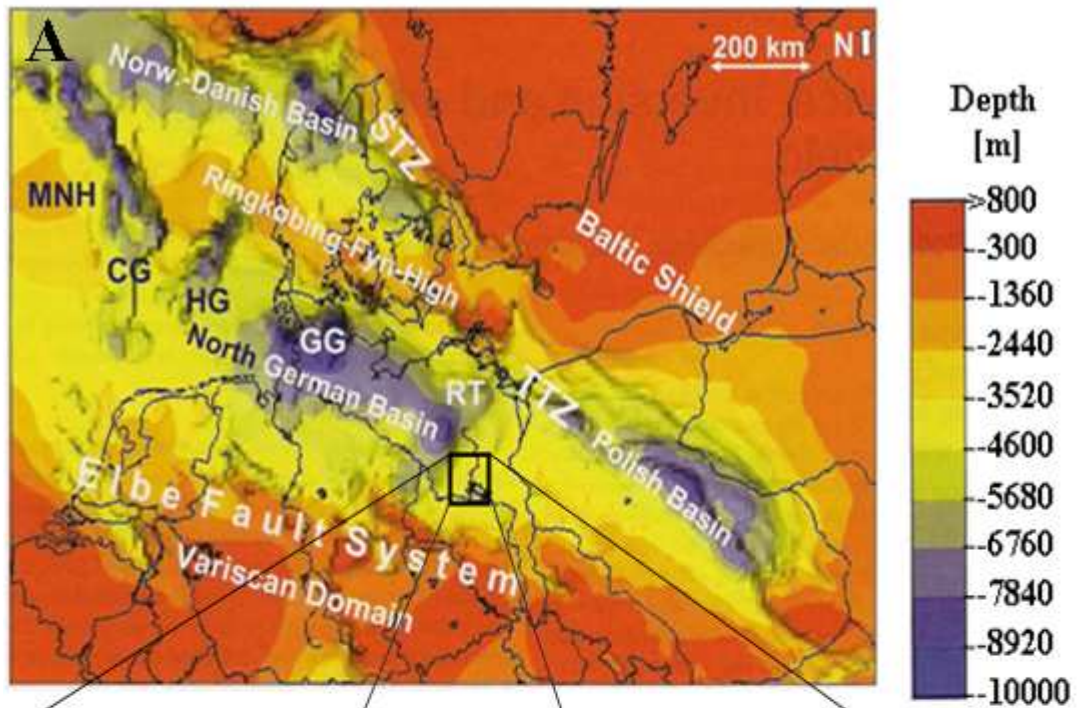
2.1 Overview

The study area is located in North Germany, on one of the major continental structural features in the world, the Central European Basin System (CEBS), shown in Figure 2.1A. The CEBS is related to the Permo-Mesozoic break up of Pangaea. It is divided into three sub-basins: (1): Norwegian-Danish basin, (2): North Germany Basin and (3): Polish basin extending from the North Sea to western Poland and is confined between the Teisseyre-Tornquist and Tornquist-Sorgenfrei zones in the NE and outcrops of the Variscan fold belt in the SW. These sub-basins evolved over a large time span from rifting during the Late Carboniferous and Permian, rifting in the Late Triassic to renewed Jurassic to Early Cretaceous rifting and subsidence, Late Cretaceous to Paleogene inversion and, finally, Cenozoic subsidence and sedimentation (Mazur and Scheck-Wenderoth 2005).

The CEBS contains thickest Permian-Cenozoic succession (> 10 km) in the central Europe. The main stratigraphic sequences of the basin infill (shown in Figure 2.1B,C) are briefly described below. The geology of study area absolutely lacks outcrops, thus, information about the subsurface can not be drawn from the surface. The subsurface geology of the study area has largely been provided by wells and geophysical data.

2.2 Upper Rotliegend

Late Carboniferous–Early Permian rifting in the area of the CEBS was accompanied by widespread volcanic activity followed by post-rift thermal subsidence with deposition of the Lower Permian Rotliegend (Mazur et al. 2005). Upper Rotliegend strata are up to 2000 m in northern Germany, the Centre of the Basin (Stollhofen et al. 2008). The upper Rotliegend succession is characterized by continental siliciclastics and minor evaporites which were deposited under arid to semi-arid climates (Glennie 1983).



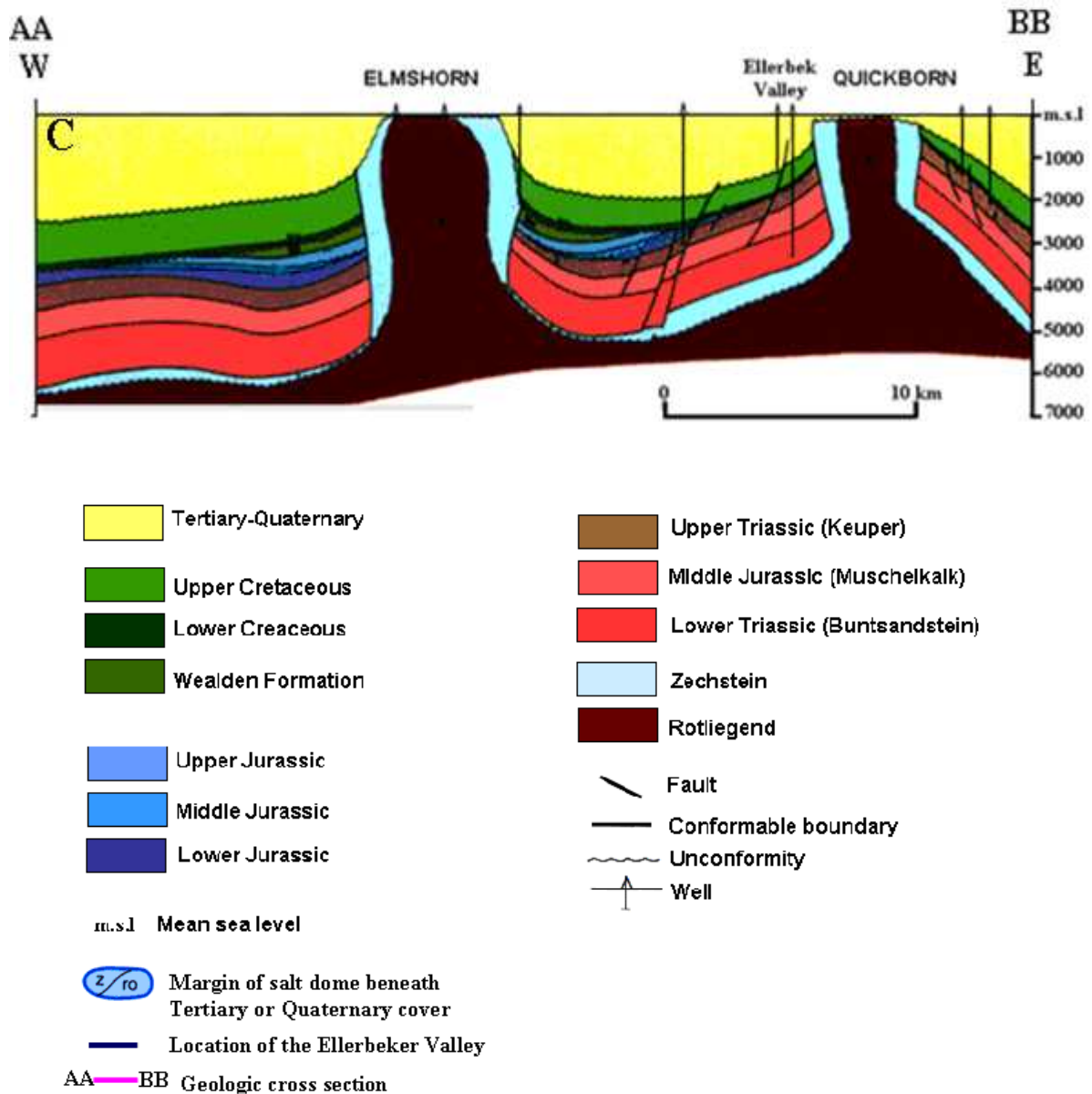


Figure 2.1: A: Structural overview of the Central European Basin system depth-to-pre-Permian surface within major NW-SE oriented fault systems: Central Graben (CG); Horn Graben (HG); Glueckstadt Graben (GG); Sorgenfrei-Tornquist Zone (STZ); Teisseyre-Tornquist Zone (TTZ); Horn Graben (HG) and Rheinsberg Trough (RT), (after Littke et al. 2008). B: Regional geological map showing sub-crop formations beneath Tertiary and Quaternary sediments (after Baldschuhn et al. 2001). The location of the Ellerbek valley is bounded by the dark blue lines. P4 and P5 represent the seismic profile4 and profile5, respectively. C: Cross section AA-BB shows the structure and geological units.

2.3 Zechstein Sequence

In Zechstein thick evaporites precipitated in the basin (Yegorova et al. 2006). The Zechstein succession consists of evaporation cycles and additional cycles dominated by clays and sandstones. At the beginning of the Zechstein, rifting in the Arctic-North Sea region, probably contemporaneous with a global sea level rise caused flooding of large parts of the CEBS (Smith and Taylor 1989) led to deposition of laminated, marly Kupferschiefer black shale of 30 cm thick (Paul 2006b) overlain by Limestones. Arid climate in combination with eustatic sea level fluctuations and/or tectonic movements repeatedly restricted sea water influx and gave rise to the development of stacked evaporation cycles. Each cycle starts with marine clays, succeeded by carbonates, Ca-sulfates and rock salts, with the climax of evaporation being reached by precipitation of Potash and magnesium salt (Warren 2008). The Zechstein evaporitic system terminated with the deposition of “Bröckelschiefer” mud and sandstones in a widespread, flat coastal sabkha environments (Stollhofen et al 2008).

2.4 Triassic Sequence

Lower Triassic “Buntsandstein” represents a predominantly terrestrial redbed sequence sandwiched between the marine Zechstein and Middle Triassic “Muschelkalk”. The lithostratigraphic subdivision of the Buntsandstein Group into seven formations reflects fining up-ward cycles (Lepper and Röhling 1998). Regional tectonic movements related to extensional faulting in the CEBS during Middle Buntsandstein triggered Zechstein salt movement leading to rafting of Buntsandstein blocks in the central parts of the North German sub-basins and within grabens (Mohr et al. 2005). Middle Triassic “Muschelkalk” Group is dominated by marine Limestones and marlstones. The base of the Muschelkalk Group is known by the “Grenzelkalk”. An important effect of Middle Muschelkalk tectonic activity is the triggering of further rafting of Zechstein salt (Mohr et al. 2005). Upper Triassic (Keuper) is characterized by arid or semi-arid intracontinental conditions. The Keuper succession consists of alternations of claystone, carbonate and evaporite series (Maystrenko et al. 2005).

Extensional structure trending NNE-SSW recognizing 3 major structures: Horn-Ems Graben, the Glueckstadt Graben and the Gihorn zone (Kockel 2002). Mobilization of Zechstein salt was triggered by rifting and caused salt pillows, salt diapirs and salt rafting (Mohr et al. 2005).

2.5 Jurassic Sequence

During Jurassic the area was covered by a large shallow epicontinental sea. The Jurassic transgression was not spontaneous, resulting in an unresolved chronostratigraphic resolution of the Triassic/Jurassic boundary in some part of the CEBS. In addition to that the Jurassic succession in the CEBS was complicated further:

- Doming in the Middle Jurassic affected the Ringkobing high. The uplift caused widespread erosion resulted in Mid-Cimmerian unconformity.
- Extensional stress during late Jurassic enforced graben formation and block faulting. It also reactivated salt movements. Salt rim synclines developed, hosting Jurassic sediments, whereas nearby the original sediment was eroded.
- Jurassic-Cretaceous boundary coincides with a major unconformity especially in the northern part of CEBS. Consequently, Jurassic sediments have been removed locally and further complicated the sedimentary pattern.
- The late Cretaceous inversion (Voigt et al. 2008) modified the remaining Jurassic strata once more by additional erosion during uplift, especially along the basin margin.

During Jurassic euxinic conditions occurred repeatedly. The first black shale intercalations appeared in Hettangian and Sinemurian, e.g. in the Netherlands and southern Germany. During the early Toarcian, a major anoxic event during deposition of the “Posidonia shale” affected wide area of Europe, providing a high class source rock. During late Jurassic, the Kimmeridge Clay Formation provided a first class source rock.

2.6 Cretaceous Sequence

The base of the Cretaceous is defined by the lowermost of the three major Lower Berriasian to earliest upper Berriasian unconformities (Late Cimmerian unconformities). It may truncate Jurassic strata or even late Triassic (Littke et al. 2008). Earliest Cretaceous tectonic activity, combined with changes in Sea level and climate, caused a termination of the later Jurassic carbonate-dominated deposition. Shallow marine carbonates were replaced by siliciclastic sediments common throughout the southernmost basins of the proto North Sea: the East Netherlands Basin, the Lower Saxony Basin and the Danish-Polish Basin which had been formed during the later Jurassic as fault bounded sub-basins of CEBS.

2.7 Tertiary Stratigraphy

The Tertiary period is characterized by the consolidation of crust. During an Early Paleocene extension phase the area of North German Basin subsided and was flooded (Voigt et al. 2008). Scandinavia is uplifted since the Paleocene and serves since then as a sediment source area of the North German Basin (Nielsen et al. 2002). Large river systems transported huge amounts of material into the basin of the ancient North Sea (BurVal Working Group 2006). Several lateral movements of the shore line caused cycles of sedimentation with an accumulation of fine grained marine sediments (e.g. mica clay) during the transgressions and a deposition of coarse grained terrigenous material (e.g. lignite sand) in phases of regression of the sea. The Tertiary strata consist of relatively uniformly distributed sequences of thick clay and sand layers (Figures 2.2B and 2.3). Since mid Pliocene the North Germany Basin has reached again a continental stadium with limnic and fluvial deposits (Voigt et al. 2008). These sediments have been partially deformed by glacial tectonic and are overlain by deposits of the glacial period and post-glacial sediments.

2.8 Quaternary Stratigraphy

At the end of the Tertiary the shoreline retreated farther to the west which was accompanied by a dramatic change in climate which led over to the Quaternary. The conditions for sedimentation and erosion changed completely (BurVal Working Group 2006). Quaternary sedimentation in northern Germany is mainly characterized by glacial activity during the Pleistocene (Gabriel et al. 2003). During several phases of glaciations, when thick ice caps covered large parts of Europe, very heterogeneous and not uniform sediments had been deposited (Piotrowski, 1994). At that time, large valley structures, formed by subglacial erosion, incised deeply into the Tertiary sediments. These valleys are characterized by steep walls with depth reaching up to 600 m (Wiederhold 2006) and widths of 1 to 2 km. With retreat of the glaciers the valleys were refilled with glacial sand, clay and till. Today they are covered by a more or less continuous till sheets. Thus, they are called “buried valleys” or “paleo-channels” (Goetze et al. 2009), since they cannot be seen at the surface today (BurVal Working Group 2006).

The formation of buried Quaternary valleys in northern Germany was dated in the last three glaciations that covered most of the North Sea and the adjacent continent. The deep North

German buried valleys are of Elsterian age, only a few or less deep structures originated during the Saalian and Weichselian glaciations (Stackebrandt 2009).

The distribution and morphology of Elsterian subglacial channels in northern Germany (after Stackebrandt 2001) are shown in Figure 1.1. Most channels have been filled with relatively fine-grained meltwater sands which contain only basal quantities of large gravels. The infill sediments are classified as glaciofluvial sand and silt and glaciolimnic silt and clay as well as boulder clay (e.g. Schwab and Ludwig 1996, Huuse and Lykke-Anderson 2000). Studies on- and offshore of northwestern Europe reveal the buried valley fill as gravel to coarse-grained sand at the bottom overlain by glaciomarine/glaciofluvial and/or glaciolacustrine fine-grained sediments (Schwab and Ludwig 1996, Huuse and Lykke-Anderson 2000, Lutz et al. 2009, Stackebrandt 2009). Till is rarely found at the base of the deep channels (Ehlers 1984). The channels, especially deeper ones, are covered with the Later Elsterian glaciolacustrine clay (Lauenburg clay) which consists of a complex glaciolacustrine clays, silt and fine sands. The Lauenburg thickness can reach 150 m in channels (Ehlers et al. 1984). The sediments fill the Ellerbek Valley is shown by BH3876 (Figure 2.2A). They can be grouped into four distinct intervals: (1) Holocene sediments, mainly intercalation of glacial tills and sandy material of outwash plains of Saalian age (0-63 m), (2) Lauenburg Clay which consists of complex glaciolacustrine clay, slit and fine sands of Late Elsterian age (63-90 m). (3), Pleistocene sands consist of glaciofluvial sands intercalated with silts and clays, and boulder clays (90-412 m) and (4) underlying the infill sediments is Lower Mica Clay (LMC) of Neogene age (412-432 m).

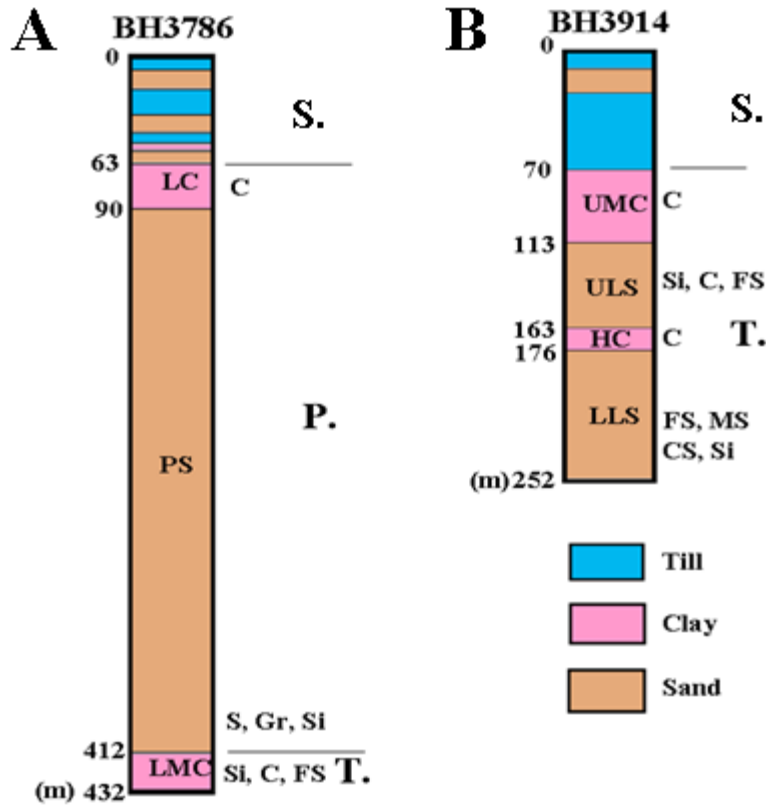


Figure 2.2: Simplified geological logs from BH3786 (A) and BH3914 (B). T. = Tertiary sediments; P. = Pleistocene sediments; S. = Saalian sediments; LC = Lauenburg Clay; PS = Pleistocene Sand; UMC = Upper Mica Clay; ULS = Upper Lignite Sand; HC = Hamburg Clay; LLS = Lower Lignite Sand; LMC = Lower Mica Clay; C=clay; Si=silt; FS=fine sand; MS=medium sand; CS=coarse sand; Gr=gravel.

2.9 Groundwater Aquifer Systems in the Study Area

In Schleswig-Holstein Quaternary and Tertiary coarse grained, sandy sediments (aquifers) and overlying fine-grained, clayey strata (protection layers) are of great importance for the drinking water supply, which is covered to nearly 100% by ground water (Scheer et al 2006). The water table is at depths just a few meters below the surface and is subject to considerable seasonal variations (Table 1.2). Different types of groundwater aquifers are summarized in Figure 2.2 after Gabriel et al (2003).

2.9.1 Tertiary Aquifers

Due to their supra-regional distribution and their huge thickness, the Tertiary aquifers can be mapped as potential rich ground water reservoirs in wide regions. In the surrounding area of the Ellerbek Buried Valley, there are two relevant aquifers, called “Upper Lignite Sand” and “Lower Lignite Sand”, which are separated by a clayey layer, called “Hamburg Clay” (Figure 2.2). These aquifers mostly consist of medium to fine grained sand with interstratified beds of humous clay and lignite. Another clayey protecting layer, the “Upper Mica Clay”, spatially covers the uppermost part of the “Lignite Sand”, except for the regions above the salt structures or in the course of the buried valleys.

2.9.2 Quaternary Aquifers

According to Scheer et al (2006) there are many types of Quaternary aquifers in Schleswig-Holstein. Caused by their predominant glacial genesis, the build-up of the Quaternary sediments and their petrography is – in contrast to the Tertiary strata – more heterogeneous. The near-surface aquifer system in the pilot area of the Ellerbek Valley is built up by medium- to coarse-grained glaciofluvial sands of mostly Saalian age. The thickness of these aquifers as well as the thickness of the covering glacial till and clay layers varies strongly. Outside the buried valleys, the total thickness of the Quaternary strata is only 20 to 60 m. Thus, the dimension of a potential groundwater extraction from the near-surface Quaternary aquifers also strongly varies. The ground water protection capability is dependent on the thickness and the permeability of the covering layers. Deeper Quaternary aquifers, often with huge thicknesses, can be found inside the buried valleys. They mostly originate from the activities of subglacial melt water during the Elsterian glaciation. Within its course, the cutting of the Ellerbek Valley eroded the Tertiary aquifers and clays and replaced them with glacial sands, tills and clay. The ratio of coarse-grained to fine-grained material varies in the different parts of the valley. Especially in the South of the Ellerbek Valley sandy strata dominate. As the youngest Elsterian sediments, the so-called “Lauenburg Clay” was deposited, which forms a thick covering layer of the buried valley aquifers nearly within the entire Ellerbek Valley. It acts as a hydraulic barrier between the aquifers above and below it (Gabriel et al. 2003). The top of the “Lauenburg Clay” can mostly be found at a similar depth as the top of the “Upper Mica” outside the buried valley.

The surface geology of the area and the surrounding region were mainly shaped during the glacial period of the youngest geological era, the Quaternary (Scheer et al. 2006). The out wash plains of the study area consist of glacial tills and sandy material of the Saalian age which form the near-surface sediments.

2.10 Groundwater Flow

The natural groundwater flow in the Quaternary and Tertiary aquifers is affected by the morphology of the landscape, which gently dips in the direction of the river Elbe as the dominant receiving river. Therefore, the general groundwater flow direction is southwest (Scheer et al. 2006). In near surface Quaternary aquifers the hydraulic gradient is locally influenced by terrain elevations or by groundwater discharge to smaller rivers. Due to the all-in-all low terrain heights, the ground water table of all aquifers is near to the surface. Groundwater recharge to the near-surface Quaternary aquifers takes place nearly in the whole pilot area, according to the rather high permeability of the covering layers and the hydraulic gradient (discharge only occurs in some lowlands along smaller rivers). The recharge areas for the deeper Quaternary aquifers in the buried valleys and for the Tertiary aquifers are restricted. A hydraulic contact between Tertiary and Quaternary aquifers is only possible in regions, where the Tertiary “Upper Mica” is not distributed, this means around the salt structures and along the edges of the buried valleys. The Elsterian “Lauenburg Clay” retards an appreciable spatial ground water recharge from the near-surface aquifers down to the deeper aquifers in the buried valley. Only at the boundary between Quaternary and Tertiary deposits of coarse-grained material has often been found what can be regarded a pathway for groundwater exchange.

The sediments in buried valleys often have higher permeabilities than the rocks of the surroundings (Scheer et al. 2006). Buried valley aquifers can be groundwater resources with a large volume. Due to their depth the aquifers are in general well protected against impacts from the surface. Hydraulic connections to surrounding aquifers can increase the amount of groundwater that can be extracted.

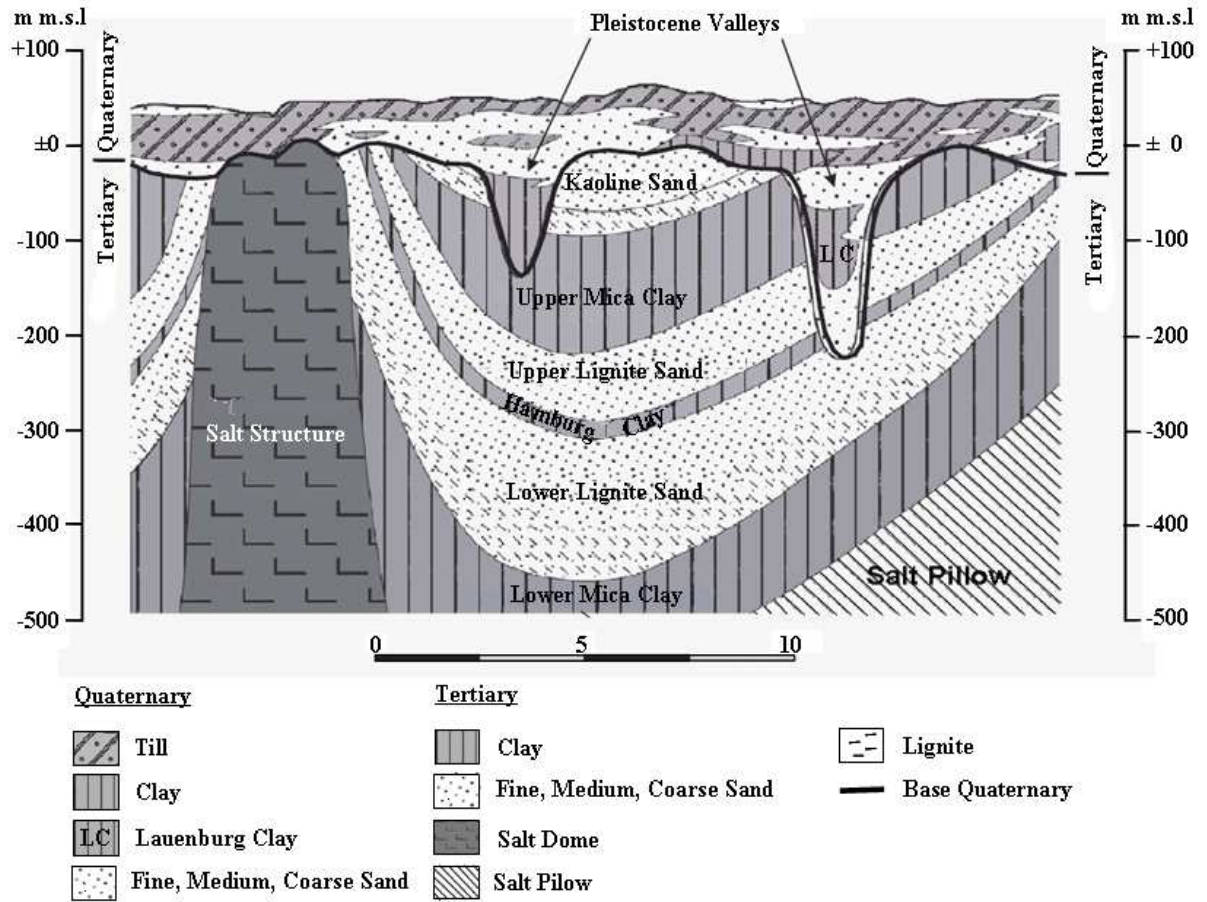


Figure 2.3: Characteristic geological structure (salt domes and buried subglacial valleys) and groundwater situation in northern Germany; aquifers: white; clayey layers: light gray (after Gabriel et al. 2003).

Table 2.1: Description of the Tertiary and Quaternary geological units in southern Schleswig-Holstein (from Wiederhold et al. 2002).

Erdzeitalter		Jahre v. h.	Geologische Schichten	hydrogeologische Bedeutung		
QUARTÄR	Holozän (Nacheiszeit)	10 000	Auelehm, Moore Flugsand, Dünen	frei bzw. abgedeckte pleistozäne Wasserleiter		
	Pleistozän Eiszeiten* und Warmzeiten*		Weichsel*		Geschiebemergel, Sande, Beckensedimente	
		Eem	organische Bildungen, marine Feinsande u. Tone	örtliche Nutzung durch kleinere Wasserversorgungen		
		Saale*	Geschiebemergel und Sande			
		Holstein	Tone, Schluffe, Feinsand	Trennschichten zwischen höheren und tieferen Wasserleitern, in Rinnen teils mit hydraulischer Barrierewirkung		
		Elster*	Tone (Lauenburger Ton)			
			ältere Warmu. Eiszeit	500 000	Geschiebemergel und Sand	tiefe pleistozäne Wasserleiter, teilweise mit hydraulischem Kontakt zu tertiären Sanden
	TERTIÄR Jungtertiär	Pliozän		2 400 000	Kaoлинsande (KS)	1. tertiärer Wasserleiter Verbreitungsgebiete beschränkt auf Trogbereiche, bei großer Tiefenlage an der Basis z. T. versalzen
			Miozän			
		Langenfelde		Oberer Glimmerton (OGT)	hydraulische Trennschicht	
Reinbek		15 000 000		Obere Braunkohlensande (OBKS)	2. tertiärer Wasserleiter in zentralen Trogbereichen teil- weise bis vollständig versalzen	
Untere-M.				Henn Moor	Hamburger Ton (HT)	hydraulische Trennschicht
		Vierlande		21 000 000	Untere Braunkohlensande- (UBKS)	vorwiegend grobkörnig feinsandig (Vierlandfeinsande VFS)
Unterer Glimmerton (UGT)					hydraulische Trennschicht, Sohlschicht der wasserwirtschaft- lich relevanten Wasserleiter	
Alttertiär		Oligozän Eozän Paläozän	23 000 000	Tone, Schluffe, Sandsteine	Anteil grundwasserführender Horizonte meist gering, in der Regel vollständig versalzen	
		frühere Erdzeitalter		65 000 000	Verschiedene Gesteinsarten	wasserwirtschaftlich nicht nutzbar

Chapter 3: Physical Parameters Evaluation and Hydrogeological Relevance

3.1 General

Geophysical methods are not only used to reveal the image or mapping of the subsurface by geophysical sections, e.g. seismic sections, but they can also be used to calculate physical parameter values characterizing the lithology of the subsurface. The use of geophysical methods in both mapping and characterizing the groundwater aquifer in the Ellerbek valley are the main objectives of the present study.

The purpose of many aquifer characterization or environmental studies is obtaining quantitative information about the hydrogeological properties of the aquifer. Compared to conventional, direct measurements (e.g. pumping tests in boreholes), which are commonly sparse and expensive, geophysical methods can provide high-resolution information over large areas and aquifer volumes. Since long time attempts have been concentrated on determination of physical parameters of sediments from borehole and surface geophysical measurements. However, determination of the physical parameters for shallow subsurface is of a considerable importance to answer questions of groundwater resources problems, engineering and environmental studies.

An attempt in this study is made to use shallow seismic P- and SH-wave profiles and VSP in addition to other geophysical data and borehole logs from BH3786 and BH3914 to image as well as determine the physical and elastic parameters of the sediments comprising the groundwater aquifers in the study area, within the limitations of the geophysical data available.

In this chapter, a brief discussion about the petrophysical and elastic parameters and their relations to seismic velocities generated from seismic data is given.

3.2 Petrophysical Parameters

The study of the physical properties of the pore system in rocks is termed petrophysics. Measurement of petrophysical parameters of the groundwater aquifers is important for management and planning the groundwater resources in the valley. Following are details about the most important petrophysical parameters in aquifer studies.

3.2.1 Porosity

Porosity is the ratio of the volume of openings (voids) to the total volume of material. Porosity represents the storage capacity of the geologic material. Using geophysical measurements the porosity of the groundwater aquifer can be estimated.

The relationship between porosity and seismic wave velocity in saturated porous media is affected by several factors such as sediments composition, pressure, depth of burial, compaction, type of fluid etc. Generally, seismic velocity increases with decreasing porosity. Figure 3.1a shows a section of clay free material and Figure 3.1b shows that increasing porosity reduces V_p seismic impedance as well as density.

Various investigations were carried out to determine porosity using surface as well as borehole geophysical measurements. Wyllie et al (1956) observed the effect of porosity (Φ) on the propagation of seismic wave velocity in bulk material and velocity in matrix and fluid, and obtained their famous equation given as follows:

$$\frac{1}{V} = \frac{1-\Phi}{V_{MATRIX}} + \frac{\Phi}{V_{PORE}} \quad (3.1)$$

where V is the bulk seismic velocity, V_{MATRIX} is the seismic velocity of the rock matrix and V_{PORE} is the seismic velocity of the pore fluid. According to Raymer et al (1980) this relationship only holds for consolidated sandstones over a porosity range of 25%–30%.

The Wyllie et al equation has been modified by Raymer et al (1980) to count for V as well as V_{MATRIX} and V_{PORE} in relation to porosity (Φ). Raymer's et al equation is expressed as follows:

$$V = V_{MATRIX} * (1-\Phi)^2 + V_{PORE} \Phi \quad (3.2)$$

Mavko et al (1998) pointed out that this equation is valid for $\Phi < 37\%$.

Seismic velocity-porosity relations for unconsolidated rocks have also been studied. Morgan (1969) measured porosities and velocities on marine sediments and derived the following equation:

$$V_p = 1.917\text{km/s} - \Phi * 0.566 \quad (3.3)$$

Salem (1990) studied the physical properties of glacial sediments in Segeberger Forst, north Germany using refraction seismic measurements. He derived the following equation for velocity-porosity relationships of the glacial sediments:

$$\Phi = -0.13564 \ln(V_p) + 1.3231 \quad (3.4)$$

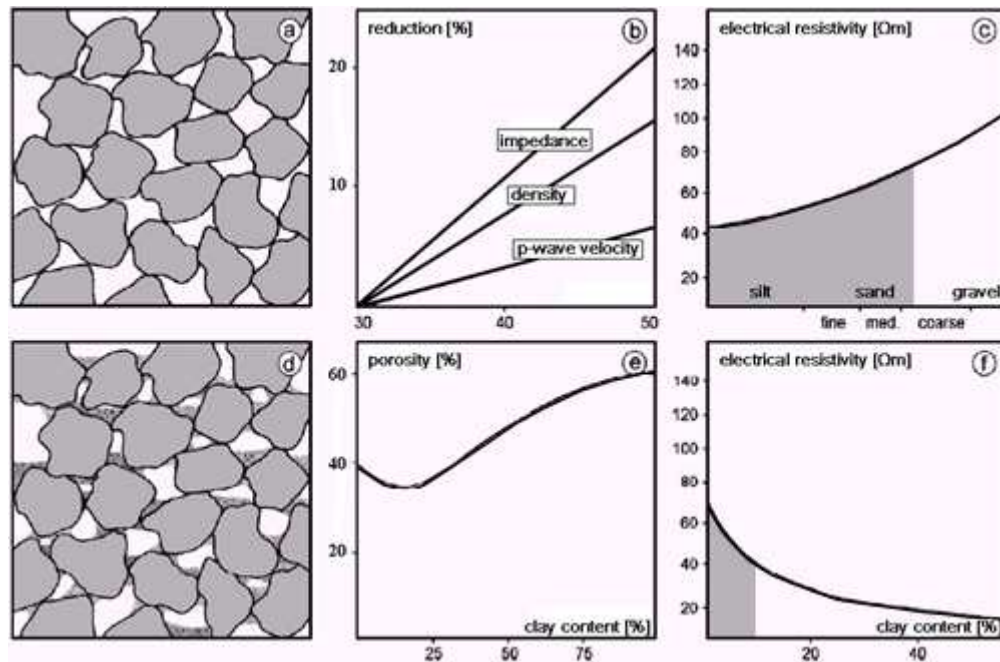


Figure 3.1: Physical properties of sediments (Gabriel et al. 2003): influence of porosity and clay content on density, seismic velocity and electrical resistivity: (a) well-sorted, clay-free sediments, (b) reduction of the seismic impedance, density and p-wave velocity of sediments as function of porosity (Morgan 1969) normalized with respect to 30% porosity; (c) electrical resistivity as a function of grain size for fresh water saturated material (after TNO 1976); (d) clayey sediment, pore space partly filled with minerals, (e) porosity as a function of the clay content (artificial sand-clay mixture, Marion et al. 1992), (f) electrical resistivity related to clay content after Sen et al (1988).

Another approach to obtain porosity of sediments is through using the electrical resistivity logs and Archie's relationship between the resistivity of the formation (R_f) and porosity (Φ) as follows:

$$R_f / R_w = a\Phi^{-m} \quad (3.5)$$

Herein a , and m are constants to be determined and R_w is the resistivity of the pore-waters (Archie, 1942). The resistivity of pore-waters (R_w) is mainly a function of the temperature and the dissolved salt content (salinity) of the pore waters. The ratio of the specific resistivity of the formation (water saturated clay free sand; R_f) to the resistivity of the pore fluid is known as the formation factor F .

A particular relation between the formation factor and porosity is proposed by the Humble Oil Company (Winsauer et al. 1952). The original formula was expressed as:

$$F=0.62/\Phi^{2.15} \quad (3.6)$$

A nearly equivalent form, with a simpler porosity exponent, is:

$$F=0.81/\Phi^2 \quad (3.7)$$

These formulae are considered to be most suitable for relatively high-porosity or granular rocks.

3.2.2 Clay Content

Clay is characterized by low hydraulic conductivity. Thus, the hydrogeological importance of clay layers is that they form hydrogeological barriers dividing aquifers and protecting them from contaminants.

The clay content of a sandy aquifer influences its hydraulic conductivity significantly. Small clay content in sand reduces porosity because clay particles fill the pore spaces. Increasing clay content reduces porosity until the entire pore spaces are filled with clay. Further increase in clay content leads to increase in porosity due to the high porosity of clay (see Figure 3.1e).

Clay content influences the electrical properties of rocks. Figure 3.1c shows that clay free materials have electrical resistivity ranging between about 50 Ωm in silt to more than 100 Ωm

in gravel. On the other hand, Figure 3.1f shows that in clayey material (like in Figure 3.1d) electrical resistivity decreases with increasing clay content and similar resistivity values can be observed.

The effect of clay content on seismic velocities was investigated by Marion et al (1992). They used artificial sand–clay mixture for laboratory experiments. They found that maximum P-wave velocities for clay contents of about 40% are as shown by Figure 3.2.

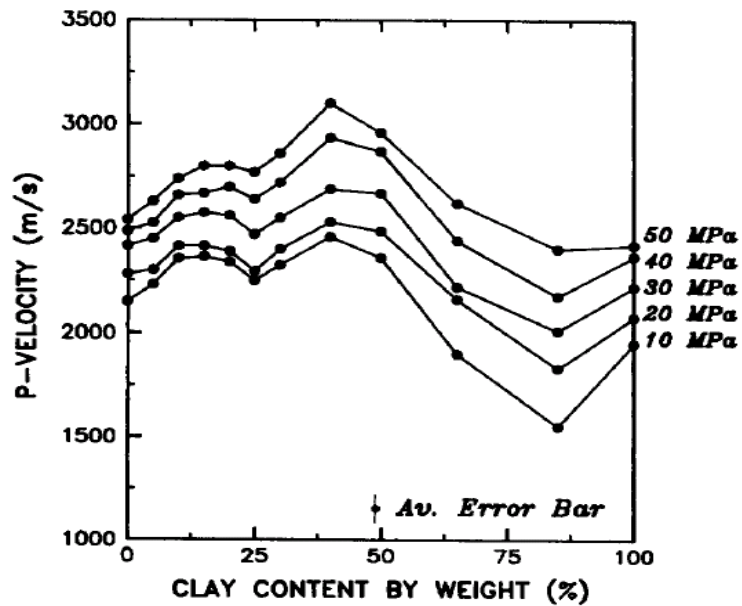


Figure 3.2: P-velocity versus clay content in saturated sand-clay samples: a peak in velocity versus clay content occurs at 40 percent clay content. Velocity at the peak is 20 to 30 percent higher than for either pure clay or pure sand. The low values of velocity for the 85 percent clay content sample are attributed to length measurement errors (after Marion et al. 1992).

The clay content can be calculated from gamma-ray log in two steps:

First a factor (I_{RA}) is calculated as follows:

$$I_{RA} = \frac{RA - RA_{cleansand}}{RA_{sh} - RA_{cleansand}} \quad (3.8)$$

where RA = radioactivity log reading in the zone of interest; $RA_{\text{cleansand}}$ = radioactivity log reading in a clay free zone and RA_{sh} = radioactivity log reading in a clay. Second, the clay volume (V_{sh}) is calculated using the formula by, e.g. Western Atlas (1985) to calculate the shale content in Tertiary rocks:

$$V_{\text{sh}} = 0.083(2^{3.7 \cdot I_{\text{RA}}} - 1.0) \quad (3.9)$$

Other expressions are also used to calculate the clay volumetric content in rocks according to the local knowledge e.g. the following equation is used to calculate clay content of older rocks:

$$V_{\text{sh}} = 0.33(2^{2 \cdot I_{\text{RA}}} - 1.0) \quad (3.10)$$

3.2.3 Density

The density (ρ) of a material is defined as its mass (m) per unit volume (v) (equation 3.11): Density of a rock sample is used to calculate porosity and pore-fluid density.

$$\rho = m/v \quad (3.11)$$

The SI-unit of density is kg/m^3 .

Relationships among velocity and density have been published by several authors such as Nafe and Drake (1957), Hamilton (1971) and Gardner et al (1974). Thus, when information about density is unavailable, it is often estimated from P-wave velocity (V_p) using such empirical relationships. Hamilton (1971) derived a relationship between P-wave velocity and density for soft, unlithified (marine) sediments from 0 to 500 m depth as follows:

$$\rho(\text{kg} / \text{m}^3) = 1135V_p(\text{km} / \text{s}) - 190 \quad (3.12)$$

Formation densities are measured using downhole logging tools as a continuous record of a formation's bulk density. This is the overall density of a rock including solid matrix and pore fluid. Knowing the matrix density and fluid density, the log density can be used to calculate porosity using the standard density-porosity relation (Serra, 1984):

$$\Phi = \frac{\rho_m - \rho_b}{\rho_m - \rho_f} \quad (3.13)$$

where Φ = porosity, ρ_m = matrix density, ρ_b = bulk density (as measured by the tool) and ρ_f = fluid density. Gardner et al (1974) suggested a useful empirical relation among P-wave velocity and density that represents an average over many rock types:

$$\rho_b = 1.741V_p^{0.25} \quad (3.14)$$

where V_p is in km/s and ρ_b is in g/cm³.

3.3 Hydraulic Conductivity

Hydraulic conductivity is a key parameter for hydrogeology. It characterizes the dynamic behaviour of an aquifer to allow for fluid flow, strongly influencing, e.g. the yield of wells, the velocity of contaminant spread, or consolidation behaviour of soil under an applied load (Kirsch and Yaramanci, 2009). Hydraulic conductivity (K) has the unit of velocity (m/s).

Hydraulic conductivity can be estimated by geophysical methods such as resistivity and seismic velocity. An empirical relation between seismic velocity V_p , porosity Φ and clay content C is found by Klimentos (1991):

$$V_p = 5.27 - 5.4\Phi - 2.54C + 0.001K \quad (3.15)$$

Some hydraulic conductivity – velocity relationships have been calculated for sandy sediments of Saale and Weichsel glaciation in Schleswig-Holstein as the following regression (after Fechner, 1998):

$$\text{Log K} = 0.004332 V_p - 12.825 \quad (\text{m/s}) \quad (3.16)$$

In chapter 6 the above mentioned physical, petrophysical and hydraulic parameters will be estimated from P- and S-wave velocities derived from seismic data.

3.4 Elastic Parameters

Determination of the elastic parameters from seismic velocities is a challenging approach in hydrogeophysical studies. These parameters have a considerable influence on porosity and permeability of rocks. They also affect the propagation of seismic waves (P- and S-waves) in porous media which are defined respectively by:

$$V_p = \sqrt{\frac{K + \frac{4}{3}\mu}{\rho_b}} \quad (3.17)$$

$$V_s = \sqrt{\frac{\mu}{\rho_b}} \quad (3.18)$$

where k is the bulk modulus, μ is the shear modulus, and ρ is the density of the material through which the waves are propagating.

Information to determine the elastic parameters can be provided by the P- and S-wave velocity along with density. Gassmann (1951a) described the effect of stress on the elastic properties of porous media. He found that the elastic moduli of a fluid-filled porous medium can be determined through both the moduli of solid and fluid substances. He applied his theory in laboratory (Gassmann, 1951b) and concluded that the medium behaves anisotropically if it is stressed under weight, and velocity increases with increasing pressure. Biot (1956 a, b) developed Gassmann's theory to treat comprehensively the propagation of elastic waves in a porous elastic solid saturated with a compressible viscous fluid under low and high frequencies. Biot pioneered the following equation for S-wave velocity (V_s):

$$V_s = \left[\frac{\mu}{\rho_b} \left\{ 1 - \left(\frac{\rho_f \Phi}{\rho_b K} \right) \right\} \right] \quad (3.19)$$

where ρ_b = solid bulk density, ρ_f = fluid bulk density, Φ = porosity and K = coupling factor.

The coupling factor describes the degree of coupling between pore fluid and matrix. Gassmann (1951a) defined the bulk incompressibility (k) as the result of bulk frame compressibility (C_b) and solid grain compressibility (C_s), pore fluid compressibility (C_f), and porosity (Φ).

3.4.1 Elastic Moduli

Elasticity deals with deformations that vanish entirely upon removal of the stresses, that cause them (Sheriff 2006). For small deformations Hook's law holds and strain is proportional to stress. The passage of a low-amplitude seismic wave is an example. The stress-strain properties of isotropic materials that obey Hook's law are specified by elastic moduli.

The elastic properties of rock are uniquely defined by elastic moduli and/or P- and S-wave velocities. These include: Rigidity (shear) modulus (μ), incompressibility (bulk) modulus (K), Young's modulus (E), Poisson's ratio (σ) and several others.

Shear Modulus (μ)

The shear or rigidity modulus (μ) is one of the critical engineering properties of sediments or soils. It is defined as the applied stress divided by the change in transversal shape (shear strain). The stress-strain ratio for simple shear (Sheriff 2006) is obtained from:

$$\mu = \frac{\Delta F / A}{\Delta L / L} \quad (3.20)$$

where ΔF = shearing force, A = cross-sectional area, L = distance between shear planes, ΔL = shear displacement.

This modulus can simply be obtained from S-wave velocity and bulk density as follows:

$$\mu = \rho_b V_s^2 \quad (3.21)$$

Bulk Modulus

The bulk modulus (k) or incompressibility ($1/c$) is defined as the stress divided by the proportional change in volume (strain) of a porous material that is it describes the volume change of the element subjected to all pressure as resistance to compression and dilatation. The stress-strain ratio under change in simple hydrostatic pressure, ΔP , (Sheriff 2006) is

$$k = \frac{\Delta P}{\Delta V / V} = 1 / c \quad (3.22)$$

Hamilton (1971) pointed out that the components of the bulk modulus are porosity (Φ), the bulk modulus of pore water (k_f), the aggregate or bulk modulus of mineral grains (k_s), and the frame bulk modulus of the sediment structure (k_b). The bulk modulus can be computed from P-wave velocity (V_p), S-wave velocity (V_s) and bulk density (ρ_b) through

$$k = \rho_b (V_p^2 - \frac{4}{3} V_s^2) \quad (3.23)$$

Young's Modulus

Young's modulus (E) is defined as the ratio of normal stress to normal strain. The stress-strain ratio for a rod pulled or compressed is

$$E = \frac{\Delta F / A}{\Delta L / L} \quad (3.24)$$

where $\Delta F/A$ = stress (force per unit area), L = original length, ΔL change in length. Young's modulus can be obtained with respect to bulk modulus and shear modulus as follows:

$$E = \frac{9k\mu}{3k + \mu} \quad (3.25)$$

In terms of the shear modulus and Poisson's ratio (σ), Young's modulus can be obtained as follows:

$$E = 2\mu(1 + \sigma) \quad (3.26)$$

Young's modulus, as a function of P- and S-wave velocities and density is calculated by the following equation:

$$E = \rho V_s^2 \left(\frac{3V_p^2 - 2V_s^2}{V_p^2 - \frac{1}{3}V_s^2} \right) \quad (3.27)$$

Poisson's Ratio

Poisson's ratio (σ) is that of transverse strain or contraction to longitudinal strain or extension resulting from a change in normal stress under compression or dilatation. When a rod of length L is pulled, it is elongated by ΔL and its width W is contracted by ΔW :

$$\sigma = \frac{\Delta W / W}{\Delta L / L} \quad (3.28)$$

In terms of velocity ratio V_p/V_s , Poisson's ratio is written as follows:

$$\sigma = \frac{V_p^2 - 2V_s^2}{2(V_p^2 - V_s^2)} \quad (3.29)$$

Generally, the elastic parameters of natural rocks mostly depend on the lithological properties. One of these properties is water saturation. When rigidity is zero, no shear wave can be transmitted. In this case σ will be 1/2 corresponding to a value for fluids. Liquid saturation of porous sediments leads to an increase in the P-wave velocity; consequently an increase in σ can be expected. Mann and Fatt (1960) indicated that the presence of aqueous solution leads to an increase in σ from a slight amount up to nearly 0.5. It is generally known that any departure of seismic wave propagation from unsaturated sediments to saturated sediments will increase the P-wave velocity and consequently, Poisson's ratio tends to increase. Since the fluid lacks rigidity, i.e., $\mu=0.0$, in turn, $\sigma=0.5$, and thus ultimately:

$$V_p = (k/\rho_b)^{1/2} \quad (3.30)$$

Gregory (1976) pointed out that at a constant pressure σ increases as water saturation increases and as porosity increases. He mentioned that for water saturated rocks σ ranges from 0.11 to 0.33 and from -0.12 to 0.12 for gas saturated rocks. Poisson's ratio also increases with decrease in porosity. Koefoed et al (1963) showed an obvious tendency between the increase of σ and the decrease of Φ . Domenico (1984) experimentally showed that 0 value of σ indicates a change in volume due to full compressibility, and the 1/2 value indicates no volumetric change that is incompressibility. This indicates that σ increases as compressibility decreases. Poisson's ratio may also be affected by grain size, i.e. σ tends to be higher when the grain size decreases. Tatham (1985) pointed out that the softer the soils (finer grain size) the higher σ , and the harder the soils (coarser grain size) the lower σ .

3.4.2 V_p – V_s Relations

An important advance in seismic methods applications is the ability to use the combination of V_p and V_s to constrain lithology, porosity and pore fluids. In oil industry the V_p/V_s ratio is found to be useful in characterizing reservoir lithology. The relation between V_p/V_s and lithology in sedimentary rocks is often indicated by a cross-plot of V_p versus V_s and/or V_p/V_s versus V_p . Prakla-Seismos (1983) mentioned that the V_p/V_s ratio is the most important parameter for interpreting P- and S-wave propagation, and for evaluating the lithological properties, as well as interpreting the field and laboratory geophysical measurements. The V_p/V_s ratio can be expressed in terms of other elastic parameters, i.e., bulk modulus (k), shear modulus (μ) and Poisson's ratio as follow:

$$\frac{V_p^2}{V_s^2} = \frac{k + \frac{4}{3}\mu}{\mu} = \frac{k}{\mu} + \frac{4}{3} \quad (3.31a)$$

$$\frac{k}{\mu} = \left(\frac{V_p}{V_s}\right)^2 - \frac{4}{3} \quad (3.31b)$$

$$\frac{V_p}{V_s} = \sqrt{\frac{2(1-\sigma)}{1-2\sigma}} \quad (3.32)$$

The relationship between V_p/V_s and k/μ gives a good representation and explanation for many physical concepts. Tatham (1982) pointed out that any relative variation between any two elastic constants can be related to variations of V_p/V_s .

Benzing et al (1983) used the V_p/V_s ratio as an indicator for porosity and lithology. Gardner and Harris (1968) used this parameter as an indicator for the presence of an incompressible fluid. They showed that values of V_p/V_s greater than 2.0 correspond to saturated unconsolidated sediments, whereas values less than 2.0 indicate either well consolidated rocks or presence of gas or air in unconsolidated sediments. Gregory (1976), Domenico (1976, 1977), and Tatham (1982) showed the importance of this parameter as evidence of the presence of gas or air in sedimentary rocks. Eastwood and Castagna (1983) showed that V_p/V_s is highly variable and sensitive to the change in lithology, whereby it is around 1.8 in quartz-rich rocks and over 5.0 in loose water saturated sediments. Stuempel et al (1984) obtained values up to 9 and Poisson's

ratio of 0.49. Meissner et al (1985) obtained values greater than 4 and high values of Poisson's ratio up to 0.48. They attributed these results to the increase in water saturation and to the presence of boulder clay. Castagna et al (1985) used this parameter as an indicator of grain size. They obtained a value of 1.45 and a Poisson's ratio of 0.1 corresponding to quartz spheres. Tatham (1985) demonstrated that silts with similar grain shapes as sands but smaller in size than sands exhibit higher values of V_p/V_s than sands even though they have the same porosities. Han et al (1986) pointed out that higher value of V_p/V_s correlate with higher porosities for saturated samples, or with the clay presence. Robertson (1987) and Zimmerman and King (1986) showed that this parameter is an increasing function of both porosity and water saturation.

Chapter 4: Application of High Resolution Seismic Methods

4.1 General

The seismic methods of exploration are based on the generation and sending of seismic waves from a selected point at the surface into the subsurface using some type of seismic energy. The generated waves (P-wave or S-wave) propagate downwards or laterally into the subsurface media according to the elastic properties of the formation. The waves behave similarly as in optic physics where they are reflected, refracted and diffracted at boundaries according to Snell's Law. The boundary is defined here as a surface separating layers of different elastic properties. Practically, the velocity of the wave in the layer is considered as the key parameters in the seismic methods of exploration.

The seismic methods are commonly employed in a variety of applications: in delineation of near-surface geology for engineering studies (Steeple and Miller 1990, Lanz et al. 1996, Bueker et al. 1998a); in coal exploration (Gochioco 1990) and mineral exploration within a depth of up to 1km (known as engineering seismology); in hydrocarbon exploration and development within a depth of up to 10 km (known as exploration seismology); in investigation of the structure of earth's crustal within a depth of up to 100 km (known as earthquake seismology).

In the present study 2-D (P- and SH-waves) high resolution seismic reflection profiling as well as Vertical Seismic Profiling (VSP) are applied to image and characterize the Quaternary aquifer system in the Ellerbek valley to a few hundred meters depth.

4.2 Fundamentals

In this section, some basic concepts of seismic methods which are relevant to the present work are briefly reviewed. The bulk of theoretical background is mainly adapted and summarized from a number of publications (e.g. Yilmaz, 1987; Sheriff and Geldart, 1995; Sheriff, 2006; Gadallah and Fisher, 2009).

4.2.1 Seismic Waves

The theory of seismic methods is based on the wave equation that was developed in a branch of physics called classical mechanics. The wave equation is applicable to any kind of wave motion including seismic wave which are mechanical waves in the solid earth. The wave equation can be written as:

$$\nabla u^2 = \frac{1}{V^2} \frac{\partial^2 u}{\partial t^2} \quad (4.1a)$$

or

$$\frac{\partial^2 u}{\partial x^2} + \frac{\partial^2 u}{\partial y^2} + \frac{\partial^2 u}{\partial z^2} = \frac{1}{V^2} \frac{\partial^2 u}{\partial t^2} \quad (4.1b)$$

where V is the propagation velocity; u is the wave field; x , y and z are the Cartesian coordinates; and t is time. Solutions of the wave equation are facilitated if certain simplifying assumptions are made about the medium through which the seismic waves are propagating. For perfectly elastic, homogeneous and isotropic media the solutions of wave equation describe four different types of waves that propagate through the body of the medium (called body waves) or restricted to the surface of the solid medium (called surface waves).

Body Waves

Body waves can propagate through the internal volume of an elastic solid and may be of two types; primary and secondary (shear) waves:

Primary waves (P-waves) are generated by some compressional force, e.g. due to firing of an energy source on a medium. The elastic character of the rock then causes an immediate rebound or expansion, followed by a dilation force as shown in Figure (4.1a). This response of the medium constitutes a primary wave “P-wave”. Particle motion in a P-wave is in the direction of wave propagation. Generally, the propagation velocity of P-waves depends on the elastic moduli and density of the medium in which the waves are traveling. The velocity of a P-wave (V_p) propagation is defined by equation (3.17).

Shear waves (S-waves) are generated when a sideways force is exerted on a medium. Particle motion of a shear wave is at right angle to the direction of propagation (Figure 4.1b). A shear wave's velocity is a function of the resistance to shear stress of the material through which the wave is traveling and is often approximately half of the material's compressional wave velocity. In an isotropic medium shear wave velocity (V_s) can be calculated by equation (3.18).

In liquids, as mentioned before, such as water, there is no shear wave possible because shear stress and strain cannot occur in liquids.

Surface Waves

Surface waves are types of seismic waves that propagate along the stress free surface of a semi-infinite medium. In exploration seismology, the near surface medium is often termed weathering layer or low-velocity layer (LVL). There are two types of surface waves: Rayleigh and Love waves.

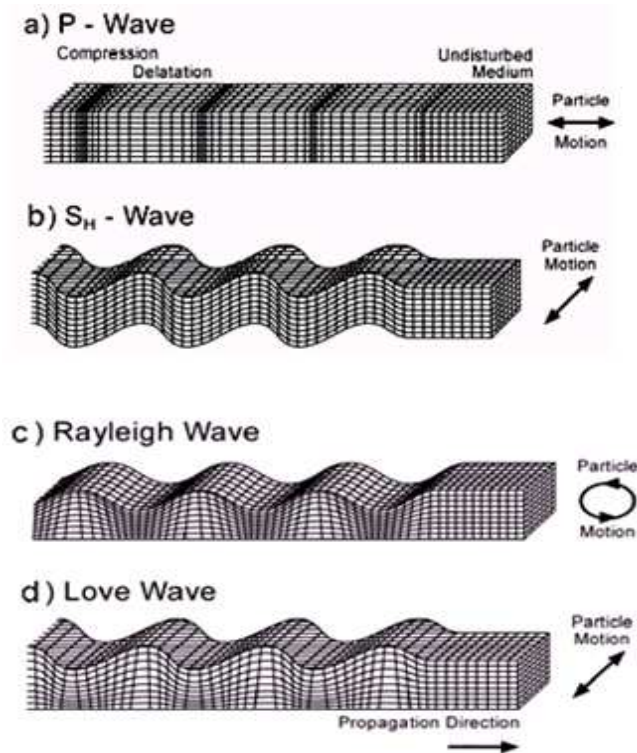


Figure 4.1: Types of seismic waves and ground particle motions: (a) P-wave, (b) S-wave, (c) Rayleigh wave and (d) Love wave (after Bolt 1982).

Rayleigh waves are of low frequency nature, traveling horizontally with retrograde elliptical motion and away from the energy source. The particle motion of this wave reduces (amplitude) with increase in depth, eventually reversing in direction. This point is in the vicinity of the base of the weathering layer. Because the motion of the ground appears to roll, this wave is commonly known as ground roll (Figure 4.1c).

The Love wave (Figure 4.1d) is a surface wave born within the LVL, which has horizontal motion perpendicular to the direction of propagation with, theoretically, no vertical motion. Such waves often propagate by multiple reflections within the LVL, dependent upon the LVL material. If such waves undergo mode conversion, a number of noise trains appear across the seismic record, obscuring reflected energy content even further.

Tube Waves

The tube wave is an interface wave that occurs in cased wellbores when a Rayleigh wave encounters a wellbore and perturbs the fluid in the wellbore. The tube wave travels down the wellbore along the interface between the fluid in the wellbore and the wall of the wellbore. A tube wave suffers little energy loss and typically retains very high amplitude which interferes with reflected arrivals and occurring later in time on the Vertical Seismic Profile (VSP) data (see section 4.4).

Converted Wave (C-wave)

When a wavefront from a conventional seismic source strikes an interface, the reflected energy is partitioned into P (pressure) and S (shear) waves. Figure 4.2 shows an incoming P-wave (P_{inc}) travelling at velocity V_1 striking the interface between the upper material and the lower material. Two reflected waves and two transmitted waves are produced as a result:

- . Reflected shear: S_{refl}
- . Reflected pressure: P_{refl}
- Transmitted shear: S_{trans}
- Transmitted pressure: P_{trans}

Note the difference in the direction of particle motion relative to the direction of wave propagation (Figure 4.2). P-waves have particle motion in the same direction as wave propagation, while shear waves have particle motion in a direction perpendicular to wave propagation.

The P-P and P-S reflectivity varies as a function of the media parameters and the incident angle. The reflection and transmission coefficients are described in the next section.

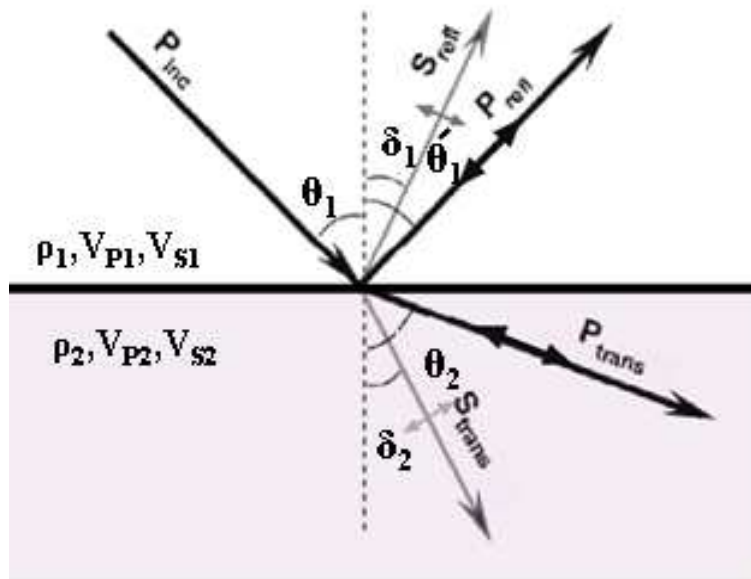


Figure 4.2: Waves generated at interface by incident P-wave. P_{inc} , P_{ref} , P_{trans} , S_{ref} and S_{trans} are the incident P-wave, reflected P-wave, transmitted P-wave, reflected S-wave and transmitted P-wave. θ_1 , θ_1 and θ_2 , are the angles of incident, reflection and transmission of P-wave. δ_1 and δ_2 , angles of reflection of S-wave. ρ_1 , V_{P1} and V_{S1} are the density the velocity of P-wave and the velocity of S-wave of the upper medium. ρ_1 V_{P2} and V_{S2} are the density P-wave velocity and S-wave velocity of medium.

4.2.2 Seismic Velocity

Seismic velocity (V) of a medium can be determined from laboratory measurements, acoustic logs, velocity analysis of seismic data (as will be shown in this section) or from vertical seismic profiling (see section 4.4). Velocity can vary vertically, laterally and azimuthally in anisotropic media such as rocks, and tends to increase with depth in the Earth because compaction reduces

porosity. Velocity also varies as a function of how it is derived from the data. For example, the stacking velocity derived from normal moveout measurements of common depth point gathers differs from the average velocity measured vertically from a check-shot or vertical seismic profile (VSP). Velocity would be the same only in a constant velocity (homogeneous) medium.

The term velocity seldom appears alone in seismic literature (Gadallah and Fisher, 2009). Instead it will occur in combinations such as the followings:

- **Instantaneous velocity:** The speed at any given moment of a wavefront in the direction of the energy propagation. It varies with wave time or propagation mode. P-wave velocity (V_p) is always the fastest. S-wave velocity (V_s) is the second fastest. The ratio V_p/V_s is greater than or equal to $(2)^{1/2}$

- **Interval velocity V_i :** The average propagation velocity through a depth or time interval. It equals the thickness of the depth interval divided by vertical time through the interval. Figure 4.3 shows a well log (A) and determination on interval velocity from the log (right) over certain depth intervals. These depth intervals are denoted by ΔZ_i , $i = 1, 2, \dots, N$. Summing these times over the indicated depth intervals gives the times Δt_i , $i = 1, 2, \dots, N$. Interval velocities are obtained from:

$$V_i = \Delta Z_i / \Delta t_i \quad (4.2)$$

- **Average velocity \bar{V} :** Total depth to a reflector Z divided by time to the reflector or twice the depth to the reflector divided by two-way, zero-offset reflection time T_i .

$$\bar{V} = 2Z / T_i \quad (4.3)$$

The average velocity can be calculated from interval velocity using:

$$\bar{V} = \frac{\sum_{i=1}^n V_i \Delta t_i}{\sum_{i=1}^n \Delta t_i} \quad (4.4)$$

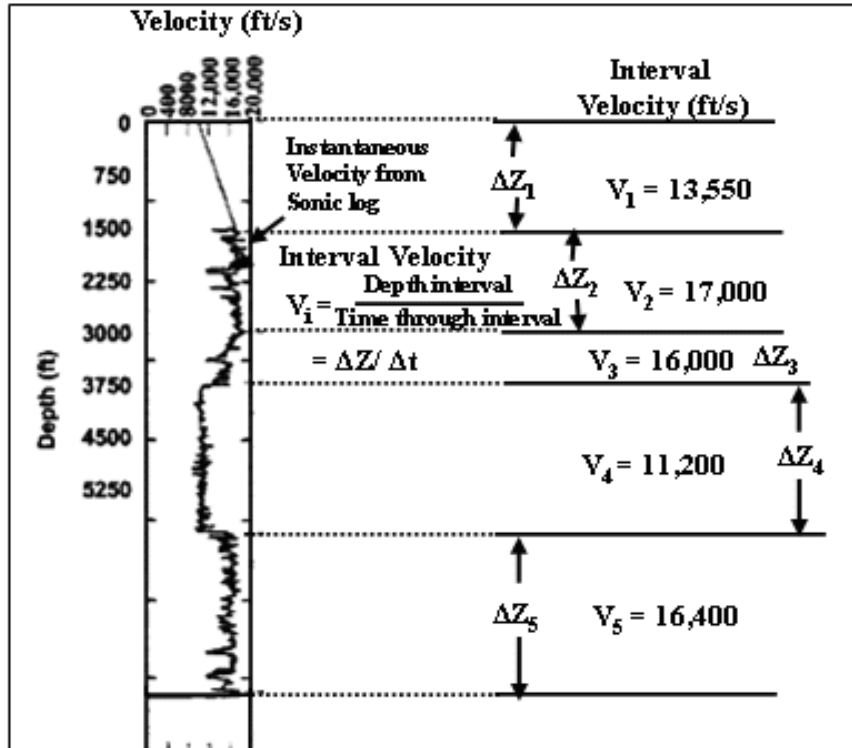


Figure 4.3: Instantaneous and interval velocities.

- **RMS velocity** V_{rms} : Square root of the average squared velocity. It is calculated from:

$$V_{\text{rms}} = \sqrt{\frac{\sum_{i=1}^n V_i^2 \Delta t_i}{\sum_{i=1}^n \Delta t_i}} \quad (4.5)$$

- **NMO velocity** V_{NMO} : The velocity used to correct for Normal Move Out (NMO) to make primary reflections on Common Mid Point (CMP) gather records occur at the same time on all traces. For isotropic horizontal layers:

$$V_{\text{NMO}} \approx V_{\text{rms}} \quad (4.6)$$

- **Stacking velocity** V_{stack} : The velocity that gives the optimum CMP stack output when used for NMO corrections.

4.2.3 Seismic Reflection and Transmission

The phenomenon in which the energy or wave from a seismic source has been returned from an interface having an acoustic impedance contrast (reflector) or a series of contrasts within the earth is called reflection. The amplitude and polarity of reflected waves depend on the acoustic properties of the material on both sides of the discontinuity (see Equation 4.9). Acoustic impedance (Z) is defined as the product of density (ρ) and velocity (V) thus:

$$Z = \rho V \quad (4.7)$$

The amplitude of the reflected wave (A_r) varies between -1 and +1 depending on the angle of incidence. The reflection coefficient (R_c) is the ratio of the amplitude of the reflected wave (A_r) to the amplitude of the incident wave (A_i). It is given by:

$$R_c = \frac{A_r}{A_i} \quad (4.8)$$

For normal incidence, R_c is given by:

$$R_c = \frac{\rho_2 V_2 - \rho_1 V_1}{\rho_2 V_2 + \rho_1 V_1} \quad (4.9)$$

and ρ_1 is the density of medium 1; ρ_2 is the density of medium 2; V_1 is the velocity of medium 1 and V_2 is the velocity of medium 2. A reflection coefficient of value 1 means that all incident seismic energy is reflected. Typical values of R_c are approximately -1 from water to air, meaning that nearly 100% of the energy is reflected and none is transmitted; ~ 0.5 from water to rock; and ~ 0.2 for shale to sand.

When the velocity is constant at both sides of a discontinuity, a density contrast will cause a reflection and vice versa. In other words, any abrupt change in acoustic impedance causes a reflection to occur. Energy which is not reflected is transmitted. With a large R_c , less transmission occurs and, hence signal-to-noise ratio reduces below such an interface. The transmission coefficient (T) of the seismic wave is calculated by the following expression:

$$T = 1 - R_c = \frac{2\rho_1 V_1}{\rho_1 V_1 - \rho_2 V_2} \quad (4.10)$$

Equations 4.9 and 4.10 are only applicable for normal incidence of a ray. In the general case reflection and transmission coefficients vary with the angle of incidence. In this case the reflection coefficient defined as a ratio of amplitudes depends on other parameters, such as the shear velocities, and is described as a function of incident angle by the Zoeppritz equations (Telford et al. 1990).

There are different types of reflections. Of interest in the interpretation of seismic data are the primary reflections. These correspond to rays travelling from their source to the reflecting surface, and then ascending directly to the surface of the ground.

Primary reflections may be accompanied by multiple reflections. These reflections, when recorded within the seismogram, should be attenuated by various methods in the processing stage.

4.2.4 Resolution of Shallow Seismic Data

Important considerations when designing shallow seismic reflection investigations are the spatial and temporal resolution. “Resolution is the ability to separate two features that are close together. The minimum separation of two bodies is the separation before their individual identities are lost on the resultant map or cross section (Sheriff, 2006). Generally, the minimum horizontal resolution of unmigrated data is restricted to the width of the first Fresnel zone (Yilmaz, 1987; Sheriff and Geldart, 1995). The Fresnel zone is defined as the subsurface area, which reflects energy that arrives at the earth’s surface within a time delay equal to half the dominant period ($T/2$). In this case ray paths of reflected waves differ by less than half a wavelength. A commonly accepted value is one-fourth of the signal wavelength. A recorded reflection at the surface is not coming from a subsurface point, but from a disk shaped area, which has a dimension equal to the Fresnel zone (Yilmaz, 1987; Sheriff and Geldart, 1995). The radius of the Fresnel zone (r) is given by:

$$r = \sqrt{\frac{Z_0 \lambda}{2}} = \frac{V}{2} \sqrt{\frac{t_0}{f}} \quad (4.11)$$

where Z_0 is the depth of the reflecting interface and $t_0=2Z_0/v$ is the two-way traveltime and f is the dominant frequency.

This equation shows that high frequencies give better resolution than low frequencies and resolution weakens with depth and with increasing velocities. The shape and size of the Fresnel zone also depend on the position of source and receiver, the velocity distribution, wave length, and on depth, dip, and curvature of the reflector (Brouwer and Helbig, 1998). Improvement of seismic resolution comes initially from improvement of the frequency bandwidth of the data (shaping the spectrum). The lower limit of vertical resolution is determined by a quarter of the dominant wavelength ($\lambda/4$, the Rayleigh criterion). The dominant wave length of seismic waves is $\lambda=v/f$, where v is velocity and f is the dominant frequency. Horizontal resolution of stacked sections may be improved by migration (see seismic data processing section). In practice, migration collapses the Fresnel zone to about the dominant wavelength (Stolt and Benson, 1986).

4.2.5 Limitations of Seismic Data

Shallow subsurface geology is characterized by heterogeneous and complex structures that may rapidly change vertically as well as horizontally, and may also dip in unpredictable directions. In such situation 2-D seismic sections may be contaminated by reflections as well as diffractions that originate from structures located out of the plan of the survey lines (3-D structures). Such unrecognized offline signals can lead to serious miss-interpretations (Green et al. 1995, Lanz et al. 1996). Therefore, such shortcomings of 2-D seismic profiling limitation are expected in high heterogeneous Quaternary sediments of the buried valleys.

4.3 2-D Seismic Reflection Profiling with P- and SH-Waves

High resolution shallow seismic reflection profiles can be useful in characterizing shallow structures and extending features identifiable in borehole lithologies within the upper few hundred meters of the subsurface. High resolution seismic reflection techniques have been developed as practical and effective methods in identifying shallow structures (Miller et al. 1986, Myers et al. 1987, Bueker et al. 1998, van der Veen and Green 1998, Wiederhold et al. 1998, Polom et al. 2008).

2-D shallow seismic P- and SH-waves are applied in the present study to image the structure of glacial sediments in the buried valley and test the applicability of SH-waves in investigating this type of structure. In addition, they are used to image the elastic properties of the sediments in 2-D by combining the velocity information derived from the 2-D shallow seismic profiles of P- and SH-waves.

4.3.1 Data Acquisition

High-resolution shallow seismic reflection surveys require use of high frequencies, therefore, appropriate seismic sources and high frequency geophones are needed (Knapp and Steeples 1986a,b). In shallow seismic techniques the main problems arise from significant changes of the seismic velocity within the shallow depth zone. In addition, the seismic records can be affected by strong noise such as ground roll, air-waves, direct arrivals, refractions, diffracted waves and multiples. Wind, rain, human activities and electromagnetic noise from powerlines and electric cables can also disturb the seismic measurements (Jefferson et al. 1998, Schuck and Lange 2007). The main components of seismic data acquisition systems are: the seismic source, seismic receivers and the recording system. The acquisition components of the present seismic data are described below.

Seismic Sources – Vibrators

Vibroseis is a seismic method in which a vibrator is used as an energy source to generate a controlled wavetrain for which a sinusoidal vibration with continuously varying frequency is applied (Sheriff, 2006). The Vibrator was initially developed by Conoco's researchers

(Crawford et al. 1960; Gadallah and Fisher, 2009). It is commonly applied in the hydrocarbon exploration industry (Polom et al. 2008). The source is widely used in seismic acquisition as it is a nondestructive method with a controllable frequency range and ideally produces a zero-phase wavelet. This type of seismic source can be operated in urban environments where other sources, like dynamite, are prohibited. Other advantages of the vibrator source include cost savings, such as the reduction in shot hole drilling associated with a dynamite source.

P-wave signals of the present data were generated by a small vibrator (MHV 2.7) developed by GGA-Institute (now LIAG) together with the firm Bohrtechnik GmbH. The vibrator can generate a signal with a bandwidth of 16 Hz to 500 Hz. Four 10-second long (50-Hz to 200 Hz upsweeps) were generated at each source station. Source stations were separated by 5 m, with the first source station at 5 m offset and the last source station near the 48th receiver station.

For the generation of SH-wave signals a new shear wave vibrator was developed and constructed by LIAG Institute in cooperation with the firm Prakla-Bohrtechnik, Peine (construction of the shear wave vibrator) and the firm Keifer, Dorfien (carrier vehicle Bokimobil). This vibrator can be rotated to emit SH-waves as well as SV-waves without changing the vehicle position. It is designed for a peak force of approximately 30 kN and a frequency range of 16 Hz to 300 Hz. Phase and amplitude control is achieved by a Pelton VibPro control unit.

For the SH-wave profile two-second long 30 Hz to 200 Hz upsweeps were recorded at each source station. The source stations were separated by 4 m with the first source station 120 m offset and the last source station near the 48 receiver station.

The Seismic Receiver

Seismic receivers (geophones) are electromechanical transducer devices that convert mechanical energy into electrical energy. More than one type of geophone is required to detect both P- and SH-waves. Vertical geophones detect P-waves, whereas SH-waves are detected by horizontal geophones.

Each fixed spread consisted of 120 (type SM 4/7, 20 Hz) vertical geophones separated by 5 m, resulting in a total spread length of 595 m. The arrangement of the geophones in relation to the

source point used in seismic data acquisition was inline spread. For details about geophone interval, offset etc see Table 4.1.

Recently, the land streamer has been introduced by van der Veen and Green (1998) to reduce labor costs and increase survey efficiency of high-resolution shallow seismic reflection techniques. It is comprised of a length of a heavy-duty nylon belt similar to that used for seat belts. Geophones are attached along the top of the belt; metal plates are then connected to the geophones from the bottom of the belt. The metal plates provide the necessary weight to couple the geophones to the ground.

The SH-wave profile was carried out using a land streamer developed by LIAG to facilitate measurements on sealed surfaces, e.g. traffic areas or factory floors. It further enables very efficient field work. It comprises 120 (10 Hz) geophones assembled every 1 m onto a belt strap. A good contact with the surface is achieved by using abrasion-resistant 3-point bearing feet. Handling in the field is done with winding drums.

Seismic Recording

The recording system is used in seismic experiments to provide an uncontaminated, precise and permanent record of data detected by receivers in the spread so that the seismic signals can be studied and analyzed at next steps.

The seismograph used for recording the seismic data was Geometrics Geode (5 geode 24 channels and 1 geode 6 channels) networked into a StrataVisor controller. Resulting uncorrelated data included 15,000 samples per trace uniformly acquired over 15-seconds record length. Geophone cables were connected to the device using self-made adapters (Gisewski G52). Power supply was realized with 24 Ah batteries embedded in self-made boxes. The single geode devices were connected with 10 cables 60 m long each and 12 geophones of 5m spacing were connected to each network cables, two of which can be interconnected. A total of 10 network cables enable a geophone layout of 600 m. The recording software is installed on a Windows XP Laptop. To achieve a fast data transmission, which is especially important for non-correlated vibroseis data, more than one network can be connected to the laptop.

Shear wave data were recorded on 5 geometrics Geode seismographs networked into a strata Visor controller. The resulting 24-bit uncorrelated data included 5000 samples per trace uniformly acquired over 5 seconds recording length.

The two P-wave reflection profiles (maximum 96-fold) and one SH-wave profile (maximum 62 fold) have been acquired perpendicular to the assumed axis of the buried valley. The data acquisition parameters and instruments of the seismic profiles are summarized in Tables 4.1 and 4.2, respectively.

Table 4.1: P-wave seismic data acquisition: equipment and parameters.

Item	Description
Instruments	
Seismic source	LIAG Kleinvibrator: MHV2.7
Sweep type	50-200 Hz Linear, 10 s
Vertical stacking	4-fold
Recording Instrument	5 Geode 24 channels, 1 Geode 6 channels
Geophone type	SM 4/7 (20 Hz)
Geometry	
Channels/record	121 (channel no. 121 is the sweep signal record)
Geophone Interval	5m
Offset	-240 m to + 595 m
Shot point spacing	5m
Number of shot points	683 (for profile 4) & 402 (for profile 5)
Spread type	2-D variable split spread
Fold coverage	96 (for profile 4) & 75 (for profile 5)
CMP spacing	2.5 m
Recording	
Sample interval	1 ms
Recording length	12000 ms
Recording filter	None
Pre-amplitude gain	36 dB
Field format	SEG2

Table 4.2: SH-wave seismic data acquisition: equipment and parameters.

Item	Description
Instruments	
Seismic source	Shear wave Vibro MHV 4
Sweep type	Sweep: 30-200 Hz 10 s, and 30-140 Hz
Vertical stacking	2-fold [+Y]-[-Y] alternated vibrations
Recorder	5 Geometrics Geode 24 channels, 1 Geode 6 channels
Geophone type	SM6 HB (10 Hz), single units attached to GGA land streamer unit
Geometry	
Channels/record	121 (channel no. 121 is the sweep signal record)
Geophone Interval	1m
Number of shot points	726
Offset	240 m to + 240 m
Shot point spacing	10m, 4m
Spread type	2-D variable split spread, SH-SH configuration 40 m roll-on streamer shift interval operation
Fold coverage	62
CMP spacing	0.5
CMP numbering	VP + GP
Recording	
Sample interval	1 ms
Recording length	15000 ms
Recording filter	None
Pre-amplitude gain	24 dB
Field format	SEG2

4.3.2 Data Analysis and Processing

The purpose of the data processing is to convert the field data into a seismic section showing the locations of reflectors along the seismic line as well as to increase the signal-to-noise ratio by increasing the reflections and suppressing noise in the data. Reflections are recognized by the hyperbolic travel times. If the reflection interface is horizontally flat, the reflection hyperbola is

symmetric with respect to zero offset. On the other hand if there is a dipping interface, then the reflection hyperbola is skewed in the up dip direction.

Most of processing operations employed routinely in deep seismic datasets can be applied to shallow seismic datasets with some considerations to avoid generating artifacts on the data like separating source generated noise from shallow reflections, careful application of NMO stretch mute and carefully muting unwanted first breaks. In this section, we analyze the raw data and then describe each processing step applied to the data.

Figure 4.4 shows typical shot gathers recorded at three locations along profile 4. Reflections are evident below 500 ms. In the upper part shots 30 and 125 show reverberating arrivals (event r) followed by clear first breaks. In shot gather 600 reflections at 500 ms and 800 ms (event d) shows distorted hyperbolic moveout, suggesting a dip-moveout (DMO) effect caused by an up-dip reflector. All records are characterized by low frequency ground roll (event g) and strong airwaves (event a). Bad traces are evident in shot gather 600 (events b).

Typical shot gathers recorded along profile 5 are shown in Figure 4.5. Reflections are evident below 500 ms. In the upper part shots 50 and 240 show reverberating arrivals (event r) followed by clear first breaks. In shot gather 351, the reflection 950 ms (event d) shows distorted hyperbolic moveout, suggesting a dip-moveout (DMO) effect caused by an up-dip reflector, whereas, a down-dip reflector is shown in shot gather 240 (event e). All records are characterized by low frequency ground roll (event g) and strong airwaves (event a).

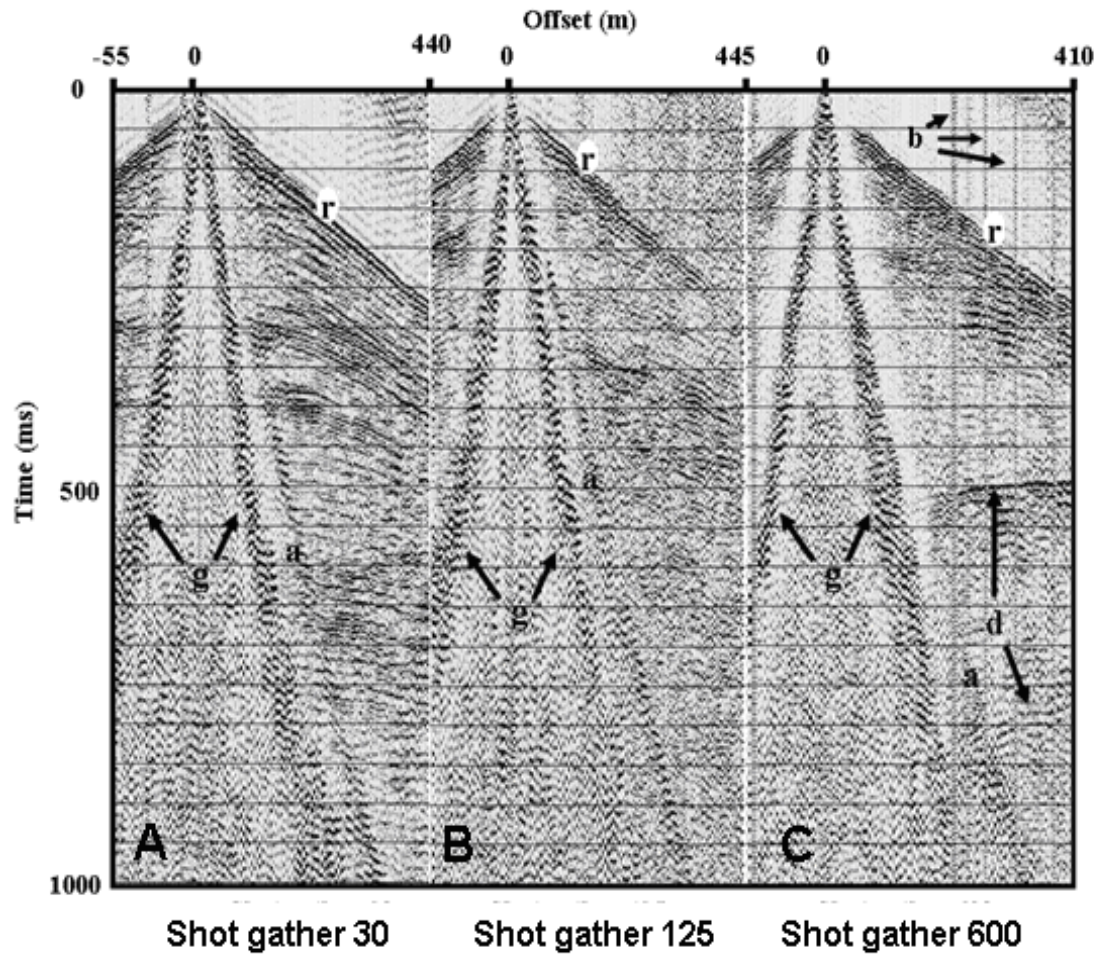


Figure 4.4: Three shot gathers with variable data quality from profile 4 with AGC (400 ms) applied. Data are displayed to 1000 ms. Shot gathers 30 (A) and 600 (C) are away from the buried valley location, whereas shot gather 125 (B) is in the location of the buried valley. The shot gathers 30 and 600 show stronger and clearer reflections than that shown by the shot gather 125. This is due to the fact that the reflections on the shot gathers 30 and 300 are from Tertiary horizons, whereas the reflections on shot gather 125 are from Quaternary sediments inside the valley. Letters highlight events: airwaves (a); noise traces (b); dipping reflectors (d); ground roll (g); first arrivals (r).

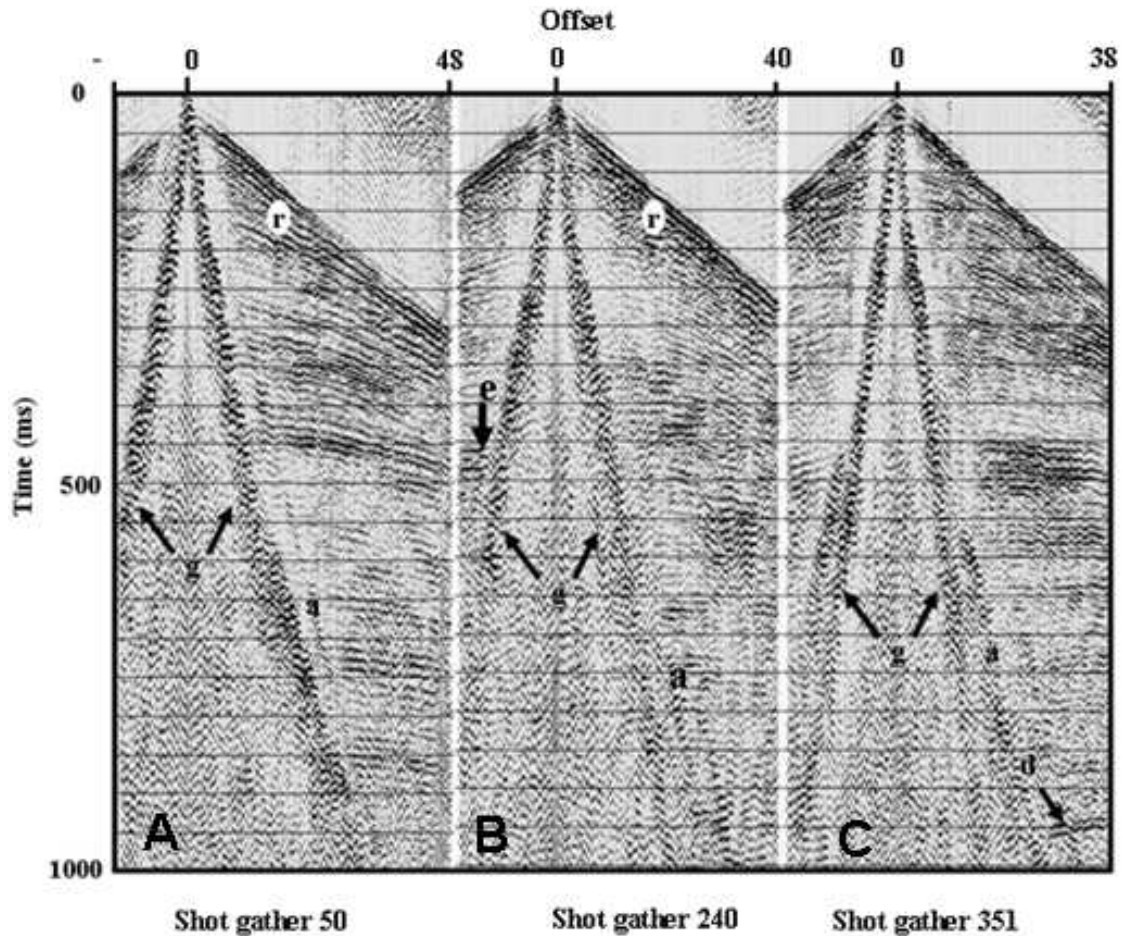


Figure 4.5: Three shot gathers with variable data quality from profile 5 with AGC (400 ms) applied. Data are displayed to 1000 ms. Shot gathers 50 (A) and 351 (C) are out of the valley, whereas shot gather 240 (B) is inside the valley. The shot gather 25 and 351 show stronger reflections than that shown by the shot gather 240. This is due to relative homogeneity and continuity of the Tertiary horizons comparing to the heterogeneity of sediments in the valley. Letters highlight events: airwaves (a); noise traces (b); dipping reflectors (d); ground role (g); first arrivals (r).

Figure 4.6 shows two raw shot gathers from the SH-wave profile. Strong reflected SH-waves (SR event) are evident at 150 ms and 300 ms two-way travel time in shot gathers 11 and 91, respectively. Surface waves of Love type (event LW) are strong in shot gather 11 and less strong in shot gather 91. Love waves can be eliminated by FK filtering. Reflected P-waves (converted waves, event PR) are seen on top of the both gathers, as they arriving faster than other types of waves. The P-wave may be muted from the data.

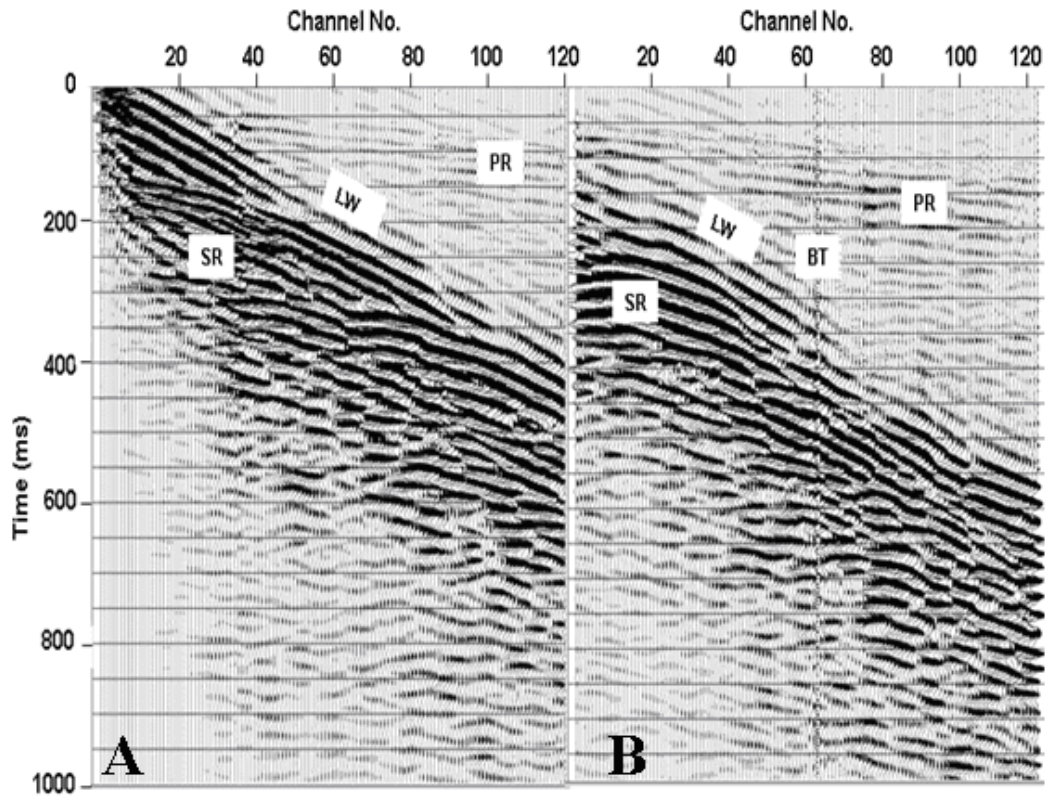


Figure 4.6: Shot gathers 11 (A) and 91 (B) from the SH-wave profile. Only, vibroseis correlation processing has been performed. SR: SH-wave reflection; PR: P-wave reflection; LW: Love wave and BT: bad trace.

Processing of P-wave data

The P-wave raw data were generally of good quality. They were processed using commercial software, i.e. Landmark ProMAX installed in a SUN workstation at LIAG.

Table 4.3 outlines the general flow of the P-wave data processing. The specific processes are discussed in detail in the following sections. The remaining steps are standard in the processing of reflection seismic data. Sheriff and Geldart (1995) and Yilmaz (1987, 2001) provide excellent references for their explanation.

Table 4.3: P-wave seismic data processing sequence.

<i>Process step</i>	Description
Data reformat	From SEG-2 to ProMAX format
Vibroseis correlation	Correlated with pilot sweep
Geometry	Defined using field notes and loaded to headers
Trace Editing	Bad / noisy traces killed
Top/ Bottom Muting	Elimination of First arrivals and surface waves.
Spherical Divergence correction	Multiply by $1/(t*v**2)$
Trace Equalization	150 ms spatially varying window
Automatic Gain Control	400 ms window
Bandpass Filter	Zero-phase Ormsby filters: 50-70-200-250 Hz
Deconvolution	Zero phase spiking Operator length: 50 ms White noise: 1 %
Static correction	Correct for near surface effects
CMP sort	Sorted from shot gathers to midpoint gathers
Velocity analysis I	Integrated analysis of shot gathers, constant velocity stacks, and semblance plots
NMO correction	Stretch mute 30%
DMO correction	Common Offset FK DMO
Velocity analysis II	After DMO applied
CMP Stacking	Applied based on optimum stacking velocities Summed NMO-corrected CMP gathers
Static correction to final datum	0m NN, 1600 m/s
F-X deconvolution	30-250 Hz, Wiener Levinson
Steep Dip FD time Migration	Using interval velocity field
Time-to-depth conversion	Using VSP velocity function

Pre-stack Processing

Vibroseis Correlation: In vibroseis data, the recorded trace has embedded sweep signals which make the seismic events unrecognizable. Therefore, it is necessary to remove the sweep from the trace to resolve the reflection events (see Figure 4.7). This is obtained with the use of cross-correlation, where the sweep is cross-correlated with the traces creating an embedded Klauder wavelet. The Klauder wavelet is the autocorrelation of a vibroseis sweep (Sheriff, 2006). The basic seismic convolutional model for a vibroseis source is:

$$x(t) = r(t) * s(t) \quad (4.12)$$

where $x(t)$ is the recorded trace, $r(t)$ is the geological reflectivity, $s(t)$ is the sweep and $*$ is the convolution operator. To remove the sweep, the trace is cross correlated (\otimes) with the sweep. The equation for the deconvolved sweep is

$$X_{cc}(t) = r(t) * s(t) \otimes S^*(t) \quad (4.13)$$

where $S^*(t)$ is the sweep input into the ground. This equation can be simplified to:

$$X_{cc}(t) = r(t) * k(t) \quad (4.14)$$

since the cross correlation of two identical sweeps is defined as Klauder wavelet, $k(t)$. Cross correlation collapses the sweep to a Klauder wavelet at impedance contrast and filters the data with sweep parameters.

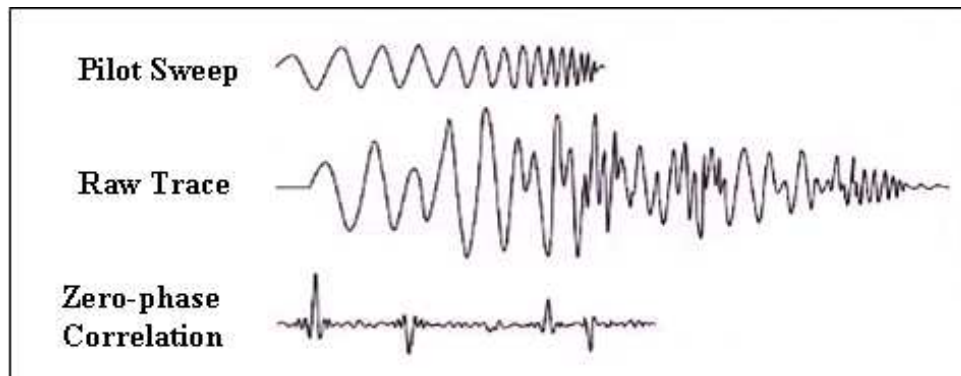


Figure 4.7: Raw and correlated vibrator traces (after Gadallah and Fisher, 2009).

Editing and Geometry assignment: The initial procedure of processing consisted of data quality check and field geometry assignment. Trace editing aimed at detection and removal of dead or very noisy traces and spikes that may induce problems with the forward Fast Fourier Transform (FFT). Top muting eliminated the first breaks (directed/ refracted arrivals) from the seismic traces and bottom muting attenuated ground roll. To examine the quality and characteristics of the raw data bandpass filters range from 30-50 Hz to 200-250 Hz were applied to the data. Automatic Gain Control (AGC) allows trace normalization (Sheriff and Geldart, 1995). The AGC operator which uses a time window of a given length (in this case 400 ms) which moved down the trace sample by sample calculated a scale factor at each location after filtering. The scale factor is equal to the inverse of the Root Mean Square (RMS) amplitude in the window. This scalar was applied to the sample at the centre sample of the time window.

Statics corrections: Statics corrections are time shifts applied to seismic data to compensate for the effects of variations in elevation, weathering thickness, weathering velocity, or reference to a datum (Figure 4.8). The objective is to determine the reflection arrival times which would have been observed if all measurements had been made on a flat plane with no weathering or low-velocity material present. These corrections are based on uphole data, refraction first-breaks, and/or event smoothing.

First-break based statics, which we applied to our data, are the most common method of making field static corrections (Wiederhold, 2006).

The term 'static' is used to denote constant time shift of whole data traces, as opposed to variable time shifts as applied by NMO corrections which are dynamic. The elevation needed for shot/receiver time correction is obtained from records. The velocity needed for calculating the time shift is obtained from refraction first break picking. The elevation corrections (also called datum correction) may be used to bring all times in a seismic record to a fixed level in the subsurface which is the final processing datum. The final processing datum could be any arbitrary level or mean sea level.

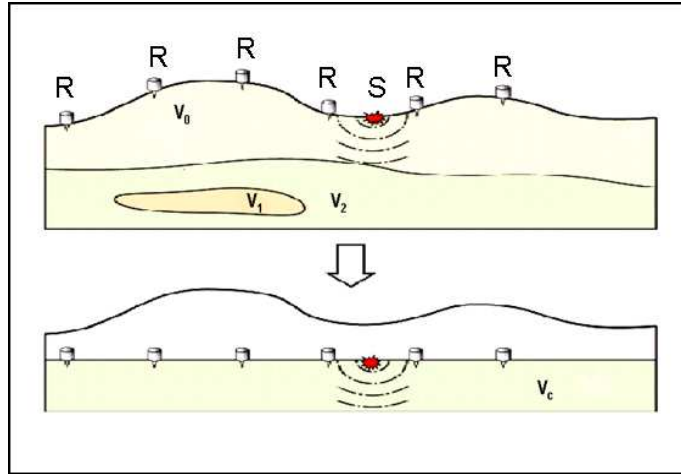


Figure 4.8: Principle of static corrections: Shot (S) and receivers (R) are moved to a flat plane, the datum or reference surface. Near surface velocity changes are replaced by a correction velocity V_c (from Wiederhold 2006).

Reflection events from a shot gather from P-wave data is shown in Figure 4.9. It shows the improvement in the alignment of the event after application of the static corrections.

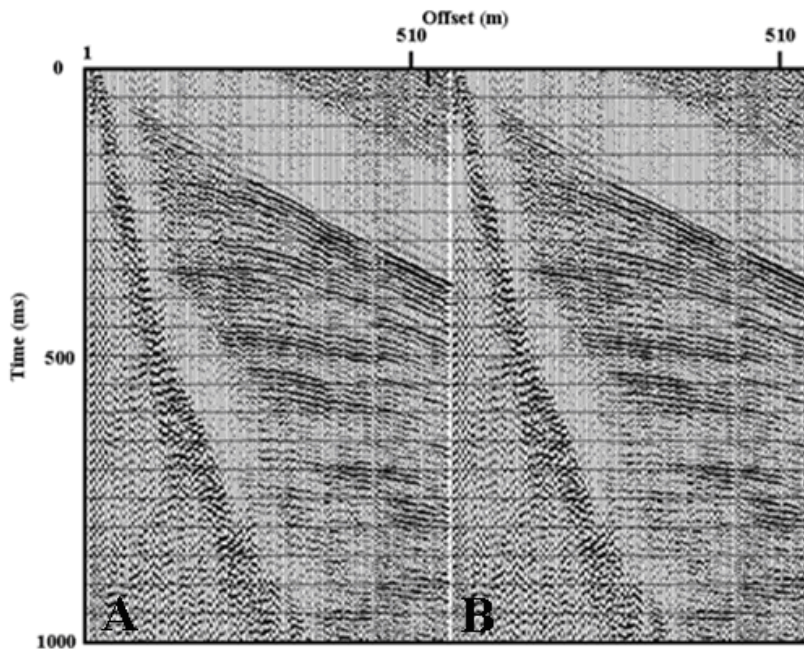


Figure 4.9: A Shot gather from profile4 without (A) and with (B) refraction statics applied. Reflection events show improvements in alignments given by the static corrections.

Deconvolution

Deconvolution is a process that improves the temporal resolution of seismic data by compressing the basic seismic wavelet (Yilmaz, 1987). It is also used to compensate for the low resolute wavelet of the Vibrator source and for some other undesirable effects included in the recorded earth response, such as reverberation and multiple arrivals. Spiking pre-stack deconvolution was applied to improve temporal resolution. Spiking deconvolution is a least squares inverse filter that compresses the seismic source wavelet into a zero lag spike.

Frequency Filtering

Frequency filtering is done to remove unwanted frequencies from the seismic data. The sweep frequencies have a range of 50 – 200 Hz and frequencies other than these are attenuated using various filtering techniques. Frequency filtering can be in the form of band-pass, band-reject, high-pass (low-cut) or low-pass (high-cut) filters.

The frequency spectrum of seismic reflections usually becomes lower with increasing arrival time as the higher-frequency components are attenuated faster by absorption, multiples, and other natural filtering processes. Hence, we often hope to shift the passband towards lower frequencies for later portions of the records, that is, we wish to accomplish time-variant filtering. By doing so, the ambient noise, which begins to dominate the signal at late times, is excluded and a section with a higher signal-to-noise ratio is obtained.

FK dip filtering

In addition to pre-stack and post-stack predictive deconvolution, another multiple suppression technique, based on frequency-wavenumber (FK) dip filtering, was applied. FK multiple reflections attenuation is a process combining: 1) velocity analysis; 2) forward Normal Moveout (NMO) correction; 3) FK dip filtering; and 4) inverse NMO correction. Multiple reflections may be recorded at nearly the same time as primary reflections, but they have lower V_{NMO} than primary reflections. Thus NMO corrections that flatten multiples overcorrect primaries. When NMO-corrected CMP records are transformed into the FK domain all primary reflections are placed in the negative half of the FK plane and the NMO corrected multiples along the $K=0$ axis. A velocity filter that passes everything except a narrow reject band centered at $K=0$ eliminates

multiples. FK multiple-attenuation offers a further gain in multiple energy suppression over stacking. The filter performs more quickly than other multiple suppression methods, and it is useful for multiple-suppression on pre-stack data.

Dip Moveout (DMO)

DMO processing or pre-stack partial migration may turn out to be a milestone on the path towards proper imaging of the subsurface structures. It was introduced to overcome efficiently the shortcomings of normal CMP stacking of steep dips. The DMO operator moves the reflection point on the dipping interface to its zero-offset location. This dip-correcting later shift involves an adjustment of the traveltimes and therefore, reducing the stacking velocities of dipping events. Consequently, events originating from the same reflector with different dips can be stacked with one and the same velocity. On the other hand, the velocity contrast is increased between steeply dipping noise and horizontal reflections observed at the same traveltime. As the stacking velocities after DMO processing are independent of dip they can be used for further imaging processes such as post-stack migration and depth migration. Thus the main goals of DMO processing can be seen as:

- Improving the zero-offset character of NMO corrected data by better approximating common reflection point data and solving the conflicting dip problem,
- Providing improved estimates of velocities, and
- Suppressing steeply dipping coherent noise.

As a final pre-stack process, we applied the Dip Moveout (DMO) correction (Yilmaz and Claerbout, 1980). The stacking velocity or NMO velocity depends on the dip of the reflector. It is well known that the conventional stacking method cannot stack both a flat and dipping layer occurring at the same time because of the dip dependence of the stacking velocity. The DMO process is a method used to improve the stack quality by compensating for the dip effect in the NMO equation. DMO correction transforms nonzero-offset seismic data in a CMP gather into the same zero-offset reflection times and reflection points for all offsets. This transformation improves velocity estimates, provides higher lateral resolution, and attenuates coherent noise (Deregowski and Rocca, 1981; Yilmaz, 1987).

DMO corrections can be applied in the common-offset domain or in the shot domain. Shot-domain DMO does not work well because shot-domain DMO is more sensitive to the errors in the NMO velocity and degrades high frequencies at steep dips. However, in our case common-offset- domain DMO indicated that, DMO not only improved velocity analysis but also it suppressed coherent noise and improved the lateral resolution. Figures 4.15 and 4.16 will show the stacked data without and with DMO applied. Hence, after application of DMO to pre-stacked data the produced stacked sections are improved.

The raw shot gathers shown in Figures 4.4 (from profile 4) and 4.5 (from profile 5) are shown after applying the pre-stack process in Figure 4.10 at top and bottom, respectively. Both subset figures show reflections from about less than 50 ms to 1000 ms.

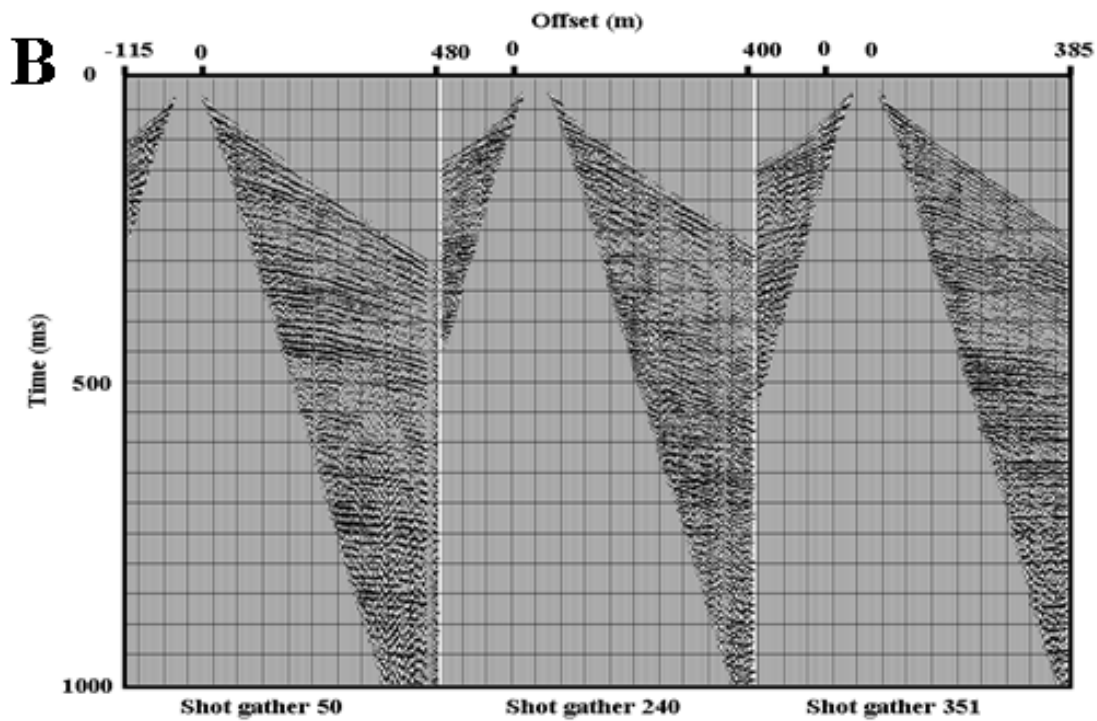
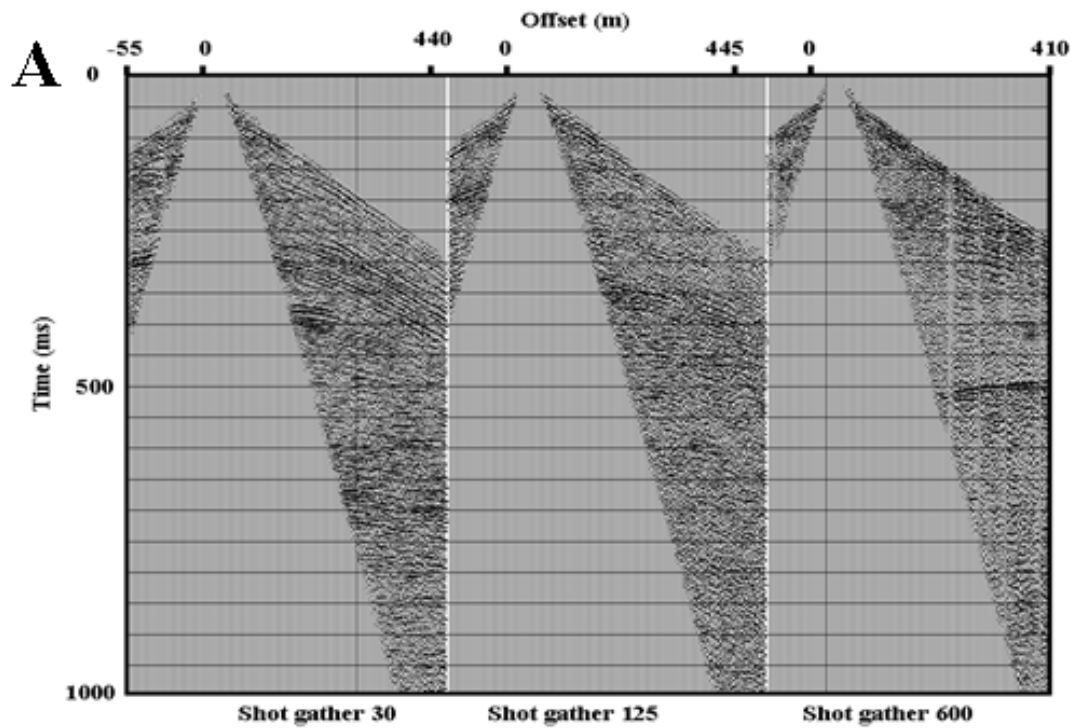


Figure 4.10: Results of applying a prestack processing sequence to typical shot gathers from profile 4 (A) and profile 5 (B). Top and bottom mute are applied to eliminate first break and surface waves, respectively. AGC 400 (ms), Bandpass filter (50-70-150-200 Hz) are applied.

Velocity Analysis

The seismic velocity is important in almost all phases of seismic data processing. It is used in normal moveout (NMO), multiple attenuation, dip moveout (DMO) and migration processes. The velocity is important for the prediction of the lithology and geological interpretation. With the wrong velocity, seismic events do not focus and reflectors are miss-positioned. Without an accurate velocity, seismic data could easily hinder rather than help the rock physicist (Claerbout, 1999), geostatistician, and reservoir engineer. Obtaining an accurate velocity estimate is one of the most difficult problems in geophysics. Velocity estimation is a nonlinear, under-determined problem. Velocity analysis is based on the hyperbolic assumption derived for a flat multi-layered earth.

There are several methods of stacking velocity analysis. The preferred method depends on the data under consideration and the preferences of the velocity picker. Almost all velocity analysis today is performed interactively on a screen using a combination display configured according to user preference. Animated displays are common and show the results of applying the NMO and stacking the data with the velocities chosen. In the past velocity analysis was considered to be a computer intensive process and some shortcuts were taken into account (such as reducing the fold of gathers). The power of modern computer systems means that short cuts are no longer required. Some systems will calculate the velocity analysis on the fly as requested by the user but most systems expect the pre-computation of the velocity analysis displays. The subsequent speed of analysis is limited only by the speed of the picker and the graphics hardware being used. On some displays the interpreter can pick several key horizons which can be used as main velocity boundaries. Depending on the geological province this method is critical, for example if velocities are to be picked for depth migration purposes. When picking horizons care should be taken to ensure the velocity interpolation stage can handle bends and other more complex geological structures.

Function velocity stacks are a common form of display in which the range of velocities used for the stack panels is defined by percentage variations from a single (best choice) function. The individual panels show high resolution but the quality of the panels depends on the accuracy of the initial function used. Figure 4.11 shows combination display the velocity spectrum (Panel A), the NMO corrected gather (Panel B) and function velocity stacks (Panel C). The gather and stack displays are interactively updated as picks are made. Dynamic (Dyn) is the stack with the currently picked velocity function. The velocity spectrum (the panel A) is calculated by

determining how well a given hyperbolic event matches real events on the central CMP gather. The maximum amplitude of coherence is expected where the hyperbola best fits a given high amplitude seismic event. The measure of coherence most often used is called semblance which is robust to noise, spatial aliasing and lateral variations in amplitude. There are various methods of displaying semblance but almost a colour contour display is used with blue representing low semblance and red representing high semblance areas. The axes of the display are velocity (horizontal) and zero-offset time (vertical). The semblance function, $S(v,t)$ is defined as a normalized cross-correlation:

$$S(v,t) = \frac{\sum_{t=\tau-dt}^{\tau+dt} \left| \sum_x p(x,t,v) \right|^2}{N \cdot \sum_{t=\tau-dt}^{\tau+dt} \left| \sum_x p(x,t,v) \right|^2} \quad (4.15)$$

here $p(x,t,v)$ is the NMO corrected trace, N is the number of traces in CDP, t is the TWT, v is the velocity and x is CMP spacing. The velocity interpreter would make picks either on the semblance clouds or on the stack displays. An edited pick is shown on the example display. Broader peaks in the deeper part of the section indicate reduced resolution and offset.

The stacking velocity is the velocity required to best stack the data using the best-fit hyperbola over the available offset range. The choice of the stacking velocity (V_{stack}) can be rather subjective. However, it turns out that an appropriate choice can cover up for a multitude of assumptions made in the CMP stacking process. For horizontal layers and small offsets V_{stack} should equal to the root mean square velocity (V_{rms}). For dipping layers a higher velocity is required since $V_{\text{stack}} = V_{\text{rms}}/\cos(\Theta)$ (where Θ is the angle of dipping).

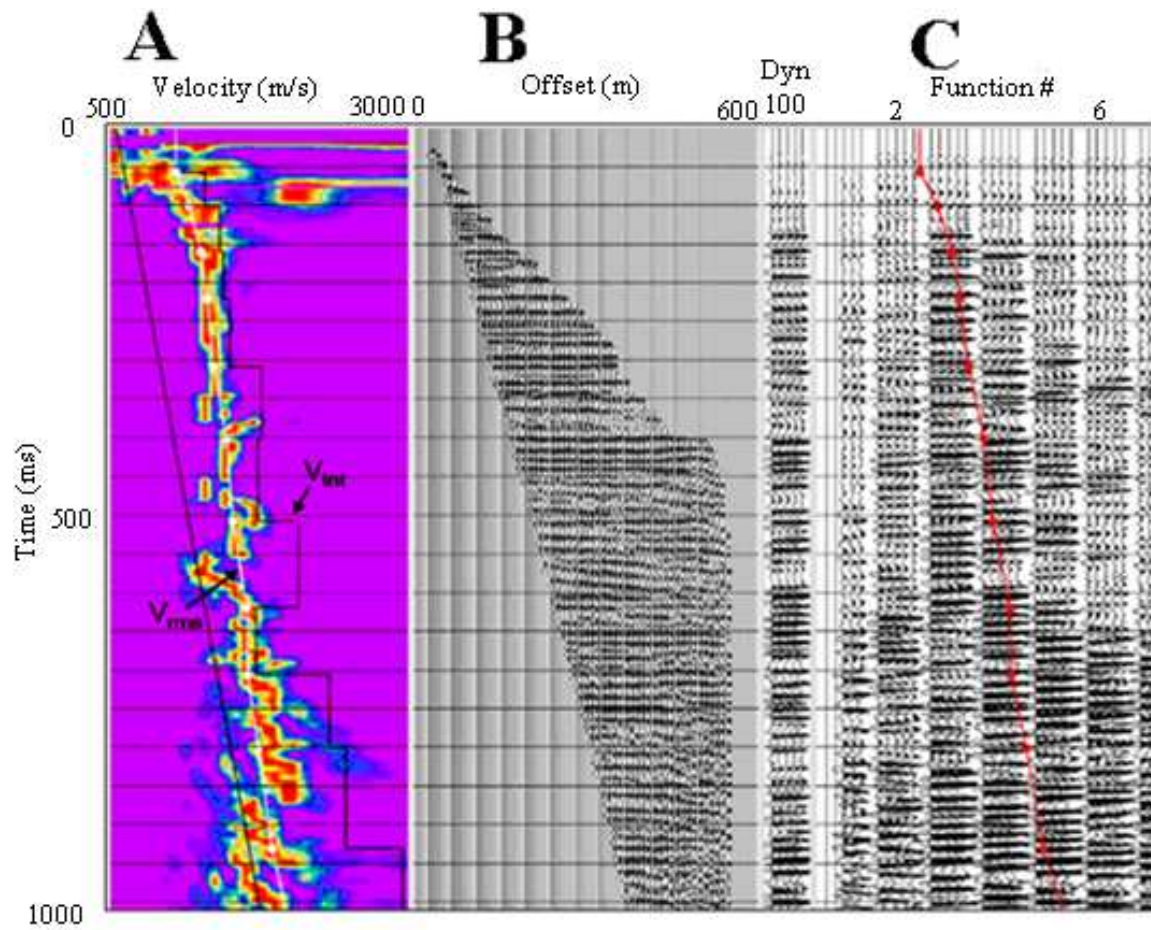


Figure 4.11: Interactive velocity analysis display with the velocity spectrum (A); the NMO corrected gather (B) and the function velocity stack (C). The semblance panel shows the estimated the RMS and interval velocity functions. The RMS velocity function is shown in the same time by the function velocity stacks panel.

The application of DMO mostly removes the effects of dip from V_{stack} such that V_{stack} approximates V_{rms} . The stacking velocity field calculated for the seismic data is shown in Figure 4.12. The stacking velocities range from 1500 to 2900 m/s for profile 4 (Figure 4.12A) and from 1600-2800 m/s for profile 5 (Figure 4.12B).

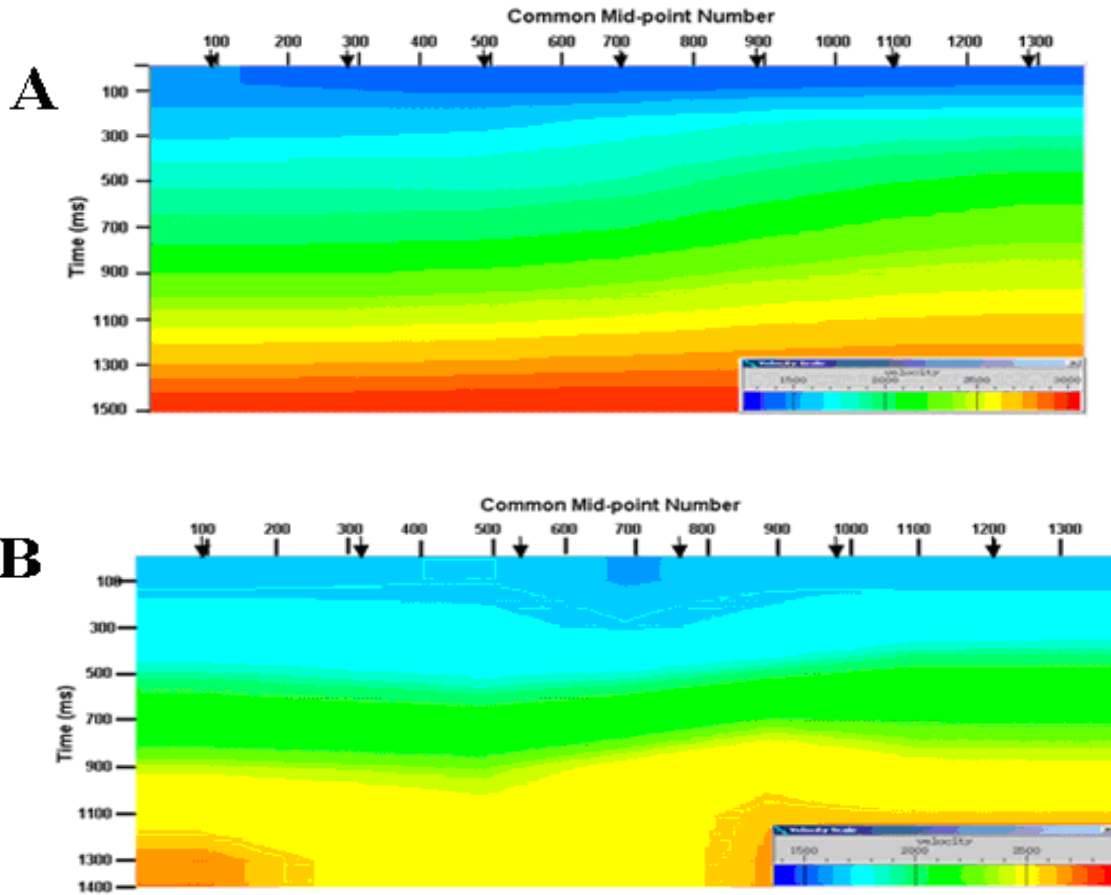


Figure 4.12: Optimum stacking velocity fields determined by interactive analysis of semblance gathers after dip moveout. A: Stacking velocity field of profile 4. B: Stacking velocity field of profile 5. Arrows on top show the CMPs at which semblance velocity analysis was conducted. The stacking velocity ranges from 1400 to 2900 m/s in profile 4 and from 1600 to 2800 m/s in profile 5.

The interval velocity is the velocity of a specific layer. Using Dix's equation (equation 4.16), Dix (1955), the RMS velocities are converted into an interval velocity model, which is displayed in Figure 4.13. The use of the Dix equation to convert RMS stacking velocities to interval velocities is based on the assumption of horizontal layers and constant velocities between the layers. Therefore, a dipping structure and vertical and lateral velocity variations can introduce significant errors into the resulting interval velocity fields. Furthermore, the error in interval velocity may be caused by picking errors in the RMS velocities. The RMS picking errors depend on the width of the maximum semblance at a reflector. Dix's equation is written as:

$$V_{\text{int}} = \sqrt{\frac{t_2 V_{\text{rms}2}^2 - t_1 V_{\text{rms}1}^2}{t_2 - t_1}} \quad (4.16)$$

where, V_{int} is the interval velocity that can be calculated for two reflectors with reflected-ray travel times t_1 and t_2 , and RMS velocities $V_{\text{rms}1}$ and $V_{\text{rms}2}$, respectively.

The calculated interval velocity fields (Figure 4.13) are characterized by an increase from about 1300 m/s at 100 ms to approximately 3000 m/s beyond 1200 ms. Such a velocity increase may be due to increasing density and decrease in porosity. The velocity fields show a decrease in velocity towards the middle, which corresponds to the location of the valley.

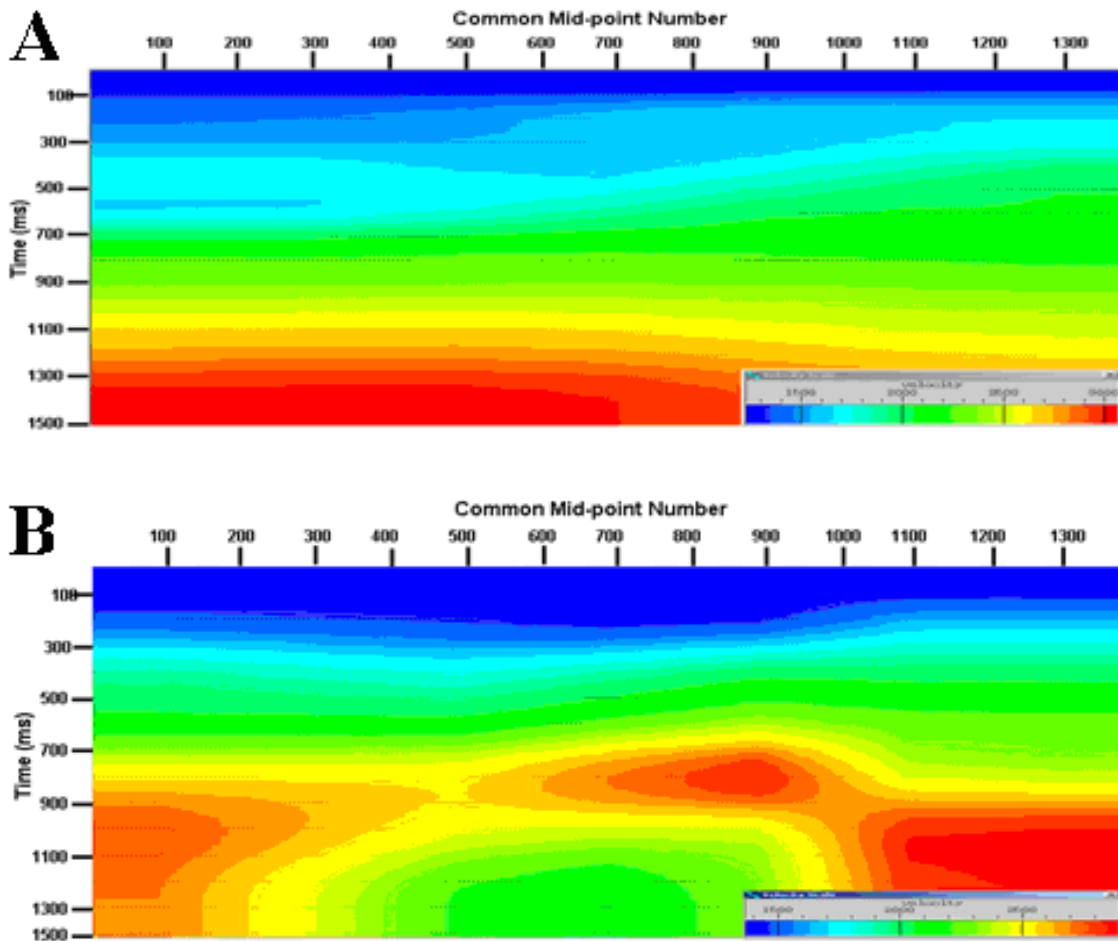


Figure 4.13: Interval velocity fields obtained from stacking velocity functions shown in Figure 4.12 A and B, respectively, using Dix's equation. A: the interval velocity field of profile 4; B: the interval velocity field of profile 5. The interval velocity ranges from 1300 to 3000 m/s in both profiles.

CMP Stacking

After DMO the data is CMP stacked. Stacking is a composite record made by combining traces from different records (Sheriff, 2006). The process of stacking is the single most powerful tool for enhancing the quality of seismic reflections (Robinson and Coruh, 1988). It combines all traces of all CMP gathers into single traces for every CMP on a line. Consequently, the stacking process greatly improves the signal to noise ratio due to the fact that noise is reduced by destructive interference as traces are combined. Wavelets on the other hand interfere constructively to produce a stronger signal. This method is very effective in attenuating several kinds of noise (Robinson and Coruh, 1988). Velocity analysis and NMO correction can be viewed as forms of stacking as well. A simple example that explains the principle of stacking is shown in Figure 4.14.

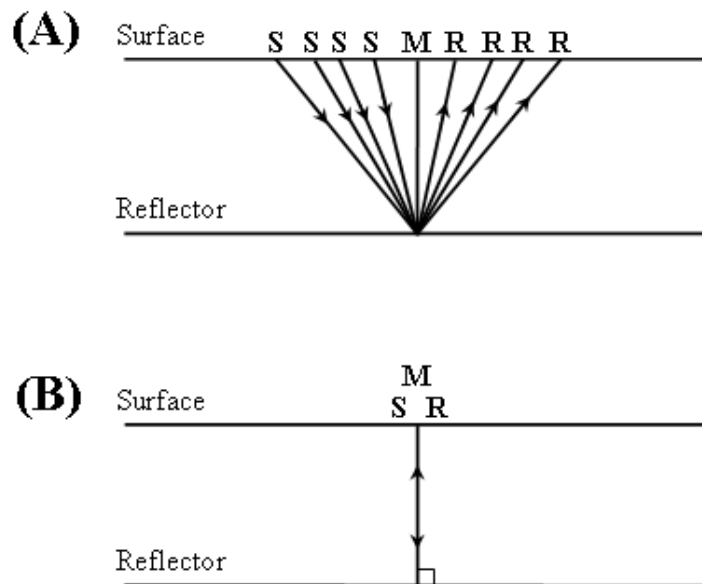


Figure 4.14: CMP traces of seismic energy (M) generated at sources points (S) reflected by a horizontal reflector and recorded at receiver points (R), before stacking (A) and after stacking (B).

Stacked sections before and after DMO and other processing applied to profile 4 and profile 5 can be seen in Figures 4.15 and 4.16, respectively. It can be seen that DMO correction has improved the seismic sections. In both seismic sections clear seismic reflections can be observed. Reflections of the base of the Quaternary are also evident at maximum TWT of about 500 ms in both seismic sections. Bowtie features due to crossing reflections are also evident.

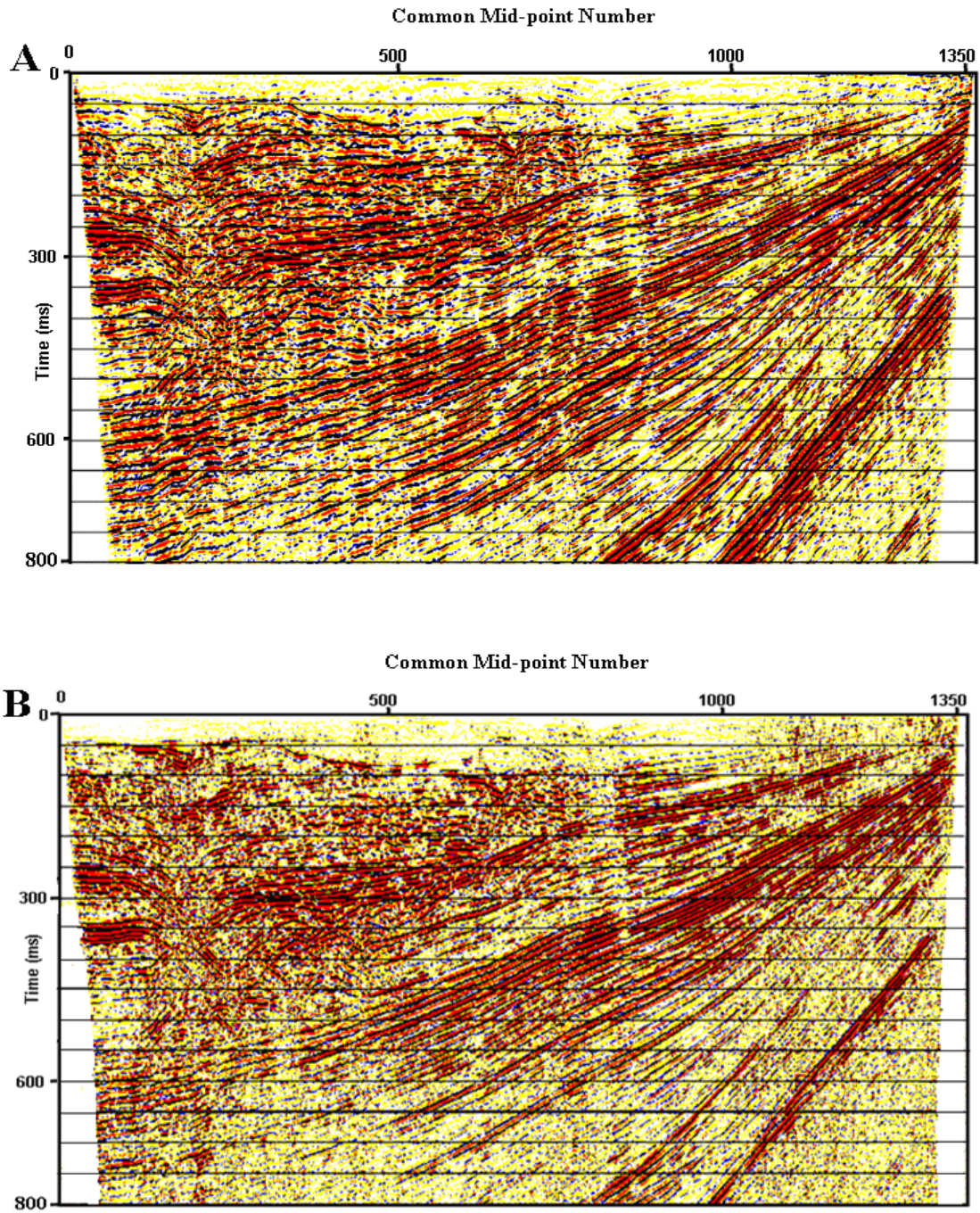


Figure 4.15: Stacked sections of profile 4 without (A) and with (B) DMO applied. Bowtie features due to crossing reflections are obvious at CMP 200 (300 ms).

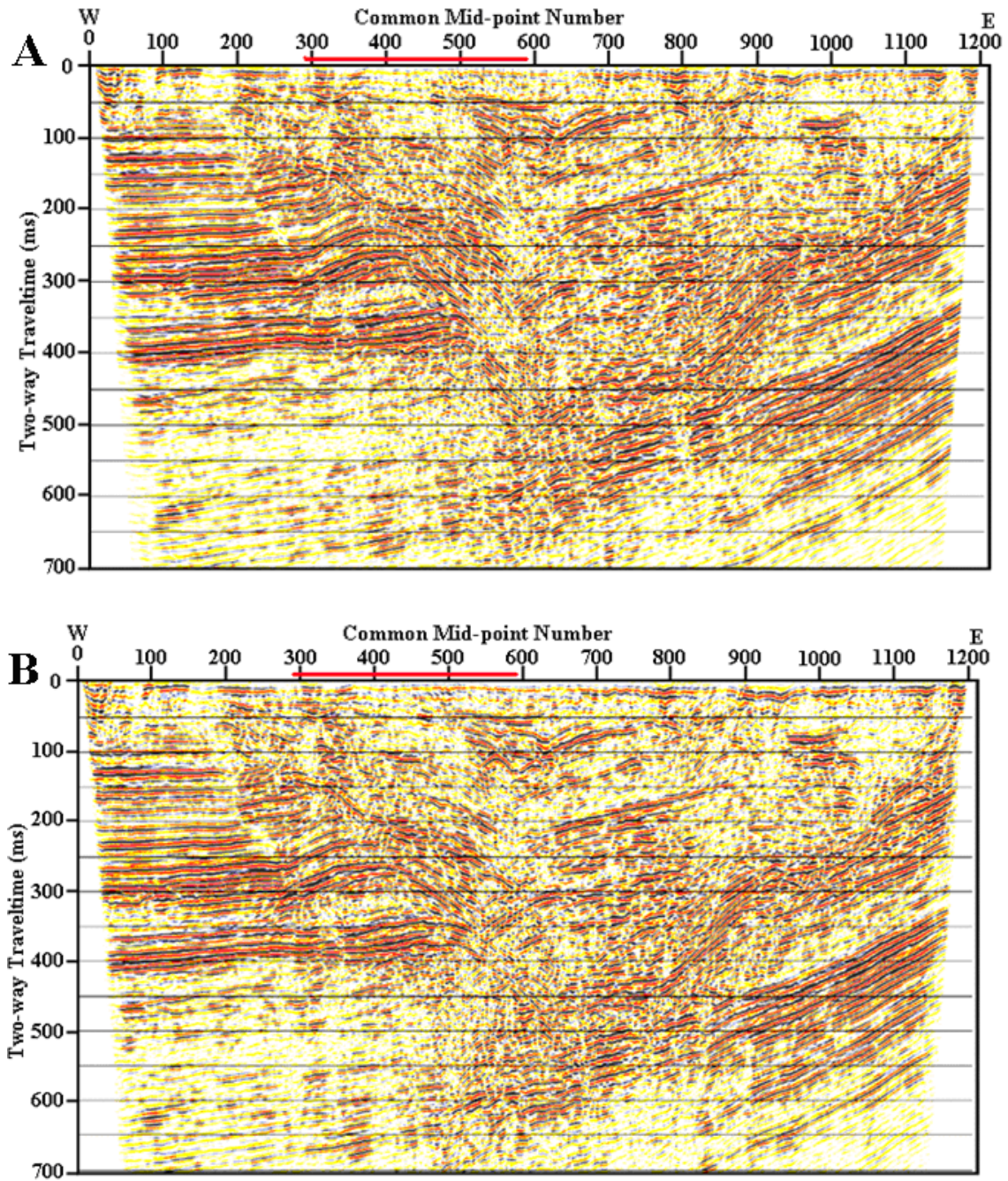


Figure 4.16: Stacked sections of profile 5 without (A) and with (B) DMO correction applied. Bowtie features due to crossing reflections are evident at CMP 600 (300 ms). The red line on top of the section (CMP 291-595) indicates the location of SH-wave profile.

Post-stack Deconvolution

Deconvolution was applied to the data after stacking to improve temporal resolution. FX deconvolution is a reliable multi channel noise-reduction filter. It preserves the most dominant dipping energy while removing random noise or dips with very low energy (Cary and Upham 1993). FX deconvolution produces a very natural looking result, with fewer artifacts than other methods (such as in FK and Radon filtering; Chase 1992). For this reason, it is highly favoured for post-stack noise attenuation. Although the danger of rejecting weak coherent signals is always there for stacked data, in practice FX deconvolution is surprisingly strong.

The FX deconvolution algorithm (Gulunay, 1986) applies (a) a Fourier transform to each trace of an input ensemble, (b) a complex Wiener prediction filter in distance for each frequency in a specified range (Robinson and Treitel 1964; Treitel 1974), and then (c) inverse transforms each resulting in frequency trace back to the time domain. Each sample in the transformed data has both real and imaginary components. Events with similar dips appear as a sinusoidally complex signals along a given frequency slice. The output trace should have less random noise than the input trace.

Migration

Migration is a process which attempts to correct the directions of the geological structures inherent in the seismic section. Migration redistributes energy in the seismic section to better image the true geological structures. It collapses the diffraction events in their apex and repositions the seismic reflectors at their correct locations. Bowtie structures are mostly corrected by the migration process.

Through the migration process, the stacked data were migrated in time, using two different algorithms: Kirchhoff migration and Steep Dip Explicit Finite Difference Time Migration (Yilmaz, 1987). Kirchhoff Time Migration performs a migration by applying a Green's function to each CDP location using a travelttime map. Travelttime maps relate the time from each surface location to a region of points in the subsurface. Kirchhoff Time migration uses a vertically and laterally variant root mean square velocity field (V_{RMS}) in time. It provides good handling of steep dips, up to 90 degrees, and of horizontal variation of velocity along the line.

A steep Dip Explicit Finite Difference Time Migration algorithm uses explicit F-X spatially-variant extrapolators to perform time migration. This migration is designed to be accurate up to approximately 70 degrees of dip. It uses a vertical and laterally-variant interval velocity field in time. The primary advantages of this approach are good handling of vertically variant velocities and relatively steep dips, and fair handling of lateral velocity variation. An example of a seismic line processed with Kirchhoff migration and with Steep Dip Migration is reported in Figures 4.17 and 4.18 for profiles 4 and profile 5, respectively.

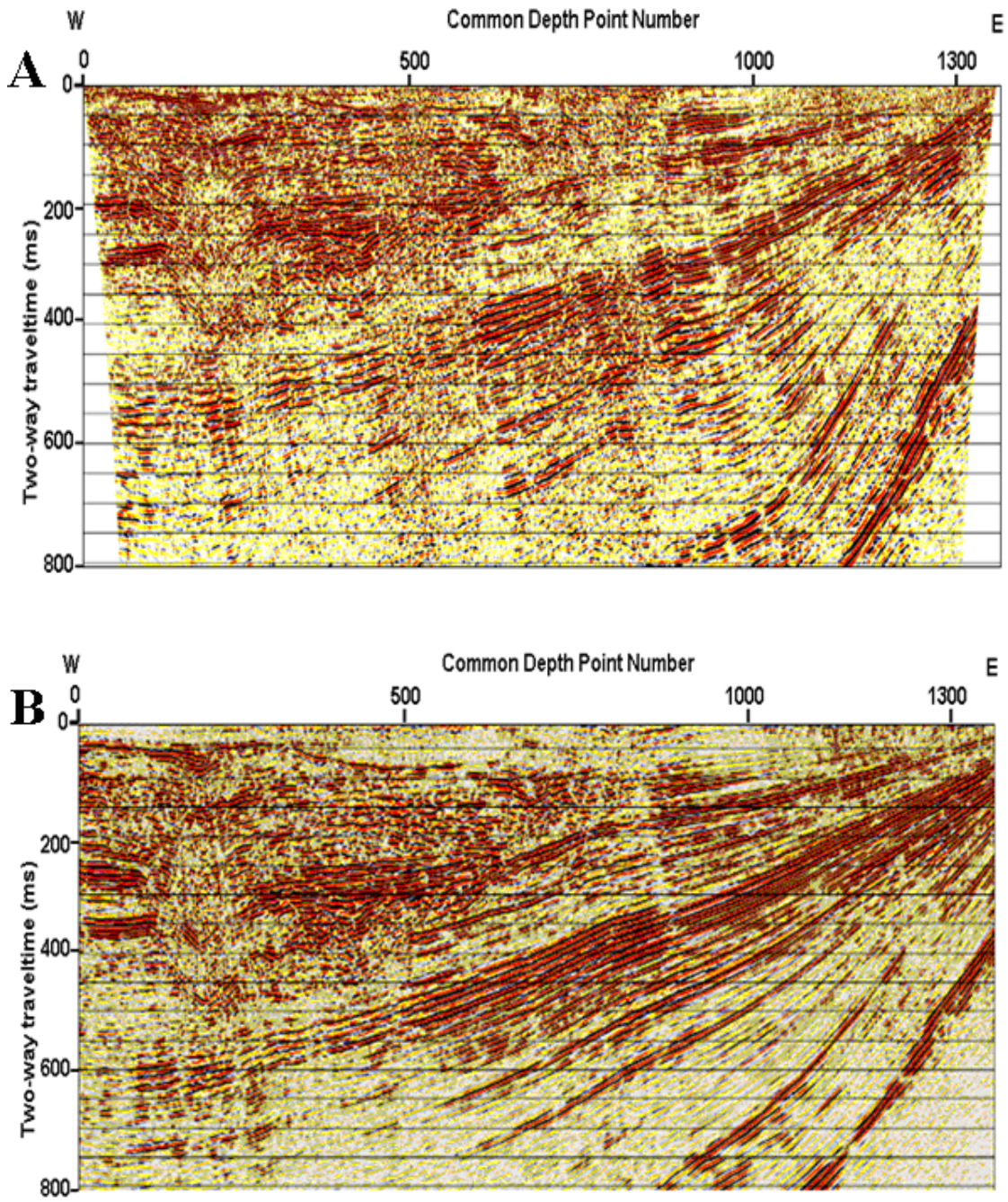


Figure 4.17: Migrated time sections of profile 4 using Kirchhoff Time Migration (A) and Steep Dip FFD Time Migration (B).

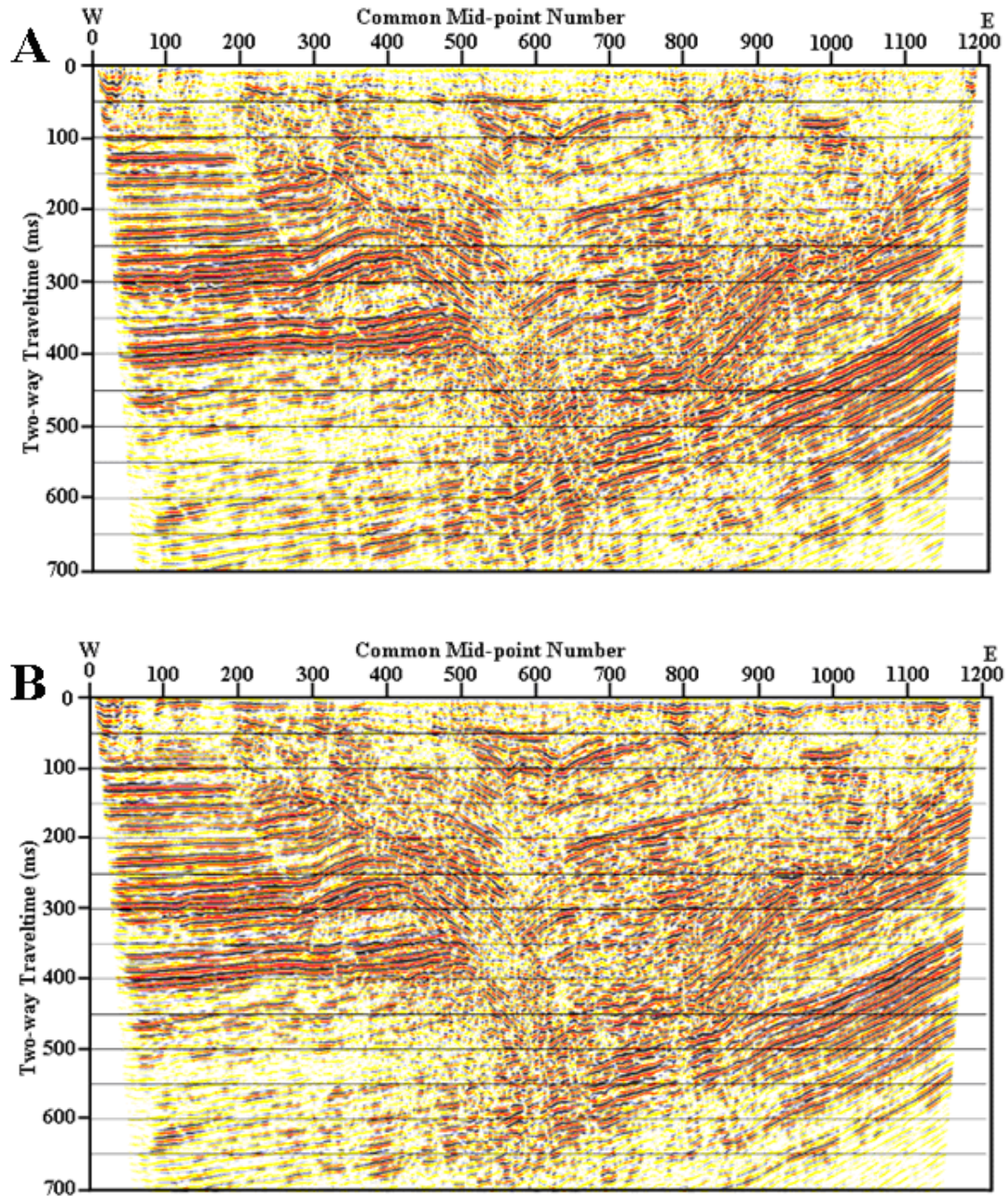


Figure 4.18: Migrated time sections of profile 5 using Kirchhoff Time Migration (A) and Steep Dip Time Migration (B).

Processing of SH-wave profile

The SH-wave seismic profile was acquired coincidentally with the P-wave seismic profile 5 between CMP291 and CMP595.

Data processing of the SH-wave survey was conducted using a sequence of steps similar to that of the P-wave data, except that the SH-wave data did not require the refraction-based static corrections. FK filtering was applied to SH-wave data to filter out Love waves which severely contaminated the data. The time-to-depth conversion was applied based on the stacking velocities used in the processing. The processing flow applied to the SH-wave data are given in Table 4.4.

Pre-stack Processing

The pre-stack processing processes include: vibroseis correlation, geometry definition, trace editing, amplitude gaining by AGC (250 ms), trace equalization and bandpass filtering (30-40-140-150 Hz).

Figure 4.19 compares between raw data with the sweep signal superimposed on the recorded signals (top) and raw data after the vibroseis correlation process has been carried out (bottom). After the vibroseis correlation events on the seismic data can be clearly identified.

Raw shot gathers from the SH-wave profile are shown in Figure 4.20A as well as the same shot gathers after the pre-stack processing was carried out (bottom).

FK Filtering

Velocity filtering is commonly used in S-wave data processing to attenuate the coherent noise. It is applied to reduce the effects of linear arriving noise (usually Love waves or refractions). On some data, these linear arrivals are easily removed or at least suppressed using slope filtering techniques.

After applying a simple FK filter using a conventional, narrow slice, focusing on the dominant linear surface wave arrival, the curved events immediately below the linear surface wave arrivals become pronounced. Based on their arrival pattern alone, they appear very reflection-

like. Without a doubt these arrivals would move out and stack coherently on CMP stacked sections. Figure 4.21 shows a shot gather from the SH-wave profile before and after application of FK filtering. The elimination of surface wave in the bottom of the Figure is evident.

Table 4.4: SH-wave seismic data processing sequence.

<i>Process step</i>	Description
Data reformat	From SEG-2 to ProMAX format
Vibroseis correlation	Correlated with pilot sweep
Geometry	Defined using field notes and loaded to headers
Trace Editing	Bad / noisy traces killed
Top Muting	Elimination of first arrivals and surface waves.
Spherical Divergence Correction	Multiply by $1/(t*v^{**2})$
Automatic Gain Control	250 ms spatially varying window
Bandpass Filter	Zero-phase Ormsby filters: 30-40-140-150 Hz
F-K filtering	Eliminate Love wave in FK domain
CMP sort	Sorted from shot gathers to midpoint gathers
Velocity analysis	Integrated analysis of shot gathers, constant velocity stacks, and semblance plots
NMO correction	Stretch mute 300%
CMP Stacking	Applied based on optimum stacking velocities, Summed NMO-corrected CMP gathers
F-X deconvolution	30-250 Hz
Steep Dip FD time Migration	Using interval velocity field
Time-to-depth conversion	Using single average velocity function

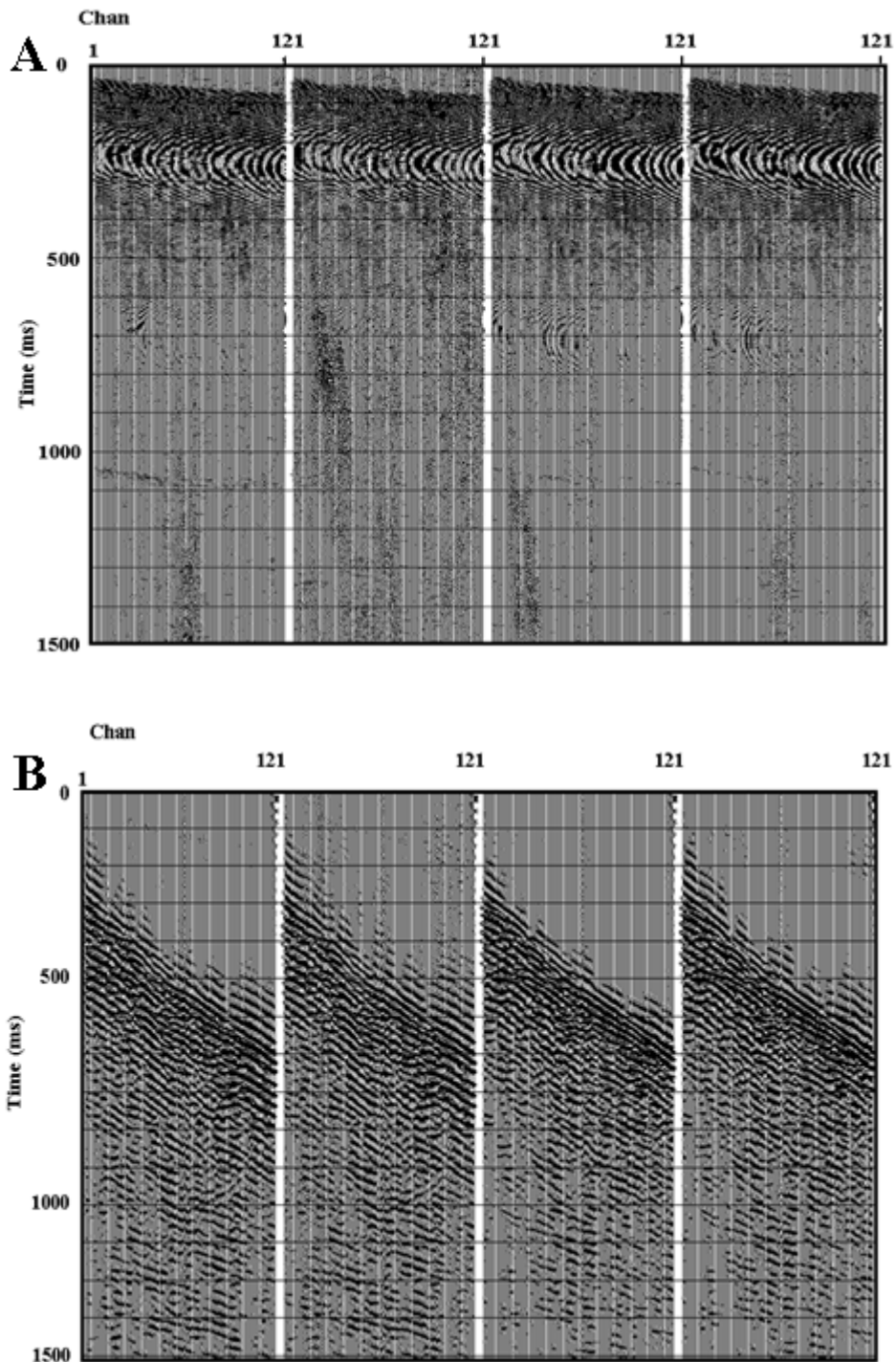


Figure 4.19: Uncorrelated (A) and correlated (B) SH-wave data (shot points 1, 2, 3 and 4) shown to first 1500 ms. Each shot point has 121 channels. Channel number 121 is the vibroseis sweep channel.

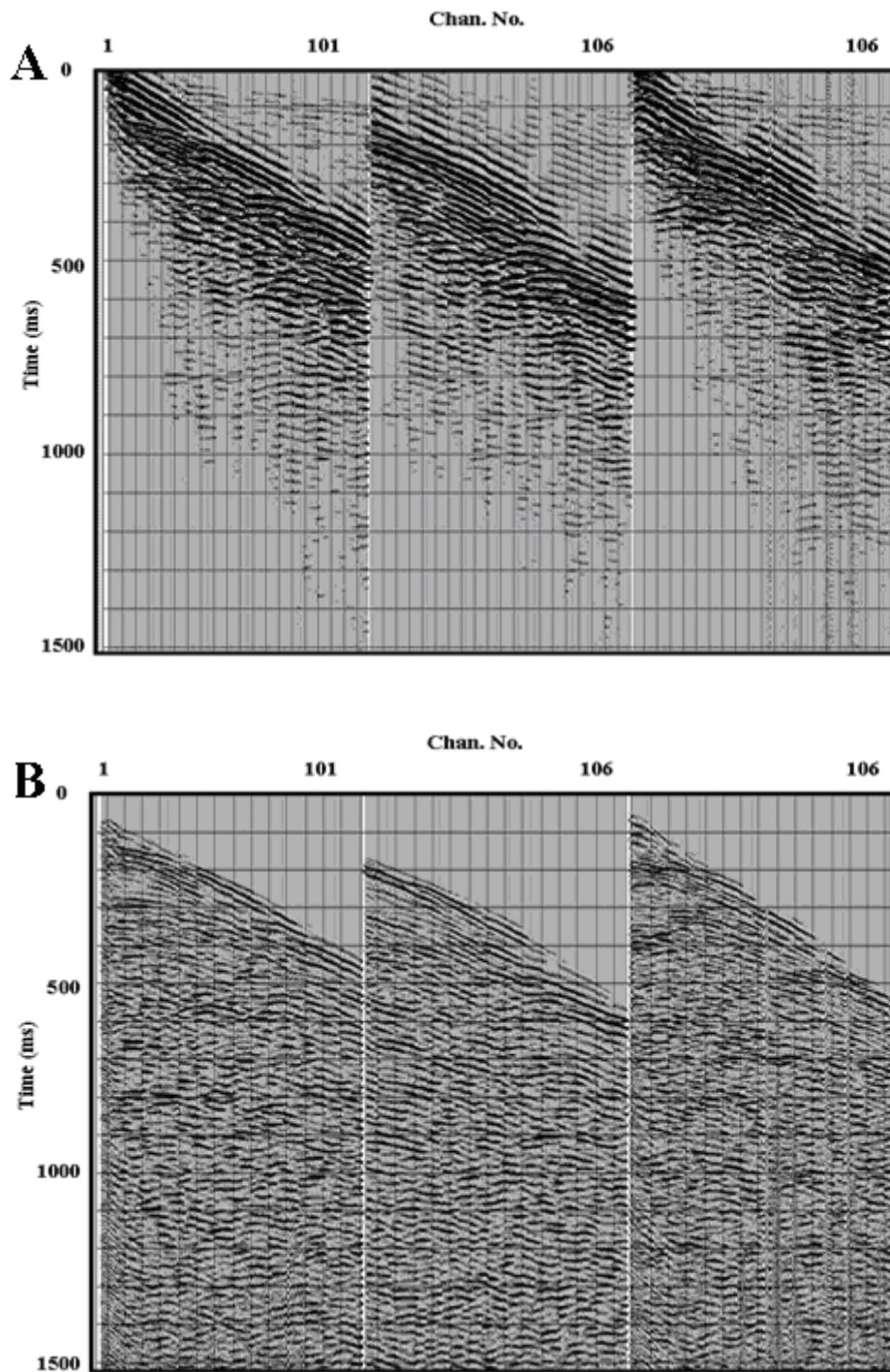


Figure 4.20: Raw shot gathers 1 (left), 2 (middle) and 3 (right) before (A) and after pre-processing applied (B).

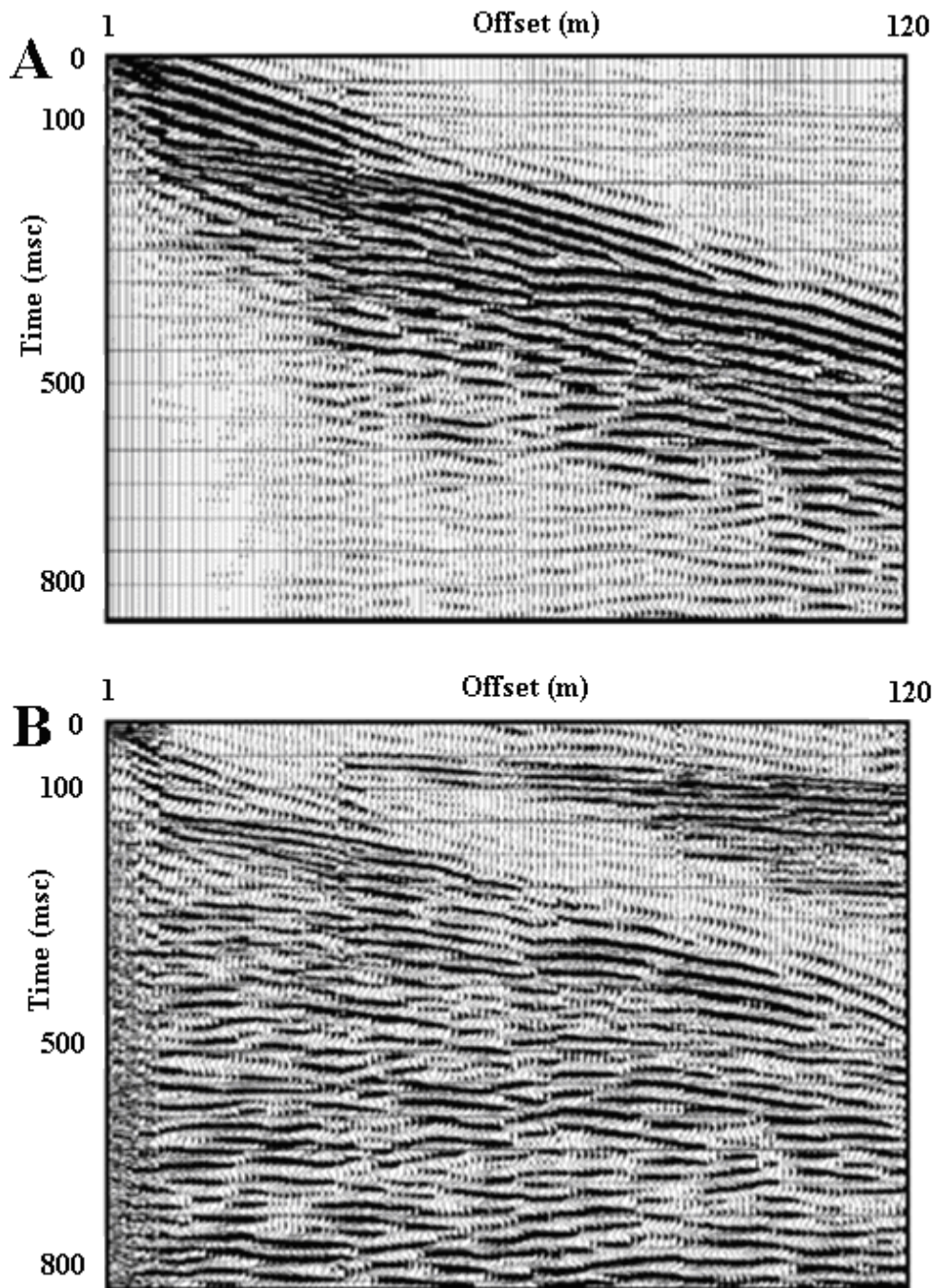


Figure 4.21: SH-wave raw shot gather before applying the FK filter (A), where coherent first arrivals are evident, and after applying the FK filter with some linear arrivals are eliminated (B).

Velocity Analysis

Constant velocity stacks (CVS) is another method of seismic velocity analysis. It allows for faster picking of velocities for maximum coherence on entire reflections. The velocity analysis on the NMO corrected seismic data is conducted using the CVS method as a first guess of velocities. Two things are important when generating CVS plots: First the maximum and minimum boundaries of the NMO velocities should be sufficiently identified. The second consideration when generating CVS plots (Figure 4.22) is ensuring that the velocity step-size is small enough between sequential CVS plots (Baker 1999). The NMO-corrected data is stacked and displayed as a panel for each different stacking velocity. Stacking velocities are picked directly from the constant velocity stack panel by choosing the velocity that yields the best stack response at a selected event. CVS has the disadvantage that the velocity is approximated as good as the distance between two test velocities. But it gives a general idea about the velocity of the reflections of interest.

Velocity analysis on the SH-wave data was conducted using CVS plots of the entire data set. The range of constant velocities used was between 200 to 800 m/s (suggested as the maximum and minimum boundaries of the NMO velocities to include the V_s shown by SH-wave data), with 40 m/s step size.

Figure 4.22 shows CVS panels from the velocity analysis on our SH-wave data. The panels show that the SH-wave data contain lateral velocity variations. However, coherent reflections, most likely to be primaries, allow picking velocities (assigned to each panel) for different record times. These velocities with times are used to orient the semblance velocity analysis of the SH-wave data.

Table 4.5 provides the sequence of velocities and times of some prominent reflections shown by the panels in Figure 4.22. The velocities and time provided are used as reference points to start the velocity analysis which is then carried out on semblance velocity plots.

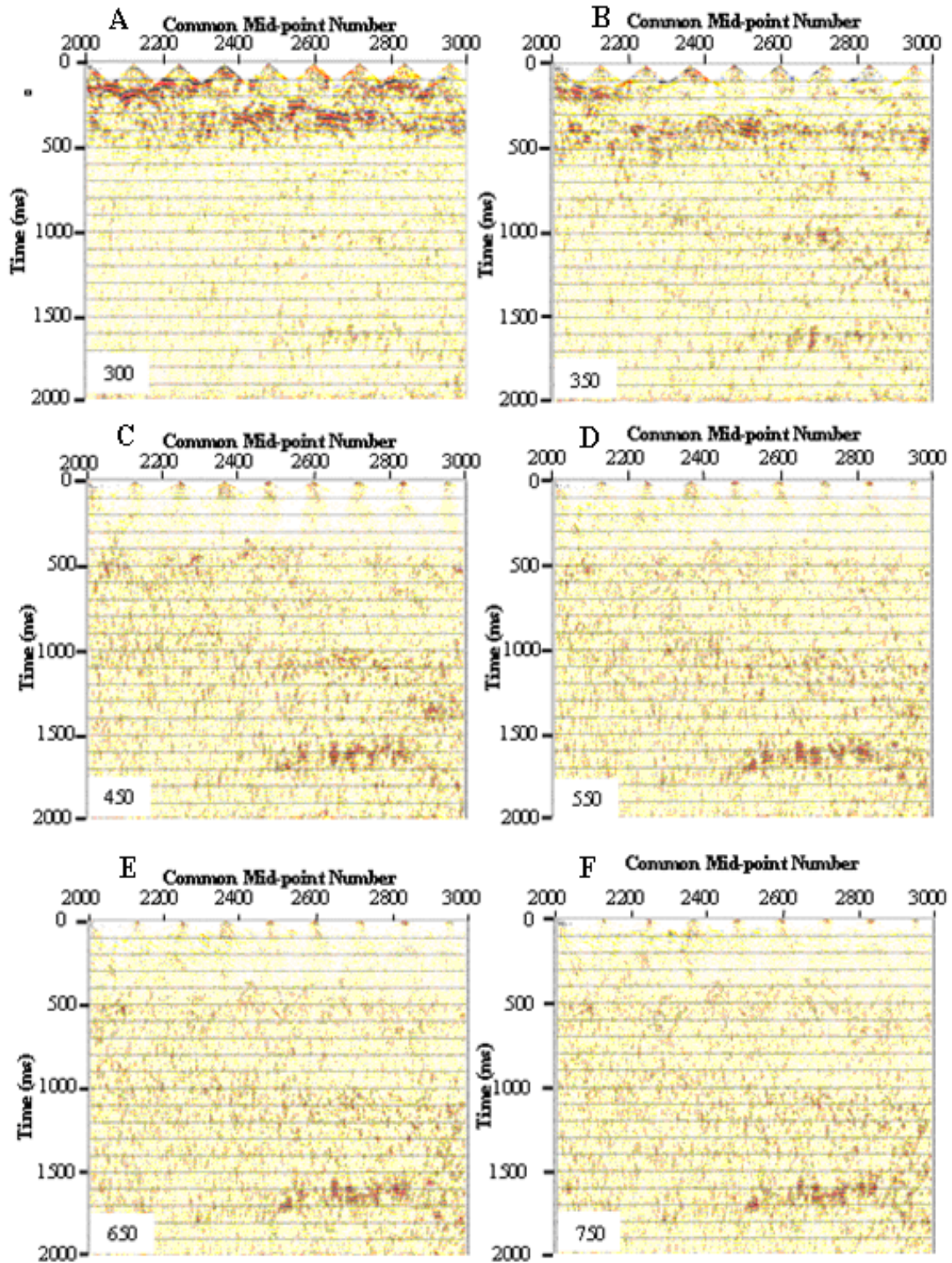


Figure 4.22: Several CVS panels (A, B, C, D, E and F) from the SH-wave profile. Each panel is assigned the velocity value in m/s with which a certain reflection becomes most coherent.

Table 4.5: Different velocities and times at which the velocities are picked for most prominent reflections in the common velocity stacks (CVS) panels from the velocity analysis of our SH-wave profile.

No.	Time (ms)	Velocity (m/s)
A	150	300
B	450	350
C	1100	450
D	1600	550
E	1650	650
F	1650	750

Figure 4.23 shows the smoothed stacking velocity field of the SH-wave profile generated from the semblance velocity analysis. The SH-wave velocity ranges from 200 m/s in the shallow parts to 720 m/s in the deeper part. Some horizontal variation in velocity shown in the lower part of the field, which indicates that Tertiary formations are characterized by higher Vs.

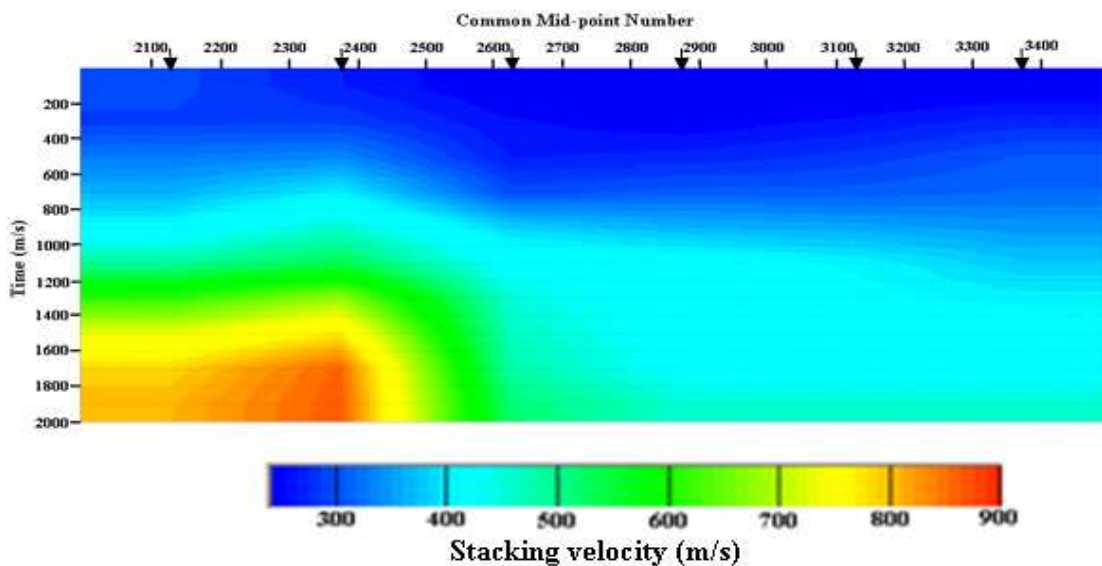


Figure 4.23: Stacking velocity field of the SH-wave profile. Arrows on top show the CMPs at which a semblance velocity analysis was conducted. The lower velocity value is about 250 m/s shown at the top of the velocity field (Quaternary sediments). Higher velocity values are shown by Tertiary sediments in the bottom left part of the velocity field (about 750 m/s). Velocity ranges from 250 m/s for Quaternary sediments to 850 m/s for Tertiary sediments.

CMP Stacking

Normal moveout (NMO) correction was performed on the CMP gathers using stacking velocities determined with constant velocity plots (Yilmaz, 2001). The CMP gathers were then stacked to produce reflection images, and to apply any necessary display processing. The location of the SH-wave section is highlighted by a double arrow line on the P-wave section in Figure 4.16 and can also be seen in Figures 1.3 and 2.1. The SH-wave stacked section in Figure 4.24 shows reflections with varying degree of resolution. The most coherent reflections are from the shallow part of the section. These reflections, highlighted by arrows on the left side of the section, are from Lauenburg Clay. Other discontinuous reflections are shown in the middle of the section at 550, 1000 and 1600 ms.

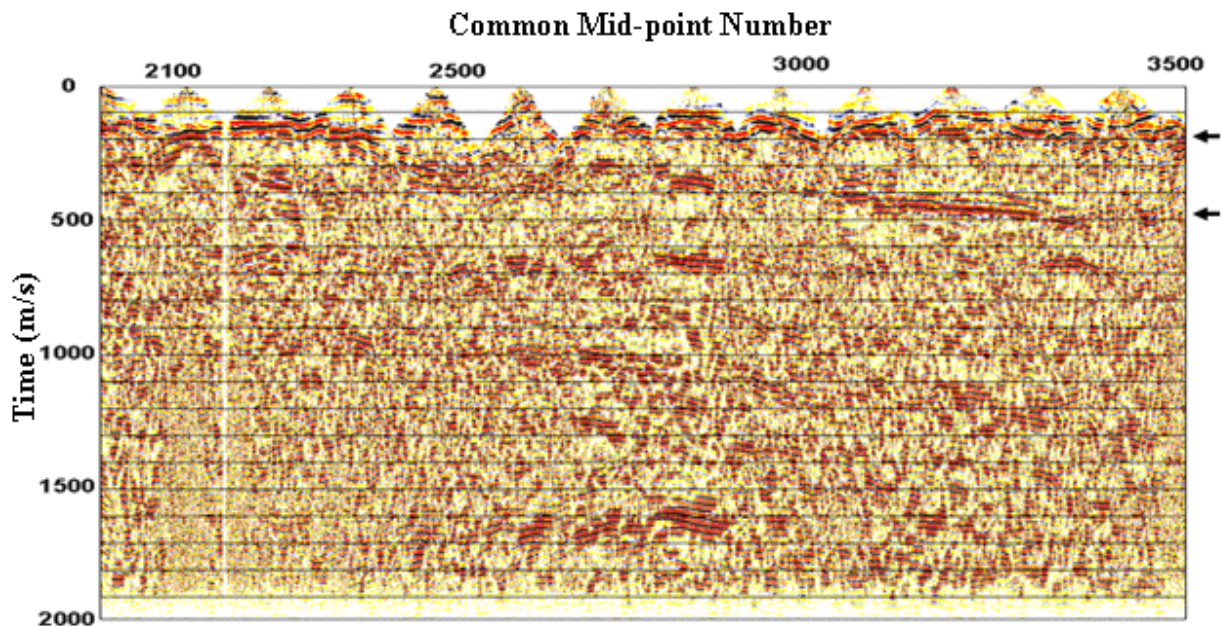


Figure 4.24: SH-wave stacked CMP section shows clear reflections of top and bottom of Lauenburg Clay at 200 and 500 ms (the two arrows on the right side). Other discontinuous reflections are also shown.

As is often the case, conversion of the time section to the depth section requires accurate velocity information. A detailed velocity field derived by interactive velocity analysis is used in converting the SH-wave time section in Figure 4.25 (A) to the depth section (B).

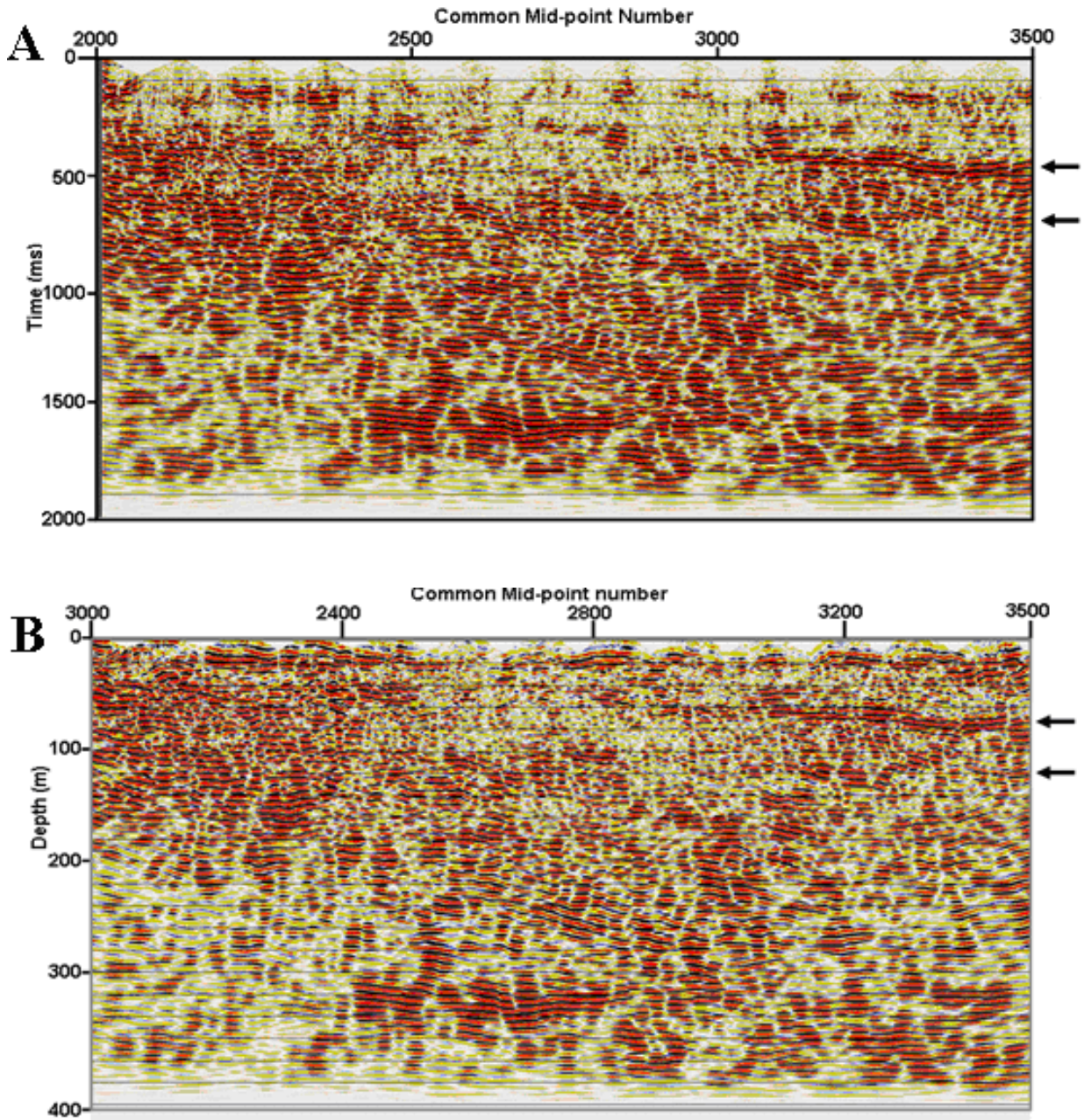


Figure 4.25: SH-wave time migrated section (top) and depth migrated section (bottom). Smearing effects due to the velocity field is evident in the bottom of the sections. The Lauenburg Clay (highlighted by two arrows on the right side) is shown between 200, 450 ms, and 30 and 70 m in top and bottom sections, respectively.

4.4 Vertical Seismic Profiling

A vertical seismic profile (VSP) is a measurement in which a seismic signal generated at the surface of the earth is recorded by geophones secured at various depths to the wall of a drilled well (Hardage, 1983). VSP has been employed to help determine the basic lithology and velocity in the vicinity of the borehole. It involves recording the complete waveform at regularly and closely spaced depth situations to extract average velocities with depth. Subsequently, these average velocities can be transformed to interval velocities. Therefore, one of the principal uses of the VSP is to determine the variation of seismic velocity with depth in-situ.

A VSP generally, gives better data than surface seismic methods, because the energy does not have to travel as far and therefore undergoes less attenuation. Consequently, the resolution of a VSP is usually significantly better than that of surface seismic data. The geologic models interpreted from VSP are more accurate and the velocity models are more useful in building a subsurface structure and stratigraphy than that extracted from surface seismic data.

4.4.1 Zero-offset VSP

There are various types of VSP surveys used in seismic exploration (e.g. Zero-offset, Offset and Walkaway VSP). Zero-offset VSP is applied in a vertical (or near vertical) borehole using a single source located near the well head. Most of the VSP surveys performed are of the zero- or near-offset type (Sheriff and Geldart 1995). The P-wave direct-arrival times from the zero-offset VSP can be used in a traveltimes inversion algorithm to obtain the P-wave interval velocities (Stewart 1984). Similarly, the arrival times of a source-generated mode-converted S-wave can be used to obtain the S-wave interval velocities. Thus a good estimate of the P- and S-wave interval velocities can be obtained from the zero-offset and offset VSP data. There is also considerable information in the reflected (upgoing) wave fields of the VSP data. The corridor stack from the zero-offset VSP can be used in a composite plot to help correlate seismic events with well logs (Stewart and DiSiena 1989). Table 4.6 highlights some objectives of Zero-offset VSP.

Table 4.6: Some objectives of Vertical Seismic Profiling (VSP) surveys (modified after Gilpatrick and Fouquet 1989).

Objectives	How achieved
Reflector identification	
Surface-to-BH correlation	Upgoing wave studies on zero-offset VSP
Increased resolution at depth	
Time-depth conversion	
Enhanced velocity analysis	First break studies on zero-offset VSP
Log calibration	
Multiple identification	
Deconvolution operator	Downgoing wave studies on zero-offset VSP
Permeability studies	Tube-wave analysis research study

The prime purpose of the present VSP data is to estimate sediment velocities as a function of depth. These velocities are then used in time-to-depth conversion of surface seismic data. They are also used in estimating physical parameters and in the lithologic delineation and mapping process by tying them with surface seismic data.

VSP data signals

Four kinds of seismic signals are detected by a geophone (receiver) placed in a well when a source located on the surface is activated. These signals are:

- (1) Direct waves causing the first breaks,
- (2) Upgoing reflections,
- (3) Downgoing reflections resulting from the reflection of upgoing waves, and
- (4) Tube waves.

The first arrival on a VSP trace is a direct arrival from above. The time of this arrival, together with the change of the time of arrival with depth of geophone is used for the velocity determination.

Tube waves can be used for permeability studies of the fractured rocks (Huang and Hunter 1981). Mjelde (1992) used high resolution tube waves to reveal layers that are too thin to be detected by body-waves.

Noise in VSP records

There may be many types of noise in VSP records from different sources such as cable waves, geophone clamping, multiple strings of well casing and resonance in multiple casing strings, mechanical and electrical noise, drill site work activities such as welding, stacking pipe and metal goods, and general rig site maintenance and tube waves on VSP data. Other factors, such as field geometry, precise depth control, recording system gain, and correct depth sampling should be considered.

4.4.2 Instrumentation and Recording of the VSP Data

In the present VSP study a vibrator seismic source was located close to the wellhead and a 3-component geophone (3-C) was lowered in the well. A schematic cross section of a typical VSP field layout is provided in Figure 4.26.

The two Zero-offset VSP surveys at BH3914 and BH3786 were carried out in 2005 (Rumpel et al. 2005a). The profile depths was from 2 to 176 m and from 4 to 302 m, respectively, with a shot point interval of 4 m, recording length 12 s and sampling rate of 1 ms. The LIAG P-wave vibrator was applied as the seismic source and the receiver was a single-level 3-C mechanically clamped geophone. The sweep frequency was varied linearly from 20 Hz to 200 Hz. The vibrator seismic sources were 9.85 m and 15 m offset from BH3914 and BH3786, respectively. Details about the field layout are provided in Table 4.7.

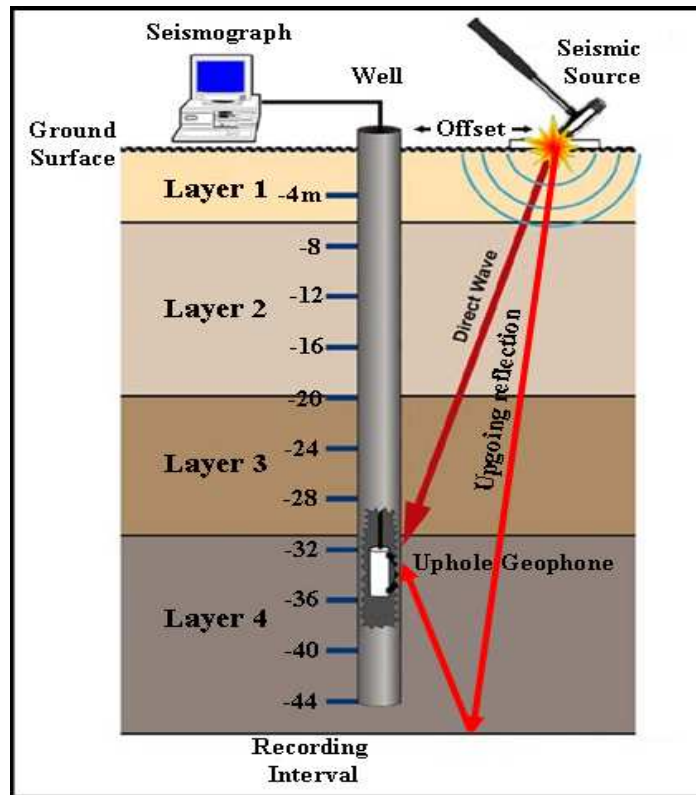


Figure 4.26: Schematic cross section of a typical VSP field layout indicating a survey borehole, seismic source, receiver, wireline and recording seismograph.

Table 4.7: VSP data acquisition: equipments and parameters.

Item	Description
Instruments	
Seismic source	LIAG Kleinvibrator: MHV2.7
Sweep type	50-200 Hz Linear, 10 s
Recording Instrument	Aladin (Antares Datensysteme GmbH, Stuhr)
VSP-sonde	Digital VSP-Sonde, type No. 1306, 3-component (x,y,z, 14 Hz)
Reference channel	P=Y
Geometry	
Station Interval	6m (BH3914), 4m (BH3786)
Source – borehole distance	9.8m (BH3914), 15m (BH3786)
Instrument orientation	314° N
Depth measured	176 (BH3914), 302 (BH3786)
Recording	
Sample interval	1 ms
Recording length	12000 ms
Pre-amplitude gain	Data=128, Reference=136 dB
Field format	SEG Standard

4.4.3 VSP Data Analysis and Processing

The present VSP data, Figures 4.27 and 4.28, show strong first arrivals and upgoing energy. The data is also contaminated by tube waves which have to be muted before the data is stacked. Nevertheless, the reflected tube waves can give hints for more permeable zones in the geologic formations penetrated by the well.

The VSP data is processed to reduce noise, separate the upgoing and downgoing wavefields and generate corridor stack sections. A standard processing procedure (Balch and Lee, 1984; Hardage 1983) is followed to process the VSP data in the two wells. Table 4.8 shows the processing sequence applied to the present data. The VSP data were processed using the ProMAX software which was used for processing surface seismic data. A module in the programme was used (VSP Module).

Table 4.8: VSP data processing sequence.

Process	Description
Vibroseis correlation	Correlate with vibroseis sweep
Correlation for tool rotation	Separate vertical component for further processing
Trace Editing	Visually inspect shots and delete excessively noisy shot traces.
Bandpass Filter	Apply zero-phase bandpass filter (40-60-200-250 Hz)
Spherical divergence corrections	Multiply by $1/(t*v**2)$
Picking of the first arrival	Calculate first breaks
Wavefield separation	Subtract downgoing wave energy from the total wavefield to yield the upgoing wave energy
Deconvolution	Design inverse deconvolution filter on the downgoing wavefield and apply to the upgoing wavefield
Two-way travelttime correction	Apply twice the first-break time to shift traces to two-way travelttime
NMO correction	Apply one way NMO correction
Stacking	Stack all levels into a single trace
Slicing	Cross correlate with CMP data

First, the raw data is correlated with the vibroseis sweep signal. Then the rotation correction to the 3-C data was carried out to separate the recorded waveform to its 3 components (X, Y and Z; Figure 4.27). Of particular interest in the present study is the Z or vertical component (Figure 4.28). From the Z-component raw data, bad traces were removed and first arrival times were picked from the raw data (Figure 4.29). Trace equalization was applied to correct for shot strength variation and near surface geology changes. Also spherical divergence was corrected.

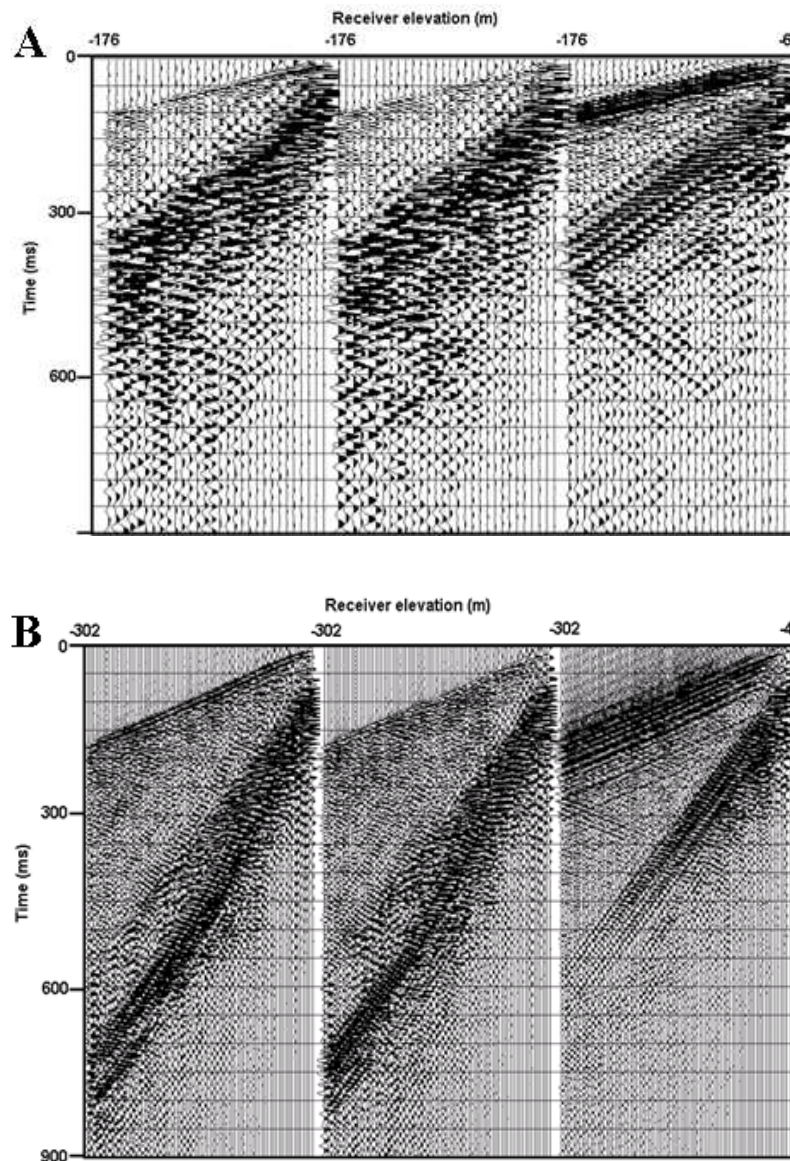


Figure 4.27: The waveform is rotated and separated to its 3 components: X (left), Y (middle) and Z (right) components. **A:** The components of the VSP at BH3914 and **B:** The components of the VSP at BH3786.

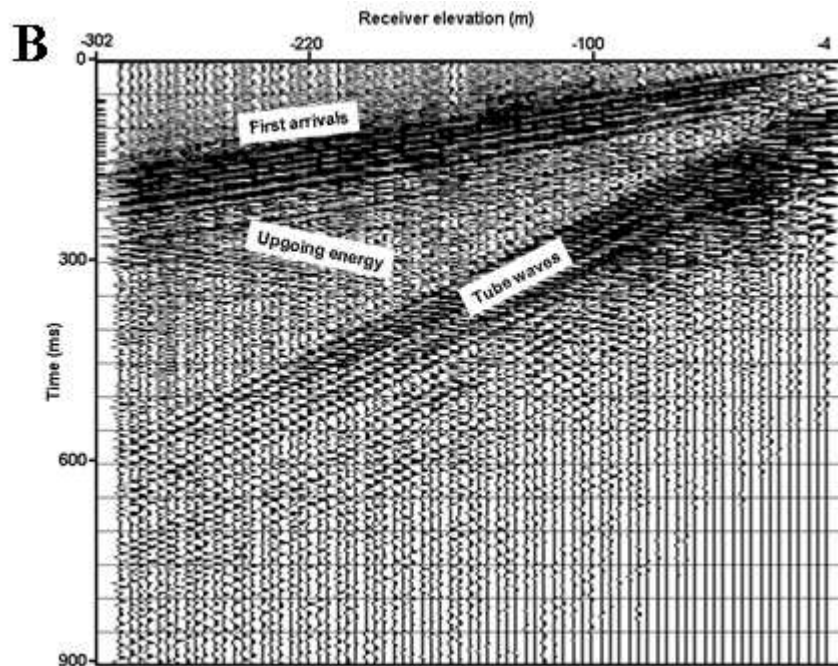
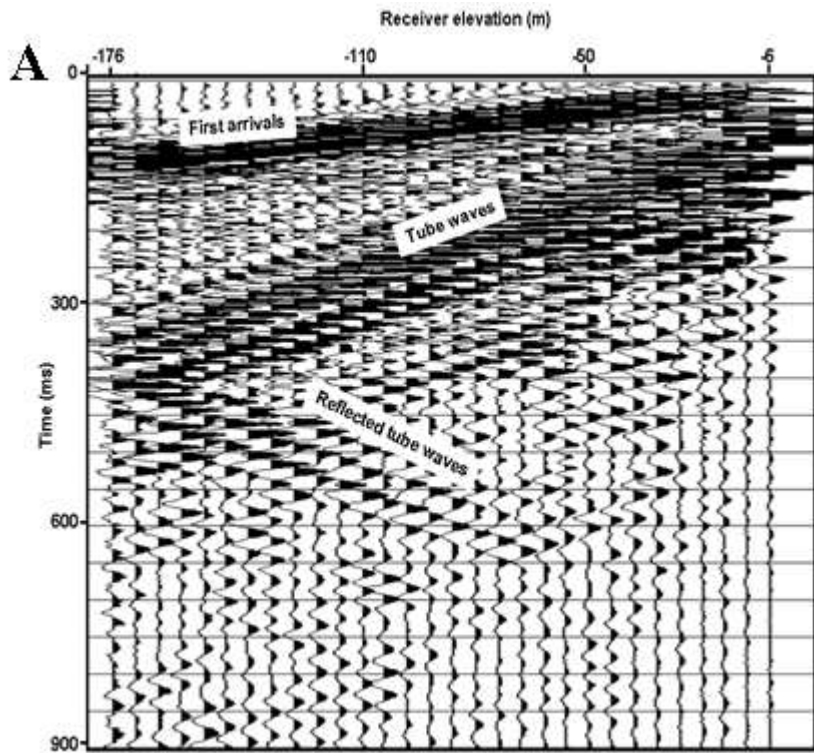


Figure 4.28: The VSP Z-component shows strong first arrivals, upgoing energy, tube waves and reflected tube waves. (A) is the Z-component of the VSP at BH3914 and (B) is the Z-component of the VSP at BH3786.

Velocity Determination

Picking of the first-break times of the first arrival waves that travel at P-wave velocity provide a time-depth profile for the sampled interval. These times must be picked as consistently and accurately as possible (see Figure 4.29). The potential for error is much greater at shallower depths because of poor coupling between the casing and the borehole wall, which leads to lower signal-to-noise ratios.

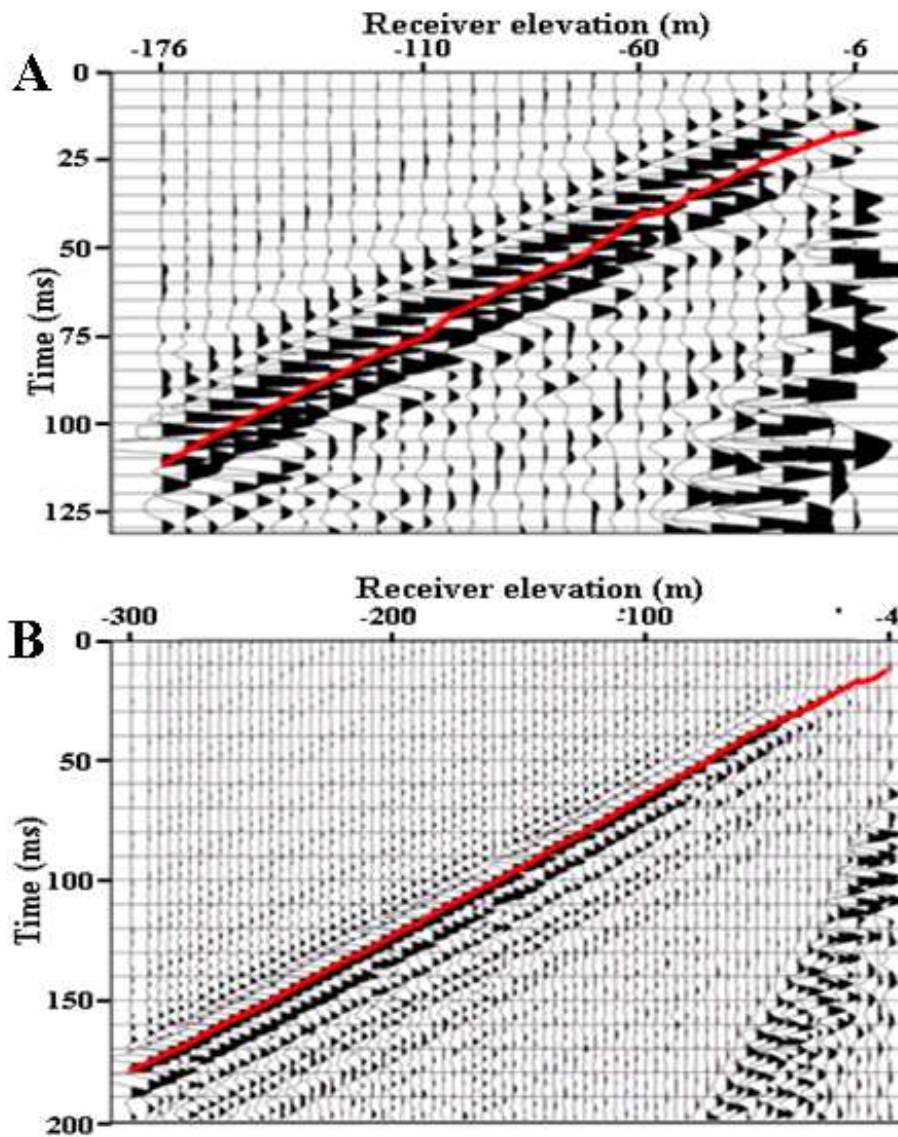


Figure 4.29: Processed VSP data of BH3914 (A) and BH3786 (B). First break picking for velocity calculation is shown by red lines.

The average velocity of the direct wave for every source-receiver pair is calculated by

$$v = r / t \quad (4.17)$$

where v is the interval velocity in depth between the source receiver pairs, r is the straight-line distance between the source and the receiver pair, and t is the first break pick time for a source-receiver pair (see Figure 4.30).

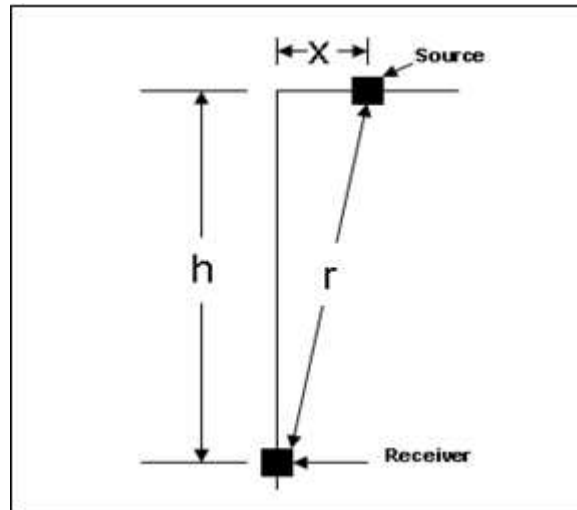


Figure 4.30: Cross section showing the source at the earth's surface and a receiver at depth h . The source is offset a horizontal distance (x) from the receiver. This configuration can be used to derive an average-velocity-with-depth function.

This calculation assumes that the waves travel from the source to a receiver with no ray bending, therefore, the error in velocity calculation decreases with decreasing distance between the well and the source and with increasing depth.

The interval velocities derived above are plotted in Figure 4.31 along with the lithological logs. There is a good correlation between the lithology and the seismic velocity data from the two wells. The both wells show a general increase of V_p and V_s with depth. The increase of velocity with depth can be related to an increase in compaction, increase in density, decrease in porosity, and/or changes in lithological composition.

There are some parts of V_p and V_s where the velocity decreases. The decrease of velocities seems to be associated with local changes in lithology.

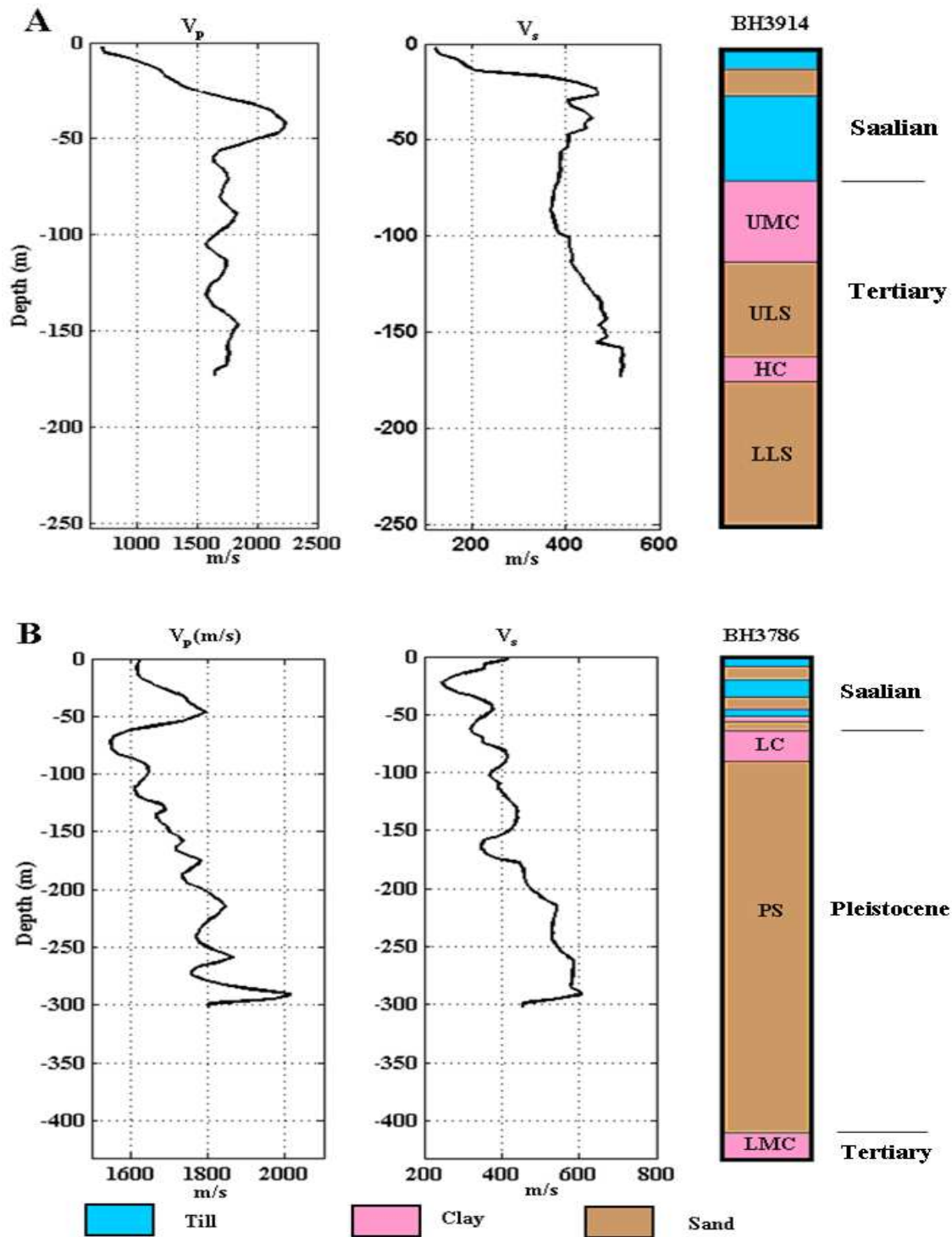


Figure 4.31: P- and S-wave interval velocities (V_p and V_s , respectively; in m/s) derived from VSP data from BH3914 (A) and BH3786 (B), correlated with the lithological logs of each borehole. Velocities are in m/s; horizontal lines follow the major geological units as shown by lithological columns. LC = Lauenburg Clay; UMC = Upper Mica Clay; ULS = Upper Lignite Sand; HC = Hamburg Clay; LLS = Lower Lignite Sand; LMC = Lower Mica Clay.

Obviously, clay layers show lower velocity values than sand layers in both Tertiary and Quaternary formations. Therefore, higher values could be related to a decrease in clay content and the low values in velocities could be related to rather high clay content in the Pleistocene sand.

Wavefield Separation

Although different types of waves are recorded by the VSP, only reflected P-waves (upgoing waves) are of interest here. Therefore, the upgoing wave field must be separated from the downgoing wave field. Reflections have a slope opposite to the first breaks. By using this difference it is possible to separate downgoing waves from upgoing waves. A variety of techniques has been developed for this purpose. Here we have tried to isolate the upgoing energy from the downgoing energy. We looked at three different methods for the separation:

1- Median.

2- FK filter.

3- Eigen Vector filter.

After testing the three filters the Median filter produces the best results. Figure 4.32 shows the separated upgoing wave fields of the VSPs at BH 3914 and BH 3786, respectively.

Deconvolution

Because we know both the input and the desired output (a single spike), a Wiener filter can be designed to remove surface multiples almost completely (VSP deconvolution).

Moreover, the downgoing and upgoing multiples differ mainly by an additional reflection at or near the surface (which acts as a simple interface); therefore, the upgoing multiples pattern will be nearly the same as that of the downgoing multiples, so the extracted upgoing wavefields were deconvolved to increase the frequency bandwidth and suppress noise, multiples and tube waves. The selection of a good deconvolution operator window size is based on its ability to collapse the downgoing energy into a single, band-limited spike. The deconvolution design

window was 200 ms with an operator length of 20 ms and 1% pre-whitening. Using the designed deconvolution operator, the upgoing wavefields were deconvolved.

Stacking

The traces of upgoing VSP energy are often stacked together to yield the pattern of primary reflections for correlating them with conventional surface seismic data. Only the portions just below the well geophone are stacked in a corridor stack: these portions are generally relatively free of multiples.

The upgoing wavefields were corrected to two-way-time and the corridor stacks of the two VSPs are shown in Figure 4.33. They are better than synthetic seismograms made for well log measurements for relating reflections to interfaces because the measurements are made at seismic frequencies and are not sensitive to logging uncertainties. Stacks of the portions of offset VSPs involving reflection points nearest to the boreholes are also used for this purpose.

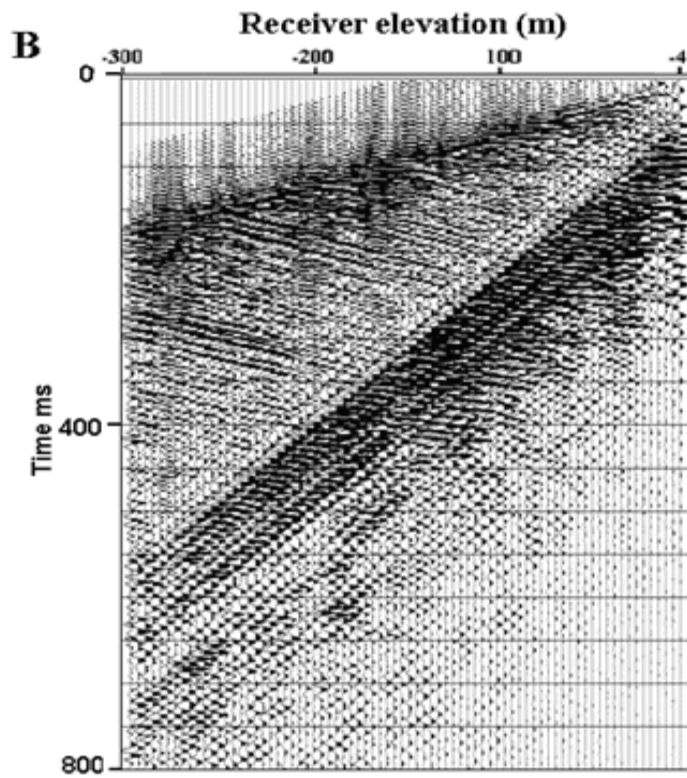
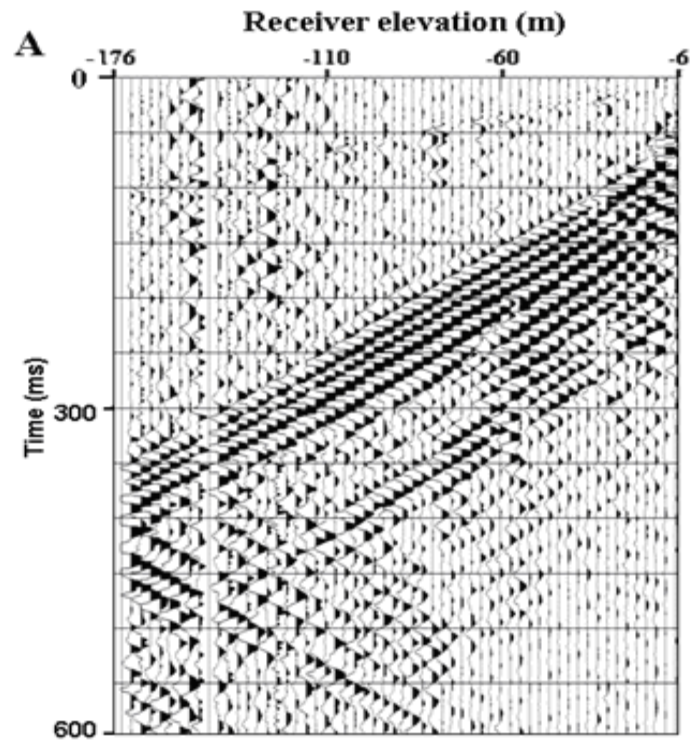


Figure 4.32: The separated upgoing energy, using median filter, of VSP at BH3914 (A) and BH3786 (B).

The corridor, a short interval following the first arrival in an upgoing VSP in the two-way-travel time, was defined and the inner corridor was muted. The corridor stack, which is a summation of some of the traces in the upgoing VSP, is repeated five times (Figure 4.33 c and f).

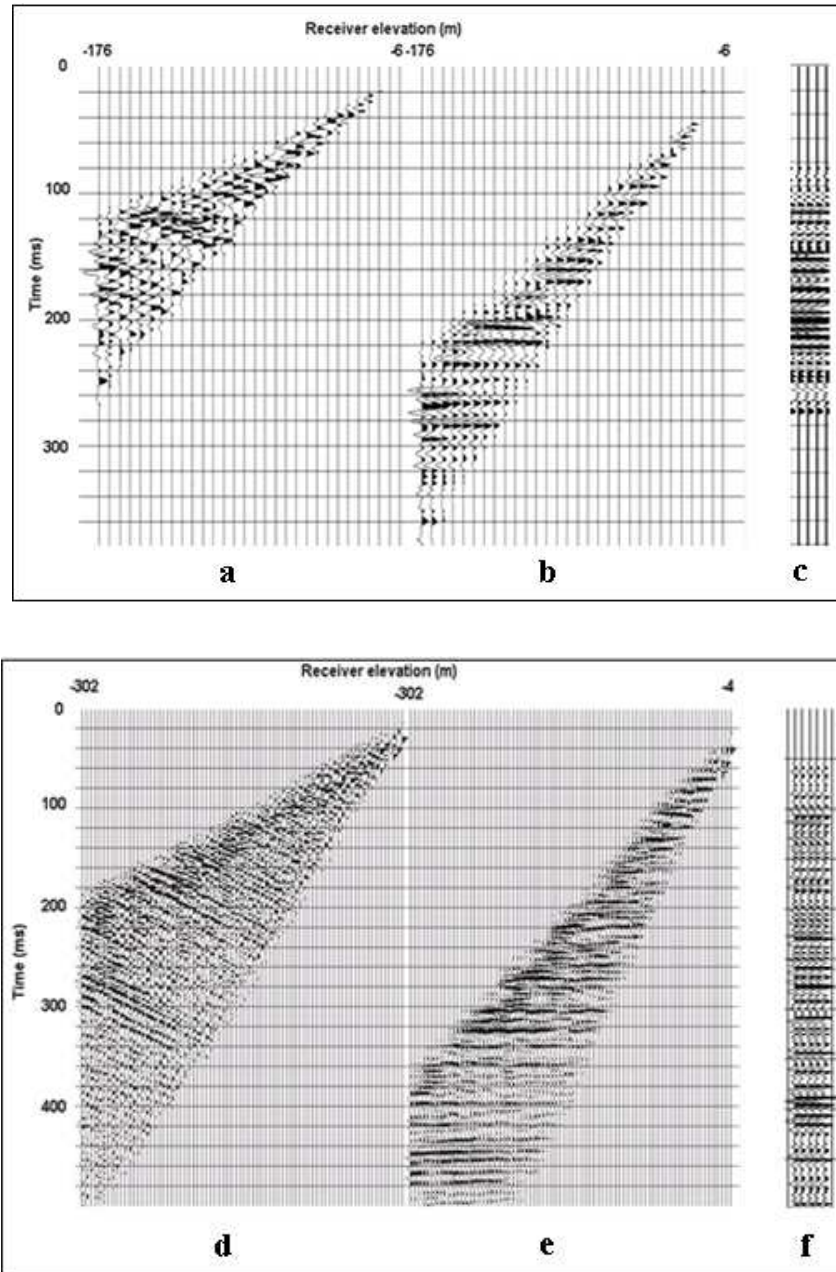


Figure 4.33: VSP results at BH3914: (a) upgoing waves, (b) upgoing waves corrected to two-way-travel time, with top and bottom mute; (c) corridor stack repeated 5 times; and BH3786: (d) upgoing waves, (e) upgoing waves corrected to two-way-travel time, with top and bottom mute and (f) corridor stack repeated 5 times.

4.5 Time-Depth Conversion of Surface Seismic Data

Time to depth conversion is a process aiming at producing a depth model, from a time interpretation, of underground geological structures. Each of the time to depth conversion processes relies on an underlying assumption on a velocity model and shows its own limitations when checking the calibration to the geological structures as seen in the wells.

As a last process, depth migration is applied to the time migrated sections. This is shown in the Figures 4.17B and 4.18B using the P-wave velocity functions derived from VSP at BH3914 and BH3786 (Figure 4.31), respectively. The resulting depth migrated sections of profile 4 and profile 5 are depicted in Figure 4.34.

Compared to the time migrated sections shown in Figures 4.17 (B) and 4.18 (B), the depth sections provided in Figure 4.34 appear clearer and events are better resolved.

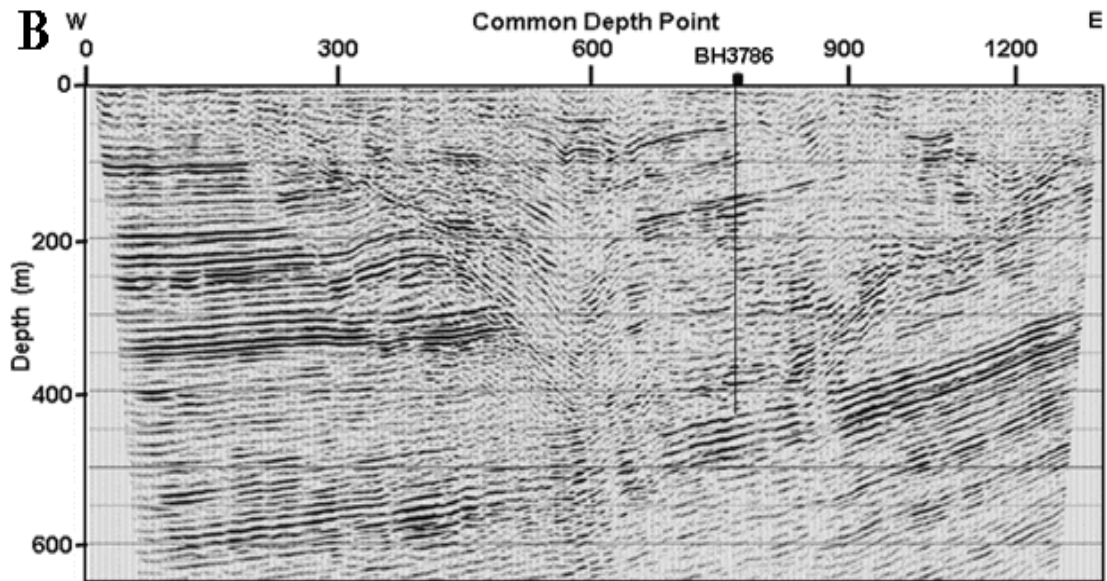
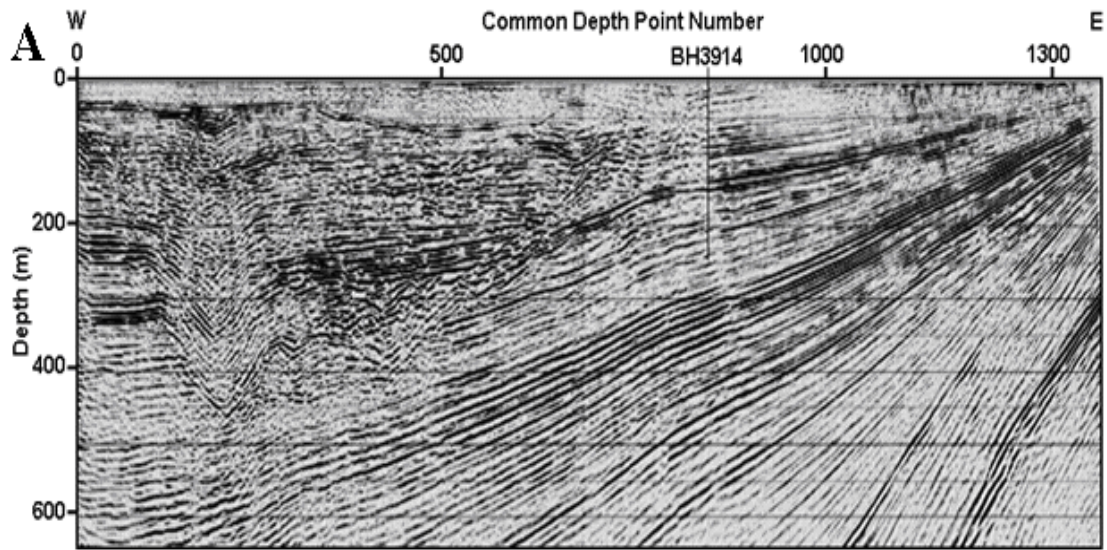


Figure 4.34: Poststack depth migrated sections of profile 4 (A) and profile 5 (B) using interval velocity functions calculated from VSP at BH3914 and BH3786, respectively.

4.6 Development of Workflow for Velocity Estimation Optimized for Geophysical Characterization

The velocity is the key parameter in seismic investigation. Obviously it is a non-linear product of all elastic properties for a given formation. The mostly one used in characterizing the subsurface is the P-wave velocity which is the fastest, associated with compressional stress and has longitudinal attitude of motion. The S-wave comes second, is associated with shear stress and has transverse motion. In seismic exploration, the variation of velocity reflects variation in elastic properties of the layers and hence variation in lithology. Estimation of the velocity is important to express correctly reflections on final stacked section.

The seismic velocity is also important for converting seismic data from the time domain to the depth domain, as shown in section 4.5, and is also an aid for geological interpretation.

The seismic velocity of different geological formations can be measured in the field by using surface as well as well logging measurements. It is also measured in the laboratory (e.g. Prasad and Meissner 1992). In the present study an integrated seismic velocity analysis has been carried out from field data including surface and vertical seismic profiling. A simple workflow was followed to calculate as accurate as possible the velocities of the highly heterogeneous Quaternary sediments in the buried valley as well as in the surrounding Tertiary horizons.

First, a velocity analysis on the NMO corrected data of the seismic profiles (P- and SH-waves) was conducted using the constant-velocity-stack (CVS) method as a first guess of the velocity. The range of constant velocities used was from 700 to 3000 m/s for P-wave profiles and from 200 to 800 m/s as maximum and minimum boundaries of the NMO velocities, with 200 m/s and 50 m/s step size, respectively.

Second, the stacking velocities were hand-picked from the displayed semblance plot, as mentioned before (see also Figure 4.35), smoothed and displayed in 2-D stacking velocity fields for P-wave and SH-wave profiles as shown by Figures 4.12 and 4.23, respectively. The velocity fields were used to initially stack the seismic data.

Third, after DMO was applied, the semblance analysis was repeated on the post-DMO CMP gathers. New stack sections were created using the new stacking velocities and compared to the

initial stacks. The new velocity fields were used to generate interval velocity fields (Figure 4.13), using Dix's equation (4.16).

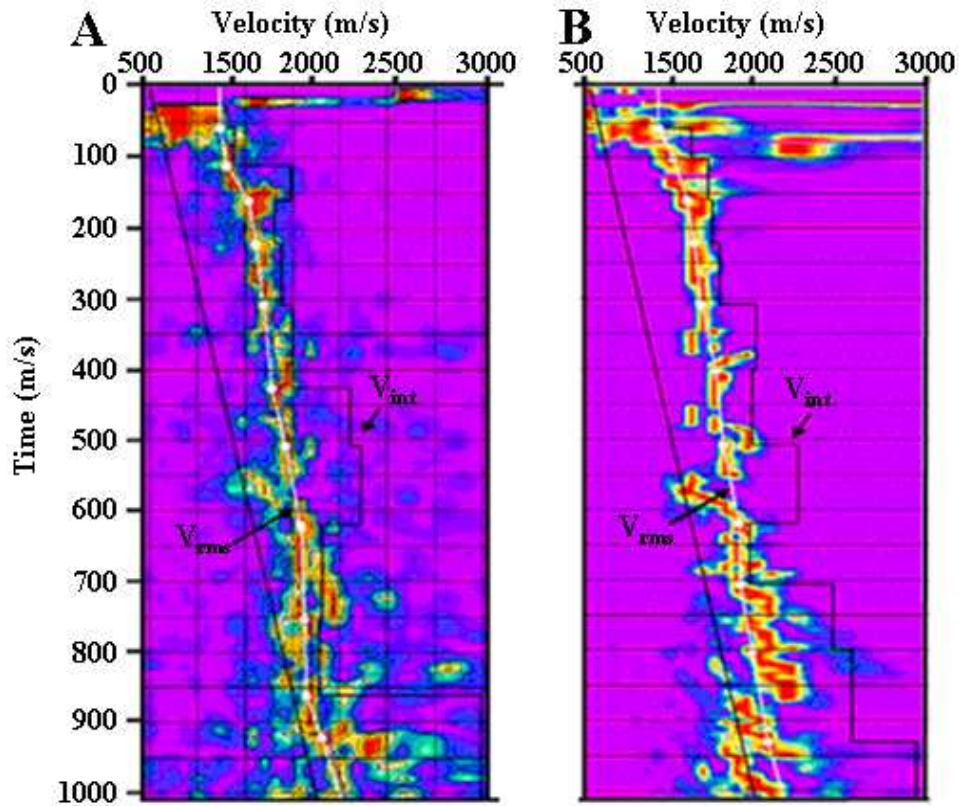


Figure 4.35: A velocity spectrum before DMO correction (A) and after DMO correction (B). Blue colour represents low semblance and red colour represents high semblance areas. V_{rms} is the RMS velocity and V_{int} is the interval velocity.

4.6.1 Comparison of CMP Seismic Velocity with VSP Data

The use of the Dix equation to convert RMS stacking velocities to interval velocities is based on the assumption of horizontal layers and constant velocities between the layers. Therefore, dipping structures and vertical and lateral velocity variations can introduce significant errors into the resulting interval velocity fields (Hajnal and Sereda 1981). As mentioned before, most of the errors in the interval velocities will be caused by picking errors in the RMS velocities.

In order to evaluate the accuracy of interval velocities calculated from CMP seismic data, they were compared with the VSP interval velocity functions obtained in BH3914 and BH3786. The

comparison can be seen in Figures 4.36, 4.37 and 4.38, where the measured interval velocity of the CMP 800 gather of profile 4, CMP 700 gather of profile 5 and CMP 3500 gather of the SH-wave profile (dotted lines) are overlain by the VSP velocity measured in BH3914 and BH3786 (solid lines), respectively. In all cases the VSP data show detailed velocity information at a few meter depths.

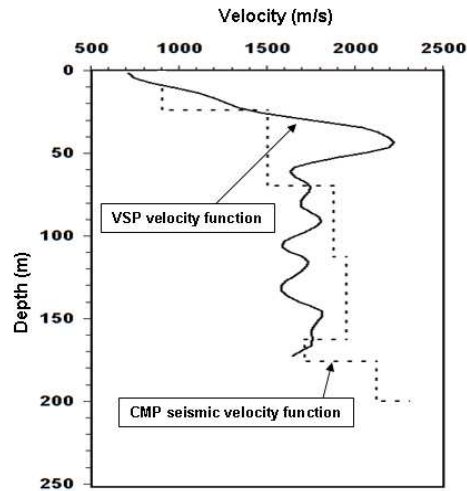


Figure 4.36: Measured interval velocity from CMP 800 of seismic profile 4 (dotted lines) compared with the VSP P-wave (V_p) interval velocity function from BH3914 (solid line).

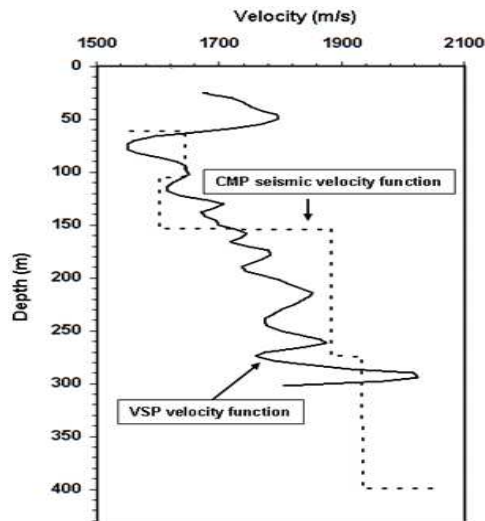


Figure 4.37: Measured interval velocity from CMP 700 of seismic profile 5 (dotted lines) compared with the VSP P-wave (V_p) interval velocity function from BH3786 (solid line).

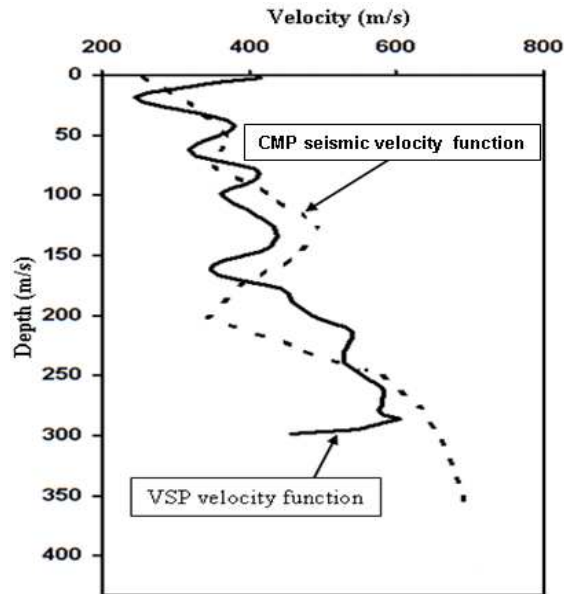


Figure 4.38: Measured interval velocity from CMP 3500 of seismic SH-wave profile (dotted lines) compared with the VSP S-wave (V_s) interval velocity function from BH3786 (solid line).

The velocity functions displayed by the VSP data show more detailed information about velocity variations with depth than that shown by velocity functions of the CMP data. However, both velocity functions show an increase in velocity with depth which can be related to variations in porosity and/or density. Discrepancies in velocity values between the two velocity functions can be seen at depths less than 100 m in case of the P-wave data. In case of the SH-wave the matching between the VSP velocity function and the CMP velocity function is higher. The discrepancies can be related to the way the waveform has propagated in this part. However, the comparison between the VSP interval velocity functions and the interval velocity functions of the CMP gathers shows that the velocity analysis of the surface data produced reliable velocity functions which can further be used in characterizing the subsurface.

Chapter 5: Interpretation

5.1 Seismic Interpretation of P-Wave Profiles

Interpretation of geophysical data is deriving a simple, plausible geologic model that is compatible with all observed data (Sheriff, 2006). The model is never unique and refining it involves a sequence of somewhat arbitrary choices. The interpretation of a seismic profile requires integration of the seismic section, velocity information, and lithological and geophysical logs from nearby boreholes. Interpretation is also dependent on some general geological and geophysical characteristics of the subsurface formations that are known from studies in the area of interest or similar areas. However, in the present area of study, only few deep boreholes that are near the seismic lines as well as a few previous geological and geophysical studies have made accomplishing a reliable interpretation of the seismic lines difficult. Moreover, chaotic reflections are dominant in the glacial sediments that fill the valley.

The interpretation of the two seismic sections of profile 4 and profile 5 is based on the depth migrated sections displayed in Figure 4.34.

5.1.1 Profile 4

Profile 4 begins from the west side of the valley near Tangstedt village and runs eastwards along an agricultural road to terminate at its east end near Hasloh village on the west periphery of the salt dome Quickborn which sits close to the surface in the east side of the valley (see Figure 2.3). This profile is parallel and 1 km to the north of profile 5 (see Figure 1.3). The length of this profile is about 3.4 km.

The detailed migrated seismic section reveals a complex stratigraphic and structural framework in valley fill sediments which extend between CMP 50 and CMP 750 (Figure 5.1).

One of the most prominent features in the seismic section is the bottom of the valley (event a) which is characterized by a high amplitude reflection signal and dipping from both the east and

west peripheries of the valley towards the axis of the valley. The maximum depth of the valley is about 450 m - that is below CMP 200. The valley is approximately 2 km wide.

The dominant feature is the regional dipping of the Tertiary horizons to the west direction which is visible throughout the entire section. The degree of dip of the Tertiary horizons increases with depth in the right side of the section which indicates the location of the salt dome in this part of the section. The valley sediments fill also shows conflicting dips from the east to the west between CMP locations 760 and 510 and from the west to the east between CMP 260 and CMP 510 (events b and c, respectively).

In the valley secondary valley features are seen between CMP 150 – 250, from 50 – 75 m depth (event b); CMP 600-750, 50-110 m depth (event c) and between CMP 320 – 660, 25 –75 m depth (event d). Beside of the mentioned features high and less reflective packages can be defined in the valley fill.

A well-defined event in profile 4 is a shallow reflection with at depth of about 50 m. The event appears as a flat event throughout the entire section, and its position agrees with the boundary between recent Holocene and Pleistocene.

A part of the valley in profile 4 between CMP 120 and CMP 250 from 150 m to the bottom of the valley is dominated by chaotic seismic facies.

The Tertiary horizons rise to the Quickborn salt dome in the east. It is found that at CMP 900 the basis of the Quaternary is at 50 m (Figure 5.1); basis of the Upper Mica Clay is 100 m; basis of the Upper Lignite Sand is 130 m; of Hamburg clay is 130 – 145 m; basis of the Lower Lignite Sand is 300 m; the Lower Mica Clay is more than 300 m deep. There are obvious breaks in the continuity of the seismic horizons of Tertiary strata. These discontinuities in the horizons are interpreted as fault planes and they are marked by dashed vertical to semi vertical lines in the seismic section.

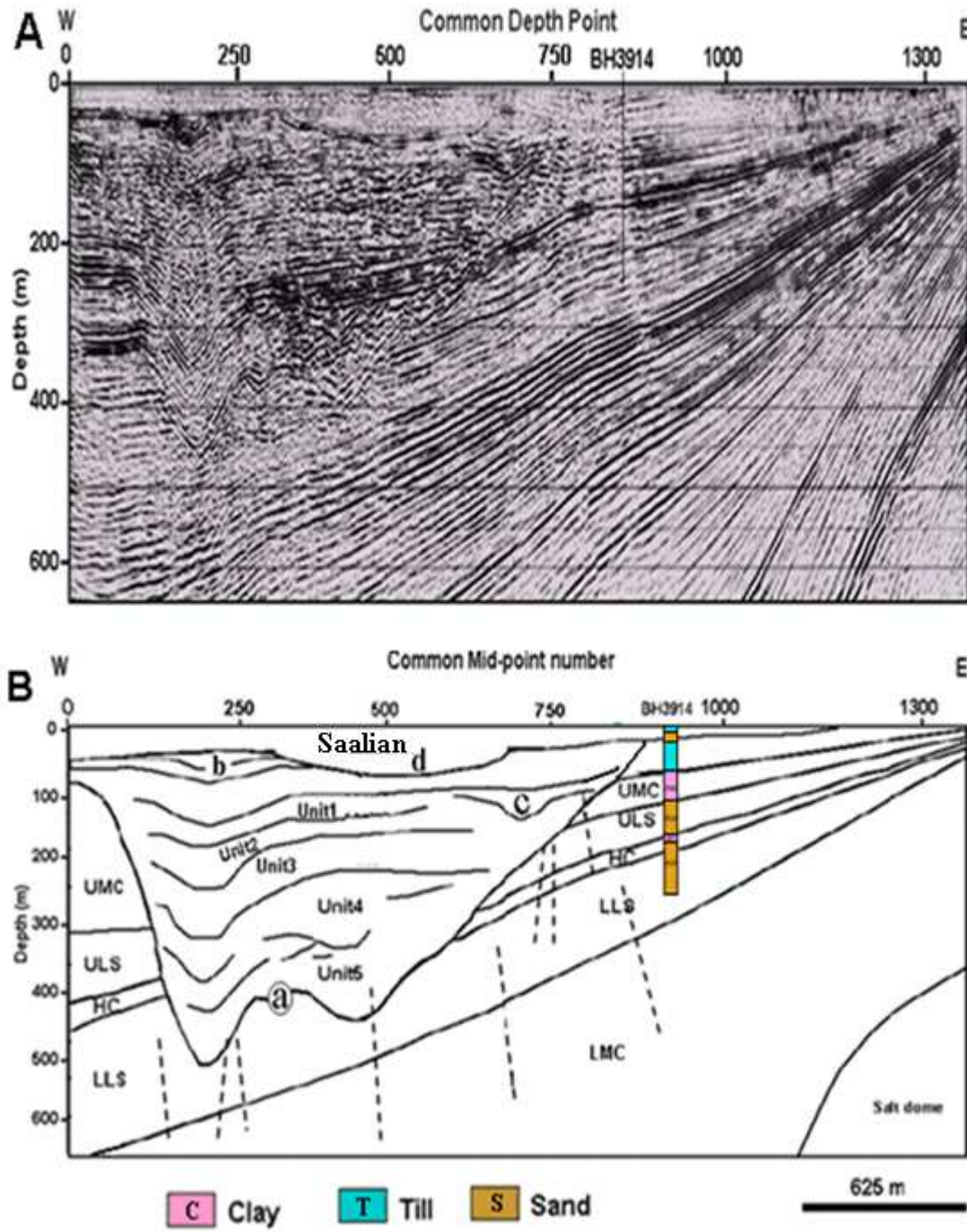


Figure 5.1: A: Migrated depth section of profile 4 and B: geological interpretation of the migrated section showing identification of reflections with BH3914 superimposed. Dashed vertical to semi vertical lines represent interpreted fault/fractures planes. a is the valley floor; b, c, and d are secondary valleys; Unit5, Unit4, Unit3, Unit2 and Unit1 are interpreted seismic facies of the valley fill. Tertiary units: LC = Lauenburg Clay; UMC = Upper Mica Clay; ULS = Upper Lignite Sand; HC = Hamburg Clay; LLS = Lower Lignite Sand; LMC = Lower Mica Clay.

5.1.2 Profile 5

Profile 5 begins from the west side of the valley south of the Tangstedt village and runs eastwards along an agricultural road to terminate at its east end near Winzeldorf village near the west periphery of the salt dome Quickborn. This profile is located south of profile 4, 1 km apart from it. The length of this profile is about 3.0 km.

The detailed migrated seismic section reveals a complex stratigraphic and structural framework in valley fill sediments which extends between CMP 200 and CMP 1200 (Figure 5.2).

One of the most prominent features in the seismic section is the bottom of the valley (event a) which is characterized by a high amplitude reflection signal and is dipping from both the east and west peripheries of the valley towards its axis. The maximum depth of the valley is about 450 m - that is below CMP 600. BH3786, located at CMP 780, taps the valley bottom at 412 m. The Ellerbek valley is roughly 2.5 km wide.

The regional dipping of the Tertiary horizons to the west direction is also evident in profile 5 with less degree compared to that in profile 4. The valley sediments fill also shows conflicting dip from the east to the west between CMP locations 650 and 600 and from the west to the east between CMP 500 and CMP 600.

In the valley secondary valley features are seen between CMP 500 – 750, from 50 – 100 m depth (event b) and CMP 1030-1150, 50-150 m depth (event c). Beside of the mentioned features high and less reflective packages can be defined in the valley fill. Strong reflections are present at depths of about 60 and 90 m in the upper part of the valley.

The seismic unit (LC) is interpreted as Lauenburg Clay which is confirmed by BH3786. Other strong reflection events are not evident in the borehole lithological log and show a gentle dipping from east to west. These events can be interpreted, through gamma-ray log, as being due to lithological changes and/or erosional surfaces. Also they can be interpreted as being due to changes of compaction in the sediments.

A part of the valley in profile 5 that is between CMP 450 and CMP 650 from 150 m to the bottom of the valley is dominated by chaotic seismic facies. The location of this structure in this profile seems to be an extension to the same phenomenon in profile 4. This structure might be interpreted as a deep secondary valley which cuts the previously deposited glacial sediments.

Strong breaking and displacement of Tertiary horizons, to the left of the valley, are shown by the section. They are interpreted as vertical to steeply dipping fault planes and marked by solid lines. These faults or some of them are most probably due to erosion of Tertiary sediments by subglacial meltwater (or may be due to melting of an iceberg), which formed a space with steep dipping walls and made the Tertiary horizons to be pulled by gravity force resulting in breaking and swelling of these horizons.

5.2 Combined Interpretation of P- and SH-Wave Profiles

The P-waves clearly image the sediments in and outside the valley but fail to trace the boundaries in shallow levels and some fault planes in Tertiary sediments. Some geological features in the shallowest units were also difficult to interpret on the P-wave sections. The ability to resolve shallow subsurface sediments is critical for groundwater pollution assessment since such sediments protect the groundwater from surface contaminants here.

Figure 5.3 displays a part of the P-wave profile 4 (left) and the SH-wave profile. Both have been scaled to match horizontally and vertically. The obvious features in both profiles is the Quaternary – Tertiary boundary which dips from west (at 140 m depth) to east direction. Layering of Quaternary sediments below 50 m is evident in both profiles, while shallower layers can be traced only on the SH-wave profile. Faults can be traced on both profiles. An integrated interpreted geological cross section is shown in Figure 5.4. The geological features traced on both profiles are compiled in this geological cross-section.

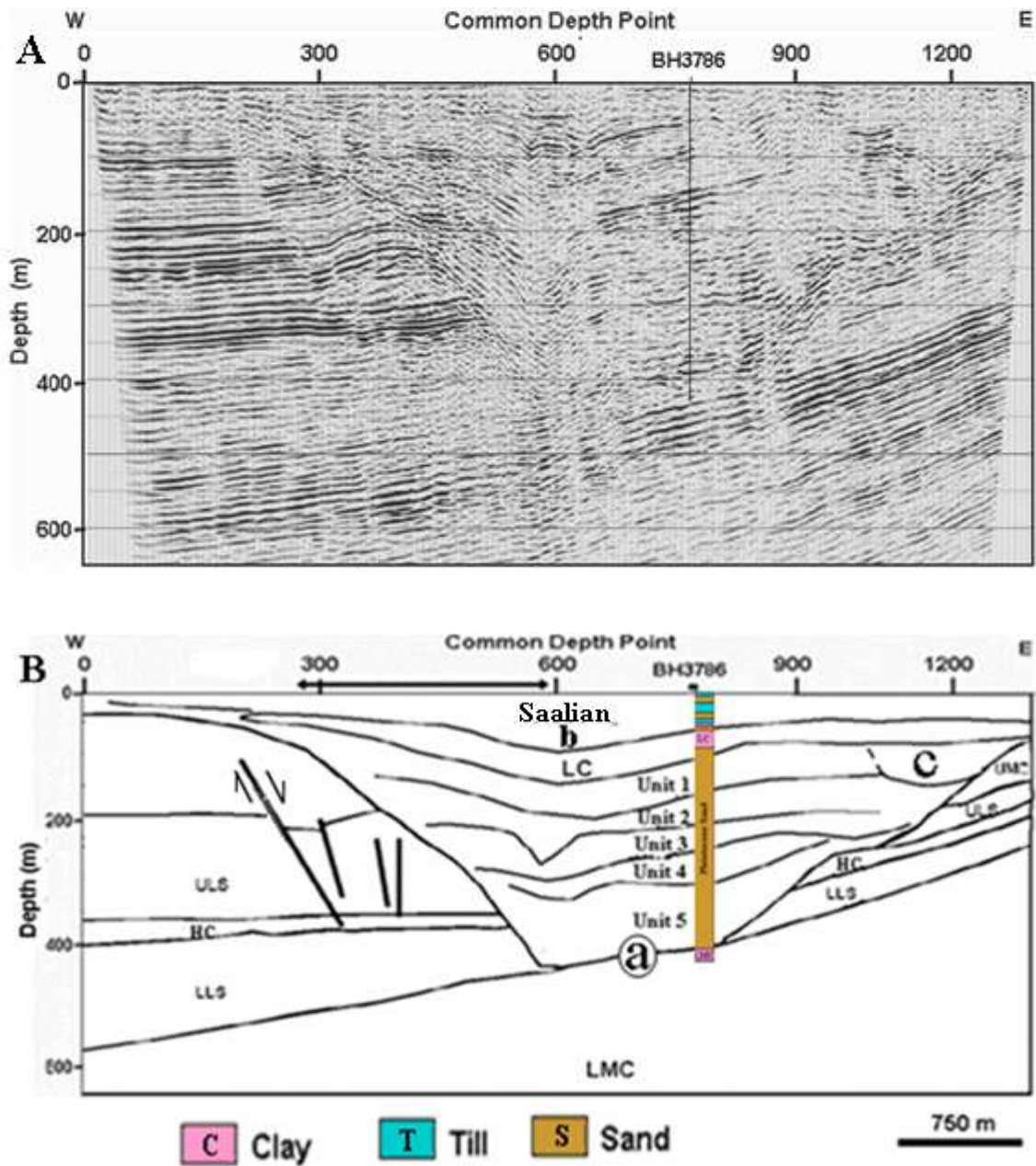


Figure 5.2: A: Migrated depth section of profile 5 and B: geological interpretation of the migrated section showing identification of reflections with BH3914 superimposed. Dashed vertical to semi vertical lines represent interpreted fault planes. a is the Ellerbek valley floor; b and c, and secondary valleys; Unit5, Unit4, Unit3, Unit2 and Unit1 are interpreted seismic facies of the valley fill. Tertiary units: LC = Lauenburg Clay; UMC = Upper Mica Clay; ULS = Upper Lignite Sand; HC = Hamburg Clay; LLS = Lower Lignite Sand; LMC = Lower Mica Clay. The double arrow line above the section highlights the corresponding location of the SH-wave section.

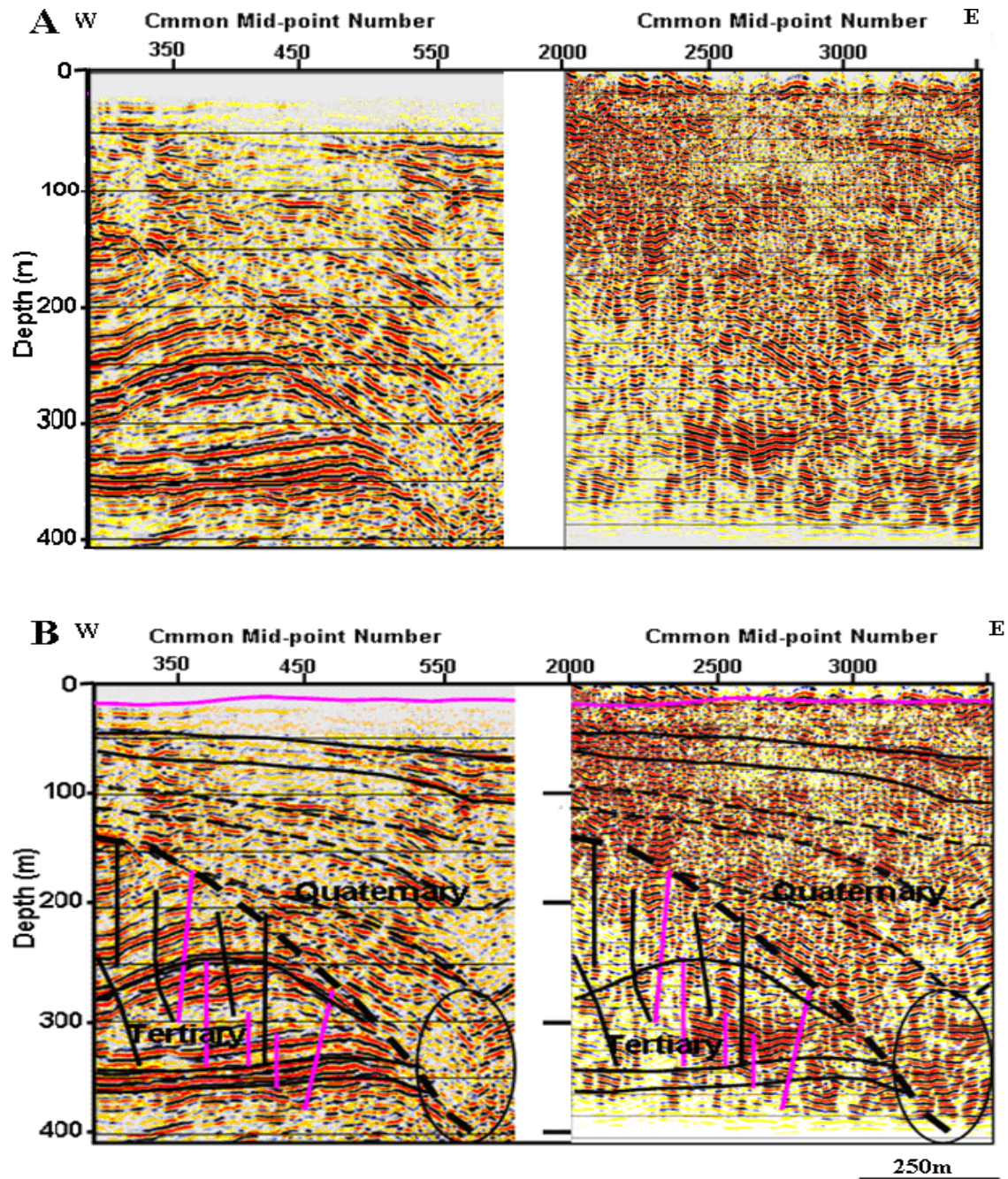


Figure 5.3: A: Part of profile 5 that is analogous to SH-profile (CMP 291 to CMP 595; left panel) and the SH-wave profile (right panel). Both are imaged and vertically positioned so as depths correlate (common mid-points numbers on P- and SH-wave sections are different). B: the seismic sections are overlain by geological interpretation. Principal interpreted stratigraphic boundaries and faults are marked. Boundaries on the SH-profile show an interpreted shallow reflection in the Holocene sediments (purple horizontal line super imposed on two sections). Black vertical lines represent faults interpreted from both sections while purple vertical lines represent faults interpreted only from SH-waves. The oval shape on the bottom right of the two sections compares the reflection configurations which are chaotic in the P-wave section and well horizontal in the SH-wave section.

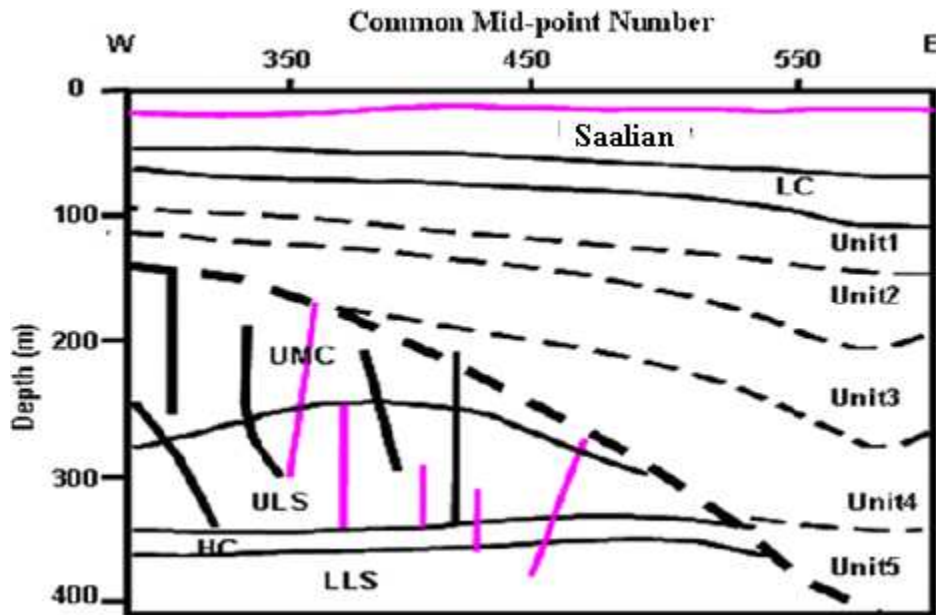


Figure 5.4: Geological model along seismic profile 5 (between CMP291 and CMP595) based on the integration of P- and S-wave depth sections. Purple coloured lines, both faults and geological boundaries, are interpreted only from the SH-wave profile. Unit1 to Unit5 are layers interpreted in Quaternary sediments bounded by unconformities (dotted thin lines). LC = Lauenburg Clay; UMC = Upper Mica Clay; ULS = Upper Lignite Sand; HC = Hamburg Clay; LLS = Lower Lignite Sand.

5.3 Integrated Interpretation

Combined data analysis and interpretation approaches have become a good practice in subsurface characterization. By combining different geophysical methods in conjunction with geological and/or hydrogeological data characterization of the subsurface structure and processes can be improved.

5.3.1 Surface Seismic and VSP Data

The zero-offset VSP data is directly comparable to the CMP seismic data by splicing the VSP corridor stack section into the surface seismic section. Figure 5.5 shows the corridor VSP stack at BH 3914 compared to the seismic reflection profile 4 at CMP 820. A prominent reflection at 125 ms is the top of the ULS. The reflection from the bottom of the ULS/ top of HC and from

the bottom of HC/ top of LLS at times of approximately 165 ms and 175 ms, respectively, are coherent in both surface seismic and VSP data. A series of high amplitude reflections around and below 200 ms are evident within the LLS layer, which suggest velocity and/or density variations within the LLS layer. There are no reflections on CMP data that compare in relative amplitude. There are, however, lower amplitude reflections of CMP data.

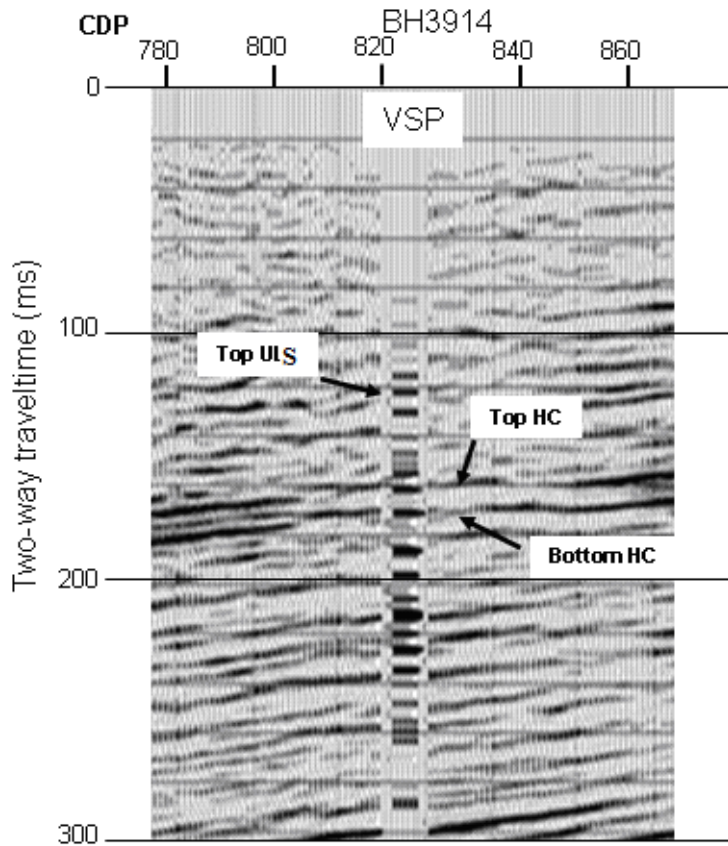


Figure 5.5: VSP corridor stack section at BH3914 spliced into the profile 4 seismic section (CMP 820) showing close match of Hamburg Clay (HC) reflections. Other reflections around and below 200 ms, within the Lower Lignite Sand layer, are evident in the VSP and to lesser degree in the seismic section of profile 4.

The VSP at BH3786 is compared to the seismic profile 5 as shown in Figure 5.6. The bottom of the Pleistocene sediments is confirmed to be at a time of 450 ms, as shown previously, on the CMP stacked section of profile 5 (Figure 4.17). A coherent reflection marked by the arrow in Figure 5.6 is evident on both datasets. The reflection from top of the LC has higher reflectivity on CMP data and low on VSP data. The base of the LC is obvious on both the CMP data and the VSP. A series of lower amplitude reflections from 300 to 450 ms seems to match well and are indicative of the lithology, the velocity and /or density variations within the Pleistocene sediments.

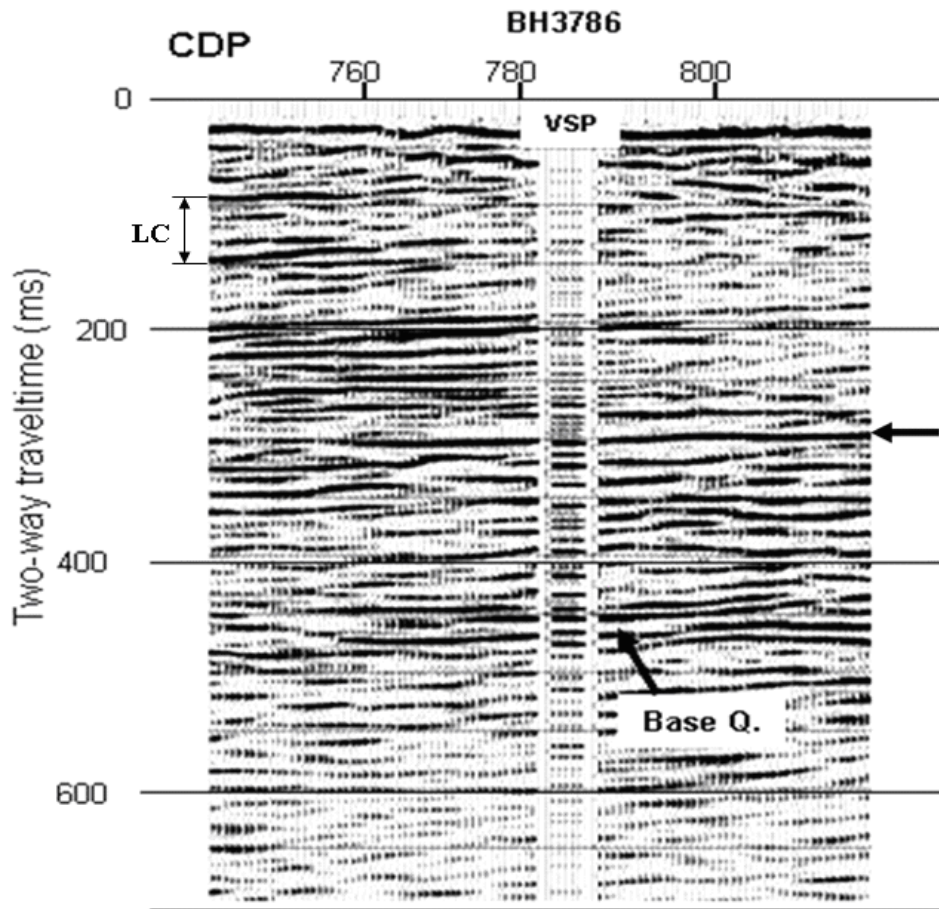


Figure 5.6: VSP corridor stack section at BH3786 spliced into the profile 5 seismic section (CMP 780) showing a good match of the base Quaternary (Base Q) signature. An excellent match is also found at 300 ms; the arrow on the right side marks a coherent reflection of both datasets.

5.3.2 Surface Seismic and SkyTEM Data

Figure 5.7 shows a SkyTEM resistivity cross-section along a flight line close to the seismic profile 4 superimposed by the interpretation of seismic profile 4 and the lithological log of BH3914. Most of the seismic interpretation boundaries are in good agreement with the SkyTEM resistivity cross-section. The LC as interpreted from seismic data and confirmed by BH3876 is in agreement with the resistivity section which shows this layer in the depth range between 60 m and 80 m with 5 to 25 Ωm .

Figure 5.8 shows a SkyTEM resistivity cross-section along a flight line close to the seismic profile 5 superimposed by the interpretation of seismic profile 5 and the lithological log of BH3786. The seismic interpretation boundaries are in reasonable good agreement with the SkyTEM resistivity cross-section. The LC as interpreted from seismic data and confirmed by BH3876 is in agreement with the resistivity section which shows this layer in the depth range between 60 m and 90 m with 5 to 25 Ωm . The bottom of the seismically interpreted unit 1 is clearly confirmed by the resistivity data near the BH3786 which shows a high resistive layer (100 Ωm) extending from the bottom of the LC at 90 m depth to about 150 m depth. This layer (Unit 1) can be considered as a good aquifer, may be sands with fresh water and covered by LC. Seismic Unit 2 can only be seen in the resistivity section close to the BH3876; there it has a resistivity of 20 to 40 Ωm . This layer can be classified as a poor aquifer compared to seismic Unit 1.

The valley boundary in the west side is well mapped by seismics and confirmed by the resistivity profile.

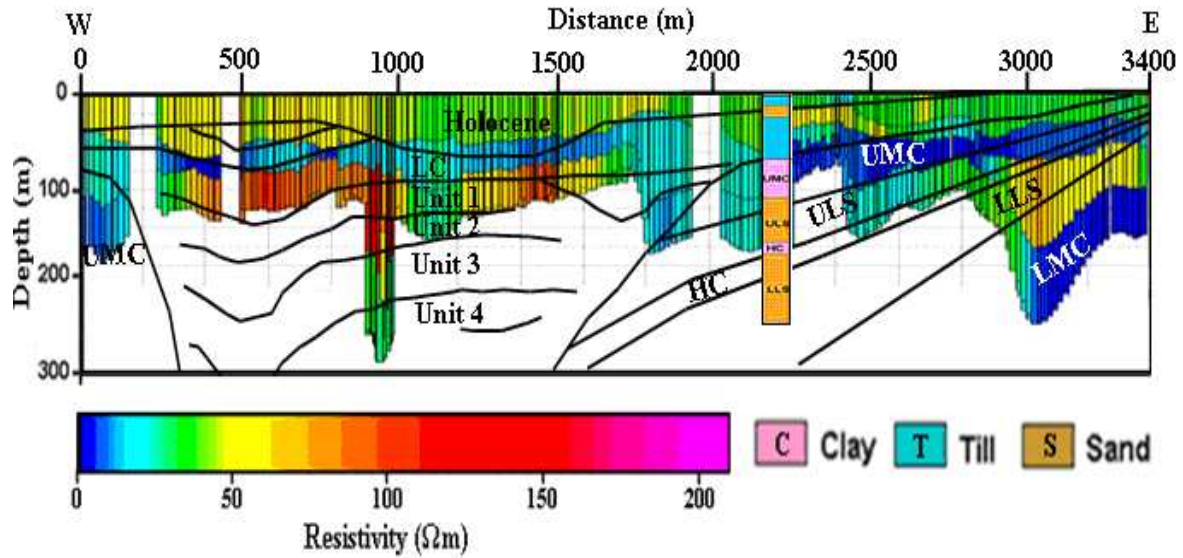


Figure 5.7: SkyTEM resistivity cross-section across the valley along a flight line close to the seismic profile 4 superimposed by seismic interpretation of profile 4 to 300m depth, and lithological log of BH3914. LC = Lauenburg Clay; UMC = Upper Mica Clay; ULS = Upper Lignite Sand; HC = Hamburg Clay; LLS = Lower Lignite Sand; LMC = Lower Mica Clay; C=clay

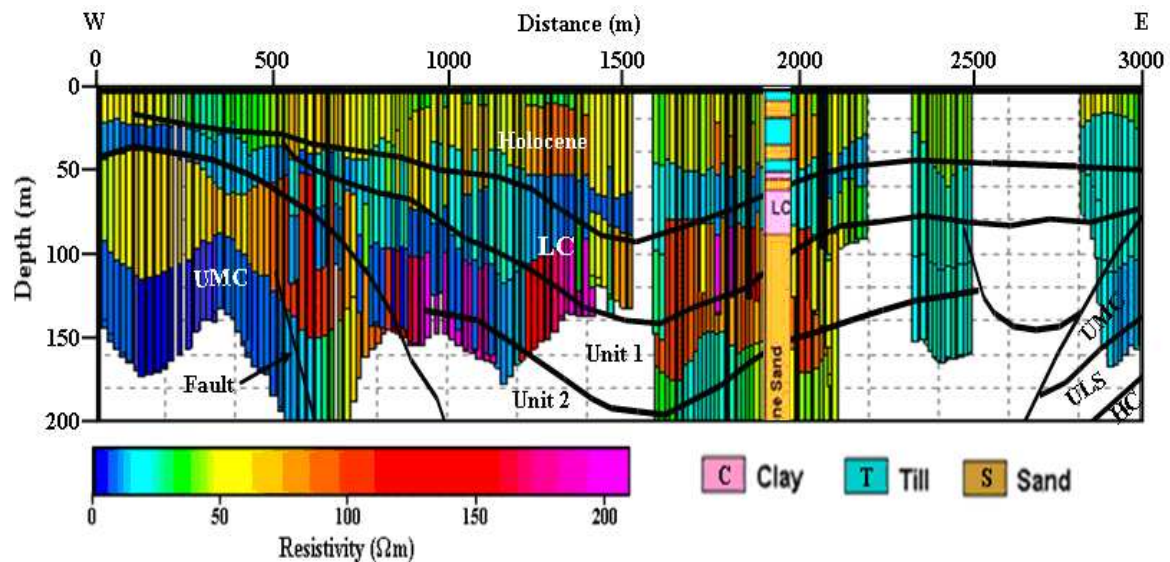


Figure 5.8: SkyTEM resistivity cross-section across the valley along a flight line close to the seismic profile 5 superimposed by seismic interpretation of profile 5 to 200 m depth, and the lithological log of BH3786. LC = Lauenburg Clay; UMC = Upper Mica Clay; ULS = Upper Lignite Sand; HC = Hamburg Clay; LLS = Lower Lignite Sand; LMC = Lower Mica Clay; C=clay

5.3.3 Seismic Data, Lithology and Well Log Data

Well logging is a technique used to make continuous profiles or point measurements of some physical and chemical properties of the surrounding rocks at discrete depths down a well. The measurements are made by lowering different types of probes (a sensor connected to a cable) into the well. Well logging techniques include resistivity, gamma-ray, etc. Log interpretation is carried out by examining the magnitudes of the rock responses for clues to the lithology. The gamma log (Figure 5.9 E) responds to clay content, and the resistivity log response (Figure 5.9 F) is inversely proportional to water content/porosity and also to clay content. A low resistivity coupled with high gamma-ray response, for example, is diagnostic of clays. Aquifers, of clean sands and gravels, are characterized by relatively high resistivity and low gamma responses. The texture of the logs provides hints to the depositional environment.

Figure 5.9 (1) shows the results of seismic profile 4, VSP at BH3914 and the lithological column of the same borehole. Resistivity and γ -ray logs and gamma-ray pattern are also shown. The Hamburg Clay (between 160 and 175 m depth) in the lithological log correlates very well with the seismic data. Below 200 m there are no changes in the lithological log shown, but there are changes in gamma log and seismic data. Therefore, this changes in acoustic and radioactive properties can be related to changes in porosity and/or lithology, because gamma ray changes with clay content and hence, porosity. VSP shows a reflection below the depth of the well. This is one of the benefits of VSP applications in imaging subsurface below drilled holes.

Figure 5.9 (2) shows the results of seismic profile 5, the VSP corridor stacked section at BH3914 and resistivity and gamma logs and gamma-ray pattern. Holocene sediments shown by borehole logs and other geophysical data as heterogeneous zone extend from the surface to the top of the LC at depth 60 m. The Lauenburg Clay at about 60 to 90 m in the lithological log correlates well with the seismic data, resistivity and gamma logs. The bottom of Unit 1 (top of Unit 2), as interpreted from seismic section, at depth of 150 m is shown by almost all data sets except the lithological log. The bottom of Unit 2 (top Unit 3) at about 220 m depth is shown by seismic data as well as by the gamma-ray log. At depth 250 m, bottom of seismic Unit 3 (top seismic Unit 4), is shown by all data. The bottom of Unit 4 (top Unit 5) at about 300 m depth is clearly confirmed by all datasets. Unit 5 is bottomed at the base of the Quaternary which is only shown by seismic sections and confirmed by lithological logs. The chaotic seismic Unit 5 at the bottom of the valley may be gravel to coarse sand (see Lutz et al. 2009).

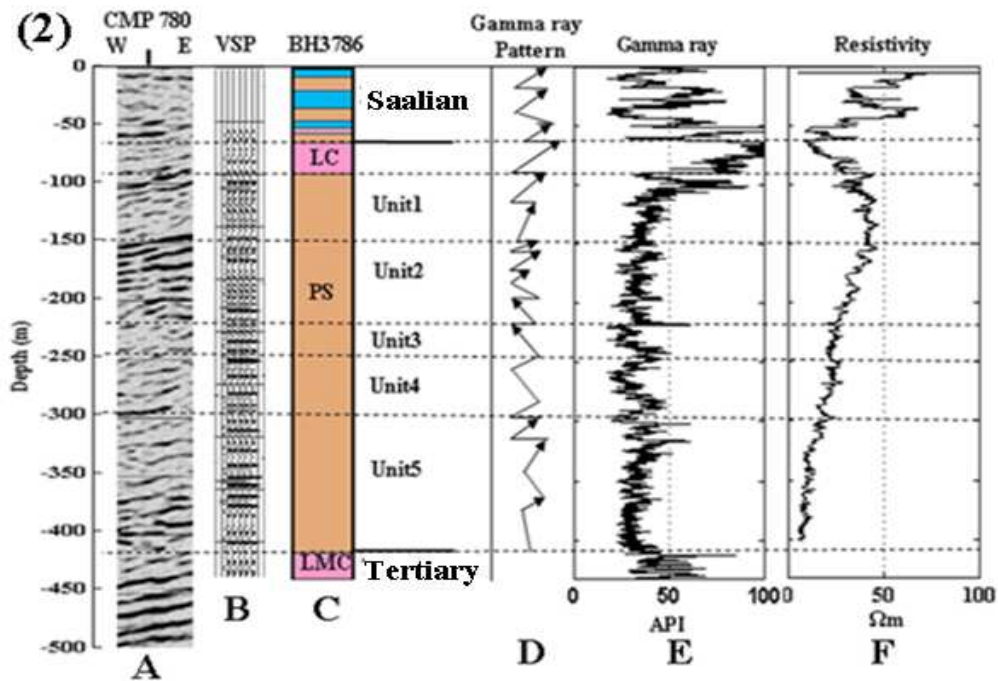
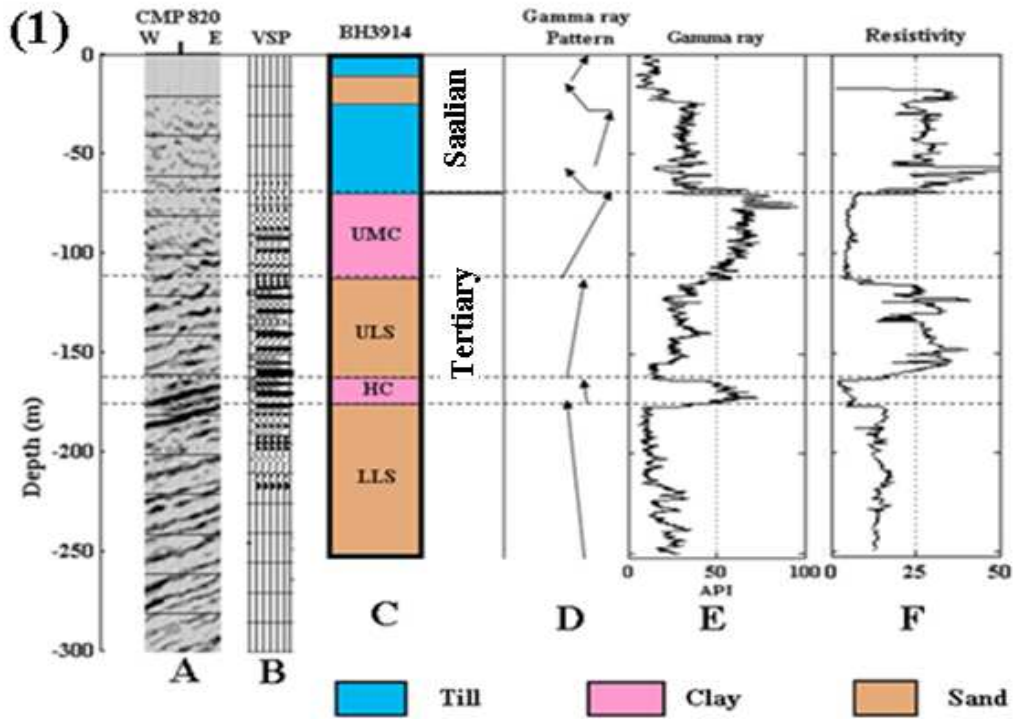


Figure 5.9: Seismic results of profile 4 (1) and profile 5 (2) and lithological and geophysical logs of BH3914 and BH3786: (A) part of seismic reflection depth section; (B) VSP corridor stack section; (C) lithological log (D) Gamma ray patterns; (E) Gamma ray log and (F) Resistivity log.

Chapter 6: Estimation of Physical Parameters

6.1 General

In chapter three some physical characteristics of rocks are discussed. In the present chapter the challenge of estimating those physical parameters from P- and S-wave velocity functions with depth, derived from borehole and surface seismic data, will be taken up. The properties of the sediments are estimated and discussed in relation to variation with depth. The parameters to be evaluated include:

- Petrophysical parameters (porosity, clay content and density),
- Hydraulic Conductivity and
- Elastic parameters (shear modulus, bulk modulus, etc).

Keeping in view the geological models interpreted from surface seismic data, each sedimentary layer can be assigned an average value of the above physical properties. The values of different physical parameters estimated in the present study should be considered as approximation.

6.2 Petrophysical Parameters

6.2.1 Porosity

Porosity of unconsolidated rocks can be estimated from borehole as well as surface seismic measurements using velocity – porosity empirical relationships which have been discussed in chapter 3. These relationships are mostly limited to certain types of rocks and/or to areas where they were derived. Some relationships require some considerations to be reliable, e.g. the rock must be isotropic (equation 3.1 after Wyllie et al. 1956). Still, some velocity-density relationships may be applicable to the present Quaternary and Tertiary sediments, e.g. equation (3.3) after Morgan (1969).

Using velocity information derived from VSP data porosities are calculated for sediments in and around well BH3914 and BH3786. The results are plotted in Figure 6.1 A to be correlated with other parameters and with the lithological logs.

The velocity-porosity relation after Morgan (1969) gave irrational results for Holocene sediments in BH3914 (0-70m depth). Therefore, to estimate the porosities of sediments in this range; equation 3.4 (after Salem 1990) has been applied resulting in reliable porosity values for this part of the subsurface.

The porosity log of BH3786 shows a general decrease in porosity with depth within the Pleistocene sediments, whereas, the porosity log of the Tertiary sediments in BH3914 does not show clear variations with depth. However, variations in porosity within individual lithological units are evident here. The average values of porosity for different lithological units is given in Table 6.1. Porosities of Quaternary unit 5 and Tertiary LLS and LMC have not been estimated since they were not measured by VSP.

6.2.2 Clay Content

The clay content is estimated from gamma-ray logs measured in BH3914 and BH3786. The estimates of the clay content are obtained through equations (3.8) and (3.9) and are shown in Figure 6.1 D. The Figure shows the clay content of the Quaternary sediments invaded by BH3914 and the clay content of Tertiary sediments in BH3786. It is obvious that the clay content is very high in Quaternary and Tertiary clayey layers (Lauenburg Clay and Upper Mica Clay, respectively) in which the clay content is > 90% close to the wells. Pleistocene sands as shown by the lithological log of BH3786 (Figure 6.1 (2)) show the lowest clay content compared to the clay content shown by Tertiary sands (Upper Lignite Sand and Lower Lignite Sand). In Pleistocene sands the clay content is about 5% whereas, in Tertiary sands it is up to 15%. This reveals that the Pleistocene sands have better hydrogeological properties than the Tertiary sands.

6.2.3 Density

The validity of velocity-density relationships is limited to specific lithologies or a certain depth interval. The relationship between P-wave velocity (V_p) and density (ρ) derived by Hamilton

(1971; equation 3.12) for soft, unlithified (marine) sediments from 0 to 500 m depth is considered to be applicable for the present environment.

Using this formula the density of the Tertiary and Quaternary sediments is calculated from P-wave velocities derived from VSPs in BH3914 and BH3876. The resulting velocities are plotted in Figure 6.1 B. The Figure shows a general increase in density with depth in BH3786 whereas BH3914 does not show such phenomenon. Density log in BH3914 shows sharp variations. These variations can be related to variations in lithological compositions as shown by the lithological log. Clay layers (UMC & HC) show higher density values but sand layers (ULS & LLS) show smaller density values. Density log in BH3786 shows smooth variation with depth as well as variations within formations. This smooth increase may be related to an increase in compaction, matrix density or pore fluid density with depth in the Quaternary sediments.

Higher density values are shown by till in the shallower part of both wells, while, the LC in BH3786 shows lower density. Variations in density within individual sediment units may be related to lithological variations. The average values of density of different sediment units are provided in Table 6.1. The density values of LLS and LMC are compiled from Gabriel (2006).

6.3 Hydraulic Conductivity

Hydraulic conductivities of different Quaternary and Tertiary sediments in the study area are estimated using the hydraulic conductivity – velocity relation (equation 3.16) after Fechner, (1998).

The results are shown in Figure 6.1C. It can be seen that Holocene sediments (till and silt) as well as LC and HC are characterized by low hydraulic conductivities, whereas, sand formations are characterized by higher hydraulic conductivities. Nevertheless there are variations in hydraulic conductivities within single units, e.g. Pleistocene sand in BH3786 has various hydraulic conductivities below 200 m. ULS in BH3914 shows low as well as high values of hydraulic conductivities. These variations in hydraulic conductivities can be related to variations in lithology.

Table 6.1 shows also the average hydraulic conductivities of the Quaternary and Tertiary sediments penetrated by BH3786 as well as BH3914. The lowest value is shown by LC, about 6×10^{-7} (m/s), whereas the highest value, about 6.9×10^{-5} (m/s), is shown by Quaternary sands.

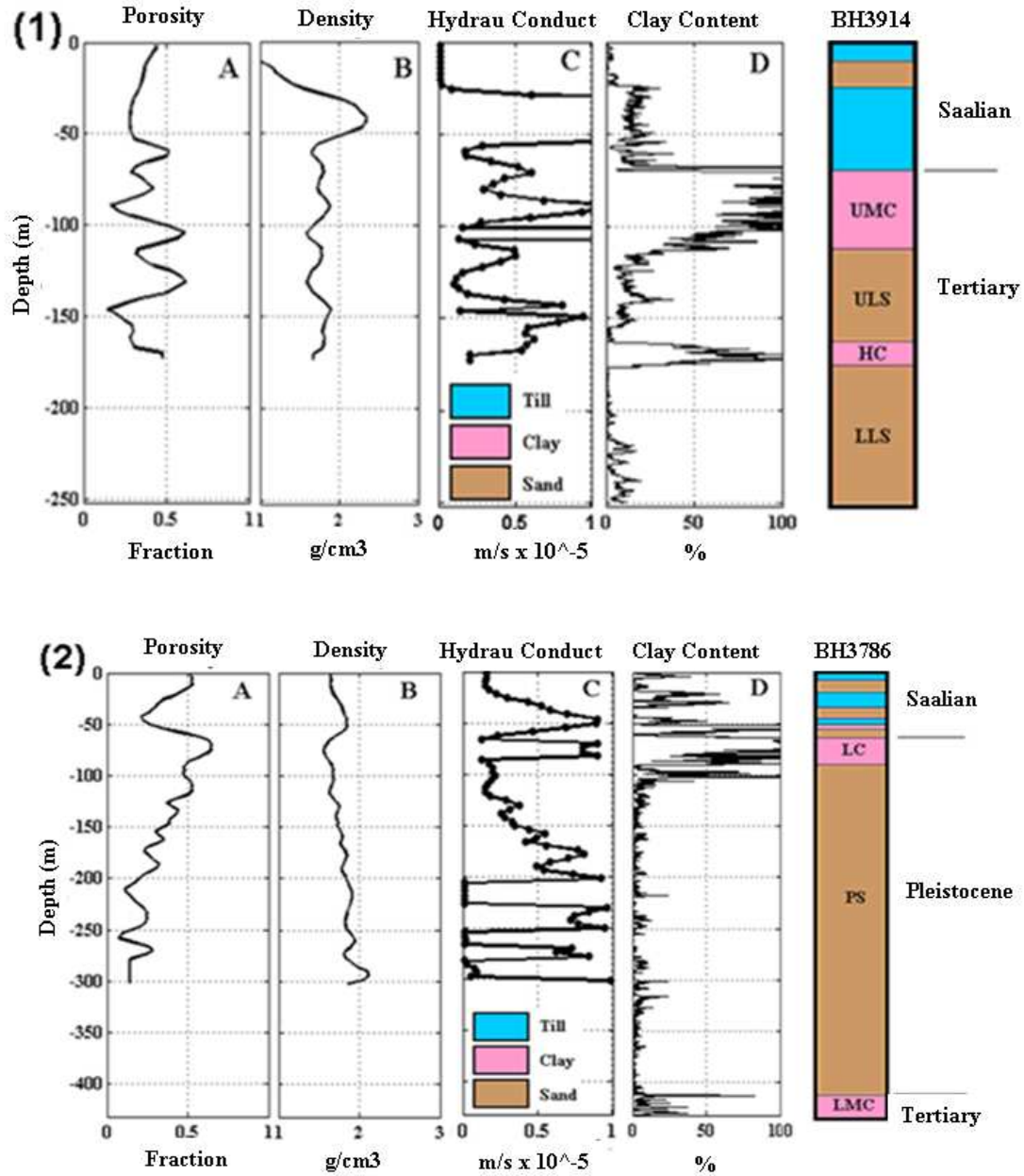


Figure 6.1: Results of physical and petrophysical parameters calculation from P-wave interval velocity function (1): at BH3914 and (2): at BH3786. (A) Porosity log calculated using the velocity – porosity relation after Morgan (1969); (B) Density log calculated from V_p interval velocity function derived from VSP data using the velocity-density empirical relation after Hamilton (1971); (C) Hydraulic conductivity calculated from velocity values using the equation of Fechner (1998), (D) Clay content calculated from gamma log using equation 3.9 (after Western Atlas 1985); and the lithological logs of BH3914. LC = Lauenburg Clay; PS = Pleistocene Sands; UMC = Upper Mica Clay; ULS = Upper Lignite Sand; HC = Hamburg Clay; LLS = Lower Lignite Sand; LMC = Lower Mica Clay.

Table 6.1: Average porosity, density and hydraulic conductivity values of the different geological units in the study area from empirical calculations.

Lithological unit	Porosity (in fraction)	Density (kg/m ³)	Hydraulic conductivity (m/s)	
Holocene	0.38	1929	5*10 ⁻⁶	
Lauenburg Clay	0.58	1935	6*10 ⁻⁷	
Pleistocene Sands (Quaternary)	Unit1	0.44	1795	3*10 ⁻⁶
	Unit2	0.24	1950	8*10 ⁻⁶
	Unit3	0.21	1790	9*10 ⁻⁶
	Unit4	0.10	1975	20*10 ⁻⁶
	Unit5	-----	2050	69*10 ⁻⁶
Tertiary	UMC	0.47	1820	10*10 ⁻⁶
	ULS	0.46	1810	9*10 ⁻⁶
	HC	0.45	1840	4*10 ⁻⁶
	LLS	-----	1858	25*10 ⁻⁶
	LMC	-----	1858	

6.4 Elastic Parameters

6.4.1 Elastic Moduli

Elastic moduli, in particular the shear modulus (μ), the bulk modulus (k), Young's modulus (E) and Poisson's ratio are calculated using P- and S-wave interval velocity functions (V_p and V_s) derived from Vertical Seismic Profiles at BH3914 and BH3786 and calculated density data (sections 4.4 and 6.2).

The shear modulus (μ) is calculated using equation (3.21). The calculated shear modulus functions at BH3914 and BH3786 are shown in Figure 6.2A. The two Figures show a general increase of the shear modulus values with depth. This increase is likely to be related to some increase of the sediments hardness due to increase of compaction with depth.

The bulk modulus is calculated using equation (3.23). The results of the calculated bulk modulus of sediments penetrated by BH3914 and BH3786 are also given in Figure 6.2B. The results show some increase of the bulk modulus values with depth especially by Quaternary sediments at BH3786. The increase of the bulk modulus with depth can be related to the increase of seismic velocity with depth as well as increase in density and decrease of porosity with depth.

Using equation (3.27) Young's modulus is calculated for Tertiary and Quaternary sediments from the P- and S-wave velocity and density functions of BH3914 and BH3786. Poisson's ratio is calculated using equation (3.29). Calculated values as functions of depth of Young's modulus as well as Poisson's ratios are provided in Figure 6.2C and D. the average values of elastic parameter values for different sediments units are provided in Table 6.2.

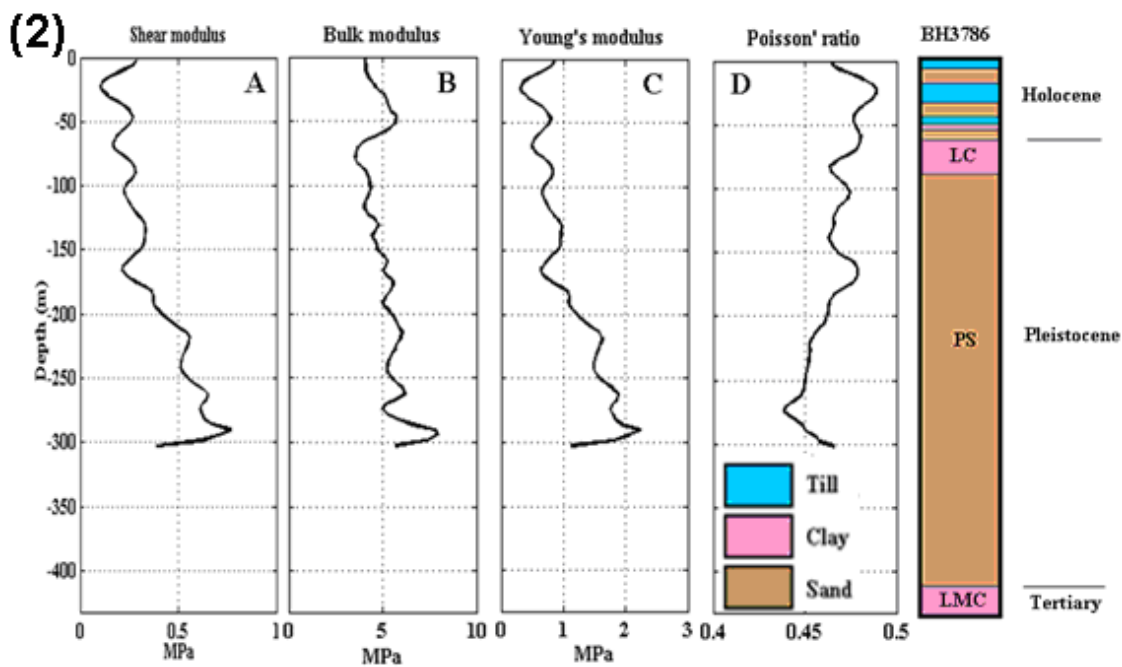
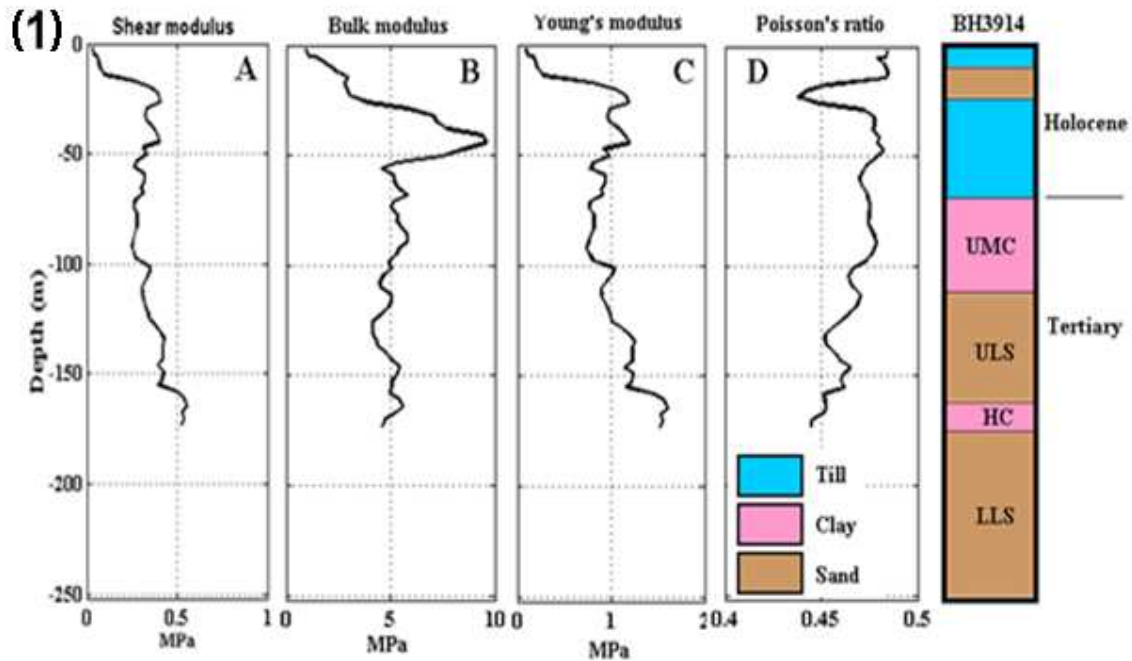


Figure 6.2: Elastic moduli derived from P- and SH-wave velocities (V_p and V_s) and densities measured (1): at BH3786 and (2): at BH3786. A is the rigidity modulus, B is the bulk modulus, C is Young's modulus and D is Poisson's ratio. LC = Lauenburg Clay; PS = Pleistocene Sands; LMC = Lower Mica Clay.

Table 6.2: Average values of elastic parameters of different lithological units observed in the Ellerbek valley and it's surrounding Tertiary horizons.

Lithological unit		μ (MPa)	K (MPa)	E (MPa)	σ
Holocene		0.15	5.0	0.7	0.47
Lauenburg Clay		0.23	3.8	0.65	0.48
Pleistocene Sands (Quaternary)	Unit1	0.28	4.5	0.83	0.47
	Unit2	0.39	5.5	1.1	0.47
	Unit3	0.55	5.5	1.6	0.45
	Unit4	0.68	6.5	2.0	0.45
	Unit5				
Tertiary	UMC	0.30	5.0	0.8	0.31
	ULS	0.42	4.8	1.2	0.30
	HC	0.54	5.1	1.6	0.31
	LLS				
	LMC				

6.4.2 V_p - V_s Relations

V_p versus V_s

To study the correlation between V_p and V_s the values of the two parameters measured by VSPs are crossplotted in Fig.6.3. Although the data points are somewhat dispersed, the P-wave velocity still correlates linearly with the S-wave velocity. Using the least-squared regression method, the linear relations derived from VSP velocity functions of BH3914 and BH3786 are, respectively:

$$V_s = 0.23V_p + 24.0 \text{ (m/s)}$$

$$V_s = 0.65V_p - 696 \text{ (m/s)}$$

V_p and V_s generally increase with depth, e.g. due to a decrease with porosity. Figure 6.3A shows V_p versus V_s of BH3914 data. A medium correlation ($R^2 = 0.5$) is shown between V_p and V_s . R^2 is the correlation factor. Obviously, Tertiary sediments are dominated by high V_p and V_s values. On the other hand Quaternary sediments (Figure 6.3B) are dominated by lower V_p and V_s velocities. This can be related to low porosity and thus less hydraulic conductivity in Tertiary sediment compared to high porosity and possibly high hydraulic conductivity in Quaternary sediments.

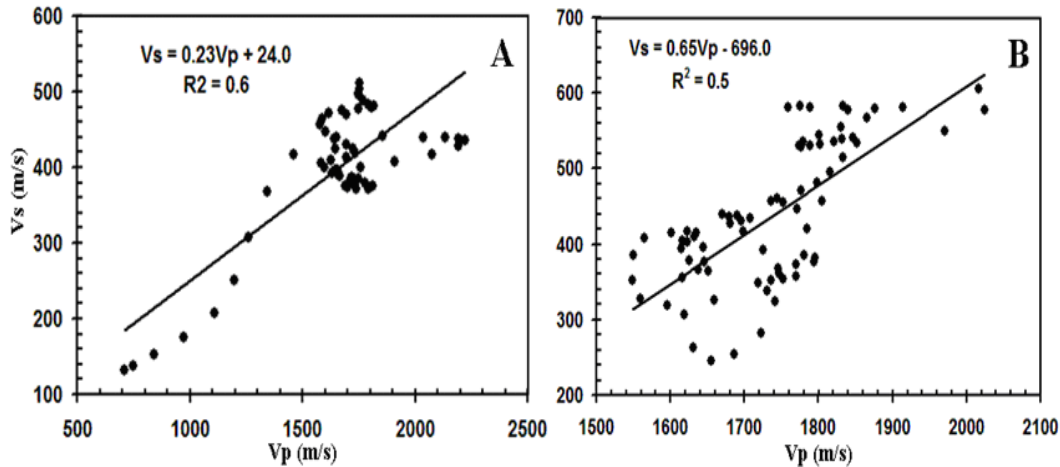


Figure 6.3: The plot of P-wave velocity (V_p) versus S-wave velocity (V_s) of BH3194 (A) and BH3786 (B). The regression linear functions are: $V_s=0.23V_p+24$ (m/s) and $V_s=0.65V_p-696$ (m/s), respectively. These equations represent the lines in the Figure. R^2 is the correlation factor.

V_p/V_s ratios

V_p/V_s ratios versus depth are calculated by dividing V_p by V_s interval velocities versus depth functions derived from VSP data from BH3914 and BH3786 (see Figure 4.31). The calculated V_p/V_s values versus depth at the two boreholes are shown in Figure 6.4. Average V_p , V_s and V_p/V_s values are given in Table 6.3.

It is obvious that the V_p/V_s ratios decrease with depth (Figure 6.4). However, within units, there sometimes increases of the V_p/V_s values are observed. V_p/V_s data versus depth can be divided into two types: steep variations found from top of the well to bottom of Holocene deposits, and gentle variations from bottom of the Holocene to the end of the measured depth of the wells. A pronounced increase in V_p/V_s values can be observed within Pleistocene sands between depths 150 m and 200 m. This is due to the increase in V_p in this zone, which may be related to a change in lithology.

V_p/V_s ratios range between 3.0 and 5.0 in Tertiary as well as Quaternary sediments (Table 6.3). This range is close to that described in the literature for saturated unconsolidated sediments (Gardner and Harris, 1968; Eastwood and Castagna, 1983; Meissner et al. 1985).

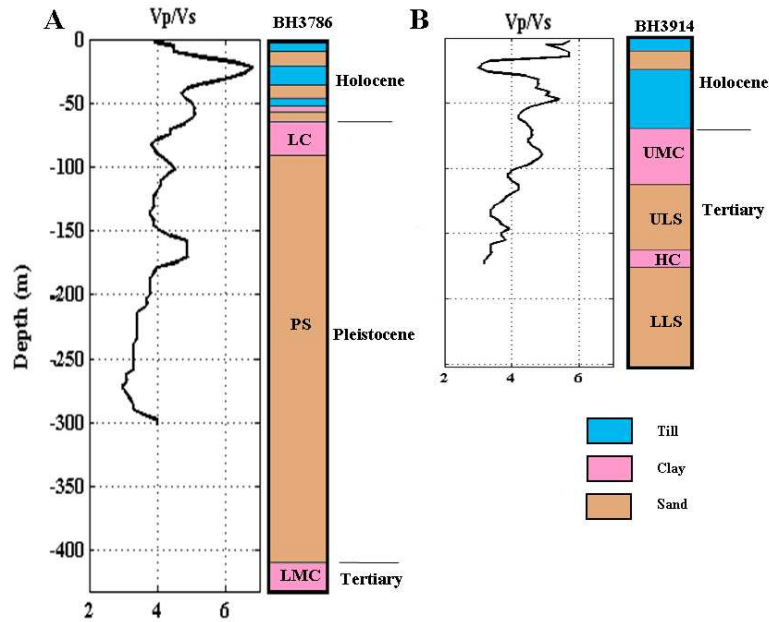


Figure 6.4: P-wave and S-wave velocity ratio (V_p/V_s) versus depth and lithological logs of BH3914 (A) and BH3786 (B) showing a general decrease in V_p/V_s ratio with depth. LC = Lauenburg Clay; UMC = Upper Mica Clay; ULS = Upper Lignite Sand; HC = Hamburg Clay; LLS = Lower Lignite Sand; LMC = Lower Mica Clay.

Table 6.3: Average values of V_p and V_s (in m/s) and of P-wave and S-wave velocity ratio (V_p/V_s) ratio for the Quaternary and Tertiary units. P-wave velocity (V_p) and S-wave velocity (V_s) values have been derived from VSP data.

Lithological unit		V_p (m/s)	V_s (m/s)	V_p/V_s
Holocene		1650	340	5.0
Lauenburg Clay		1590	370	4.3
Pleistocene Sand (Quaternary)	Unit1	1660	410	4.1
	Unit2	1780	440	4.1
	Unit3	1800	530	3.4
	Unit4	1870	570	3.3
	Unit5	2000*	650*	3.1
Tertiary	UMC	1700	390	4.4
	ULS	1710	470	3.7
	HC	1680	450	3.8
	LLS	1900*		
	LMC			

Note: values marked by stars have been estimated from surface seismic data since they were not measured by VSP.

2-D V_p/V_s ratios can be calculated by dividing the 2-D interval velocity of P-wave profile 5 by the 2-D interval velocity field of SH-wave profile. The 2-D P-wave velocity field used in calculating 2-D V_p/V_s ratios is the part of the field extending between CMP 300 to CMP 600 to depth of 500 m to match the 2-D SH-wave velocity field. Figure 6.5 shows that all the V_p , V_s and V_p/V_s fields vary vertically as well as in lateral directions.

The V_p field (Figure 6.5A) shows velocity values ranging between 1350 and 2850 m/s. It shows a general increase of velocity with depth and can be divided vertically into three zones:

- Low velocity zone from 0 to 200 m depth,
- Medium velocity zone from 200 to 400 m, and
- High velocity zone from 400 to the end of the section.

There is a clear anomalous velocity zone across the Tertiary-Quaternary boundary below CMP500 at 400 m depth with average velocity of 1400 m/s. Looking horizontally at the V_p velocity field it can be seen that the Tertiary formations have higher velocities than the Quaternary formations.

The V_s velocity model (Figure 6.5B) also shows a general increase of the velocity with depth. It shows a better resolution of the velocity change, but horizontally there are large differences in velocity distributions. A low velocity anomalous zone is found within the Quaternary part at about 150 m depth with average velocity of about 300 m/s.

The V_p/V_s ratio range (see Figure 6.5C) calculated from these velocities varies vertically as well as laterally. The 2-D V_p/V_s ratio field shows a better distinction between different formations. A general decrease in V_p/V_s ratio is evident. The shallow part shows homogeneous lateral variation whereas the deep part shows more heterogeneity in V_p/V_s ratio values. The ratio variations fit the Tertiary-Quaternary boundary. The values vary between 2.0 and 6.8, with an average value of 4.0 which is typical for shallow poor consolidated materials. A low V_p/V_s ratio is evident in the bottom of the Quaternary sediments.

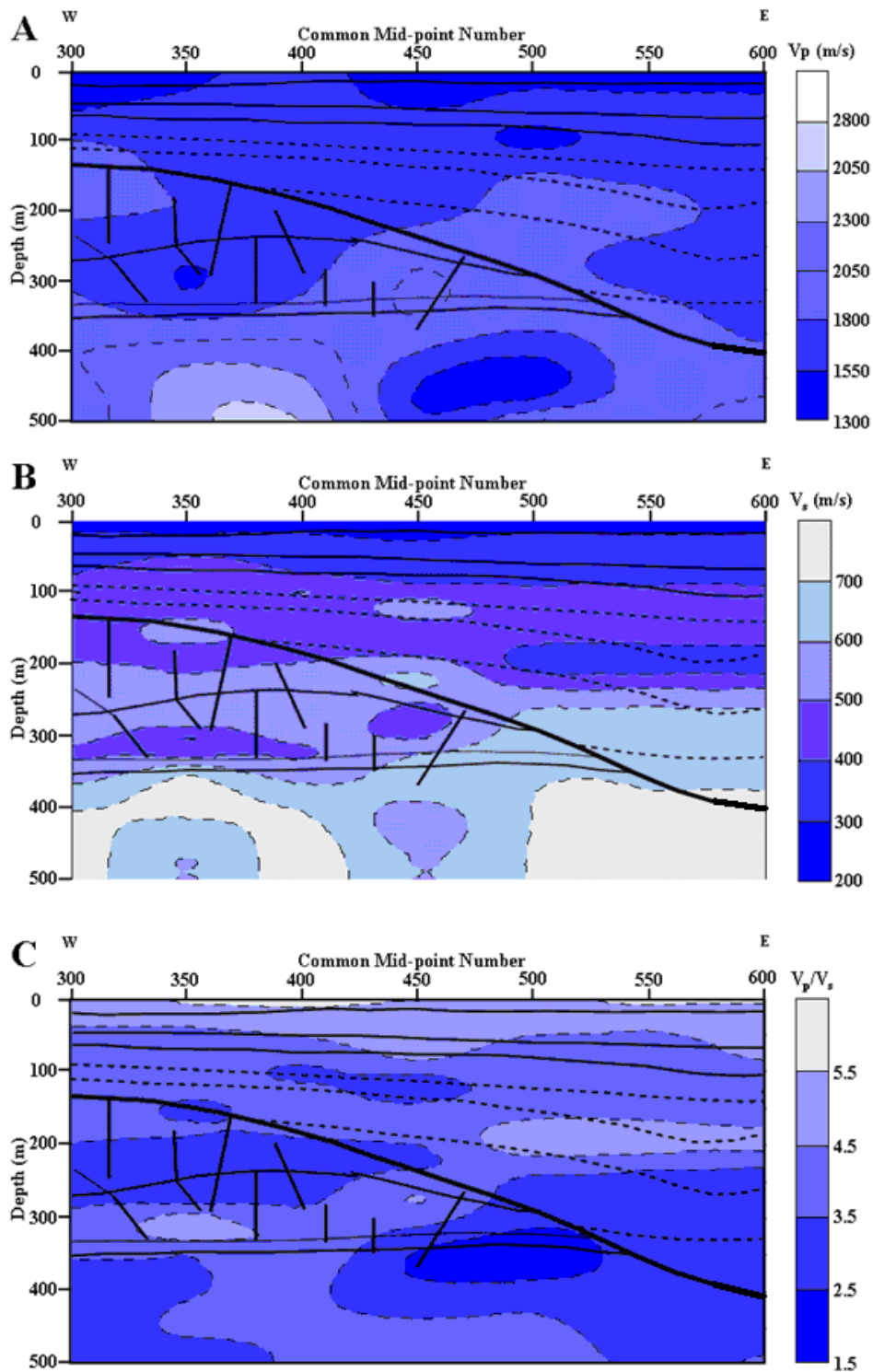


Figure 6.5: 2-D interval velocity fields of P-wave profile 5 (A), SH-wave (B) and the P-wave and S-wave velocity ratio (V_p/V_s) (C). The 2-D P-wave interval velocity is resampled (between CMP300 to CMP600) to match the 2-D SH-wave velocity field. All fields are superimposed by the integrated interpretation of P- and SH-wave seismic data shown in Figure 5.4.

V_p/V_s versus depth

A general decrease of V_p/V_s with depth is observed in the two wells. This relation is demonstrated in Figure 6.6. Examples of regression lines for the wells are given in Table 6.4. The lines are fit from top to bottom of the measured Tertiary and Quaternary at BH3914 and BH3786 respectively.

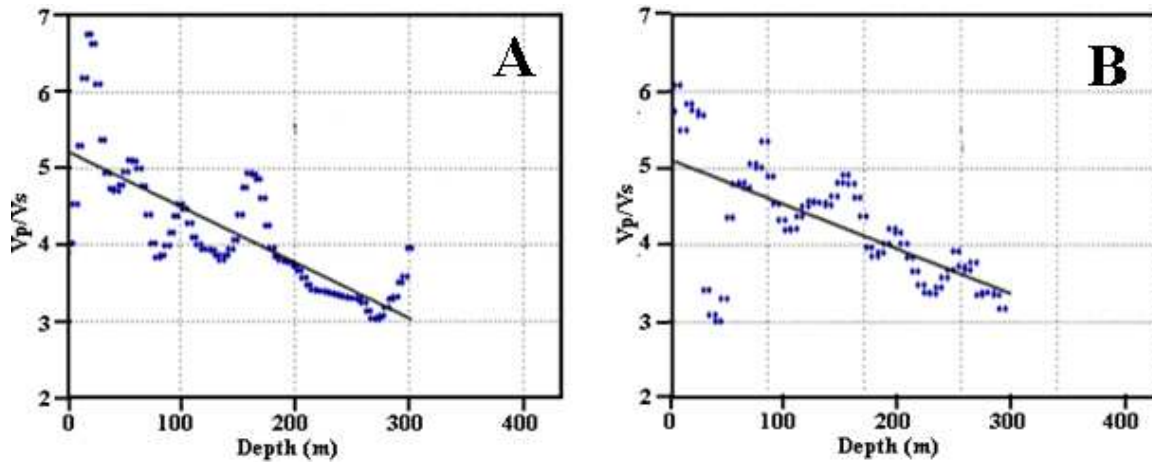


Figure 6.6: P-wave and S-wave velocity ratio V_p/V_s versus depth from BH3914 (A) and BH 3786 (B). The regression lines, fit over the whole well, are shown ($V_p/V_s = -0.01z + 5.1$ and $V_p/V_s = -0.7z + 5.2$, respectively, when z is the depth in meters).

Table 6.4: Representative line fit equations for V_p/V_s versus in BH3914 and BH3786.

Well	Representative line fit equation; z in meters
BH3914	$V_p/V_s = -0.01z + 5.1$
BH3786	$V_p/V_s = -0.7z + 5.2$

V_p/V_s versus V_p and V_s

Figure 6.7 shows V_p/V_s versus V_p as a cross-plot. The plot demonstrates that sediments are significantly separated into clusters. Tertiary clays are better discriminated from Tertiary sands as shown in Figure 6.7A compared to the discrimination between Quaternary clays and sands as shown in Figure 6.7B. The data plotted in Figure 6.7 are provided in Appendix (A).

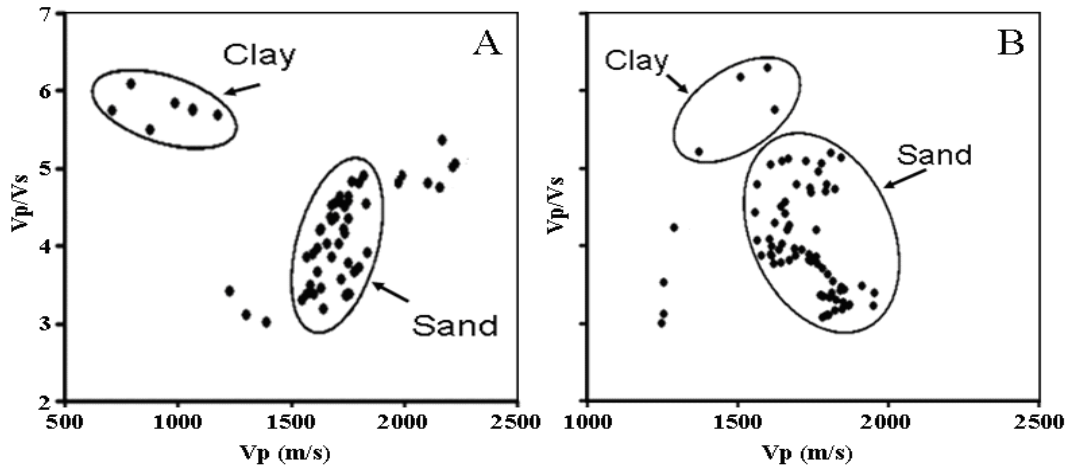


Figure 6.7: P- and SH-wave velocities are determined using full waveform VSP from BH3914 (A) and BH3786 (B). Plots of P-wave and S-wave velocity ratio (V_p/V_s) versus P-wave velocity (V_p) show tendency of the data to form clusters which correlate to certain types of sediments.

Figure 6.8 shows the plots of V_p/V_s versus V_s . The plots show that, the Quaternary sediments show higher correlation between V_p/V_s and V_s ($R^2 = 0.9$) than Tertiary sediments ($R^2 = 0.6$). The plotted data in this Figure is provided in Appendix A.

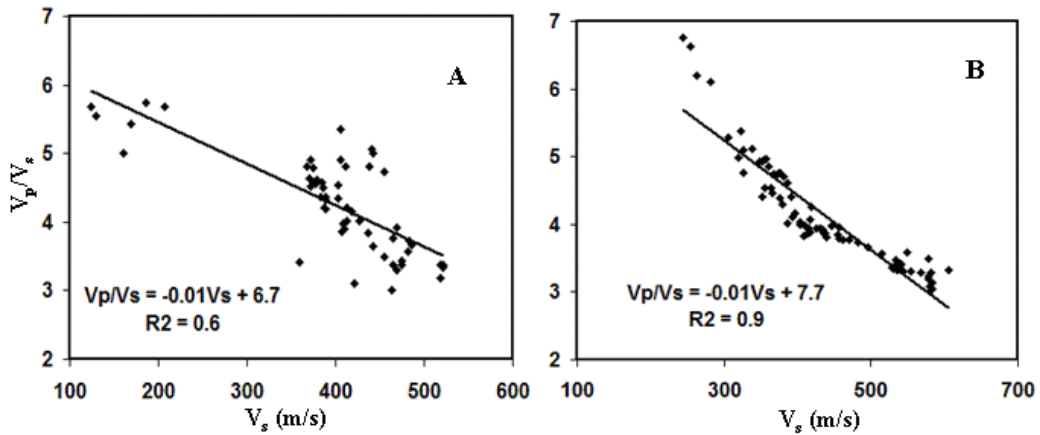


Figure 6.8: Correlation between P- and S-wave velocity ratio (V_p/V_s) versus S-wave velocity (V_s) from BH3914 (A) and BH3786 (B).

Chapter 7: Discussion

7.1 Overview

Over the last few decades geophysical methods have been used extensively to aid in solving a wide range of hydrogeological problems. Taking advantage of the fact that the different geophysical methods are sensitive to different properties, the geophysical methods are used in solving three main objectives: hydrogeological mapping, hydrogeological parameter estimation and hydrogeological monitoring.

The main goal of the present study is to use an integrated approach of geophysical methods to image and characterize the Quaternary aquifers in glacial sediments that fill the Ellerbek Buried Subglacial valley as well as the surrounding Tertiary horizons.

Geophysical data acquisition, processing and interpretation were highlighted in the previous chapters. This chapter discusses the result of the geophysical methods applied to image and characterize the Quaternary aquifer systems in Ellerbek Valley and its surrounding Tertiary sediments. Integrated interpretations of geophysical data as well as correlation with other similar and related studies are also discussed.

7.2 Surface Seismic Profiling

Processing of the P-wave seismic profiles

2-D high resolution shallow seismic reflection profiles were acquired over high complex structure filled and covered with heterogeneous glacial sediments; therefore it required much effort to generate improved images of the subsurface. In seismic processing stage standard processing operations have been applied to the seismic data. But significant improvements have been achieved by applying dip-moveout (DMO) processing. To image reflections in regions of such high structural complexity it was necessary to resort to either partial pre-stack depth migration or DMO processing (Hale 1984). Deregowski (1986) claimed ten benefits for DMO processing however, common offset f-k DMO scheme (after Notfors and Godfrey 1987) was tested which has improved the seismic data by elimination of dipping effects and attenuation of

noise. The partial migration character of the DMO operation suggests it is best applied before doing the velocity analysis and the stack (Veeken 2007). Significant improvements of velocity spectrums were observed after application of DMO (see Figure 4.35) which can be related to the improvement of the seismic data due to noise attenuation by DMO. Consequently, this resulted in improvement of the migrated seismic sections. In other words, application of DMO lowered the level of migration noise (Notfors and Godfrey 1987). It was observed that DMO followed by post-stack time migration becomes approximately equivalent to pre-stack migration, but at significantly reduced computing cost (Jakubowicz, 1990).

Conventional velocity analysis of CMP gathers after (e.g. Sheriff and Geldart 1995; Yilmaz 2001) was carried out on the seismic data to calculate the interval velocity functions. Consequently, a simple and effective workflow for velocity estimation was developed. This workflow comprises three steps: (1) CVS analysis (see Baker 1999) was done first to select certain velocities for certain reflections; (2) following Yilmaz (2001), semblance gather analysis was conducted before and after DMO applied to seismic data and (3) the resulting RMS velocity functions were converted to interval velocity functions by Dix's equation (Dix 1956). The reliability of the interval velocity functions derived from surface seismic data was checked by interval velocity functions derived from VSP data. There were good correlations between the velocity functions. The common offset FK DMO data were then stacked using the RMS velocity functions resulting in good stacked sections. The NMO stacked sections in Figures 4.15 and 4.16 reveal complex structures characterized by diffractions or bowtie reflections which required migration processing to be eliminated.

Migration process greatly improved the images of the seismic profiles by collapsing the diffraction events in their apex and repositioned the seismic reflectors at their correct locations. This is, particularly, evident comparing the shape of the secondary channels within the Quaternary sediments before and after migration. Two types of migration algorithms were applied to collapse the diffraction events. The FD time migration for steep dips (up to 50°; Soubaras 1996) gave a better result than the Kirchhoff time migration (Schneider 1978). This may be due to the fact the FD algorithm allowed to include lateral and vertical velocity variations and provided images that were free of major artifacts. After time migration, the data were depth converted to image the subsurface in depth using interval velocity functions derived from VSP data. Interval velocity derived from VSP is supposed to be more accurate and therefore useful in depth migration than the velocity derived from CMP seismic Data.

Processing of the SH-wave seismic profile

An experimental 2-D SH-wave profile (about 750 m long) was carried out (coincident with P-wave profile 5 between CMP 291 and CMP 595) in order to test the potential of S-wave seismic in imaging buried valley structures and to image the shallow situations in which P-wave reflection exploration is ineffective (see Young and Hoyos 2001). The processing flow of the SH-wave profile is shown in Table 4.4. The main problem of SH-wave data was Love wave which is very evident across the seismic records (see Figure 4.21A). Love wave in SH-wave gathers can be compared to Rayleigh wave in P-wave gathers. However, Love wave velocity is closer to S-wave velocity than Rayleigh wave velocity is to P-wave velocity. To deal with the Love wave recorded in the present SH-wave data, two types of processing were applied to the shot gathers: f-k filtering (e.g. Sheriff and Geldart 1995) to minimize Love wave amplitude and top mute to remove what is remain. In acquisition stage the SH-wave profile was carried out with SH-wave streamed laid on asphaltic road (fast over slow geology) to suppress Love wave (Haines and Ellefsen 2006). Even though the strong Love wave that interfere with the direct arrival SH-waves (Figure 4.21B) was successfully eliminated, the shot gathers are still noisy (may be with mode converted waves) which seem to be stacked with the primary reflections as shown in the SH-wave stacked sections (Figure 4.24). This uncertainty can be related to the situation in the field regarding the source and receivers coupling with the locations and also to the heterogeneity of the surface soil. However, the overall image shown by SH-wave profile for the subsurface is good since confident events observed after CMP stacking can be tracked and confirmed by P-wave profile.

Interpretation of the seismic data

In general, the use of 2-D seismic data in imaging buried valleys showed variable results. However, the 2-D seismic imaging of buried valleys can be improved by acquiring the data with several vertical stacks at the shot points (Gabriel et al. 2003) and high CMP fold (Lutz et al. 2009). These factors can improve the signal-to-noise ratio and resolve internal structure of buried valleys. Using 24-fold seismic profile, Gabriel et al (2003) successfully imaged the internal structure of the Ellerbek valley near Bevern village, north of the present study area. Lutz et al (2009) pointed out that using 2-D seismic data with fold up to 81 the internal structure of buried valley fill can be resolved. The quality of seismic data, collected for buried valleys investigation, is also varying. Jorgensen and Sanderson (2006) pointed out that onshore seismic

data is poorer than offshore seismic data which hampers their geological interpretation. In combination with borehole and other geophysical data, it is, however, possible to construct detailed geological models (Jorgensen et al. 2003). Other authors e.g. Wolfe and Richard (1996) observed that seismic reflection surveys over a buried valley did not show fine stratigraphic details. They related that to the attenuation of the high-frequency seismic waves, needed for high resolution, by glacial materials.

In the present study area two 2-D P-wave seismic profiles were acquired with high resolution parameters (Table 4.1) resulting in high fold data (96- and 75-fold) and the processing flow used generated good quality seismic sections. The seismic reflection profiles are located across the valley axis (Figure 1.2). They show useful information about the valley infill stratigraphy and the substratum. They clearly indicated the presence of the buried valley by revealing the Tertiary/Quaternary (the valley floor) and the Pleistocene/Holocene boundaries which are characterized by high amplitude reflections at maximum depth of about 450 m and 60 m, respectively.

The Valley substratum – Tertiary Stratigraphy

The substratum has been cut by subglacial erosion to maximum depth of about 450 m (Figures 5.1 and 5.2). They consist of Tertiary deposits made up of sands and clay layers of Marine environment. These deposits are shown by the lithological log of BH3914 which shows abrupt shift in lithology from clay dominated layers to sand dominated layers. They can easily be traced from the well log to the coherent reflections on the seismic data. Coherent seismic reflections are related to impedance contrasts which are associated with bedding that represents the geologic structure (Sheriff and Geldart 1995). Almost all lithological boundaries recognized in the BH3914 (252 m) correspond with seismic facies units. The seismic facies below the well are confirmed from previous work (e. g. Scheer et al. 2006). The dip of Tertiary horizons due to the Quickborn salt dome emplacement is very clear in the seismic sections.

The Valley infill stratigraphy

The stratigraphy of the valley infill sediments can be discussed based on the seismic profiles (Figures 5.1 and 5.2) with lithological log and gamma-ray control provided by BH3786 placed closed to the middle of the valley as well as correlation with the results of other studies. The

seismic facies of valley infill sediments can be divided into five basic seismic facies units (Unit 1-5). Mitchum et al (1977) defined seismic facies units as mappable three dimensional seismic units composed of groups of reflections whose parameters differ from those of adjacent facies units. These units have no clear lithological boundaries as shown by the BH3786 lithological log. On the other hand, they show strong reflections on the seismic profiles. They must probably represent multiple erosional events (Lutz et al. 2009). Gamma-ray log shows abrupt changes in size of deposited sediments corresponding to the major reflections on the seismic data indicating changes of the depositional environment.

Unit5 represents the sediments deposited at the bottom of the valley up to 150 m (~ 450-300 m) thick. It is a chaotic to an irregular stratified facies unit. Usually, chaotic facies found in the bottom of the valley fill and it has been described based on seismic data by many authors. Kluiving et al (2003) and Praeg 2003 interpreted the chaotic seismic facies at the bottom of the valley with the help of well data as gravel to coarse grained sand. Similar interpretation, based on 3-D seismic data has been done by Lutz et al (2003). Different lithological compositions have also been interpreted to the chaotic facies at the bottom of valley fill. Gabriel et al (2003), using 2-D seismic and gravity data, interpreted the chaotic seismic facies at the bottom of the Ellerbek valley on profile 1 as Boulder Clay (see Figure 1.2 for the location of the seismic profile 1). O’Cofaigh (1996) described the chaotic facies at the bottom of the valley fill as is typically comprises the basal member of infill and to be the collapse and slumping of unstable sediments along the valley flanks. The upper boundary of this unit is easily identified as a erosional truncation. Here, this chaotic layer is interpreted as coarse grained sands with gravel based on the present seismic data correlated with BH3786 lithology (Figure 2.2A).

Unit 4 is a layered and stratified seismic facies with high amplitude reflections in profile 4 and of low amplitude reflection in profile 5. Seismic facies unit3 lacks internal reflections and therefore no stratified change in acoustic properties. It is interpreted as no change of lithologic facies (Sheriff 1980). Unit 2 is characterized by moderate amplitude and laterally continuous reflections lie conformably below their top boundary. Unit 1 similar to unit 3 also does not have internal reflections and therefore no stratified change in acoustic properties. Units 4 to 1 mostly consist of finer sands (as gamma-ray log shows a general fining upward) than that compose unit 5, and represent horizontally stratified sediments.

Comparable observations on the lithology of the sedimentary infill of buried valleys were made by e.g. Huuse and Lykke-Anderson 2000, Kluiving et al. 2003, Praeg 2003, Lutz et al. 2009.

They interpreted the buried valley fill as chaotic/ disturbed seismic facies most likely represents glaciofluvial sand, while the well layered seismic facies is glaciolacustrine/ Glaciomarine fine grained sediments and displaying onlap fill. Similar succession was also described in north Germany by Ehlers et al (1984).

Figure 7.1 shows chaotic or deformed and inclined reflections highlighted by the rectangles. These chaotic zones extend between CMP 120 and CMP 250 and between CMP 450 and CMP 650 in profile 4 and profile 5, respectively, from below 100 m to the bottom of the valley. They can be interrelated in two different ways: (1) they could represent strata deposited on top of dead ice as described by Stephan (1974) and Grube (1979). During deglaciation, collapse of ice and sediment into the channel might be stilled at the bottom of the channel for some period of time (Kehew et al. 1999, Kozlowski et al. 2005, Jørgensen & Sanderson 2006). Sediment from more recent glacial events may be deposited over the filled channel, leading to crosscutting relationships that would be hard to explain without the presence of buried ice (Kehew et al. 1999). Gradual melting of the buried ice creates the final valley form, destroying the characteristics of the original valley sediments like bedding planes; (2) the other possible explanation for the chaotic structuring and dipping reflection in the western parts of the two profiles is that it might be a different valley (secondary?) that could be trace by the chaotic area (valley B below CMP 600 in Figure 7.2) which its relation to the major valley (valley A) and to the fault system need to be explained.

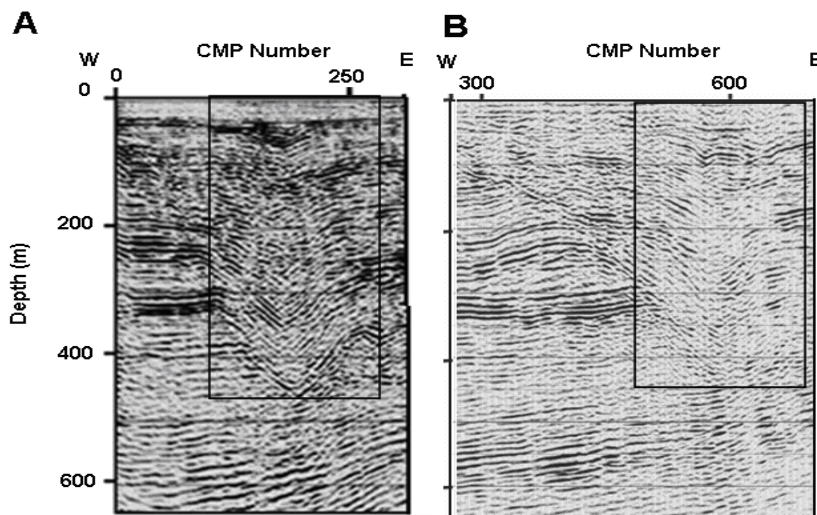


Figure 7.1: Part of the migrated seismic sections **A**: from profile 4 between CMP 120 and CMP 300; **B**: profile 5 between CMP 450 and CMP 650 show chaotic curve-like reflections in the areas marked by the rectangles.

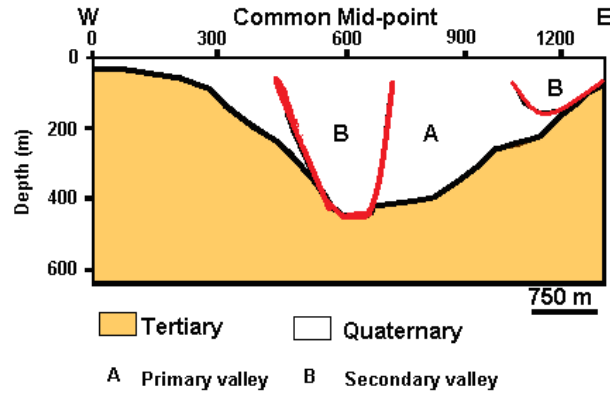


Figure 7.2: A simplified geological section interpreted from profile 5 to illustrate a possible large secondary (?) valley (B) within the major Ellerbek valley (A).

Two systems of faulting are interpreted from seismic data: (1) faulting Tertiary deposits - Pre-Quaternary Faulting - is shown in migrated section of profile 4 below the buried valley (Figure 5.1), and (2) fault system to the west of the valley (shown in Figure 5.2). The former fault system was most probably due to salt structure or tectonic events, whereas the later can be related to gravitational sliding of the western wall of the valley due to erosion of Tertiary sediments by subglacial meltwater (or may be due to melting of a buried iceberg), which formed a space with steep dipping walls and thus, the Tertiary horizons were pulled by gravity force resulting in breaking and moving of these horizons down slope. It can also be related to reactivation of previously existing faults that can be evident by the presence of Marine Mica Sand (Figure 7.3; after Scheer et al. 2006) which is found in the west of the valley protected by faulting against post-faulting weathering activities.

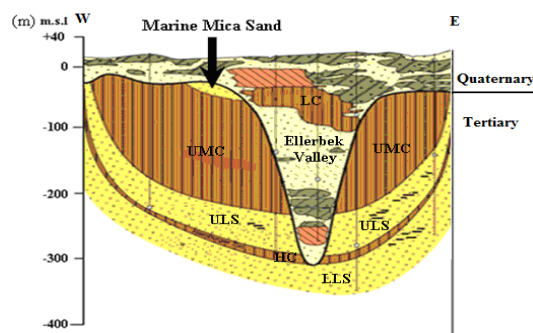


Figure 7.3: Geological section across the Ellerbek Valley showing the Quaternary sediments fill the Ellerbek valley as well as Tertiary sediments. LC = Lauenburg Clay; UMC = Upper Mica Clay; ULS = Upper Lignite Sand; HC = Hamburg Clay; LLS = Lower Lignite Sand. The arrow points to Marine Mica Sand which appears on the west side of the valley.

Combined interpretation of P- and SH-wave profiles

The Ellerbek buried valley and underlying Tertiary sediments have also been mapped by SH-wave profile to a depth of about 400 m. Attenuation of SH-wave signal in the low velocity sediments (Bexfield et al. 2006) may be the reason of limiting the depth. On the other hand, P-wave failed to interpret geological boundaries in the shallow part. Therefore, combination of P- and SH-wave seismic profiles (Figure 5.3) increases the scope of interpretation by providing different levels of resolution: SH-wave profile shows shallow reflection and adds more information about faulting in Tertiary sediments; P-wave mapped deeper to the bottom of the valley as well as Tertiary sediments. Decreasing spatial sampling interval on the SH-wave survey (0.5 m) allows obtaining high resolution image of the subsurface. Combining P- and SH-wave profiles conclude a detailed subsurface structure shown in Figure 5.4.

7.3 VSP and Seismic velocities derived physical parameters

Most of the VSP surveys performed are of the zero- or near-offset type, which is primarily used for velocity determination (Stewart 1984) and surface seismic correlation. Two zero-offset vertical seismic profiles (VSP) were carried out in BH3914 and BH3786. They were used in deriving P- and S-wave interval velocity models (Figure 4.31) of Tertiary and Quaternary sediments. These velocities were then used in deriving some physical properties of the sediments and therefore characterizing the groundwater aquifers. The velocities were also used in depth imaging of the seismic data. A three components (3-C) uphole geophone was used in acquiring the VSP data permitted to generate converted shear wave component in addition to the P-wave component. Therefore, converted V_s were combined with V_p to give additional information on lithology.

To demonstrate the usefulness of VSP data in the Quaternary and Tertiary aquifer characterization they need to be correlated with other geophysical and geological data. The two corridor stacks produced from VSP data at BH3914 and BH3786 (Figure 4.33) were spliced into surface seismic lines for correlation and integrated interpretation. Both datasets show excellent correlation of major seismic events in Quaternary as well as Tertiary sediments as shown in Figures 5.5 and 5.6.

As mentioned before, V_p and V_s models derived from VSP data are compared with the velocity models derived from CDP seismic data. The both datasets show acceptable matching which means the reliability of the velocity analysis of surface seismic data. This enables quantitatively use of these velocity fields in characterizing the groundwater aquifers in the study area. The P-wave velocities observed by VSP are in the range 1590-2000 m/s. Likewise; the S-wave velocities are in the range 250-650 m/s. These velocities can be compared to velocities calculated from similar sedimentary environments. Here are some examples of V_p (m/s) from other studies: 2100 – 2400 for saturated till (Häni 1986); 1550 – 1740 for saturated sediments (Omorinbola 1983); 1457 - 2060 for saturated glacial sediments (Salem 1990); 1350 – 1550 for saturated glacial sediments Silver and Linkeback (1972); 1700 – 2800 for Boulder Clay (Stuempel et al. 1984); 1600 for Lauenburg Clay and 2300 for Till (Gabriel et al. 2003); 1300-1800 for saturated sand and 500-2800 for clay (Fertig 2005). Examples of V_s (m/s): 536-863 for saturated glacial sediments (Salem 1990); 110-155 for clay (Fertig 2005). Most of the work done to estimate velocity of sediments from shallow seismic data was for marine sediments (e.g. Hamilton 1978, 1979). The average values of P-wave velocities derived from global compilations of marine sedimentary rocks are commonly between 1500-2200 m/s (Hamilton 1978) and for S-wave are < 1500 (Hamilton 1979). Figure 4.31 shows significant increase of interval velocities of P- and S-waves (V_p and V_s) with depth which can be related to several factors. Yilmaz (2001) pointed out that several factors influence interval velocity within a rock unit with a certain lithologic composition: e.g. pore shape, pore pressure, pore fluid, confining pressure and temperature. Increase of V_s in saturated sediments can be due to variations of the grain size (Stuempel 1984), consolidation (Meissner et al. 1985) and to decrease in porosity (Bourbie et al. 1987 and Schön 1998). However, the most likely explanation for the increase of velocity values with depth, of the present data, is that unconsolidated sediments have experienced a significant reduction in porosity with depth due to compaction; the principal compaction mechanism is most probably ice sheets during the Quaternary. However, velocities obtained from the seismic data fall within a range reasonable for unconsolidated saturated sediments.

The interval V_p and V_s models and V_p/V_s ratio (Figure 6.4) provided constrain on possible variations in the subsurface physical properties to depth of 300 m. Empirical relationship between V_p and V_s is evaluated by regression analysis which shows good relationship in Tertiary sediments and poorer in Quaternary sediments (Figure 6.3). In this evaluation, only one trend line is attempted to be derived for each well. The correlation factors between V_p and V_s

are 0.6 and 0.5 in BH3914 and BH3786, respectively, indicating that there may be similar factors controlling V_p and V_s . Such analysis was carried out by Castagna et al (1985) for clastic sediments and by Hamilton (1979) for water saturated sands. Statistical relationships have also been carried out between V_p/V_s , V_p and V_s . The cross plots between V_p/V_s and V_s show poor correlation ($R^2 = 0.6$) in Tertiary sediments but strong correlation ($R^2 = 0.9$) in Quaternary sediments (Figures 6.8). This indicates that the main factor controlling the V_p/V_s ratio in Quaternary sediments is the variation in V_s and, consequently, the factors controlling its propagation in Quaternary sediments. On the other hand the factor controlling the V_p/V_s ratio in Tertiary sediments may be the variations in both velocity types. Because V_p and V_s increase with decreasing porosity (Domenico 1984) and V_p/V_s is directly correlated to porosity (Han et al. 1986), therefore, the high V_p/V_s (low V_s) values at depth range 150-180 m and most probably below 270m (Figure 6.4A) may indicate high porosity zones.

The combined use of V_p and V_s relationship as lithology indicator is based of the fact that seismically derivable parameters are very sensitive to lithology variation. A very demonstrative case shows that Limestones, sands and shales are perfectly separated in $V_p(V_p/V_s)$ domain, while they overlap on the V_p scale (Garotta 1999). Similarly, Tertiary and Quaternary clays and sands are separated in $V_p(V_p/V_s)$ domain as shown by Figure 6.7 but there is still an overlap. However, the idea shows a promising result in using crossplots of different $V_p - V_s$ relationship to differentiate between different lithologies.

An approach to estimate physical and hydrogeological properties from seismic data using well-known equations modified for unconsolidated sediments was deployed. In-situ estimated physical parameters include porosity, bulk density and hydraulic conductivity. Applying equation 3.3 (after Morgan 1969) to P-wave interval velocity (V_p) derived from VSP yields porosity values which range from 0.45 to 0.47 for Tertiary sediments and from 0.21 to 0.58 for Quaternary sediments. The lower end of the range of the Quaternary porosity (0.21) probably represents porosity of a relatively clean clastic unit (Pleistocene sands, Unit3). The high velocity value is shown by Lauenburg Clay. On the other hand Tertiary aquifers show medium to high porosity values which may be due to fine sand and/or sand intercalated with clay (the composition of Tertiary deposits as described by Scheer et al (2006). Porosity estimates obtained from seismic velocity data fall within a range of values reasonable for sandy aquifers.

In-situ bulk density as a function of depth was calculated for Tertiary and Quaternary sediments from V_p velocity functions derived at BH3914 and BH3876, using a linear density-velocity

relationship (equation 3.12; after Hamilton 1971). The density range of Quaternary sediments is higher (1795-2050 kg/m³) than in the Tertiary sediments (1820-1858 kg/m³). The higher end of the density range of the Quaternary sediments represents the density of the sedimentary unit at the bottom of the valley (unit 5). Similar valley was calculated for boulder clay at the bottom of the valley below the seismic profile 1 (Gabriel 2006) indicating that the density of different valley fill sediments can not be used as an indicator for sediments. However, densities of sediments calculated for Tertiary and Quaternary units are comparable to those calculated by others authors (Wuestenhagen et al. 1990, Hänig et al. 1994, Gabriel et al. 2003). Both decrease of porosity and an increase of density with depth are more evident in Pleistocene sands fill the Buried Valley than in the Tertiary sediments.

Hydraulic conductivity deduced from V_p indicate that Pleistocene sands exhibit higher values whereas, LC exhibits the lowest value. This situation reflects presence of a good aquifer structure in the Quaternary Valley: high productive or permeable sands (aquifer) covered by high impermeable clay layer (aquitards). Nevertheless, due to heterogeneity in Quaternary sediments there are variations in hydraulic conductivity (Figure 6.1) indicating that hydraulic conductivity is highly sensitive to heterogeneity. The reliability of the hydraulic conductivity measured from seismic data can be checked if compared with hydraulic conductivity measured by other methods (e.g. pumping test, which is described and many hydrogeological textbooks).

Elastic properties of the sediments are determined from knowledge of the seismic wave velocities of the medium (Gassmann 1951). The shear modulus, the bulk modulus, Young's modulus and Poisson's ratio were estimated from seismic velocities and density values. The all parameters show clear increase with depth which might be attributed to increase in compaction of sediments with depth. The V_p/V_s are used to compute Poisson's ratio according to equation 3.27. The values ranged among 0.44 and 0.49 and are very close to the limit of 0.5, indicating that the bulk compressibility of the sediments is very low. The high values and low variability of Poisson's ratios indicate that the bulk compressibility of the Quaternary sediments is mostly controlled by the pore fluid than by the elastic properties of the sediment framework. The values of Poisson's ratio calculated here are typical to values previously derived for unconsolidated saturated sediments (e.g. Stuempel et al. 1984, Meissner et al. 1985). The shear modulus in Quaternary sediments shows average value of 0.48 MPa and in Tertiary sediments 0.42 MPa. Average Young's modulus of Quaternary sediments is 1.4 MPa and of Tertiary sediments is 1.2 MPa. The increase of Young's modulus with depth may be attributed to the increase of stress

which produces more deformation in the rock matrix and reducing the pore spaces. Due to that Young's modulus increases.

7.4 Other Geophysical Data

General valley fill stratigraphic models can be determined by lithological logs, whereas, more detailed 1D as well as 2-D stratigraphy can be determined by surface and borehole geophysical data calibrated by the lithological logs. Resistivity models derived from airborne electromagnetic methods show consistency with the seismic data (Figures 5.7 & 5.8) down to depth of about 200 m. It is clear that Tertiary clay layers as well as the Lauenburg Clay are shown by low resistivity layers (5-25 Ωm). On the other hand, Tertiary and Quaternary sands show higher resistivity values ($> 50 \Omega\text{m}$). The short coming of the electromagnetic methods in this area is the penetration depth. The depth of penetration of electromagnetic methods is limited by the clay layers at shallow depths which trap the electrical current (Tezkan et al. 2009). They related the shallow depth to the use of small electromagnetic transmitter (50 m by 50 m). To overcome the problem of shallow penetration depth Tezkan et al (2009) proposed using of larger electromagnetic transmitter (400 m by 400 m). They applied the larger loop in Cuxhaven resulting in mapping the bottom of the valley at depth 309 m, where the small loop could penetrate only few tens of meters in their study area. However, the resistivity structures shown by Ellerbek valley confirmed the interpretation of the seismic interpretation and successfully map the Lauenburg Clay.

Assumptions on seismic features

The evolution of the Ellerbek buried valley can be explained in the following hypothetical schematic illustration.

Figure 7.4,1 shows the Pre-Quaternary situation when the Tertiary horizons were not eroded by subglacial melt water drainage. There might be possible drainage system or faulting and fracturing and /or a pre-existing open or buried valley cutting in the Tertiary sediments running parallel to the direction of the present buried valley. This hypothesis can be inferred from the theory mentioned by many authors that: (1) the present deep valleys are following pre-Quaternary drainage system or structures like faulting (e.g. Jørgensen and Sanderson 2006,

Stackebrandt 2009) and (2) the deepest incision into the older sequences is strongly controlled by the neotectonically active Central Europe subsidence zone (Garetzky et al 2001, 2003).

Figure 7.4, 2 shows the valley structure deposition of the Pleistocene glacial sediments. The erosional surface steeply dips in the west side and gently dips in the east side. Thus, the Tertiary sediments in the west side had been pulled down slope by the force of gravity as shown by arrows. Stackebrandt (2009) pointed out that the primary shape of the channels was altered by gravitational sliding and other reworking processes. The valley cut the pre-Quaternary sediments (Tertiary) to depth about 500 m. Gabriel et al (2003) show a depth below 360 m of the valley by seismic profile 1. This may indicate difference in depth along the valley as a characteristic of the glaciated valleys which have highly irregular longitudinal profiles with multiple occurrences of lows and thresholds (Jørgensen and Sanderson 2006). The arrows in the Figure show a proposed gravitational sliding direction due to excavation of Tertiary sediments by glacial ice sheets. The shape of the valley floor can be related to many factors e.g. the erodability of the substratum (Jørgensen and Sanderson 2006). The eastern flank of the valley is steeply dipping at Tertiary sands and gently to flat over the Tertiary clays (e.g. Hamburg Clay).

Figure 7.4, 3 shows the present day structures after the depositional of the Pleistocene sands and the Holocene sediments cover. The faulting shown in this figure may be interpreted due to down slope movements of the Tertiary sediments. The infill sediments are interpreted to consist of five major seismic facies of Pleistocene sands, generally fining upward, which represent the groundwater aquifer, and covered by Lauenburg Clay which represents the aquifer seal. The Figure shows also secondary structures discussed as to be secondary valleys (the structures below CMP 600 and CMP 1200) or deformed structure (the structure B below CMP 600) due to melting or thawing of buried block of old ice. Thawing of buried block of old ice might be the cause of gravitation sliding and mass flow of the material of steep valley flanks into the valley (Stackebrandt 2009).

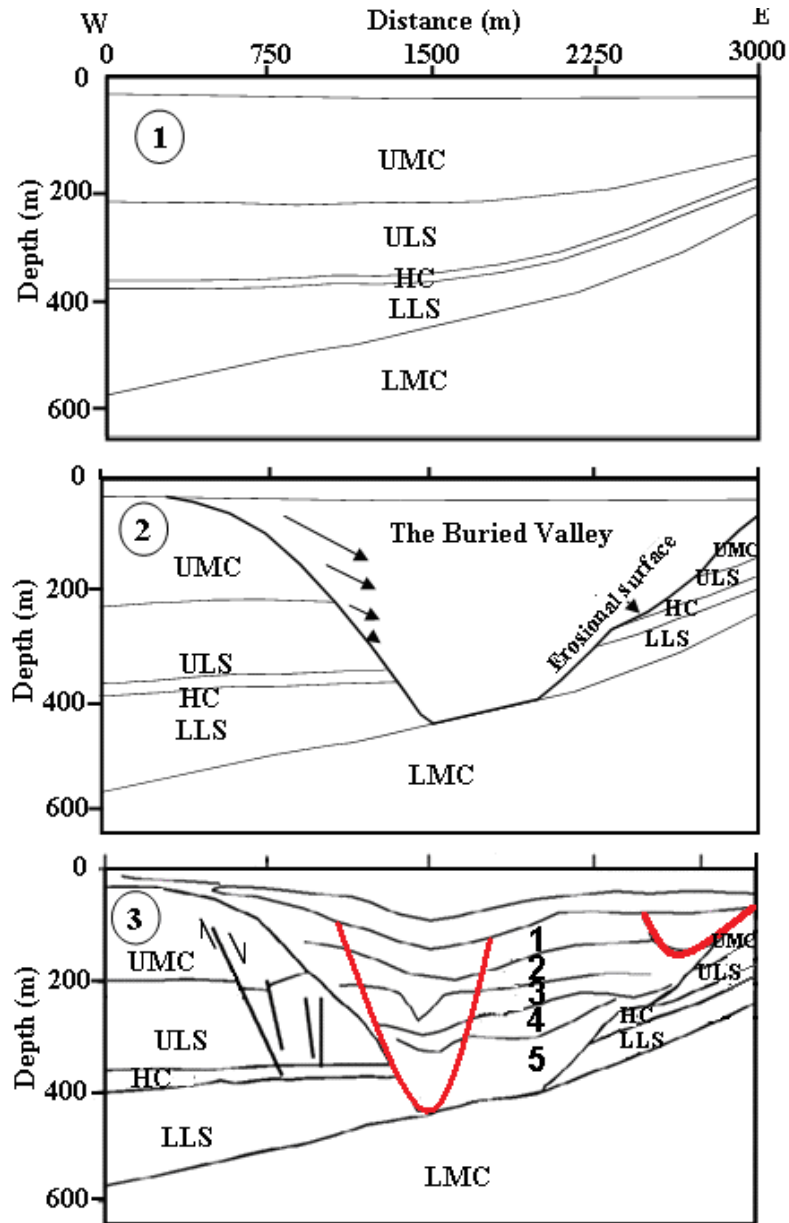


Figure 7.4 Hypothetical schematic illustrations for the interpreted structural evolution of the Ellerbek Valley: (1) the Pre Quaternary situation; (2) after the Tertiary horizons were eroded by glacial activities and (3) the present day situation. Red boundaries are secondary valleys. LC = Lauenburg Clay; UMC = Upper Mica Clay; ULS = Upper Lignite Sand; HC = Hamburg Clay; LLS = Lower Lignite Sand; LMC = Lower Mica Clay. Numbers 1-5 represent sediment units of the valley infill as interpreted from seismic data.

Chapter 8: Conclusions and Recommendations

8.1 Conclusions

Buried valleys occur across Northern Germany, yet no systematic study has been completed of the scale, style, and hydrogeological significance of these aquifer types. The present thesis reviews geological, hydrogeological and geophysical knowledge of the Ellerbek Valley aquifers in North Germany. The Buried valley is incised into Tertiary deposits and filled with Pleistocene glacial deposits.

The geophysical methods carried out offered possibilities for imaging the structures and geometry as well as obtaining representative physical and hydrological properties of unconsolidated saturated sediments of Quaternary and Tertiary formations

The 2-D high-resolution P-waves seismic reflection profiling has yielded high-resolution images of the Ellerbek buried valley, a complex incision cut the Tertiary horizons and filled with glacial, glaciofluvial and glaciolacustrine sediments showing general fining upward sequence. The fill is mainly composed of gravel and coarse sands at the bottom of the valley to fine sands towards the top with small amount of clays. Within the main valley there are other sub-valleys with different geological and geophysical characteristics. The valley is comparable to buried valleys elsewhere in formally glaciated areas.

The SH-wave reflection profile has been contaminated by many types of seismic noise, particularly Love waves. However, it has been favorable for imaging stratigraphy at the Ellerbek valley because SH-waves are very sensitive to compositional contrasts such as the interfaces between the sand aquifers and clay aquitards. In contrast to P-waves, SH-waves are largely insensitive to pore fluids, and thus are not affected by the water saturation in the valley. The SH-wave reflection method provides good images of the valley stratigraphy to a depth of about 400 m. The seismic images provide the thickness of the Lauenburg Clay and underlying Pleistocene sands in the valley and indicate that there are lateral variations within these layers that may affect the areal extent of their hydraulic behaviour. The Tertiary-Quaternary boundary below the seismic profiles has also been delineated. The SH-wave seismic images suggest that the Quaternary sediments show greater lateral heterogeneity than Tertiary layers, in agreement

with P-wave images. This information can provide important constraints for hydrogeological modeling. Because, the Lauenburg Clay layer is dominated by clay composition may be coherent enough to prevent flows from or near the surface. SH-wave data also added more information to P-wave data especially in the shallowest part of the subsurface. Combined information of P- and SH-waves profiles show more detailed images of the subsurface.

The VSP derived velocities are likely to be representative of the seismic velocities of the drilled section. The VSP corridor stacks show detailed images of the subsurface that match the surface seismic sections. The velocity models derived from seismic data provide possible variations in the subsurface lithology and physical properties of the sediments.

Results from geophysical surveys of the Ellerbek valley study area provided valuable information on the hydrogeological framework of the Pleistocene sandy aquifers and the covering low permeable clay layer. The Lauenburg clay unit probably forms a confining layer over much of the aquifer, and thus plays a significant role in the hydraulic behaviour of the groundwater flow system.

In addition to the mapping of the aquifer and the sealed units, geophysical data formed the basis for estimating the physical characteristics of the aquifer by applying well-known equations. Ranges of values for these physical parameters acceptable for unconsolidated saturated sediments were obtained.

The results of this study demonstrate that geophysical methods, especially seismics, can be used to image the sedimentary architecture of unconsolidated glacial sediments aquifers, even when the lithologic contrasts between units are subtle

8.2 Recommendations

Based on the results of this study, future seismic reflection studies should be dominated by shear waves because they show superiority to P-wave data in providing useful information regarding aquifer stratigraphy inside the buried valley.

The present SH-wave survey collected data that was superimposed by Love waves which can be related to the geophone-surface coupling, or more specifically, to the surface layer that should

have high velocity, (i.e., compacted soils, concrete or asphaltic ground), to suppress Love waves which are normally generated with SH-waves.

The present SH-wave survey used large offset which produced gathers that suffer from arriving waves other than SH-waves. Also the penetration depth was not deep enough to map the bottom Quaternary valley. Therefore the field setup used in this survey needs to be enhanced for future surveys.

Other problem in this present SH-wave seismic data was the noise related to rain and winds, which required that many shot-gathers had to be muted from the data. This, in turn, decreases the resolution of the seismic sections. Though noise levels could perhaps be reduced by carrying the data in times when there are no or not much rain and winds.

The high resolution P- and SH-wave seismic profiling were processed using ProMAX, a programme designed to process seismic data mostly collected for deep investigations, like oil explorations. Therefore, using a program designed for shallow seismics to process the data may enhance signal to noise ratio.

Although the present 2-D P- and SH-wave seismic data has yielded good information on the Quaternary sediments in the study area, uncertainty on the true dip and lateral extension of the individual reflectors can be resolved with more confidence by applying 3-D seismic surveying. Therefore, 3-D shallow seismic surveying is recommended to be carried out for further detailed images of the sediments therefore their hydrogeological parameters should be varied.

Considering the information gained from VSP data in this study, carrying out cross-hole seismic surveying using the existing wells may be useful to extrapolate the estimated physical and petrophysical characteristics of the sediments. Secondary valleys within the buried valley might be of superior hydraulic characteristic if they filled with coarse sands or gravels, therefore, more detailed investigation targeting these channels should be carried out.

More investigation boreholes should be drilled to carry out a proper and detailed hydrogeological and geophysical measurements for a more reliable and comparable studies.

REFERENCES

- ARCHIE GE (1942). The electrical resistivity log as an aid in determining some reservoir characteristics. Transactions of the American Institute of Mining, Metallurgical and Petroleum Engineers, **146**: 54–62.
- BAINES D, SMITH DG, FROESE DG, BAUMAN P, NIMECK G (2002). Electrical resistivity ground imaging (ERGI): A new tool for mapping the lithology and geometry of channel-belts and valley-fills. Sedimentology, **49**: 441–449.
- BAKER GS (1999). Processing near-surface seismic-reflection data. A prime, Society of Exploration Geophysics.
- BALCH AH, LEE MW (1984). Vertical seismic profiling technique applications and case histories. Internat. Human Resources Devel. Corp.
- BALDSCHUHN R, BINOT F, FLEIG S, KOCKEL F (2001). Tectonic Atlas of Northwest Germany and the German North Sea Sector - Structures, Structural Development and Palaeogeography. Geol. Jb., A 153, 88 S., 3 CDs; Hannover.
- BEBLO M (1997). Umweltgeophysik. Ernst Verlag, Berlin.
- BENN DI, EVANS DJA (1998). Glaciers and Glaciation. Edward Arnold, London, 734 pp.
- BENZING WM, BYERLY PE, HOPKINS JR (1983). Shear and compressional wave data interpretation-Midland Basin, Texas. Paper pres. at 53rd Ann. Int. SEG Mtg., Las Vegas.
- BERSEZIO R, GIUDICI M, MELE M (2007). Combining sedimentological and geophysical data for high-resolution 3-D mapping of fluvial architectural elements in the Quaternary Po Plain (Italy). Sedimentary Geology, **202**: 230–248.
- BIOT MA (1956a). Theory of propagation of elastic waves in a fluid-saturated porous solid: I. Low-frequency range. Journal of the Acoustical Society of America, **28**: 168-178.
- BIOT MA (1956b). Theory of propagation of elastic waves in a fluid-saturated porous solid: II. Higher-frequency range. Journal of the Acoustical Society of America, **28**: 179-191.
- BOLT BA (1982). Inside the Earth: evidence from Earthquake. W. H. Freeman, Sanfrancisco, 191 pp.
- BOSCH AJH, MAKKER MAJ, GUNNINK JL, PAAP BF (2009). Airborne electromagnetic measurements as basis for a 3D geological model of an Elsterian incision. In: Journal of the German Society for Geosciences ZDGG, **160**: 249-258.
- BOULTON GS, HINDMARSH RCA (1987). Sediment deformation beneath glaciers: rheology and geological consequences. Journal of Geophysical Research **92**: 9059-82.

- BOYD R, SCOTT DB, DOUMA M (1988). Glacial tunnel valleys and Quaternary history of the Outer Scotian shelf. *Nature*, **333**: 61–64.
- BRADFORD JH, SAWYER DS, ZELT CA, OLDOW JS (1998). Imaging a shallow aquifer in temperate glacial sediments using seismic reflection profiling with DMO processing. *Geophysics*, **63**: 1248-1256.
- BROUWER J, HELBIG K (1998). *Shallow high-resolution reflection seismics*. Elsevier Science Ltd, Amsterdam.
- BUEKER F, GREEN AG, HORSTMAYER H (1998). Shallow 3-D seismic reflection surveying: Data acquisition and preliminary processing strategies. *Geophysics*, **63**: 1434-1450.
- BURVAL WORKING GROUP (2006). Groundwater resources in buried valleys – a challenge for geosciences.- 314 S.; ed R.Kirsch, H.M. Rumpel, W. Scheer, and H. Wiederhold. Leibniz Institute for Applied Geosciences, Hannover.
- BURVAL WORKING GROUP (2009). Buried Quaternary valleys – a geophysical approach. In: *Journal of the German Society for Geosciences ZDGG*, **160**: 237-247
- CARY P, UPHAM W (1993). Noise attenuation with 3D FXY deconvolution. *Canadian Society of Exploration Geophysics; CSEG Convention Abstracts*, 22-23.
- CASTAGNA JP, BATZLE ML, EASTWOOD RL (1985). Relationships between compressional and shear-wave velocities in clastic silicate rocks. *Geophysics*, **50**: 551–570.
- CHASE M (1992). Random noise reduction by FXY prediction filtering, in *62nd SEG Convention Abstracts*, 1152-1153.
- CLAERBOUT J (1999). *Geophysical estimation by example: Environmental soundings image enhancement: Stanford Exploration Project*. <http://sepwww.stanford.edu/sep/prof/>.
- CRAWFORD JM, DOTY WEN, LEE MR (1960). Continuous signal seismograph. *Geophysics*, **25**: 95-105.
- CUTLER PM, COLGAN PM, MICKELSON DM (2002). Sedimentologic evidence for outburst floods from the Laurentide Ice Sheet margin in Wisconsin, USA: Implications for tunnel-channel formation. *Quaternary International*, **90**: 23–40.
- DANIELSEN J.E, AUKEN E, JØRGENSEN F, SØNDERGAARD V, SØRENSEN KI (2003). The application of the Transient Electromagnetic method in hydrogeophysical surveys: *Journal of Applied Geophysics*, **53**: 181–198
- de BROEKERT PP (2002). *Origin of Tertiary inset-valleys and their fills, Kalgoorlie, Western Australia*. PhD thesis, Australian National University, Canberra.
- DEREGOWSKI S M (1986). What is DMO? *First Break*, **4**: 7, 7-24

- DEREGOWSKI SM, ROCCA F (1981). Geometrical optics and wave theory of constant offset sections in layered media. *Geophysical Prospecting*, **29**: 374-406.
- DIX CH (1955). Seismic velocities from surface measurements. *Geophysics*, **20**: 68–86.
- DOMENICO SN (1976). Effect of brine-gas mixture on velocity in an unconsolidated sand reservoir. *Geophysics*, **41**: 882 – 894.
- DOMENICO SN (1977). Elastic properties of unconsolidated porous sand reservoirs. *Geophysics*, **42**: 1339-1368.
- DOMENICO SN (1984). Rock lithology and porosity determination from shear and compressional wave velocity. *Geophysics*, **49**: 1188–1195.
- EASTWOOD RL, CASTAGNA JP (1983). Basis for interpretation of V_p/V_s ratios in complex lithologies. Soc. Prof. Well Log Analysts 24th Annual Logging Symp.
- EHLERS J (1996). *Quaternary and Glacial Geology*. Wiley Chichester, 578 p.
- EHLERS J, LINKE G (1989). The origin of deep buried channels of Elsterian age in northwest Germany. *Journal of Quaternary Science* **4**: 255-65.
- EHLERS J, MEYER KD, STEPHAN HJ (1984). Pre-Weichselian glaciations of north-west Europe. *Quaternary Science Review*, **3**: 1-40.
- EHLERS J, WINGFIELD R (1991). The extension of the late Weichselian/late Devensian ice sheets in the North Sea basin. *Journal of Quaternary Science*, **6**: 313-26.
- FECHNER T (1998). Seismische Tomographie zur Beschreibung heterogener Grundwasserleiter. *Tuebinger Geowissenschaftliche Arbeiten*, C40.
- FERTIG J (2005). Geschwindigkeits- und Dichtewerte in Sedimenten. In: Knödel K, KRUMMEL H, LANGE G: *Handbuch zur Erkundung des Untergrundes von Deponien und Altlasten*, **3**, Geophysik. Springer, Berlin.
- GABRIEL G (2006). Gravity investigation of buried Pleistocene subglacial valleys. *Near Surface Geophysics*, **4**: 315-326.
- GABRIEL G, KIRSCH R, SIEMON B, WIEDERHOLD H (2003). Geophysical investigation of buried Pleistocene subglacial valleys in Northern Germany. - In: HUUSE M, LYKKE-ANDERSEN H, PIOTROWSKI JA (eds.), *Geophysical Investigations of Buried Quaternary Valleys in the Formerly Glaciated NW European Lowland: Significance for Groundwater Exploration (Special Issue)*. *Journal of Applied Geophysics*, **53**: 159-80.
- GADALLAH MR, FISHER RL (2009). *Exploration Geophysics: An Introduction*. Springer Berlin.
- GARDNER GHF, GARDNER LW, GREGORY AR (1974). Formation velocity and density – the diagnostic basics of stratigraphic traps. *Geophysics*, **39**: 770-780.

- GARDNER GHF, HARRIS MH (1968). Velocity and attenuation of elastic waves in sands. Soc. Prof. Well Log Analysts 9th Ann Symp, Transactions, M1–M19.
- GAROTTA R (1999). Shear Waves from Acquisition to Interpretation. Society of Exploration Geophysicists.
- GASSMANN F (1951a). Ueber die Elastizität poröser Medien. Vierteljahr. Naturforsch. Gesel. Zurich, **96**: 1–23.
- GASSMANN F (1951b). Elastic waves through a packing of spheres. Geophysics, **16**: 673-685.
- GILPATRICK R, FOUQUET D (1989). A user's guide to conventional data VSP acquisition. The Leading Edge, **8**: 34-39.
- GLENNIE KW (1983). Early Permian (Rotliegendes) palaeowinds of the North Sea. Sedimentary Geology, **34**: 245-265.
- GREEN AG, PUGIN A, BERES M, LANZ E, BUEKER F, HUGGENBERGER P, HORSTMAYER H, GRASMUECK M, DE IACO R, HOLLIGER K, AND MAURER HR (1995). 3-D high-resolution seismic and georadar reflection mapping of glacial, glaciolacustrine and glaciofluvial sediments in Switzerland: Ann. Symp. Environ. Engin. Geophys. Soc. (SAGEEP), Expanded Abstracts, 419-434.
- GREENHOUSE JP, KARROW PF (1994). Geological and geophysical studies of buried valleys and their fills near Elora and Rockwood, Ontario. Canadian Journal of Earth Science, **31**: 1838-1848.
- GRUBE F (1979). Uebertiefe Täler im Hamburger raum. Eiszeitalter und Gegenwart **29**: 157-172.
- GOCHIOCO LM (1990). Seismic surveys for coal exploration and mine planning. The Leading Edge, **9**: 25-28.
- GÖTZE HJ, GABRIEL G, GISZAS V, HESE F; KIRSCH R; KÖTHER N; SCHMIDT S (2009). The ice age paleo-channel to channel Ellerbek integrated 3D gravity study. In: Journal of the German Society for Geosciences ZDGG, **160**: 279-293
- GREGORY AR (1976). Fluid saturation effects on dynamic elastic properties of sedimentary rocks. Geophysics, **41**: 895-921.
- GULUNAY N (1986). FX decon and the complex Wiener prediction filter for random noise reduction on stacked data. Paper presented at the Society of Exploration Geophysicists 56th Annual International Meeting, Houston, TX.
- HAINES S, ELLEFSEN K (2006). Aquifer characterization with seismic shear wave reflection profiling: Proceedings, Symposium on the Application of Geophysics to

- Environmental and Engineering Problems, Environmental and Engineering Geophysical Society, 929-937.
- HAJNAL Z, SEREDA IT (1981). Maximum uncertainty of interval velocity estimation. *Geophysics*, **46**: 1543-1547.
- HALE D (1984). Dip-moveout by Fourier transform. *Geophysics*, **49**: 741-757.
- HAMILTON EL (1971). Elastic properties of marine sediments. *Journal of Geophysical Research*, **76**: 579-604.
- HAN DH, NUR A, MORGAN D (1986). Effect of porosity and clay content on wave velocities in sandstones. *Geophysics*, **51**: 2093-2107.
- HARDAGE B (1983). Vertical seismic profiling: Part A: Principals: Geophysical Press Pergamon Press, London, UK.
- HASBROUCK WP (1991). Four shallow-depth, shear-wave feasibility studies. *Geophysics*, **56**:1875-1885
- HOLZSCHUH J (2002). Low-cost geophysical investigations of a paleochannel aquifer in the Eastern Goldfields, Western Australia. *Geophysics*, **67**: 690–700.
- HOOKE RL, JENNINGS CE (2006). On the formation of the tunnel valleys of the southern Laurentide Ice Sheet. *Quaternary Science Reviews*, **25**: 1364–1372.
- HUANG CF, HUNTER JAM (1981). Identification and correlation of tube wave events on borehole seismic records. Atomic Energy of Canada, Ltd Ottawa, Technical Record TR-32.
- HUUSE M, LYKKE-ANDERSEN H (2000). Overdeepened Quaternary valleys in the eastern Danish North Sea: morphology and origin. *Quaternary Science Reviews*, **19**: 1233–1253.
- HUUSE M, PIOTROWSKI JA, LYKKE-ANDERSEN H (2003). Geophysical investigations of buried Quaternary valleys in the formerly glaciated NW European lowland: Significance for groundwater exploration. *Journal of Applied Geophysics*, **53**: 153–157.
- JAKUBOWICZ H (1990). A simple efficient method of dip-moveout correction: *Geophysical Prospecting*, **38**: 221-245.
- JEFFERSON RD, STEEPLES DW, BLACK RA, CARR T (1998). Effects of soil moisture content on shallow seismic data. *Geophysics*, **63**: 1357 – 1362.
- JØRGENSEN F, SANDERSON PBE (2006). Buried and open tunnel valleys in Denmark – erosion beneath multiple ice sheets. *Quaternary Science Reviews*, **25**: 1339–1363.
- JØRGENSEN F, SANDERSON PBE (2009). BURIED VALLEY MAPPING IN DENMARK: EVALUATING MAPPING METHODS In: *Journal of the German Society for Geosciences ZDGG*, **160**: 271-278.
- JØRGENSEN F, LYKKE-ANDERSEN H, SANDERSON PBE, AUKEN E, NORMARK E (2003). Geophysical investigations of buried Quaternary valleys in Denmark: An

- integrated application of transient electromagnetic soundings, reflection seismic surveys and exploratory drillings. *Journal of Applied Geophysics*, **53**: 215–228.
- KEHEW AE, LORD ML, KOZLOWSKI AL (2007). Glacial landforms of erosion. In: Elias SA (ed.) *Encyclopedia of Quaternary Science*. Elsevier, 818–831.
- KEHEW AE, NICKS LP, STRAW WT, (1999). Palimpsest tunnel valleys: Evidence for relative timing of advances in an interlobate area of the Laurentide Ice Sheet. *Annals of Glaciology*, **28**: 47–52.
- KILNER M, WEST LJ, MURRAY T (2005). Characterisation of glacial sediments using geophysical methods for groundwater source protection. *Journal of Applied Geophysics*, **57**: 293–305.
- KIRSCH R (2006). *Groundwater Geophysics: A Tool for Hydrogeology*, Springer Berlin.
- KIRSCH R, YARAMANCI U (2009). Geophysical characterization of aquifers.- In: Kirsch, R. (Hrsg.): *Groundwater geophysics, a tool for hydrogeology*, 2nd Ed.: 491 – 509; Springer, Heidelberg
- KLIMENTOS T (1991). The effects of porosity-permeability-clay content on the velocity of compressional waves. *Geophysics*, **56**: 1930-1939.
- KLUIVING SJ, BOSCH JHA, EBBING JHJ, MESDAG CS, WESTERHOFF RS (2003). Onshore and offshore seismic and lithostratigraphic analysis of a deeply incised Quaternary buried valley-system in the northern Netherlands. *Journal of Applied Geophysics*, **53**: 249–271.
- KNAPP RW, STEEPLES DW (1986a). High-resolution common-depth-point seismic reflection profiling: Instrumentation. *Geophysics*, **51**: 276-282.
- KNAPP RW, STEEPLES DW (1986b). High-resolution common-depth-point seismic reflection profiling: Field acquisition and parameter design. *Geophysics*, **51**: 283-294.
- KOCKEL F (2002). Rifting processes in NW-Germany and the German North Sea sector. *Netherlands Journal of Geosciences / Geologie en Mijnbouw*, **18**: 149-158.
- KOEFOED O, OOSTERVELD MM, ALONS IJG (1963). A laboratory investigation into the elastic properties of Limestones. *Geophysical Prospecting*, **11**: 300-312.
- KOZLOWSKI AL, KEHEW AE, BIRD BC (2005). Outburst flood origin of the central Kalamazoo River valley, Michigan, USA. *Quaternary Science Reviews*, **24**: 2354–2374.
- KRISTENSEN TB, HUUSE M, PIOTROWSKI JA, CLAUSEN OR (2007). A morphometric analysis of tunnel valleys in the Eastern North Sea based on 3D seismic data. *Journal of Quaternary Science*, **22**: 801– 815.

- LANZ E, PUGIN A, GREEN AG, HORSTMAYER H (1996). Results of 2- and 3-D high-resolution seismic reflection surveying of surficial sediments. *Geophysical Research Letters*, **23**: 491–494.
- LEPPER, J. & RÖHLING, H.-G. (1998): Buntsandstein.- In: BACHMANN GH, BEUTLER G, LERCHE I. (Hrsg.): Excursions of the International Symposium on the Epicontinental Triassic.- *Hallesches Jahrb. Geowiss.*, **6**: 27-34; Halle (Saale).
- LITTKER R, SCHECK-WENDEROTH M, BRIX MR, NELSKAMP S (2008). Subsidence, inversion and evolution of the thermal field. In: Littke R, Bayer U, Gajewski D, Nelskamp S (eds) *Dynamics of Complex Intracontinental Basins - The Central European Basin System*. Springer: 125-141.
- LUTZ R, KALKA S, GÄDICKE C, REINHARD L, WINSEMANN J (2009). Pleistocene tunnel valleys in the German North Sea: spatial distribution and morphology. In: *Journal of the German Society for Geosciences ZDGG*, **160**: 225-235.
- MANN RL, FATT I (1960). Effect of pore fluids on the elastic properties of sandstone. *Geophysics*, **25**: 433-444.
- MARION D, NUR A, YIN H, HAN D (1992). Compressional velocity and porosity in sand-clay mixtures. *Geophysics*, **57**: 554– 563.
- MAVKO G, MUKERJI T, DVORKIN J (1998). *The Rock Physics Handbook: Tools for seismic analysis in porous Media*, Cambridge, Cambridge University Press.
- MAYSTRENKO J, BAYER U, SCHECK M (2005) The Glueckstadt Graben, a sedimentary record between the North- and Baltic Seas in North Central Europe. *Tectonophysics*, **397**: 113–126
- MAZUR S, SCHECK-WENDEROTH M (2005). Constraints on the tectonic evolution of the Central European Basin System revealed by seismic reflection profiles from Northern Germany. *Netherlands Journal of Geosciences / Geologie en Mijnbouw*, **84**: 389-401.
- MAZUR S, SCHECK-WENDEROTH M, KRZYWIEZ P (2005). Different modes of the Late Cretaceous – Early Tertiary inversion in the North German and Polish basins. *International Journal of Earth Sciences*, **49**: 782-798.,
- MCCANN T (2008). *The Geology of Central Europe*. Geological Society, London.
- MEISSNER R, STUEMPEL H, THEILEN F (1985). Shear wave studies in shallow sediments: In *Seismic Shear Waves, Handbook of Geophysical Exploration, Part B, Applications*, Ed. By Helbig K. and Treiter S., 15 B, Geophysical Press, London – Amsterdam, 225-253.

- MILHOLLAND P, MANGHNANI MH, SCHLANGER SO, SUTTON GH (1980). Geoacoustic modeling of deep-sea carbonate sediments. *Journal of the Acoustical Society of America*, **68**: 1351-1360.
- MILLER RD, PULLAN SE, WALDNER JS, HAENI FP (1986). Field comparison of shallow seismic sources. *Geophysics*, **51**: 2067-2092.
- MILLER RD STEEPLES DW (1990). A shallow seismic reflection survey in basalts of the Snake River Plain, Idaho. *Geophysics*, **55**: 761-768.
- MITCHUM JRM (1977). Seismic stratigraphy and global changes of sea level. Part 11: glossary of terms used in seismic stratigraphy. In: Payton CE (Ed.), *Seismic Stratigraphy—Applications to Hydrocarbon Exploration*. American Association of Petroleum Geologists, *Memoir*, **26**: 205– 212.
- MJELDE R (1992). Reflection and polarization of tube waves as seen in VSP data. *Geophysical Prospecting*, **4**: 605 – 617.
- MØLLER MJ, OLSEN H, PLOUG C, STRYKOWSKI G, HJORTH H (2007). Gravity field separation and mapping of buried Quaternary valleys in Lolland, Denmark, using old geophysical data. *Journal of Geodynamics*, **43**: 330–337.
- MOHR M, KUKLA PA, URAI JL, BRESSER G (2005). Multiphase salt tectonic evolution in NW Germany: seismic interpretation and retro-deformation. *International Journal of Earth Sciences*, **94**: 917-940.
- MORGAN NA (1969). Physical properties of marine sediments as related to seismic velocities. *Geophysics*, **34**: 529– 545.
- MOOERS HD (1989). On the formation of tunnel valleys of the Superior Lobe, central Minnesota. *Quaternary Research* **32**: 24–35.
- MYERS PB, MILLER RW, STEEPLES DW (1987). Shallow seismic-reflection profile of the Meers fault, Comanche County, Oklahoma. *Geophysical Research Letters*, **14**: 749-752.
- NAFE JE, DRAKE CL (1957). Variation with depth in shallow and deep water marine sediments of porosity, density and velocities of compressional and shear waves. *Geophysics*, **22**: 523-552.
- NOTFORS CD, GODFREY RJ (1987). Dip moveout in the frequency-wavenumber domain. *Geophysics*, **52**: 1718-1721.
- O'COFAIGH C (1996). Tunnel valley genesis. *Progress in Physical Geography* **20**: 1–19.
- PAUL J (2006b) Field Trip F1: Zechstein around the Harz Mts. A geotraverse across an evaporite platform. In: v Eynatten H, Dunkl I, Fischer C, Karius V, Rupper H (eds) *Sediment 2006, Schriftr, DGG*, **45**: 193-212.

- PIOTROWSKI JA (1994). Tunnel-valley formation in northwest Germany - geology, mechanisms of formation and subglacial bed conditions for the Bomhoved tunnel valley. *Sedimentary Geology*, **89**: 107-41.
- PIOTROWSKI JA (1997). Subglacial hydrology in north-western Germany during the last glaciation: groundwater flow, tunnel valleys, and hydrological cycles. *Quaternary Science Reviews*, **16**: 169– 185.
- POLOM U, ARSYAD I, KUEMPEL H-J (2008). Shallow shear-wave reflection seismics in the tsunami struck Krueng Aceh River Basin, Sumatra. *Advanced Geosciences*, **14**: 135–140.
- PRAEG D (1996). Morphology, stratigraphy and genesis of buried Mid-Pleistocene tunnel-valleys in the southern North Sea basin. PhD Thesis, University of Edinburgh.
- PRAEG D (2003). Seismic image of mid-Pleistocene tunnel-valleys in the North Sea Basin – high resolution from low frequencies. *Journal of Applied Geophysics*, **53**: 273-298.
- PRAKLA-SEISMOS (1983). Scherwellen-Seismik: Hannover, Prakla-Seismos AG
- RAYMER LL, HUNT ER, GARDNER JS (1980). An improved sonic transmit time – porosity transform. *Soc. Prof. Well Log Analysts 21st Annual Logging Symp., Transactions*, 1-10.
- RIDER MH (1996). *The Geological Interpretation of Wireline Logs*. Whittles Publishing, 280pp.
- ROBINSON ES, CORUH C (1988). *Basic Exploration Geophysics*. John Wiley & Sons, New York, 163-210.
- ROBERTSON JD (1987). Carbonate porosity from S/P traveltimes ratios. *Geophysics*, **52**: 1346-1354.
- ROBINSON EA, TREITEL S (1964). Principles of digital filtering. *Geophysics*, **29**: 395-404.
- RUMPEL HM, GRELL T, HÖLSCHER F, STOLL M (2005a). Vertikales Seismisches Profil (VSP) zur teufenabhängigen Geschwindigkeitsbestimmung im BurVal Messgebiet Ellerbeker Rinne – Bericht zur techn. Durchführung und Processing. GGA-Institut Hannover.
- RUMPEL HM, GRUENEBERG S, RODE W, TAMIRU G, WEITMUELLER W, WIEDERHOLD H (2005b). Reflexionsseismische Untersuchungen der Ellerbeker Rinne bei Tangstedt und Schnelsen – Bericht zur technischen Durchführung und Processing. GGA-Institut Hannover.
- SALEM HS (1990). A theoretical and practical study of petrophysical, electric, and elastic parameters of sediments. PhD dissertation, Kiel University.
- SCHEER W (2001). Untersuchungsprogramm zur Ermittlung des nutzbaren Grundwasserdargebotes in schleswig-holsteinischen Nachbarraum zu Hamburg, Suedwest-Holstein. Landsamt fuer Natur und Umwelt, Flintbek.

- SCHEER W, KRÖGER J, KIRSCH R, ZARTH M (2006). Ellerbeker Rinne. In: Kirsch R., Rumpel HM, Scheer W & Wiederhold H. (Eds.): Groundwater resources in buried valleys, a challenge for geosciences. - Report GGA: 303 S., Hannover.
- SCHUCK A, LANGE G (2007). Seismic Methods. In: Environmental Geology, Handbook of Field Methods and Case Studies. Springer.
- SCHWAB G, LUDWIG AO (1996). Zum Relief der Quartärbasis in Norddeutschland, Bemerkung zu einer neuen Karte, -Z. geol Wiss. 24: 343-349; Berlin.
- SEN PN, GOODE PA, SIBBIT A (1988). Electrical conduction in clay bearing sandstones at low and high salinities. Journal of Applied Physics, **63**: 4832– 4840.
- SERRA O (1984). Fundamentals of Well-Log Interpretation (Vol. 1): The Acquisition of Logging Data: Dev. Pet. Sci., 15A: Amsterdam (Elsevier).
- SHERIFF RE (1980). Seismic stratigraphy: International Human Resources. Development Corporation, Boston.
- SHERIFF RE (2006). Encyclopedic Dictionary of Exploration Geophysics, 4th ed. Society of Exploration Geophysicists.
- SHERIFF RE, GELDART LP (1995): Exploration Seismology, Cambridge University Press, II Ed., 419 p.
- SIEGENTHALER C; HUGGENBERGER P (1993). Pleistocene Rhine gravel: deposits of a braided river system with dominant pool preservation. In: Best JL, Bristow CS (eds) Braided rivers. Geological Society Special Publication **75**: 147–162
- SIEMON B, RÖTTGER B, EBERLE D (2001). Airborne geophysical investigation of saltwater intrusions and coastal aquifers in NW Germany. – In: Proceedings 7th Meeting Environmental and Engineering Geophysics: 228-229.
- SMED P (1998). Die Entstehung der dänischen und norddeutschen Rinnentäler (Tunneltäler)— Glaziologische Gesichtspunkte, Eiszeitalter und Gegenwart **48**: 1–18.
- SMITH DB; TAYLOR JCM (1989). A ‘North-west Passage’ to the southern Zechstein Basin of the UK North Sea. Proc. Yorkshire Geological Society, **47**: 313-320.
- STACKEBRANDT W (2009). Subglacial channels of Northern Germany – a brief review. In: Journal of the German Society for Geosciences ZDGG, **160**: 203-210.
- STACKEBRANDT W, LUDWIG AO, OSTAFICZUK S (2001). Base of Quaternary deposits of the Baltic Sea depression and adjacent areas (map 2). Brandenburgische Geowissenschaftliche Beiträge **8**: 13–19.
- STEEPLES D, MILLER R (1990). Seismic reflection methods applied to engineering, environmental, and groundwater problems: In Society of Exploration Geophysics

- Investigations in Geophysics No. 5. Geotechnical and Environmental Geophysics, volume 1: Review and Tutorial, 1-30.
- STEPHAN HJ (1974). Sedimentation auf Toteis in Schleswig-Holstein, diskutiert anhand einiger Beispiele. – *Meyniana* **25**, 95-100
- STEWART RR (1984). Vertical-seismic-profile (VSP) interval velocities from traveltimes inversion. *Geophysical Prospecting*, **32**: 608 - 628.
- STEWART RR, DISIENA JP (1989). The values of VSP in interpretation. *The Leading Edge*, **8**: 16-23.
- STOLLHOFEN H, BACHMAN GH, BARNASCH J, BAYER U, BEUTLER G, FRANZ M, KÄSTNER M, LEGLER B, MUTTERLOSE J, RADIES D (2008). Upper Rotliegendes to Early Cretaceous basin development.- In: Littke R, Bayer U, Gajewski D, Nelskamp S (Eds.) *Dynamics of complex basins. The Central European Basin System*. Springer: 181-210.
- STOLT RH, BENSON AK (1986). *Seismic Migration, Theory and Practice*, Geophysical Press, London, 382 p.
- STUEMPEL H, KÄHLER S, MEISSNER R, MILKEREIT B (1984). The use of seismic shear waves and compressional waves for lithological problems of shallow sediments. *Geophysical Prospecting*, **32**: 662-675.
- TAMIRU G (2009). Lithological relevance of the near-surface seismic velocity model. PhD Dissertation, Gottfried Wilhelm Leibniz Universität Hannover.
- TATHAM RH (1982). V_p/V_s and lithology. *Geophysics*, **47**: 336-344.
- TATHAM RH (1985). Shear waves and lithology: In *Seismic Shear Wave, Handbook of Geophysical Exploration, Part B, Applications*, ed. Helbig K, Treiter S, 15B. Geophysical Press London – Amsterdam, 87-133.
- TELFORD WM, GELDART LP, SHERIFF RE (1990). *Applied Geophysics*, Cambridge University Press.
- TEZKAN B, MBIYAH MH, HELWIG SL, BERGRERS R (2009) Time domain electromagnetic (TEM) measurements on a buried subglacial valley in Northern Germany by using a large transmitter size and a high current. In: *Journal of the German Society for Geosciences ZDGG*, **160**: 271-278.
- THOMSEN R, SØNDERGAARD VH, SØRENSEN KI (2004). Hydrogeological mapping as a basis for establishing site-specific groundwater protection zones in Denmark. *Hydrogeology Journal*, **12**: 550–562.

- TNO (1976). Geophysical well logging for geohydrological purposes in unconsolidated formations. Groundwater Survey TNO. The Netherlands Organization for Applied Scientific Research, Delft.
- TREITEL S (1974). The Complex Wiener Filter. *Geophysics*, **39**: 169-173.
- VAN DER VEEN M, GREEN AG (1998). Land streamer for shallow data acquisition: evaluation of gimbal-mounted geophones. *Geophysics*, **63**: 1408-1413.
- VAN DIJKE JJ, VELDKAMP A (1996). Climate - controlled glacial erosion in the unconsolidated sediments of northwestern Europe, based on a genetic model for tunnel valley formation. In: Earth surface processes and landforms. The journal of the British geomorphological research group, **21**: 327-340.
- VEEKEN PCH (2007). Seismic Stratigraphy, Basins Analysis and Reservoir Characterisation. Elsevier, Amsterdam. 509 p.
- VOIGT T, REICHERTER K, VON EYNATTEN H, LITCKE R, VOIGT S, KLEY J (2008). Sedimentation during basin inversion. In: Littke R, Bayer U, Gajewski D, Nelskamp S (Eds.) Dynamics of complex intracontinental basins. The Central European Basin System. Springer, 211-232.
- WARD SH (1990). Geotechnical and environmental geophysics, Soc. Expl. Geophys.
- WARREN JK (2008). Salt as sediment in the Central European Basin System as seen from a deep time perspective. In: Littke R, Bayer U, Gajewski D, Nelskamp S (Eds.) Dynamics of complex intracontinental basins. The Central European Basin System. Springer: 249-276.
- WESTERN ATLAS (1985). Log Interpretation Charts. Atlas Wireline Services, Huston, 207 p.
- WIEDERHOLD H (2006). Seismic methods. In: BurVal Working Group (eds.): Groundwater Resources in Buried Valleys – a challenge for Geosciences: 227-240; Hannover (Leibniz Institute for Applied Geosciences).
- WIEDERHOLD, H., GABRIEL, G. & GRINAT, M. (2005): Geophysical exploration of the Bremerhaven- Cuxhaven valley in the area of research drilling Cuxhaven. - Zeitschrift für Angewandte Geologie, **51**: 26-36
- WIEDERHOLD H, BUNESS AH, BRAM K (1998). Glacial structures in Northern-Germany revealed by a high-resolution shallow reflection seismic survey. *Geophysics*, **63**: 1265-1272.
- WIEDERHOLD H, AGSTER G, GABRIEL G, KIRSCH R, SCHENCK PF, SCHEER W, VOSS W (2002). Geophysikalische Erkundung quartärer Grundwasserleiter im südlichen Schleswig-Holstein. *Zeitschrift für Angewandte Geologie*, **48**: 13-26.

- WIEDERHOLD H, RUMPEL HM, AUKEN E, SIEMON B, SCHEER W, KIRSCH R (2008). Geophysikalische Verfahren zur Erkundung und Charakterisierung von Grundwasserleitern in quartären Rinnen. *Grundwasser-Zeitschrift der Fachsektion Hydrogeologie* **13**: 68–77.
- WINGFIELD R (1990). The origin of major incisions within the Pleistocene deposits of the North Sea. *Marine Geology*, **91**: 31-52.
- WINSAUER WO, SHEARIN HM, MASSON PH, WILLIAMS M (1952). Resistivity of Brine-Saturated Sands in Relation to Pore Geometry. *AAPG Bulletin*, 36: 253-277.
- WOLFE PJ, RICHARD BH (1996). Integrated Geophysical Studies of Buried Valley Aquifers. *Journal of Environmental and Engineering Geophysics*, **1**: 75-84.
- WUESTENHAGEN K, BAERMANN A, BRUNS J, BUSSE R, GEYH M, SCHNEIDER W, WIENBERG R (1990). Glazial geprägter Glimmerton als Schadstoffbarriere im Elbtal des Hamburger Raums. *Geologisches Jahrbuch. Reihe, C* **55**: 3– 162.
- WYLLIE MRJ, GREGORY AR, GARDNER LW (1956). Elastic wave velocities in heterogeneous and porous media. *Geophysics*, **21**: 41-70.
- WYLLIE MRJ, GREGORY AR, GARDNER GHF (1958). An experimental investigation of factors affecting elastic wave velocities in porous media. *Geophysics*, **23**: 459-493.
- YEGOROVA T, BAYER U, THYBO H, MAYSTRENKO Y, SCHECK-WENDEROTH M, LYNGSIE SB (2006). Gravity signals from the lithosphere in the Central European Basin System. *Tectonophysics*, **429**: 133-163.
- YILMAZ O (1987). *Seismic Data Processing*, Society of Exploration Geophysics, Tulsa.
- YILMAZ O, CLAERBOUT JF (1980). Prestack partial migration. *Geophysics*, **45**: 1753-1777.
- YILMAZ O (2001). *Seismic Data Analysis - Processing, Inversion and Interpretation of Seismic Data*. SEG, Tulsa Oklahoma USA.
- YOUNG RA, HOYOS J (2001). Near-surface, SH-wave surveys in unconsolidated, alluvial sediments. *The Leading Edge*, **20**: 936-948.
- ZIMMERMAN RW, KING MS (1986). The effect of the extent of freezing on seismic velocities in unconsolidated permafrost. *Geophysics*, **51**: 1285-1290.

APPENDICES

APPENDIX A

The following tables provide V_p , V_s and V_p/V_s values from BH3914 (A1) and BH3786 (A2) used in Figures 6.6 and 6.7.

A1:

Depth (m)	V_p (m/s)	V_s (m/s)	V_p/V_s	Depth (m)	V_p (m/s)	V_s (m/s)	V_p/V_s
2	703.8	123.8	5.7	89	1825	372	4.9
5	800.7	159.9	5.0	92	1799.7	375	4.8
8	919.5	169.5	5.4	95	1754.2	379.3	4.6
11	1066.9	185.8	5.7	98	1676	383.7	4.4
14	1178.7	207.3	5.7	101	1619	407.8	4.0
17	1228	359.4	3.4	104	1571.7	407.4	3.9
20	1304	421	3.1	107	1597.8	410.1	3.9
23	1390.4	463.1	3.0	110	1660.9	413.1	4.0
26	1547.8	469.2	3.3	113	1734.7	412.5	4.2
29	1755.7	403.4	4.4	116	1737.5	417.8	4.2
32	1974.3	411	4.8	119	1714.5	426.3	4.0
35	2106.6	438.3	4.8	122	1678.7	436.8	3.8
38	2158.8	455.4	4.7	125	1616.4	442.4	3.7
41	2228.7	440.5	5.1	128	1585	454.6	3.5
44	2216.9	442.5	5.0	131	1570.5	464.8	3.4
47	2169.8	405.5	5.4	134	1601.5	474.8	3.4
50	1988.8	405.8	4.9	137	1635.3	475.1	3.4
53	1831.1	403.2	4.5	140	1720.9	481.9	3.6
56	1680.1	388.1	4.3	143	1784.8	485.4	3.7
59	1628	388.7	4.2	146	1836.2	469.3	3.9
62	1632.7	387.9	4.2	149	1801	483.4	3.7
65	1698.4	388.3	4.4	152	1782.4	485.9	3.7
68	1740.3	386.3	4.5	155	1752.3	465.2	3.8
71	1756.4	384.2	4.6	158	1748.5	521	3.4
74	1720.1	378	4.6	161	1758.7	521	3.4
77	1701.9	374.1	4.5	164	1751.1	517.7	3.4
80	1681.5	372.2	4.5	167	1744.1	521.2	3.3
83	1715.8	370.2	4.6	170	1645.9	517.8	3.2
86	1769.2	367.1	4.8	173	1645.9	517.8	3.2

A2

Depth (m)	V _p (m/s)	V _s (m/s)	V _p /V _s	Depth (m)	V _p (m/s)	V _s (m/s)	V _p /V _s
2	1622.4	416.7	3.9	154	1725.1	392.1	4.4
6	1616.3	356	4.5	158	1735.5	351.7	4.9
10	1616.3	356	4.5	162	1718.8	348.7	4.9
14	1618.1	305.8	5.3	166	1718.8	348.7	4.9
18	1631.4	263.6	6.2	170	1747.1	360	4.9
22	1655	244.7	6.8	174	1779.9	385.6	4.6
26	1685.7	254.2	6.6	178	1771.6	446.8	4.0
30	1722.4	282	6.1	182	1752.4	454.7	3.9
34	1741.1	323.6	5.4	186	1736	456.4	3.8
38	1751.5	354.4	4.9	190	1736	456.4	3.8
42	1769.5	373.2	4.7	194	1744.7	461	3.8
46	1794.4	375.8	4.8	198	1775.9	470.3	3.8
50	1769.2	357	5.0	202	1798.5	481.9	3.7
54	1730.6	338.8	5.1	206	1815.1	496.3	3.7
58	1659.5	326.2	5.1	210	1833.2	514.6	3.6
62	1595.6	319.6	5.0	214	1846.7	540.5	3.4
66	1559.4	327.1	4.8	218	1831.7	539.8	3.4
70	1548.9	352.2	4.4	222	1820.9	536.4	3.4
74	1548.9	352.2	4.4	226	1801.8	532.9	3.4
78	1550.3	385.7	4.0	230	1788.6	530.2	3.4
82	1565	408.8	3.8	234	1776.9	528.9	3.4
86	1600.8	414.2	3.9	238	1773.1	530.4	3.3
90	1632.5	409.9	4.0	242	1773.1	530.4	3.3
94	1644.8	395.8	4.2	246	1779.6	535.2	3.3
98	1646	376.1	4.4	250	1800.9	544	3.3
102	1638	366.1	4.5	254	1830.4	554.4	3.3
106	1625.4	379.1	4.3	258	1865.8	567.6	3.3
110	1614.6	393.5	4.1	262	1833	583.6	3.1
114	1614.6	393.5	4.1	266	1774.8	582.8	3.1
118	1616.1	404	4	270	1758.5	581.6	3.0
122	1635.5	415.1	3.9	274	1758.5	581.6	3.0
126	1680.5	426.4	3.9	278	1788.5	580.8	3.1
130	1690.1	437.8	3.9	282	1840.2	577.6	3.2
134	1670.1	438.8	3.8	286	1913.3	581.5	3.3
138	1670.1	438.8	3.8	290	2016.4	605.9	3.3
142	1679.2	435.2	3.9	294	1970	549.4	3.6
146	1696	430.6	3.9	298	1805.2	456.9	4.0
150	1698.8	417.1	4.1	302	1805.2	456.9	4.0

APPENDIX B

The following tables (**B1** and **B2**) provide porosity, density and hydraulic conductivity values from BH3914 and BH3786, respectively.

1. Porosity (Φ) $\Phi = -0.1356 \ln(V_p) + 1.3231$ (after Salem 1990).
2. V_p km/s = $1.917 \text{ km/s} - \Phi * 0.566$ (after Morgen 1969)
3. Density (ρ) $\rho (\text{kg} / \text{m}^3) = 1135 V_p (\text{km} / \text{s}) - 190$ (after 1971)
4. Hydraulic Conductivity (K) $\text{Log K} = 0.004332 V_p - 12.825$ (m/s) (after Fechner 1998)

B1:

Depth (m)	Φ (fraction)	P (g/cm ³)	K (m/s)*10 ⁻⁶	Depth (m)	Φ (fraction)	P (g/cm ³)	K (m/s)*10 ⁻⁶
2	0.43	1.96	0.0002	89	0.48	1.88	12
5	0.42	2.17	0.00044	92	0.48	1.85	9.36
8	0.41	2.23	0.00144	95	0.48	1.8	5.95
11	0.39	2.08	0.00626	98	0.47	1.71	2.73
14	0.37	2.19	0.0191	101	0.47	1.65	1.54
17	0.36	2.14	0.0312	104	0.46	1.59	963
20	0.35	1.99	0.0667	107	0.46	1.62	1.25
23	0.35	1.86	0.158	110	0.47	1.7	2.34
26	0.33	1.87	0.759	113	0.47	1.78	4.89
29	0.32	2.06	6.04	116	0.47	1.78	5.03
32	0.30	2.05	53.4	119	0.47	1.76	4
35	0.29	2.2	200	122	0.46	1.72	2.8
38	0.28	2.26	336	125	0.46	1.64	1.5
41	0.28	2.34	676	128	0.46	1.61	1.1
44	0.28	2.33	601	140	0.46	1.76	4.27
47	0.28	2.27	375	143	0.46	1.84	8.07
50	0.29	2.07	60.17	146	0.47	1.89	1.35
53	0.47	1.89	12.8	149	0.46	1.85	9.48
56	0.47	1.72	2.84	152	0.46	1.83	7.88
59	0.47	1.66	1.69	155	0.46	1.8	5.83
62	0.47	1.66	1.77	131	0.45	1.59	0.951
65	0.47	1.74	3.41	134	0.45	1.63	1.3
68	0.47	1.79	5.18	137	0.45	1.67	1.82
71	0.47	1.8	6.08	158	0.45	1.79	5.62
74	0.47	1.76	4.23	161	0.45	1.81	6.22
77	0.47	1.74	3.53	164	0.45	1.8	5.76
80	0.47	1.72	2.88	167	0.45	1.79	5.38
83	0.48	1.76	4.05	170	0.45	1.68	2.02
86	0.48	1.82	6.91	173	0.45	1.68	2.02

B2:

Depth (m)	Φ (fraction)	ρ (g/cm ³)	K (m/s)*10 ⁻⁶	Depth (m)	Φ (fraction)	P (g/cm ³)	K (m/s)*10 ⁻⁶
2	0.52	1.65	1.6	154	0.30	1.77	4.45
6	0.53	1.65	1.6	158	0.32	1.79	5.47
10	0.53	1.64	1.5	162	0.35	1.78	4.93
14	0.50	1.65	1.53	166	0.30	1.76	4.18
18	0.46	1.66	1.75	170	0.24	1.79	5.54
22	0.41	1.69	2.21	174	0.23	1.83	7.68
26	0.34	1.72	3	178	0.26	1.84	8.08
30	0.31	1.76	4.33	182	0.29	1.82	7.07
34	0.29	1.79	5.22	186	0.32	1.80	5.84
38	0.26	1.80	5.79	190	0.30	1.78	4.95
42	0.21	1.82	6.92	194	0.25	1.79	5.4
46	0.22	1.85	8.99	198	0.21	1.83	7.38
50	0.26	1.85	8.88	202	0.18	1.85	9.25
54	0.33	1.82	6.91	206	0.15	1.87	0.1
58	0.45	1.77	4.7	210	0.11	1.89	0.13
62	0.57	1.69	2.31	214	0.12	1.91	0.16
66	0.63	1.62	1.22	218	0.15	1.91	0.15
70	0.65	1.58	9	222	0.17	1.89	0.13
74	0.65	1.57	8	226	0.20	1.88	0.12
78	0.62	1.57	8	230	0.23	1.86	9.6
82	0.56	1.59	9	234	0.25	1.84	8.38
86	0.50	1.63	1.29	238	0.25	1.83	7.45
90	0.48	1.66	1.77	242	0.24	1.82	7.18
94	0.48	1.68	1.99	246	0.21	1.83	7.66
98	0.47	1.68	2.02	250	0.15	1.85	9.47
102	0.49	1.68	2.12	254	0.09	1.89	0.13
106	0.52	1.67	1.87	258	0.07	1.93	0.13
110	0.53	1.65	1.65	262	0.15	1.94	0.2
114	0.53	1.64	1.48	266	0.25	1.89	0.13
118	0.50	1.64	1.5	270	0.28	1.82	7.3
122	0.42	1.67	1.82	274	0.23	1.81	6.2
126	0.37	1.72	2.85	278	0.14	1.84	8.4
130	0.40	1.75	3.76	282	0.14	1.90	0.14
134	0.44	1.73	3.14	286	0.14	1.98	0.3
138	0.42	1.71	2.57	290	0.14	2.10	0.81
142	0.39	1.72	2.81	294	0.14	2.11	0.9
146	0.39	1.74	3.33	298	0.14	2.05	0.5
150	0.34	1.74	3.42	302	0.14	1.86	9.89

APPENDIX C

The following tables (C1 and C2) provide elastic parameters values from BH3914 and BH3786, respectively.

Formulas used for calculating elastic parameters

5. Shear modulus (μ)

$$\mu = \rho_b V_s^2$$

6. Bulk Modulus (k)

$$k = \rho_b (V_p^2 - \frac{4}{3} V_s^2)$$

7. Young's Modulus (E)

$$E = \rho V_s^2 \left(\frac{3V_p^2 - 2V_s^2}{V_p^2 - \frac{1}{3} V_s^2} \right)$$

8. Poisson's Ratio (σ)

$$\sigma = \frac{V_p^2 - 2V_s^2}{2(V_p^2 - V_s^2)}$$

C1:

Depth (m)	μ (MPa)	k (MPa)	E (MPa)	σ (ratio)	Depth (m)	μ (MPa)	K (MPa)	E (MPa)	σ (ratio)
2	0.03	0.93	0.09	0.48	89	0.25	5.79	0.75	0.48
5	0.04	1.08	0.11	0.48	92	0.25	5.41	0.74	0.48
8	0.06	1.82	0.19	0.48	95	0.26	5.24	0.77	0.48
11	0.07	2.29	0.21	0.48	98	0.28	4.9	0.81	0.47
14	0.09	2.94	0.28	0.48	101	0.35	5.04	1.03	0.47
17	0.27	2.82	0.79	0.45	104	0.34	4.66	1.01	0.46
20	0.35	2.93	1.03	0.44	107	0.32	4.48	0.95	0.46
23	0.4	3.05	1.15	0.44	110	0.3	4.5	0.89	0.47
26	0.41	3.91	1.19	0.45	113	0.31	5	0.9	0.47
29	0.33	5.83	0.98	0.47	116	0.31	5.01	0.92	0.47
32	0.32	7.04	0.96	0.48	119	0.33	4.86	0.96	0.47
35	0.33	7.21	0.98	0.48	122	0.34	4.55	0.99	0.46
38	0.37	7.72	1.08	0.48	125	0.34	4.11	1	0.46
41	0.39	9.4	1.15	0.48	128	0.38	4.11	1.11	0.46
44	0.4	9.57	1.19	0.48	131	0.41	4.12	1.19	0.45
47	0.31	8.47	0.92	0.48	134	0.43	4.3	1.25	0.45
50	0.33	7.51	0.98	0.48	137	0.42	4.41	1.22	0.45
53	0.28	5.32	0.81	0.47	140	0.42	4.8	1.23	0.46
56	0.26	4.55	0.77	0.47	143	0.42	5.09	1.22	0.46
59	0.32	5.15	0.93	0.47	146	0.39	5.43	1.14	0.47
62	0.32	5.18	0.93	0.47	149	0.42	5.31	1.24	0.46
65	0.3	5.37	0.89	0.47	152	0.42	5.05	1.22	0.46
68	0.31	5.8	0.9	0.47	155	0.39	5.06	1.15	0.46
71	0.26	5.12	0.77	0.47	158	0.5	4.96	1.45	0.45
74	0.26	5.02	0.77	0.47	161	0.54	5.38	1.56	0.45
77	0.28	5.35	0.81	0.47	164	0.55	5.57	1.6	0.45
80	0.28	5.32	0.82	0.47	167	0.53	5.19	1.53	0.45
83	0.27	5.53	0.81	0.48	170	0.54	4.69	1.55	0.45
86	0.26	5.79	0.78	0.48	173	0.52	4.6	1.52	0.45

C2

Depth (m)	μ (MPa)	k (MPa)	E (MPa)	σ (ratio)	Depth (m)	μ (MPa)	k (MPa)	E (MPa)	σ (ratio)
2	0.29	4.06	0.84	0.46	154	0.27	4.99	0.8	0.47
6	0.27	4.08	0.79	0.47	158	0.24	5.22	0.72	0.48
10	0.21	4.09	0.61	0.47	162	0.22	5.14	0.65	0.48
14	0.15	4.16	0.46	0.48	166	0.21	4.99	0.63	0.48
18	0.12	4.31	0.34	0.49	170	0.23	5.24	0.69	0.48
22	0.1	4.52	0.3	0.49	174	0.27	5.53	0.8	0.48
26	0.11	4.79	0.33	0.49	178	0.32	5.53	0.95	0.47
30	0.14	5.1	0.42	0.49	182	0.36	5.35	1.07	0.47
34	0.19	5.23	0.55	0.48	186	0.37	5.15	1.09	0.46
38	0.23	5.29	0.67	0.48	190	0.37	4.99	1.09	0.46
42	0.25	5.44	0.75	0.48	194	0.38	5.07	1.11	0.46
46	0.27	5.69	0.79	0.48	198	0.4	5.35	1.18	0.46
50	0.26	5.69	0.77	0.48	202	0.43	5.56	1.26	0.46
54	0.23	5.46	0.69	0.48	206	0.46	5.7	1.34	0.46
58	0.2	5.11	0.6	0.48	210	0.5	5.85	1.46	0.46
62	0.18	4.48	0.53	0.48	214	0.54	6.02	1.58	0.45
66	0.17	3.96	0.49	0.48	218	0.56	5.94	1.62	0.45
70	0.17	3.67	0.5	0.48	222	0.55	5.79	1.6	0.45
74	0.19	3.57	0.57	0.47	226	0.54	5.68	1.57	0.45
78	0.23	3.54	0.69	0.47	230	0.53	5.5	1.53	0.45
82	0.27	3.62	0.78	0.46	234	0.52	5.37	1.5	0.45
86	0.28	3.89	0.82	0.46	238	0.51	5.26	1.48	0.45
90	0.28	4.15	0.82	0.47	242	0.51	5.22	1.49	0.45
94	0.26	4.27	0.77	0.47	246	0.52	5.27	1.52	0.45
98	0.24	4.31	0.7	0.47	250	0.55	5.46	1.59	0.45
102	0.22	4.36	0.66	0.47	254	0.58	5.74	1.68	0.45
106	0.22	4.25	0.66	0.47	258	0.62	6.09	1.8	0.45
110	0.24	4.13	0.7	0.47	262	0.65	6.18	1.88	0.45
114	0.25	4.03	0.75	0.47	266	0.64	5.71	1.86	0.44
118	0.27	4.03	0.79	0.47	270	0.62	5.13	1.78	0.44
122	0.29	4.17	0.84	0.47	274	0.61	4.97	1.76	0.44
126	0.31	4.54	0.92	0.47	278	0.62	5.26	1.79	0.44
130	0.33	4.77	0.97	0.47	282	0.63	5.8	1.83	0.45
134	0.33	4.61	0.97	0.46	286	0.67	6.58	1.94	0.45
138	0.33	4.43	0.96	0.46	290	0.77	7.76	2.23	0.45
142	0.33	4.51	0.95	0.46	294	0.7	7.94	2.05	0.46
146	0.32	4.67	0.94	0.47	298	0.62	7.32	1.8	0.46
150	0.3	4.71	0.89	0.47	302	0.39	5.67	1.14	0.47

Curriculum Vitae

Name: Mohammed El Mahdi Siddig Abdelrahman.

Date of birth: May 23, 1971.

Nationality: Sudanese.

Address: University of Khartoum, Faculty of Science, Dept. of Geology, P.
O. Box: 321, 11115 Khartoum, Sudan. Mobile: +249912959343.
mohdmahdi@hotmail.com

Education:

PhD candidate at Leibniz University of Hannover, Germany, since 2006. Dissertation title: *Geophysical and lithological Characterization of the Ellerbek Valley Aquifer System*.

M. Sc. in Geology, University of Khartoum, Faculty of Science, Department of Geology, Sudan, 2001.

Postgraduate Diploma in Geo-information Science and Earth Observation, International Institute for Geo-Information Science & Earth Observation (*ITC*), the Netherlands, 2002.

B. Sc. (*Honours*) in Geology, University of Khartoum, Sudan, 1996.

Employment

1997-2001 Teaching Assistant at the Department of Geology, University of Khartoum.

2001- Lecturer at Department of Geology, University of Khartoum.

Hannover, September 2010